Illinois U Library

Transactions

of the

ASME

Symposium on Coal Hydrogenation

The Coal-Hydrogenation Demonstration Plant at Louisiana, Mo. . *J. A. Markovits* 349
High-Pressure Vessels in Coal-Hydrogenation Service . . . . *J. T. Donovan, M. Josenhans, and J. A. Markovits* 357
High-Pressure (10,300 Psi) Piping, Flanged Joints, Fittings, and Valves for Coal-Hydrogenation Service . . . . *J. H. Sandaker, J. A. Markovits, and K. B. Bredtschneider* 365
Instrumentation for Coal-Hydrogenation Service . . . . *G. L. Bruno, F. W. Geyer, and J. A. Markovits* 373
Metallurgical and Fabrication Considerations in the Coal-Hydrogenation Demonstration-Plant Construction . . . . *B. H. Leonard, Jr., G. D. Gardner, and J. A. Markovits* 379
Design of Preheaters and Heat Exchangers for Coal-Hydrogenation Plants . . . . *P. W. Laughrey, W. I. Gwillim, H. Schappert, and J. A. Markovits* 385
A Simple Hydrodynamic Thrust Bearing . . . . *F. R. Archibald* 393
Density-Pressure Relationships for Two Low-Viscosity Dimethyl Siloxanes . . . . *S. B. Gunst* 401
A Mathemetical Evaluation of Pressures in a Grease-Lubricated Bearing . . . . *K. B. Lawrence* 409
Investigation of Lubricants for Power Circuit Breakers . . . . *R. R. Bush* 415
Heat Transfer to Superheated Steam at High Pressures . . . . *W. H. McAdams, W. E. Kennel, and J. N. Addoms* 421
Philadelphia Electric Company Adopts Mobile Coal-Handling Equipment . . . . *E. C. Russell* 429
Storing and Reclaiming Coal With Earth-Moving Equipment at the Oswego Steam Station . . . . *J. N. Ewart* 435
Vibration of Marine-Turbine Blading . . . . *R. W. Nolan* 439
Theory of the Mechanical Properties of Hot Plastics . . . . *S. J. Loring* 447
Extrapolation of Static Tests to Predict Operation of Jet Engines in Flight . . . . *C. A. Meyer* 465

MAY, 1950

VOL. 72, NO. 4

Transactions

of The American Society of Mechanical Engineers

Published on the tenth of every month, except March, June, September, and December

OFFICERS OF THE SOCIETY:

James D. Cunningham, *President*

Joseph L. Kopf, *Treasurer*
C. E. Davies, *Secretary*

COMMITTEE ON PUBLICATIONS:

Ronald B. Smith, *Chairman*

John Haydock
George R. Rich

C. B. Campbell
Paul T. Norton, Jr.

H. G. Wenig
D. R. Thomas *Junior Advisory Members*

George A. Stetson, *Editor*
K. W. Clendinning, *Managing Editor*

REGIONAL ADVISORY BOARD OF THE PUBLICATIONS COMMITTEE

Kerr Atkinson—I
Otto de Lorenzi—II
W. E. Reaser—III
F. C. Smith—IV
Hendley Blackmon—V
R. E. Turner—VI
R. G. Roshong—VII
M. A. Durland—VIII

Published monthly by The American Society of Mechanical Engineers. Publication office at 20th and Northampton Streets, Easton, Pa. The editorial department is located at the headquarters of the Society, 29 West Thirty-Ninth Street, New York 18, N. Y. Cable address, "Dynamic," New York. Price $1.50 a copy, $12.00 a year for Transactions and the *Journal of Applied Mechanics;* to members and affiliates, $1.00 a copy, $6.00 a year. Changes of address must be received at Society headquarters three weeks before they are to be effective on the mailing list. Please send old as well as new address.... By-Law: The Society shall not be responsible for statements or opinions advanced in papers or ... printed in its publications (B13, Par. 4).... Entered as second-class matter March 2, 1928, at the Post Office at Easton, Pa., under the Act of August 24, 1912.... Copyrighted, 1950, by The American Society of Mechanical Engineers. Reprints from this publication may be made on condition that full credit be given the Transactions of the ASME and the author and that date of publication be stated.

The Coal-Hydrogenation Demonstration Plant at Louisiana, Mo.

By J. A. MARKOVITS,[1] LOUISIANA, MO.

The 200 to 300-bbl per day capacity demonstration plant hydrogenates coal at 700 atm pressure in two stages. First, coal paste is liquefied with finely divided iron catalyst at 525 atm hydrogen partial pressure, then the middle oil distillate is further hydrogenated in the vapor phase on fixed catalyst beds. The hydrogen is made by catalytic reforming of natural gas with steam.

INTRODUCTION

BACKGROUND information on the national liquid-fuel situation and status of the American synthetic-fuel research has already been presented by Dr. Schroeder.[2] The report mentioned Bureau of Mines demonstration-plant activities at Louisiana, Mo. Two plants were erected adjacent to the government-owned synthetic-ammonia plant: A 200 to 300-bbl per day capacity coal-hydrogenation plant and an 80 to 100-bbl per day capacity gas-synthesis plant.

The gas-synthesis plant will not be discussed in this presentation. For general orientation it may be mentioned that, when completed, it will produce synthetic fuels by the Fischer-Tropsch synthesis method from hydrogen and carbon-monoxide mixtures derived from gasification of pulverized coal with oxygen and superheated steam. Major component parts of this installation are the 1-ton per hr capacity Linde-Frankl oxygen plant, the pulverized-coal gasification plant, the gas-purification plant, the Fischer-Tropsch synthesis plant, and the product-recovery unit or refinery. The total plant construction is nearing completion, but the component parts were started up as soon as progress of the construction made it possible. The oxygen plant started producing 98 per cent pure tonnage oxygen as early as January, 1949, and pulverized coal was gasified in the plant with oxygen and superheated steam in May. Operation of the integrated plant is anticipated in 1950.

The coal-hydrogenation-plant construction was completed in January, 1949, but partial test runs were under way by November, 1948. The plant produced the first synthetic liquid fuels from lignite derivatives in April, 1949. In this presentation the process will be described as it is practiced in the demonstration plant. Details of conventional procedures will have to be omitted for brevity.

The plant was designed and built by the Bechtel Corporation of San Francisco, Calif., under technical direction and supervision of the Bureau of Mines. In the plant, 10,000 psi operating pressures are combined with temperatures up to 1000 F, and the materials to be processed at these conditions range from gases to mixtures of viscous liquids containing high percentages of abrasive solid particles. These service conditions presented many unusual engineering problems. Coal has been hydrogenated in Germany on a rather extensive scale for the past 20 years, but the process was new in the United States. Few items were commercially available for the chosen process. Where there was a choice between importing equipment from Germany or building it here, the latter was done. It was the hard way, but it was considered desirable to acquire design "know-how" and to give American manufacturers an idea of the basic requirements for the design of future commercial-size plants. Within the limitations of the project the equipment was chosen and sized so that the results of operations would be representative of those expected in modern full-scale hydrogenation plants.

THE PROCESS

Coal and petroleum differ in appearance but are similar in chemical composition. The main constituents of both are carbon and hydrogen, although the carbon:hydrogen ratio, the arrangement of the atoms in the molecule, and the molecular weights are different. In addition, coal contains more oxygen, nitrogen, sulphur, and mineral impurities or ash. To convert coal into gasoline the carbon and hydrogen atoms have to be rearranged, the hydrogen:carbon ratio must be approximately doubled, and the ash has to be removed.

In the demonstration plant all this is done at the 700-atm pressure level and in two stages. In liquid-phase hydrogenation a pulverized coal-oil paste is liquefied with hydrogen at elevated temperatures in the presence of a finely divided catalyst, such as iron oxide. In the vapor phase the middle-oil cut of the liquefied coal, which boils below 625 F, is converted into gasoline and byproducts with hydrogen over a solid bed of catalyst containing tungsten or molybdenum. Fig. 1 is a simplified flow diagram and shows the two main steps in proper relation to the necessary auxiliary operations.

The raw coal is first crushed to minus $^3/_4$-in. size, then pulverized to minus 60 mesh in a ball mill and dried to 1 or 2 per cent moisture content by a gas-fired recirculating drier. The pulverized coal is mixed with a small quantity of catalyst, such as iron oxide or tin oxalate and with heavy oil, previously obtained from the liquid-phase process into a paste, containing approximately 47 per cent solids.

The viscous paste is injected into the paste preheater by steam-driven plunger pumps working at 10,000 psi. The preheater is of modified radiant type, in which the high-pressure tubing is protected by a superheated-steam jacket. Before the paste enters the preheater, a small volume of hydrogen is injected to reduce the viscosity. The mixture is then heated in the first section to about 570 F. At this stage, additional hot hydrogen and recycle heavy oil are added to jump the temperature to the 640 F level, circumventing coal-swelling difficulties that would occur around 600 F. After passing through the remainder of the preheater, the mixture leaves at about 815 F and passes into the first of two converters. For 95 per cent conversion of the coal to liquid and gaseous products, the residence time is approximately 1 hr. The reaction is highly exothermic, and to maintain the reaction temperature at 930 F, cooling hydrogen is added to the converters in controlled amounts at different points.

After the second converter, the reacted products enter the

---

[1] Assistant Chief, Coal-to-Oil Demonstration Branch, Office of Synthetic Liquid Fuels, Bureau of Mines.

[2] "Synthetic Liquid Fuels in the United States," by W. C. Schroeder, *Mechanical Engineering*, vol. 69, 1947, pp. 989–995.

Contributed by the Petroleum Division and presented at the Petroleum Mechanical Engineering Conference, Oklahoma City, Okla., October 2–5, 1949, of THE AMERICAN SOCIETY OF MECHANICAL ENGINEERS.

NOTE: Statements and opinions advanced in papers are to be understood as individual expressions of their authors and not those of the Society. Paper No. 49—PET-3.

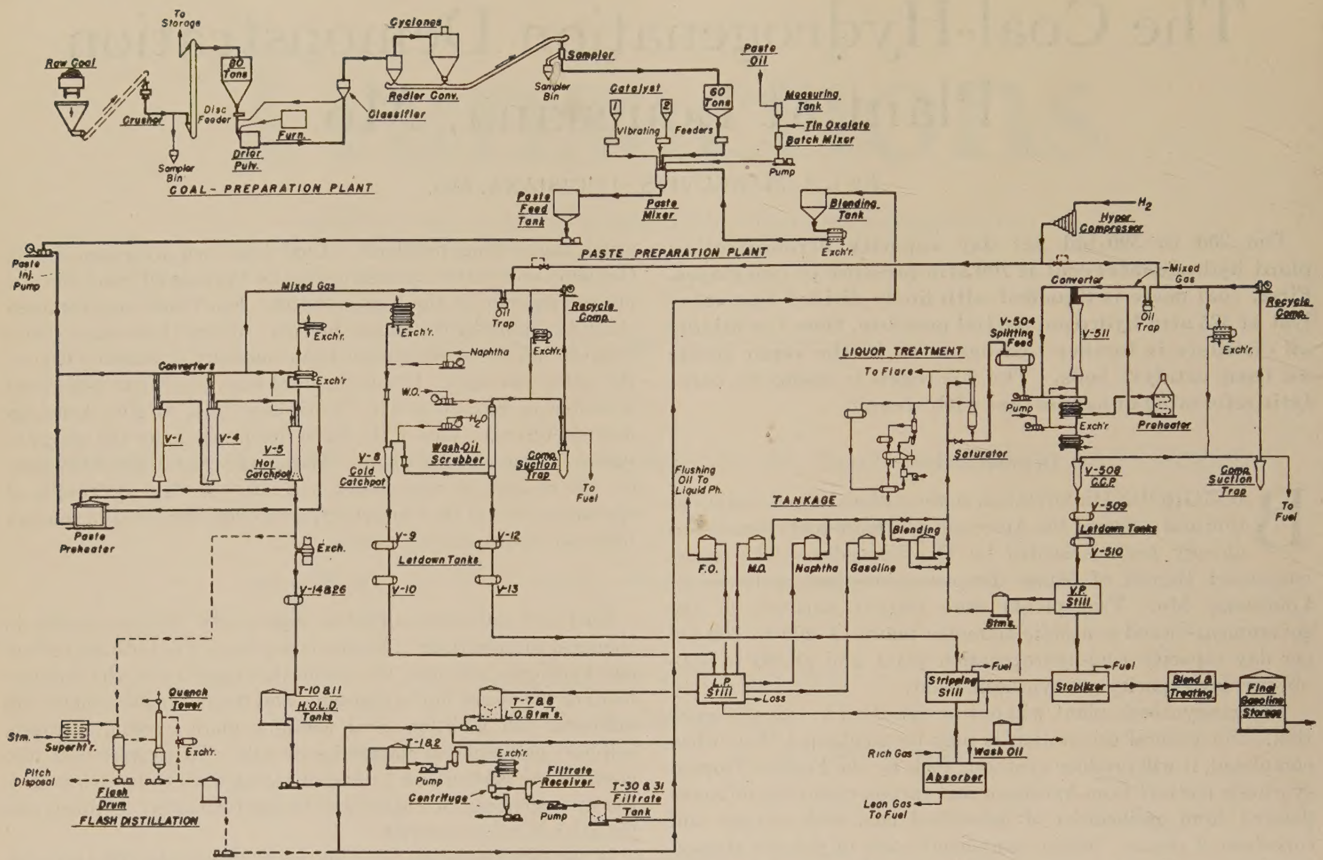

Fig. 1 Process-Flow Diagram of Coal-Hydrogenation Demonstration Plant

"hot catchpot," where the hydrogen and light ends separate from the solid-containing heavy-oil fraction. "Letting down" the heavy oil to near atmospheric pressure is the next step. This is extremely difficult, because the hot liquid contains large quantities of absorbed gases and up to 30 per cent of abrasive solids. The heavy-oil letdown valve, therefore, is considered one of the critical pieces of equipment and will be described in detail in a companion paper.

Two methods are provided for removing ash, catalyst, and unreacted coal from the heavy-oil letdown (HOLD). The first is a flash distillation unit (see Fig. 2), consisting mainly of a gas-fired heater for superheating steam to 1100 F, and a flash tower with high-velocity nozzles for instantaneous mixing of the hot steam and HOLD. The resulting mixture is quenched with saturated steam to prevent coking in the flash tower, which is 5 ft diam and 15 ft in height. Residue is withdrawn by steam-driven pumps and injected into a water-spray chamber for quenching. It is expected that the pitch will be hard and suitable for fuel; if not, other methods will be studied for the utilization of this waste product. The vapors from the flash tower pass to a quench tower and are cooled with oil of controlled temperature, to prevent congealing in the vessel. The recovered heavy oil is used in the pasting-oil cycle.

The alternate method consists of a Bird and a Sharples centrifuge, with facilities for blending and diluting the feed as well as for temperature control on the inlet and jacketed drums and for collecting the filtrate and residue. The filtrate is used in the pasting-oil cycle and the residue burned or otherwise disposed of.

The gases and vapors leaving the top of the hot catchpot are cooled in a heat-exchanger and water-cooler system from about 850 F to 150 F, and the condensed liquid and vapor are separated in the "cold catchpot." The gas from the cold catchpot, containing about 70 per cent hydrogen, is washed with water at full operating pressure for the removal of NH_3, H_2S, and water-soluble salts and is scrubbed with oil obtained in the liquid-phase distillation unit to separate the light hydrocarbons. After this purification, the hydrogen stream is recycled through the system with fresh make-up hydrogen. The liquid products from the cold catchpot and from the wash-oil scrubber go through let-down systems, where the pressure is reduced in two steps, first to 25 and then to 7 atm, and are then charged to the liquid-phase distillation unit. This two-step letdown facilitates economical separation of the C_1 and C_2 rich tail gases from the liquefied petroleum gases.

The bottoms from the liquid-phase distillation unit join the pasting-oil stream. Gasoline, naphtha, and middle-oil cuts are separated to establish weight relations and to prepare, by blending, after the separation of the washing oil, a feed stock of uniform composition for the vapor-phase hydrogenation. This stock is combined with a nearly equal amount of vapor-phase recycle middle oil and saturated with H_2S or with sulphur for the vapor-phase-hydrogenation step. The addition of some form of sulphur is necessary to preserve the activity of the vapor-phase catalyst.

The vapor-phase injection pumps, working at 10,000 psi, feed the charge, to which hydrogen is added, through a feed-product exchanger and a radiant-type vapor-phase preheater. The stream leaves the preheater at around 850 F completely vaporized. This vapor enters a single converter containing six fixed-catalyst beds. The catalyst is fuller's earth, treated with hydrofluoric acid and impregnated with compounds of zinc, molyb-

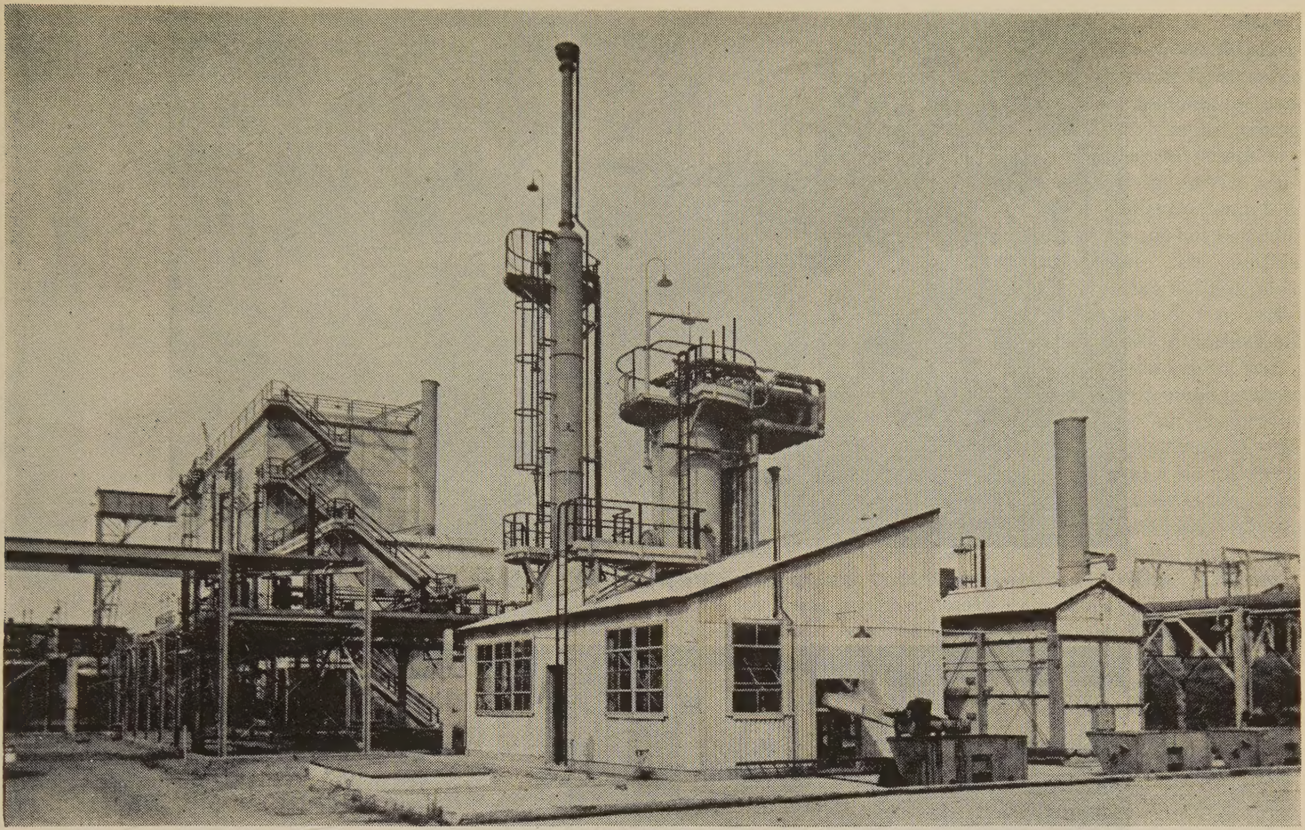

FIG. 2 HEAVY OIL LETDOWN FLASH DISTILLATION

denum, chromium, and sulphur. The catalyst is very rugged and at 700 atm performs the triple duty of the former German saturation, splitting, and dehydrogenation operations. The reaction is quite sensitive to temperature variations, and recirculated cooling hydrogen is added at every catalyst bed to keep the temperature between the 912 and 930 F operating limits. After the reaction is balanced, the feed-product exchanger provides most of the heat necessary, and the duty of the preheater becomes negligible.

The products then pass through a cooler and a cold catchpot, where the condensed oil and hydrogen are separated. The hydrogen is returned to the circulating compressors, and the liquid passes through a two-step letdown system to the vapor-phase distillation unit. The primary purpose of this unit is to separate the finished product from the recycle oil. Since conversion in the vapor-phase hydrogenation unit generally varies between 40 and 60 per cent, the distillation unit makes about 40 to 60 per cent bottoms, which are recirculated to the vapor-phase hydrogenation system; the overhead is stabilized to a 10-lb RVP gasoline, washed with caustic and water, and sent to final storage. Tail gases pass through an absorber before being used for fuel. Ammonia, CO_2, and H_2S liquors are treated with sulphuric acid before going to the sewer, and the recovered H_2S is utilized to saturate the vapor-phase charge.

Make-up hydrogen of about 11 per cent by weight of the moisture- and ash-free coal is furnished from the former Missouri Ordnance Works' natural-gas reformer, scrubber, and compressor system. Here natural gas is cracked with steam at 1700 F, and the resulting H_2 and CO are shifted with more steam at 800 F to H_2 and CO_2. The mixture is stored in a 300,000-cu-ft gas holder and compressed through three stages of a 7-stage 210,000-cu-ft per hr capacity compressor to 450 psi (see Fig. 3), at which pressure the CO_2 is scrubbed out with water. After the 7th stage, around 11,000 psi, the remaining CO is changed by catalytic reaction into methane and water. The resulting 95 per cent pure hydrogen is ready for injection into the gas-circulating system.

The recirculating compressors shown in Fig. 4 provide the large excess of hydrogen necessary to keep the partial pressure of the system at 525 atm. Approximately 250 standard cu ft of recycle gas is circulated for each gallon of paste. The reaction is highly exothermic, and the circulating gas must be kept cold for temperature control. Failure of the gas-recycle system would result in coking up of the converters, runaway temperatures, and disaster. So important is this function, that the circulating gas is called the "bloodstream of the process." One steam-driven and one motor-driven recycle compressor are operated continuously for each hydrogenation phase at half load, so that in case of failure of any unit, the other would immediately pick up the whole load. The units are single-stage double-acting reciprocating compressors and are designed to maintain a pressure differential of 750 psi with a 450,000 standard cu ft per hr output.

PLANT EQUIPMENT

The facilities required to carry out the operations described can be subdivided into the following groups:

1 Coal preparation.
2 Paste preparation.
3 Hydrogen manufacture.
4 Hydrogen compression and purification
5 Gas recycle and scrubbing.
6 Liquid-phase hydrogenation.
7 Liquid-phase distillation.
8 Vapor-phase hydrogenation.
9 Vapor-phase distillation
10 Ash removal.
11 Heavy-oil blending.
12 Gas recovery.
13 Storage and transfer.
14 Instruments.
15 Auxiliaries

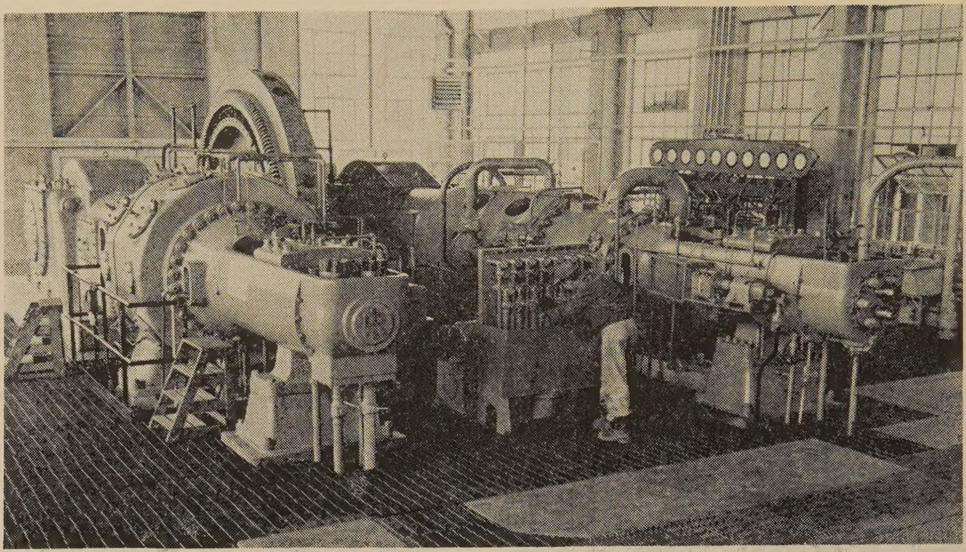

Fig. 3 Make-Up Hydrogen Compressor

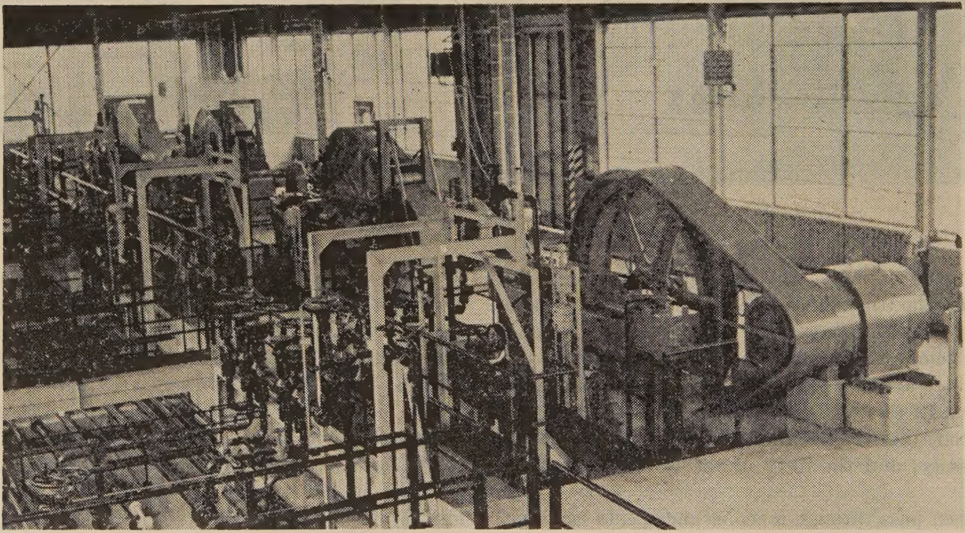

Fig. 4 Circulating Hydrogen Compressors

Detailed discussion of the foregoing groups will be omitted; and only a few comments will be offered, where necessary, to augment the process description. Thorough analyses of the more difficult coal-hydrogenation-equipment problems are given in companion papers elsewhere in this issue.

The coal-preparation plant was designed and furnished by Roberts & Schaefer Company, Chicago, Ill. It consists of track hopper, plate feeder, scraper conveyer, primary crusher, crushed-coal storage bin, feeder, gas-swept ball mill, gas-fired flue-gas heater, cyclones, fans, and water tumbler. It will pulverize and dry 10 tons per hr to 99 per cent minus 60 mesh, 85 per cent plus 200 mesh, 10 to 2 per cent moisture. Coal washing was eliminated from the original plans but may be added later if necessary.

The paste-preparation unit consists of a pulverized-coal storage bin, weighing feeder, paste mixer, paste storage tank, and facilities for mixing and adding measured quantities of dry or wet catalyst.

Paste is kept above 210 F and is circulated by Moyno pumps past the suction intake of the high-pressure injection pumps. Although all lines and containers are steam-jacketed, viscosities as high as 1300 centipoises are encountered at this temperature. Coal and paste-preparation plants are shown in Fig. 5.

Hydrogen manufacturing, compression, purification, gas-recycle, and scrubbing facilities were described with the process. The technique employed and equipment used are adaptations of the Hercules Powder Company's 15,000-psi ammonia-synthesis practice. Make-up compressors and recycle-gas circulators were furnished by Ingersoll-Rand. The metallic packings used are quite satisfactory for these services.

The liquid and vapor-phase hydrogenation units are completely new in American industry. The high-pressure vessels, preheaters, exchangers and coolers, tubing, flanging, valves and instrumentation are subjects covered by companion papers.

The severe service conditions of the coal-paste injection pumps place them in the critical category. The paste has a viscosity of 4750 centipoises at the 200 F pumping temperature and 10,300 psig discharge pressure. The pumps are Union Steam Pump Co., 250-lb steam-driven, double-acting, duplex, forged-steel

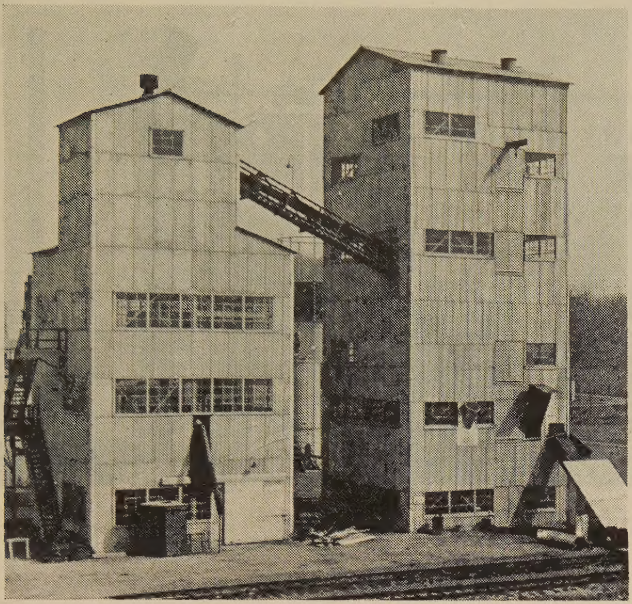

FIG. 5 COAL-AND-PASTE PREPARATION PLANT

plunger pumps, working at 50 psi suction and 10,300 psi discharge pressure. With 24-in. × $2^3/_4$-in. bore and 18-in. stroke, capacity is 25 gpm at 14.6 rpm, and the developed hydraulic horsepower is 150. Application of this time-proved direct pumping method is a promising deviation from the oil-driven hydraulic pumps used previously. Oil, naphtha, and water-injection pumps are similar to the paste-charge pumps, except that the service conditions are not quite so severe. The heavy-oil recycle pump is a steam-driven plunger-type surge pump. It returns hot bottoms to the preheater at 750 F and 10,000 psi pressure. The pump is separated from the hot valve block, and cold, clean flushing oil is the surge medium. An Aldrich-Groff 40-hp motor-driven, vertical-triplex, variable-stroke injection pump is used in flushing-oil service, mainly to determine its adaptability for this type of work. This pump has Teflon packing. The Union Steam pump plunger packings were furnished by Garlock and have four Neoprene-impregnated chevron rings. The 8-in-deep stuffing box, as well as the steam end, is oil-lubricated. It is felt that a lot will have to be learned by experience about high-pressure seals at the given operating conditions before the problem can be considered solved.

The most troublesome problem of the ash-removal and heavy-oil-blending steps is viscosity and settling of solids. Lines and pumps are steam-jacketed; tanks are equipped with heaters and mixing devices. An elaborate flushing-oil system is provided for these and other parts of the plant to eliminate plugging during shutdown periods.

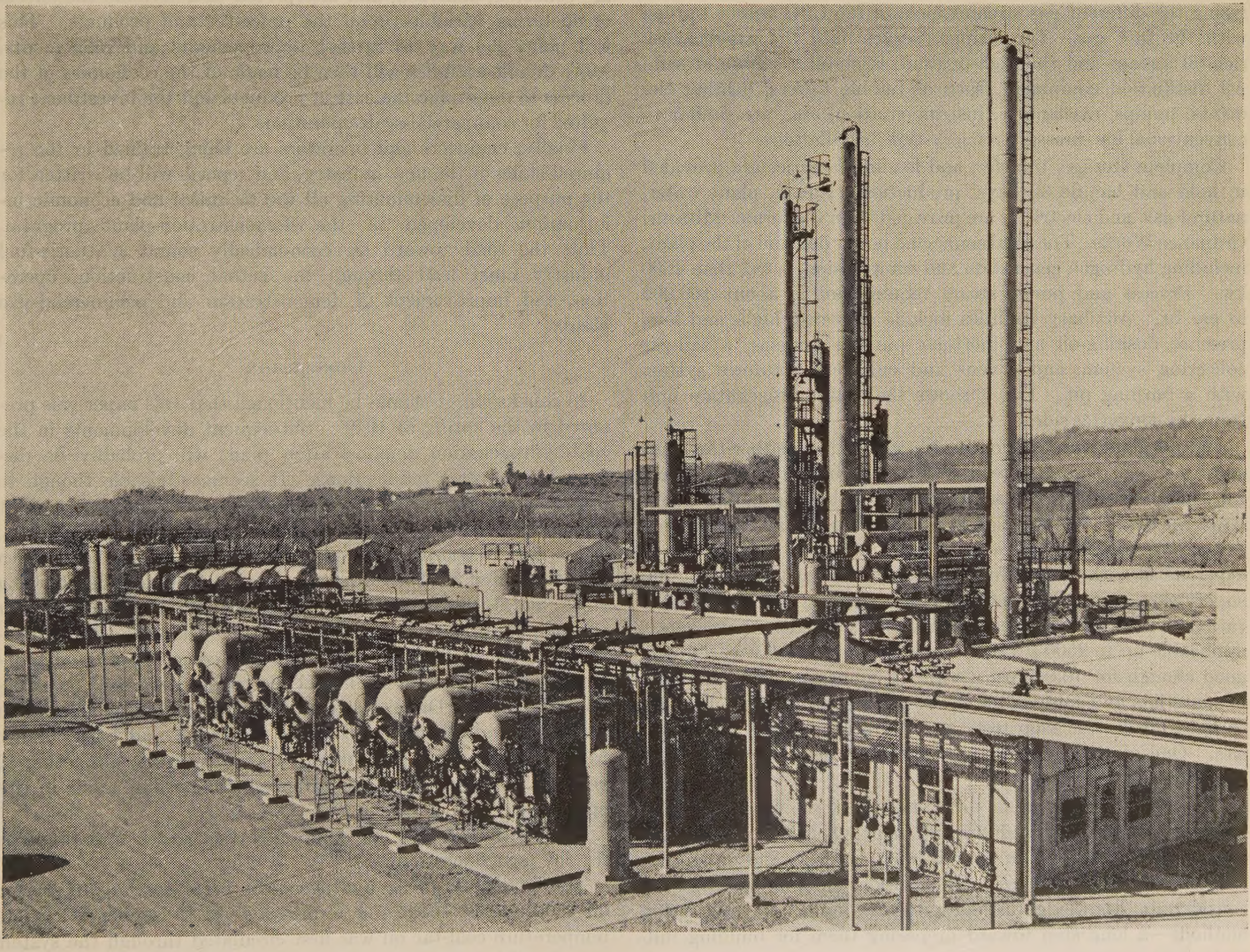

FIG. 6 COAL-HYDROGENATION DISTILLATION PLANT

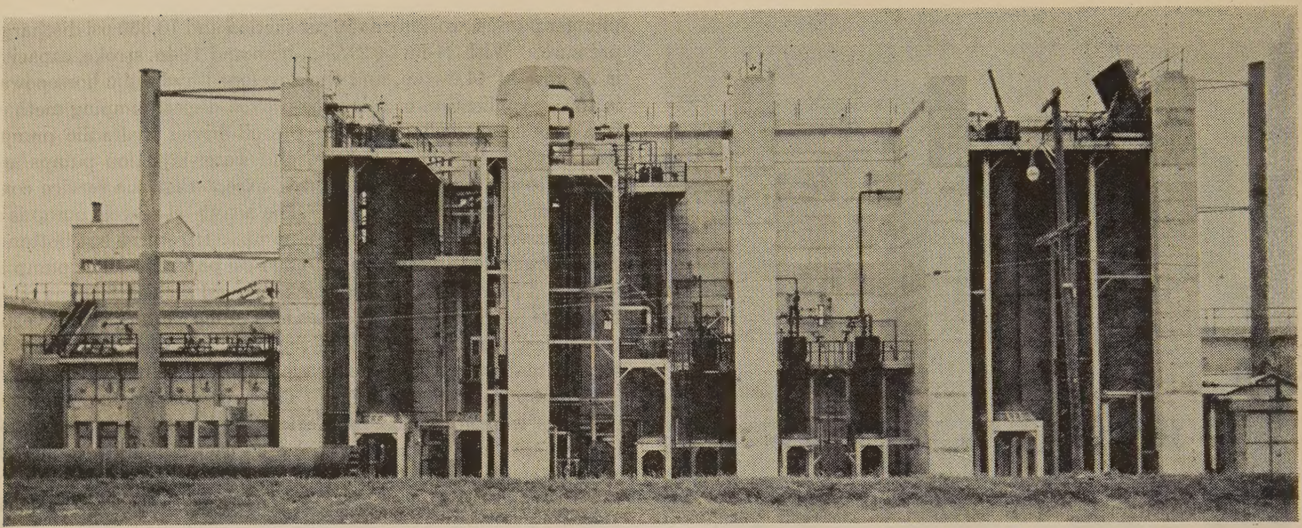

Fig. 7 Looking South at Open End of Stall

The liquid-phase distillation, vapor-phase distillation, gas-recovery, and liquor-treatment units are shown in Fig. 6. Gas recovery consists essentially of an oil absorber to recover enough butane to provide vapor-pressure control in the finished gasoline. No provisions are made for total C_3, C_4 recovery, and after analyzing the different gas streams most of the LPG will be burned with the fuel gas. The stripper serves both the gas-recovery rich-oil stream and the high-pressure wash-oil scrubber stream. All distillation equipment, such as bubble towers, heating elements, pumps, exchangers, instrumentation, etc., are similar to conventional low-pressure refinery-type installations.

Complete storage, transfer, and loading facilities are provided to hold and handle 30 days' production. Steam, plant water, natural gas, and electricity are provided from the former Missouri Ordnance Works. The total connected power demand of the plant, including hydrogen generation and compression, is less than 4000 kw. Process and power steam requirement is about 100,000 lb per hr. Auxiliary facilities include elaborate high- and low-pressure flushing-oil and inert-gas purging systems, a tail-gas collecting system, and a vent and emergency letdown system with a burning pit. Fig. 7 shows the coal-hydrogenation unit from the converter side.

During plant construction it was found that neither the average American manufacturer nor the construction forces realized fully the severity of the service in a coal-hydrogenation plant. After the design was completed in painstaking detail and reasonably severe specifications were drawn, repeated difficulties were experienced with their enforcement. The importance of careful supervision, inspection, and testing during every step of the fabrication and installation became evident. Standards of excellence, applicable up to 2500-psi service conditions, were not necessarily good enough for 10,000-psi work. In numerous instances flaws in materials and unsatisfactory workmanship were not brought to light until after shop tests, or even after delivery to the job site. One of the companion presentations discusses these problems in detail.

It became evident at an early stage that the demonstration-plant program is really fulfilling its main functions. During the construction and break-in periods, many process and design improvements were developed. In addition, manufacturers gained considerable knowledge in high-pressure design and fabrication methods—a long step toward preparing them for building full-scale plant equipment.

Operation of an Integrated Plant

The second phase of the work is under way. It is the demonstration of the operation of an integrated plant, producing synthetic liquid fuels from coal. During this period, operating data are collected, analyzed, and interpreted to determine the effects of operating variables upon the processes and products. This will point the way to further improvements and refinements. More detailed studies will then be made of the economics of the process to determine the cost of products and the investment required for commercial-scale operations.

Finally, engineers and operators are being trained in the required skills of the new industry, and reports will be written for the purpose of disseminating all the technical and economic information developed in the demonstration-plant program. Thus the road toward an economically sound synthetic-fuel industry must lead through the actual construction, operation, and improvement of demonstration and commercial-size plants.

Conclusion

In conclusion, it should be mentioned that this paper was prepared in the spring of 1949. Subsequent developments in the coal-hydrogenation demonstration plant will probably be discussed in several publications. It seems advisable though to bring the six papers of this symposium up to date with a short reference to the two completed hydrogenation runs.

The first 10,000-psi vapor-phase hydrogenation run in America was conducted in April, first using a petroleum-crude charging stock, and, thereafter, hydrogenating low-temperature lignite tar oil, mainly into gasoline and Diesel fuel. The actual hydrogenation period lasted 9 days. At the May dedication of the demonstration plants, part of the Diesel oil produced was used on a 200-mile trial run in a Diesel-electric locomotive hauling a loaded 8-car passenger train from St. Louis to Louisiana and back. Since May all plant passenger autos, trucks and cranes, altogether 55 vehicles, have been operated on synthetic gasoline made in this operation.

During the summer all equipment was tested and prepared for the next operation.

The first liquid-phase hydrogenation break-in run was started on October 12, 1949, and terminated on December 2. High-temperature coal-tar oil was first circulated through the system at reduced temperatures, then hydrogenated. On November 25, a paste was introduced containing 25 per cent of Rock Springs, Wyoming coal. Hydrogenated products from both charging stocks were nearly identical and consisted mainly of naphtha and middle oil suitable for vapor-phase hydrogenation stock.

Hydrogenation at 700 atm was never before attempted in this country, and the work was conducted with inexperienced operators in a brand new plant containing untried equipment and experimental instruments; hence, the run was considered highly successful. All objectives of both the vapor- and liquid-phase hydrogenations were achieved.

High-Pressure Vessels in Coal-Hydrogenation Service

By J. T. DONOVAN,[1] M. JOSENHANS,[2] and J. A. MARKOVITS[3]

The converters have to be built to resist 10,000 psi pressure and 1000 F temperature, complicated by hydrogen attack and H_2S corrosion. The three different designs proposed by American manufacturers are compared, and the vessels accepted for the plant are described in detail. The German spirally wound construction is discussed, and its expected advantages are enumerated.

Introduction

PRESSURES up to 15,000 psi have been used commercially in the synthesis of anhydrous ammonia and there is evidence of higher pressures applied for limited industrial production of plastics. These ranges, however, are unusual in American industry. Hydrogenation of coal combines working pressures of 10,300 psi with temperatures of 1000 F. The steels used must resist attack by high partial pressures of hydrogen and the corrosive effect of 1 per cent by weight of hydrogen sulphide, besides retaining adequate strength at elevated temperatures.

The 200-bbl per day demonstration plant required reaction vessels of 32 in. ID × 39 ft $1\frac{1}{2}$ in. length. The vessels were sized to provide adequate residence time, proper space velocity, and complete accessibility upon removal of the top and bottom heads. To utilize a low-alloy steel it was desirable to keep the shell temperature as low as 500 F. This was accomplished by providing a 3-in-thick asbestos-cement liner separating the reaction space from the shell.

Comparison of Proposed Designs

Manufacturers of high-pressure vessels proposed three different types of construction for this service as follows:

A A laminated wall of perforated carbon-steel plates with a 12 per cent chrome-alloy liner.

B A two-layer compound cylinder with a perforated carbon-moly jacket over a 3 per cent chrome grooved inner shell.

C A simple cylinder or solid wall forging of 3 per cent chrome.

Table 1 gives a comparison of the salient features of each design, and Figs. 1, 2, and 3 show the analysis of wall stresses as computed by the Lamé formula, stipulated by the API-ASME Code for vessels having wall thickness greater than 10 per cent of the inside diameter.

The laminated construction had many points in its favor, including the low-cost carbon steel, the close control of the wall material (insuring homogeneous construction), elimination of waste inherent in forging operations, and uniform stress distribution through the entire wall as shown in Fig. 1. On the other hand, the built-up ends, where the solid flange is welded to the laminated wall section, gave certain fabrication difficulties that caused undesirable increase in both weight and cost.

TABLE 1 VESSEL COMPARISONS

	A	*B*	*C*
Wall thickness, in.	$10\frac{1}{2}$	11	$8\frac{3}{4}$
Shell construction	Laminated $\frac{1}{4}$-in. plates	Forged compound cylinder	Solid forged
Type of steel	Carbon steel	5-in. inner shell-3% Cr 6-in. jacket-carbon moly	3% chrome
Maximum shell working stress, psi	17940	21460	25000
Ultimate tensile stress, psi	75000	90000	100000
Yield stress, psi	45000	50000	55000
Safety factor (based on ultimate tensile strength)	4	4	4
Vessel weight, lb	312000	285000	180000
Vessel price, dollars	79876	88350	62600
Price per lb, cents	25.6	31	34.8

The compound cylinder construction, similar to that used on large-caliber gun barrels, was considered an excellent and time-proved design for operation at high pressure. However, the close machining inherent in this method of fabrication, in addition to the $\frac{1}{2}$ in. heavier wall, resulted in the most expensive unit. This design required perforation of the pervious jacket and machining of grooves on the outer surface of the inner cylinder to permit the uniform release of the hydrogen, which diffuses through the alloy layer. These operations also contributed to the higher costs.

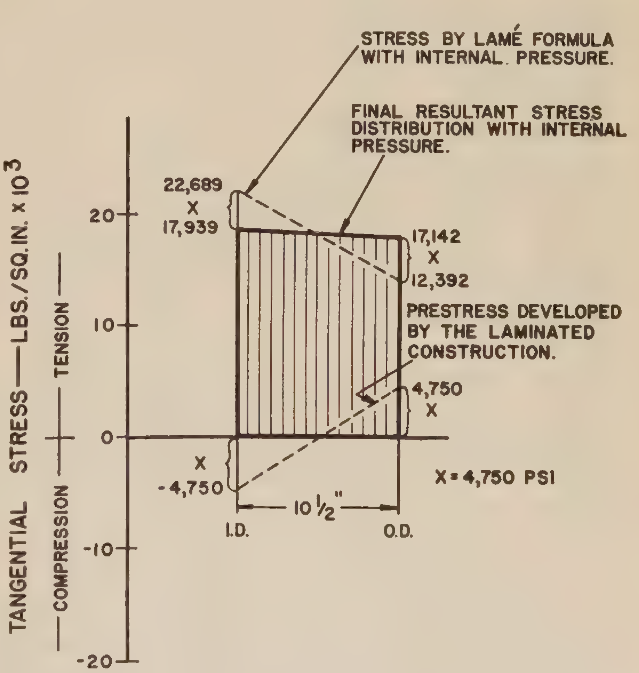

FIG. 1 Wall Stresses of Multilayer Construction

Referring again to Table 1, it is apparent that the solid-forged construction has the most points in its favor—it is lightest and lowest in cost; it combines the best physical and noncorrosive properties in one material.

---

[1] Mechanical Engineer, Coal-to-Oil Demonstration Branch, Office of Synthetic Liquid Fuels, Bureau of Mines, Louisiana, Mo.

[2] Special Engineer, Koppers Company, Inc., Louisiana, Mo.

[3] Assistant Chief, Coal-to-Oil Demonstration Branch, Office of Synthetic Liquid Fuels, Bureau of Mines, Louisiana, Mo.

Contributed by the Petroleum Division and presented at the Petroleum Mechanical Engineering Conference, Oklahoma City, Okla., October 2–5, 1949, of The American Society of Mechanical Engineers.

Note: Statements and opinions advanced in papers are to be understood as individual expressions of their authors and not those of the Society. Paper No. 49—PET-6

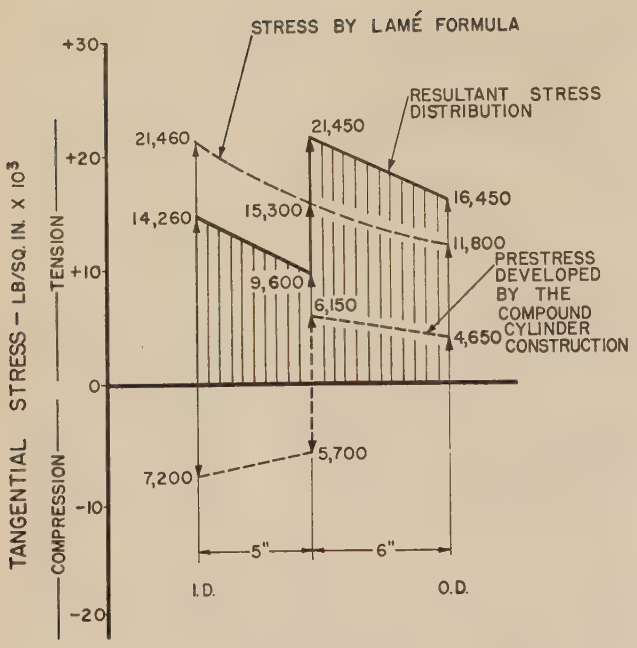

FIG. 2 WALL STRESSES OF COMPOUND CYLINDER

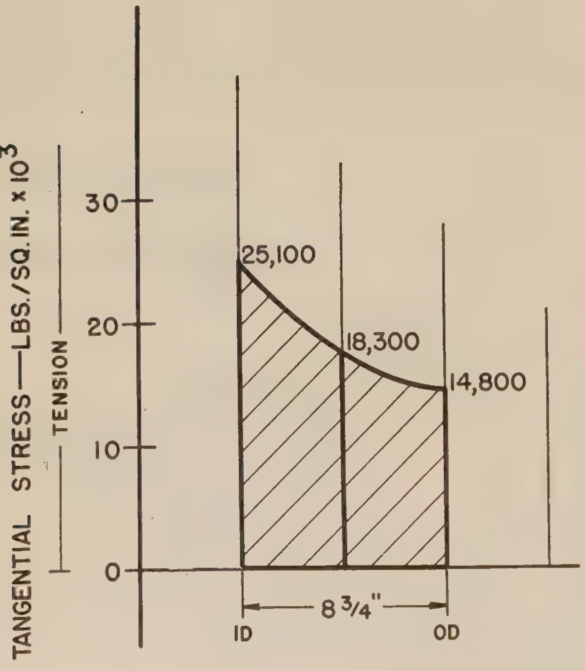

FIG. 3 WALL STRESSES OF SOLID FORGING

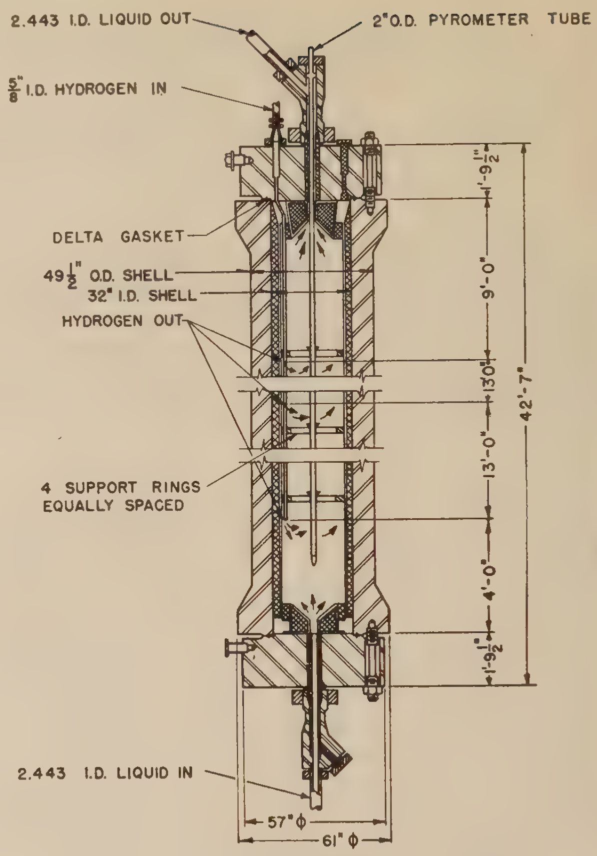

FIG. 4 LIQUID-PHASE CONVERTER ASSEMBLY

DEMONSTRATION-PLANT HIGH-PRESSURE VESSELS

The final design of these units furnished by the Midvale Company of Philadelphia, Pa., is as follows:

Liquid-Phase Converters. These vessels, shown in Fig. 4, are alloy-steel forgings, 32 in. ID × $49^1/_2$ in. OD × 39 ft $1^1/_2$ in. length, face to face of end flanges, with the ends flanged out to 61 in. OD. The heads are flat steel forgings, $21^1/_2$ in. thick × 57 in. diam, provided with the necessary openings for the entry of the coal paste and hydrogen, and the exit of the products of reaction. There are no openings in the converter shell. The shell steel has 3 per cent chrome with 0.65 per cent nickel, 0.30 per cent molybdenum, and 0.25 per cent carbon, an ultimate tensile strength of 100,000 psi, and an elastic limit of 55,000 psi.

Past experience has shown that a minimum of 3 per cent chromium is desirable to resist penetration of hydrogen and the corrosive effect of H_2S at 500 F and 10,000 psi. The other constituents are necessary for adequate strength in an $8^3/_4$-in-thick converter wall, where the thickness is based on working unit stress of one fourth of the ultimate tensile strength at the shell temperature as required by the API-ASME Code. All vessels were tested hydrostatically to $1^1/_2$ times the operating pressure.

The converter heads are subjected to more severe temperature conditions; consequently, it was decided to use a slightly higher content of the same alloying elements, with heat-treatment to provide approximately the same physical properties. The head steel is 4 to 6 per cent chrome with 1 to 1.25 per cent nickel, and 0.40 to 0.80 per cent molybdenum. The head studs, of which there are 12 in each head on a $45^1/_2$-in-diam bolt circle, are $5^3/_4$ in. diam, of SAE-4340, with an ultimate tensile strength of 120,000 psi and an elastic limit of 90,000 psi. The stud nuts are of SAE-4140, with an ultimate tensile strength of 100,000 psi and an elastic limit of 70,000 psi. The shell proper weighs about 80 tons, each head about $7^1/_2$ tons, and the assembled converter, with internals, about 105 tons.

In determining the required head thickness the problem was approached by assuming a head thickness of 18 in. and substituting this value in Roarks' formulas[4] for determining tension stresses in flat bolted cover plates

$$S_t = \frac{3w}{2\pi m t^2}\left[m + (m+1)L_n\frac{a}{r_0} - (m-1)\left(\frac{r_0}{2a}\right)^2\right]$$

---

[4] Roarks' Formulas for Stress and Strain, p. 188.

where

$a = 22.75 \text{ in.} = \dfrac{\text{bolt circle diameter}}{2}$

$r_0 = 16.625 \text{ in.} = \dfrac{\text{gasket contact diameter}}{2}$

w = 8,960,000 lb = total force on head from internal pressure
t = 18 in. head thickness
m = 3, reciprocal of Poisson's ratio

Then

$$S_t = \frac{3 \times 8{,}960{,}000}{2\pi \times 3 \times 324}\left[3 + 4\left(L_n \frac{22.75}{16.625}\right) - (3 - 1)\left(-\frac{16.625^2}{4 \times 22.75^2}\right)\right]$$

S_t = 17,500 psi (without holes)

This stress was then checked by using the API-ASME Code formula stipulated in paragraph W-316.

In an 18-in-thick head this gives a value of 19,500 psi (without holes).

The thickness was then analyzed, taking into consideration the weakening effect of the large centrally located hole in the head.

Using formula[5]

$$S_t = \frac{Wk_1}{t^2}$$

where

S_t = allowable tensile stress at outer edge of hole = 25,000 psi
W = total force from internal pressure = 8,960,000 lb
k_1 = 1.25 (derived from graph on ratio of bolt circle to gasket circle radii)

then t becomes 21.2 in.

It was decided to use a thickness of $21^1/_2$ in. owing to possible higher temperatures which might occur on heads, and to reduce the elastic strain which might result in undesirable gasket action.

The bolts were sized in the conventional manner, based on a working load of 8,960,000 lb, which resulted in a working stress for the twelve $5^3/_4$-in-diam studs of 30,500 psi, or about one third of the elastic limit.

The asbestos-cement lining for the converter shell is mixed in the proportion of 1:1:1 by volume of granulated asbestos, quick-setting Portland cement and water. The mixture is poured and tamped in sections in the annular space between the shell and the basket. The basket is stainless-steel, ASTM-A240-347, and has a reaction space of about 110 cu ft. This steel was chosen for its good hydrogen and corrosive-gas resistance at temperatures up to 1000 F. The basket is $25^1/_2$ in. ID with $^1/_4$-in-thick wall, perforated with $^5/_{16}$-in-diam holes on 3-in. centers for pressure equalization.

The heads of the converter are insulated on the inside with 12 in. of asbestos cement and are sealed to the flanged ends by annealed SAE-1020 steel gaskets. The self-sealing gasket shown in Fig. 5 is of triangular cross section. The 33.250-in-ID gasket fits into 0.35-in-deep grooves in head and shell flange. About 0.002-in. copper plating was added to the polished gasket faces which improved the seal considerably by eliminating the galling of contact surfaces during fluctuation in pressure. The initial seal is created on opposite tips of the gasket by the bolting force. The gasket becomes deformed after internal pressure is applied as shown by dotted lines in Fig. 5. Sealing actually takes place along faces marked a and b in the cross section. The soft-iron gasket is of small cross section and the internal pressure forces the entire gasket to expand in diameter when the pressure forces the bolted head away from the shell. At this writing it is still controversial how often a gasket can be re-used.

Temperature measurement within the converter is taken through a centrally located 40-ft-long, 2-in-OD, $^7/_8$-in-ID seamless-steel pyrometer tube. This tube, held in place by several steel spiders, has a closed bottom and is designed to withstand an external pressure of 10,300 psi at 1000 F. Inside the tube is a $^1/_8$-in. schedule-40 pipe of ASTM-A276-304 stainless steel, to which are attached six thermocouple elements on 6-ft centers. These elements transmit the temperatures at the various levels to a recording instrument located in the instrument house.

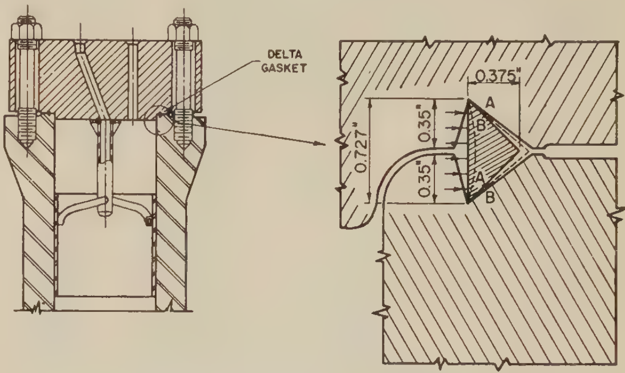

FIG. 5 DELTA GASKET ASSEMBLY

Vapor-Phase Converter. The vapor-phase converter, shown in Fig. 6, is identical with the liquid-phase converter in dimensions and composition of shell and heads. The inner insulation is also the same, except that the liner is $^1/_{16}$-in. perforated stainless steel. The insulation is recessed for the $^3/_8$-in. cooling hydrogen lines, so that the space inside of the insulation is unobstructed for the insertion and removal of the catalyst basket.

The removable catalyst basket, shown in detail in Fig. 6, is 24 in. ID, 36 ft $4^3/_4$ in. long, and made of $^3/_8$-in. ASTM-A240-347 stainless-steel plate. Both top and bottom ends are bell-shaped and bolted to the body of the basket. Pressure equalization between basket and shell is obtained by holes in the top bell. The catalyst space of about 100 cu ft in the basket is subdivided into six compartments by perforated grids covered by a wire screen to support the 10-mm-diam × 10-mm-long pelleted catalyst. The grids are so constructed that they also serve as a gas-distribution chamber for uniform distribution of the hydrogen supplied to the bottom of each grid by separate $^3/_8$-in. supply lines through the top head.

The pyrometer tube is similar to that in the liquid-phase converter, except that inside of the 2-in-OD pyrometer tube there is a $^3/_4$-in-diam solid rod which carries 12 thermoelements for measuring the temperature at two points in each of the six catalyst chambers. The pyrometer tube is enclosed in a shielding pipe, permitting removal of the tube without disturbing the catalyst. The shield is closed at the bottom and made of ASTM-A240-347, schedule-160 pipe.

Hot Catchpot. This vessel receives the products of reaction from the liquid-phase converters. The heavy oil is drawn off at the bottom, while gases and vapors leave through the top of the hot catchpot. The general construction and dimensions shown in Fig. 7, as well as the materials of construction, are the same as for

---

[5] "Stress and Deformation in Flat Circular Cylinder Heads," by Gilbert Dudley Fish, Trans. ASME, vol. 43, 1921, p. 615, No. 1805.

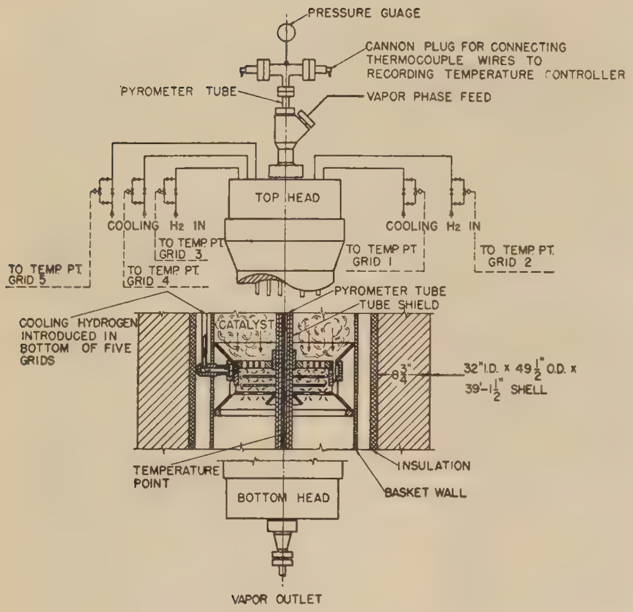

Fig. 6 Vapor-Phase Converter Internals

the liquid-phase converter, except that the shell is 25 ft $5^1/_2$ in. face to face of end flanges. The liquid inlet pipe extends downward through the top head a distance of 13 ft 6 in. The normal level of the liquid is about 5 ft above the bottom, while the liquid outlet pipe projects upward through the center of the bottom head to a height of 4 ft. To prevent settling of solids and coking at the bottom, a $^1/_2$-in. size perforated, schedule-40 pipe bent to a $23^1/_2$-in-diam ring is provided a few inches above the bottom for agitating and cooling the liquid with hydrogen.

Measuring and regulating the liquid level in the hot catchpot is a very important but troublesome operating function; and, in an attempt to make it foolproof, various methods were provided and are expected to work simultaneously. These methods are described in a companion paper on instrumentation.

The temperature of the hot-catchpot contents is observed by pyrometer readings. The pyrometer tube extends upward from the bottom about 2 ft above the normal liquid level. The thermoelements are spaced 12 in. on centers with at least two elements in the vapor space.

Cold Catchpots. Fig. 8 shows an assembly of these vessels. They are 24 in. ID, $37^3/_4$ in. OD, and 16 ft $11^3/_8$ in. inside length. They are flanged at the top to 47 in. OD and tapered at the bottom to a 2-in-diam liquid outlet. The top head is 45 in. OD, and $18^7/_8$ in. thick, and is provided with product inlet and gas outlet openings. The $2^1/_2$-in-diam product inlet pipe extends 2 ft below the head, where it is divided into two $1^1/_2$-in-diam pipes, terminating in $^3/_8$-in. × $1^7/_8$-in. rectangular outlets, discharging downward at 15 F, and tangentially along the inner surface of the shell. This arrangement will provide efficient separation of gases from liquids without foaming. At the elevation of the impinging stream, the vessel is lined with an interchangeable carbon-steel wear cylinder, 2 ft long × $^3/_8$-in. wall thickness. The shell analysis is 2.50 to 3.25 per cent nickel, 0.75 per cent chromium, and 0.30 to 0.40 per cent molybdenum, and has an ultimate tensile strength of 100,000 psi and an elastic limit of 55,000 psi. The heads are carbon steel, and the head studs, nuts, and gaskets are the same as for the converters and the hot catchpot.

Since the normal operating temperatures are low, 150 F for the liquid phase, and 80 F for the vapor phase, the cold catchpots are neither insulated nor lined on the inside. For the same reason,

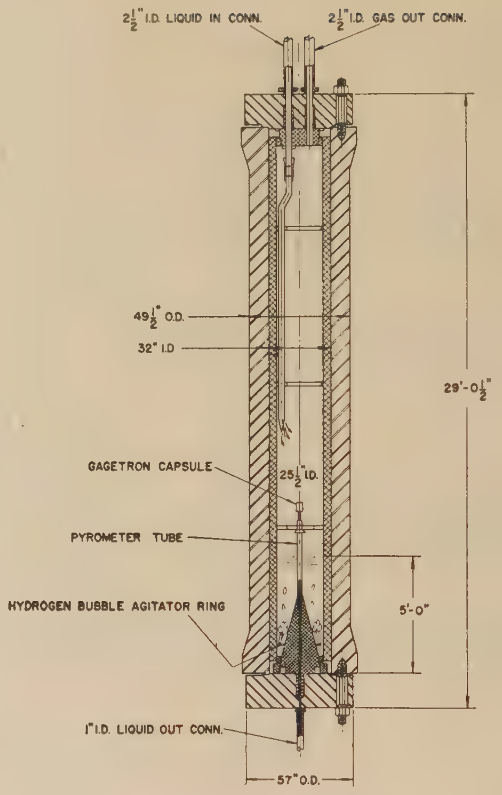

Fig. 7 Hot-Catchpot Assembly

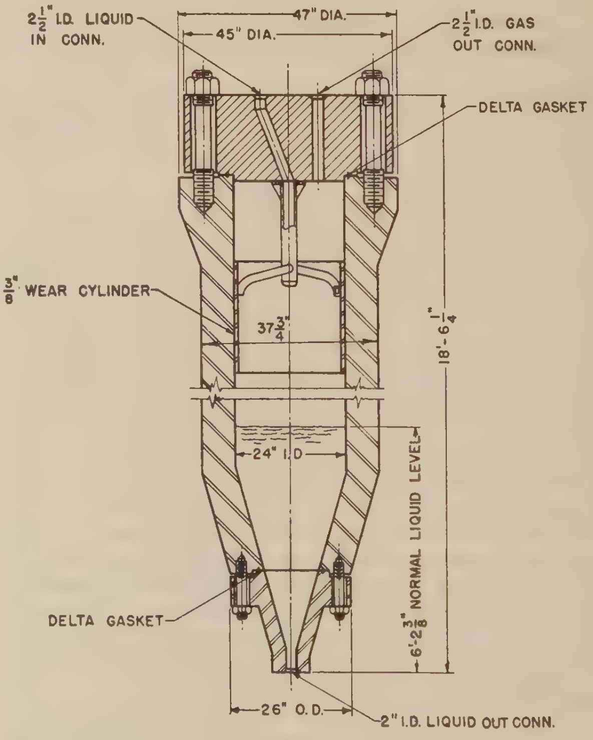

Fig. 8 Cold Catchpots and Compressor Suction Traps

the shell steel contains only enough alloy metals to meet the required physical properties. The normal liquid level in the cold catchpot is 7 ft $8^3/_8$ in. above the bottom outlet flange.

Compressor Suction Traps. These vessels, also shown in Fig. 8, are installed in the recycle gas-compressor suction lines from the cold catchpots, to trap the moisture from the gas before it reaches the compressors. They are identical with the cold catchpots.

Wash-Oil Scrubber. The wash-oil scrubber is installed in the liquid-phase recycle gas-suction line between the cold catchpot and the compressor suction trap. The purpose of the scrubber is to wash out the hydrocarbons and impurities from the gaseous products of hydrogenation in order to maintain the partial pressure of hydrogen in the recycle gas at a minimum of 80 per cent. The scrubber is packed with $1^1/_2$-in. × $1^1/_2$-in. steel Raschig rings.

The design conditions are similar to those for the cold catchpot, 10,300 psi at 120 F. In details of the shell, heads, and closures, materials of construction and general dimensions, the scrubber is identical with the cold catchpot, except that it is much longer, being 41 ft $7^1/_4$ in. over-all. Like the cold catchpot, it is tapered at the bottom from 24 in. ID in the body to a 2-in-diam bottom outlet. The wash-oil inlet pipe through the top head extends down 6 ft to a perforated-steel distribution plate, below which is a packing space 28 ft 8 in. deep. The steel Raschig-ring packing is supported by a steel grate 3 ft $2^3/_8$ in. above the bottom head flange. The gas-inlet pipe extends up from the bottom to a point just below the packing grate and is surmounted by a serrated bubble cap. The normal liquid level in the scrubber is 4 ft above the packing grate. The liquid level is indicated and controlled in the same manner as in the cold catchpot.

Stall Structure and Repair Pit

All high-pressure vessels are located within a heavy-walled reinforced-concrete structure 193 ft long, 28 ft wide, and 58 ft high, open on the top and rear. To minimize the danger of possible fires or explosions, the structure is divided into six stalls by 14-in. reinforced-concrete walls. A 130-ton gantry crane with a 70-ft lift and 60-ft span straddles the structure and facilitates handling of the heavy equipment. Fig. 9 shows the gantry crane carrying a converter to the stalls visible in the right background.

The two end compartments of the stalls house the preheaters. Next to the preheater are the hot stalls of each phase, containing the converters, high-temperature exchangers, and hot catchpot. In the center are the two cold stalls with the cold catchpots, coolers, and compressor suction traps. In a full-scale plant it is not considered necessary to enclose the cold vessels and preheaters. The experimental nature of the operation justified this extra precaution in the demonstration plant.

Adjacent to the stall area is a reinforced-concrete repair pit 35 ft deep. This pit facilitates the repair and cleaning of the large vessels by permitting vertical removal of internals.

New Developments in High-Pressure-Vessel Design

The demonstration-plant high-pressure vessels described were built in accordance with the established practice of forged construction. However, during the initial stages of plant design, consideration was given to layer-vessel design and to the spirally wound vessels (Wickelofen) still in the industrial development stage in Germany. The carbon-steel-plate layer vessels proved to be too heavy and expensive, while the spirally wound vessels were not available from American manufacturers.

Latest investigations indicate that the spirally wound vessels have excellent possibilities in future American full-scale operations. Therefore a detailed description of this method seems to be pertinent to this paper. The Germans developed this method of pressure-vessel construction shortly before the second world war as a modification to the layer vessel designed and constructed by the A. O. Smith Company of Milwaukee, Wis. Figs. 10, 11, and 12 help to visualize the spirally wound method of construction. The principle of design utilized by this method is the shrinkage of each successive layer of the wound strip upon the layer or core beneath. Shrinkage of the layers is achieved by continuously heating each strip electrically to between 1100 and 1550 F just before winding, followed by cooling to atmospheric temperature after it is pressed onto the underlying layer. The resultant predetermined contraction of the metal strip will set up circumferential prestressing necessary for minimum wall thickness. The intimate interlocking of the wound strips provides the necessary longitudinal strength.

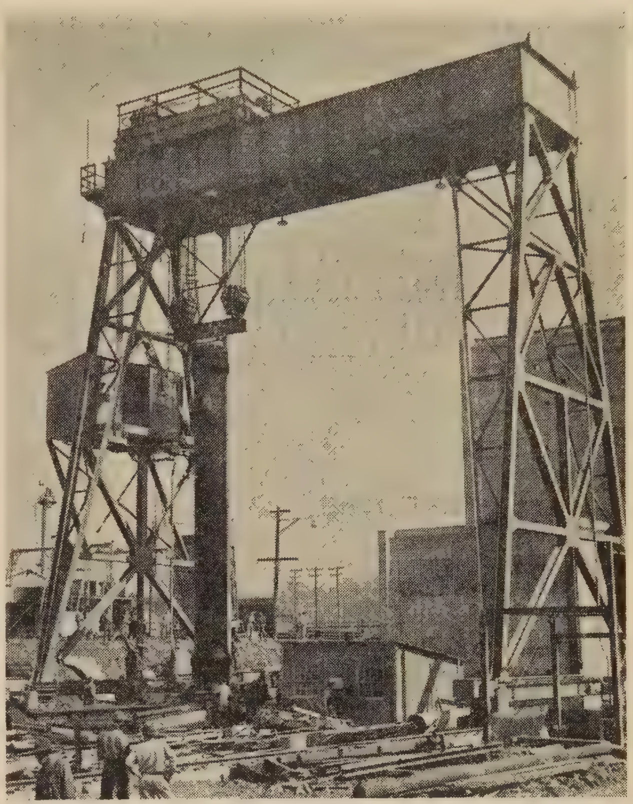
FIG. 9 PANORAMA OF STALL SHOWING GANTRY CRANE

The wound vessel is fabricated essentially as follows: The inner tube, which forms the core, may vary in thickness from $^7/_8$ in. for 30-in-ID to $1^1/_4$ in. for a 48-in-ID vessel. The inner tube must resist corrosion and hydrogen attack at high temperature and pressure. A 3 per cent chrome steel with 0.2 per cent C, 0.4 per cent Mn, 0.3 per cent Si, and 0.15 per cent V was normally used by the Germans for this purpose. A plate of commercial width is rolled to the desired diameter and butt-welded longitudinally. As many of these cylinders as are necessary for the desired length of the vessel are butt-welded together, and then stress-relieved. Dummy ends of plain carbon steel are welded to the ends of the inner tube. These dummy ends, to which the strip ends are welded, are later cut off when the vessel is finished.

The strip may vary in thickness from $^1/_4$ in. to $^3/_8$ in., and the width is usually about 10 times the thickness. It may be of plain carbon steel for the lower pressure and temperature ranges or low-alloy steel for higher temperatures and pressures, depending upon operating conditions or strength of material desired. As

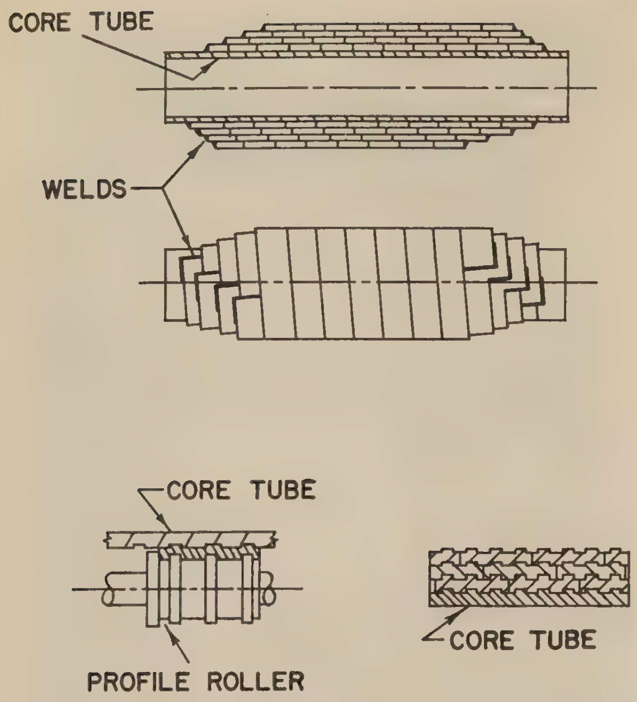

Fig. 10 Detail of Wickelofen Wrapping

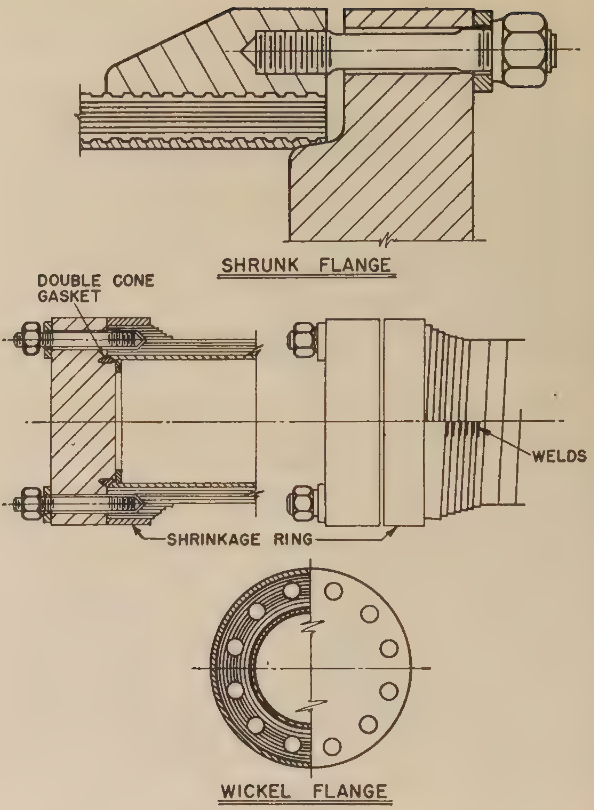

Fig. 11 Wickelofen Flanges

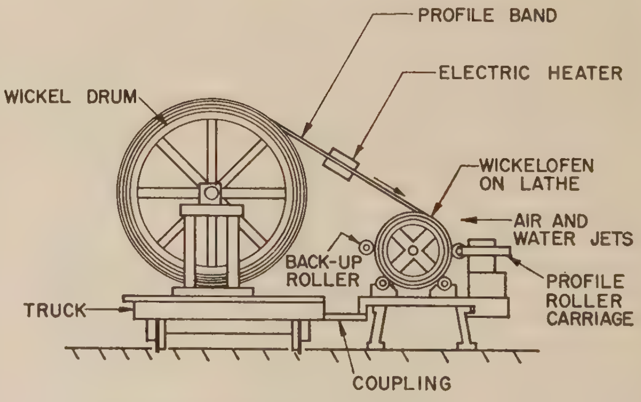

Fig. 12 Wickelofen Wrapping Lathe

shown in Fig. 10, the strip is rolled to a tongue-and-groove profile, preferably three or more grooves in width, so that the upper layer of strip can overlap by at least one third its width and still interlock amply for axial strength.

The wrapping lathe can be the same type used for machining solid wall vessels, Fig. 12. The tool carriage can be altered to run on a special track and accommodate a reel of strip, the strip heating and cooling equipment, and a profiled back-up roller. The strips, as received in mill lengths, are butt-welded end to end to a length required to wind a complete layer in one run.

The inner tube with its dummy ends is set on the lathe, and cooling water is turned on inside the tube. Spiral grooves are then cut into the outside face of the tube to match the tongues on the strip, at a pitch equal to the width of the strip, plus a slight clearance.

Before wrapping is started the end of the strip is welded to the dummy end of the inner tube at an angle corresponding to the pitch. The strip passes between guide rollers and is pressed against the vessel by two 6-in-diam profiled rollers diametrically opposite each other, to prevent distortion of the tube. The load on these rollers is about 1 ton. The guide rollers act as the connection for the electric current, which heats the strip as it unwinds from the reel onto the vessel. The power required to heat the strip to between 1100 and 1550 F is furnished at 30 to 40 volts and 4000 to 6000 amp.

After passing under the profiled roller, the strip is quenched by compressed-air jets and about five or six turns later by cold-water jets. The speed of wrapping is about 15 fpm.

After the first layer of strip is completely wrapped, the end is welded to the dummy end of the inner tube and the carriage returned to the other end of the lathe. The next strip is then welded to the first layer strip (see Fig. 10), so that it will overlap the joints of the underlying layer by one third of the width of the strip. The succeeding strips are then wrapped exactly like the first and second, until the required wall thickness is obtained.

To finish the ends of the vessel a flange is formed by the same wound method, a steel ring is shrunk over the strip ends, and the dummy inner-tube ends are cut off to the proper length Fig. 11. Instead of a wound flange of strips, a solid forged-steel flange may be screwed or shrunk on, if desired. Fig. 13 shows a German Wickelofen of the type described.[6]

Full-Scale Plant Converter. A layout has been made of a full-scale plant converter employing the spirally wound principle. A sectional sketch with the main dimensions and materials is shown in Fig. 14.

In order to take the best advantage of this type of construction, the wrapping strip steel should have a high yield strength. Also, the yield should not exceed 75 per cent, nor be less than 60

---

[6] For further particulars on the construction of the "Wickelofen" refer to "Engineering in Hydrogenation Plants in Germany," by J. F. Ellis, published by the British Intelligence Objectives Subcommittee, 32 Bryanston Square, London, W.I., or the office of Technical Services, U. S. Dept. of Commerce, Washington, D. C.

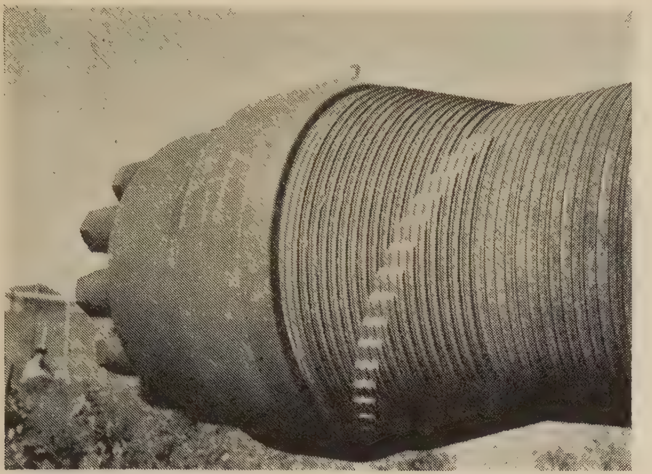

Fig. 13 Flanged End of Wickelofen

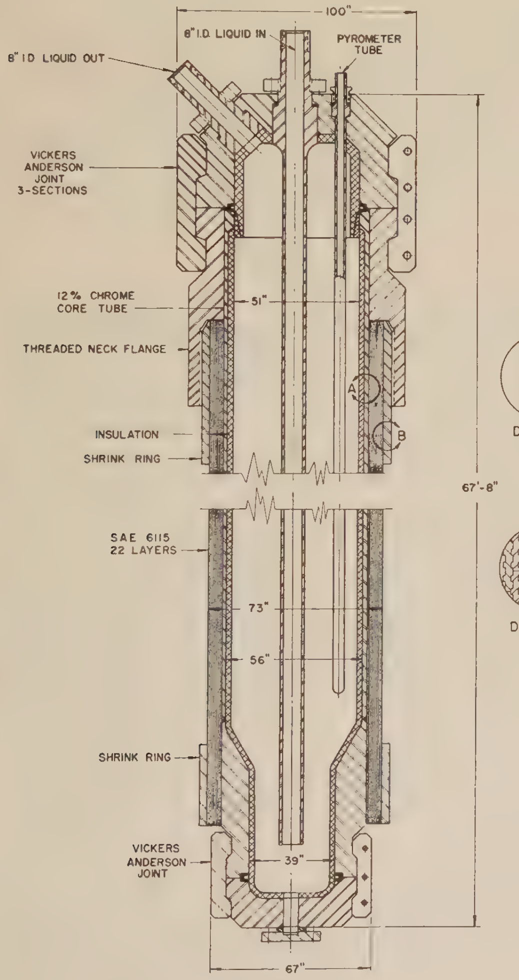

Fig. 14 Full-Scale Plant Converter

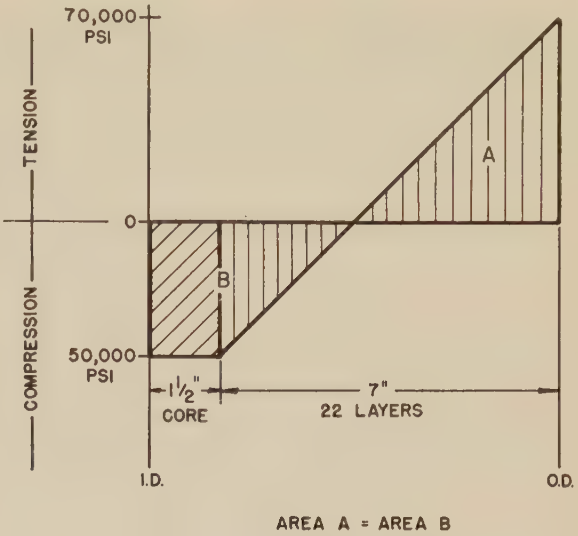

Fig. 15 Wall-Stress Diagram

per cent of the ultimate tensile strength. The elongation should not be lower than 17 per cent. It is believed that a low-chrome vanadium steel similar to SAE 6115 could be heat-treated in the wrapping procedure to secure the desired properties.

In designing the vessel shown in Fig. 15, a steel with 90,000 psi yield strength and about 130,000 psi ultimate tensile strength is used. In arriving at the wall thickness, the strip was stressed to 70,000 psi on the outside layer, resulting in compressive stress on the core tube of similar magnitude, Fig. 15. Twenty-two $^5/_{16}$-in. layers were required over a $1^1/_2$-in. inner tube. This resulted in an $8^1/_2$-in. wall for the specified 56-in-ID vessel, weighing only 316 tons.

Conclusions

Many improvements are still possible in high-pressure vessel fabrication, particularly for large diameters required in commercial-scale hydrogenation plants.

The spirally wound construction is especially promising. A brief summary of the advantages claimed follows:

1 Economy in corrosion and hydrogen-resistant material, since only the core tube needs these properties.

2 The thin strips permit treating and forging operations to penetrate the innermost crystals. Thus the safety factor required for nonhomogeneous solid walls can be reduced.

3 The method of construction gives higher stress distribution on the outside layers, causing these to stretch uniformly, and thereby permitting visual inspection of amount of growth.

4 Reduction of wall thickness from increased physical properties secured by controlled heating and cooling of strip.

5 Material lost in machining is only one sixth of that lost in forging solid-wall vessels.

6 Fewer operators are required, and the manufacturing time is reduced to one fifth of that required in forging.

7 Wound vessels can be made at the plant-site shop, thus simplifying handling and transportation problems.

8 The size of vessels is limited only by the capacity of crane handling equipment in the field.

High-Pressure (10,300 Psi) Piping, Flanged Joints, Fittings, and Valves for Coal-Hydrogenation Service

By J. H. Sandaker,[1] J. A. Markovits,[2] and K. B. Bredtschneider[3]

The high-pressure piping components used in the coal-hydrogenation process are described briefly. Some factors considered in design are given. In addition, a short discourse on future design for commercial-scale plants is included.

Introduction

The coal-hydrogenation demonstration plant required large quantities of 10,300-psi piping, flanged joints, fittings, and valves of various types. Service conditions introduce unique problems which have to be considered in the design of these elements. Some of these problems are touched upon briefly and resulting designs are described.

At this time it appears probable that most piping in future coal-hydrogenation plants would be made lighter by the use of higher-strength steels. However, the other piping components are unlikely to be changed radically in design.

Piping

Design and standardization of the 10,300-psi-working-pressure piping presented numerous problems. In selecting materials and determining wall thicknesses, consideration had to be given to process-flow requirements, prevailing pipe-manufacturing practices, permissible stresses, including creep stress at high temperature, and the effect of corrosion, erosion, and hydrogen attack. In addition, however, it early became apparent that large unit weights were involved; so that it became imperative to design for minimum weight consistent with safety and reliability.

It was realized that the many theories available to explain the failure of thick-walled cylinders from excessive internal pressure gave widely different results at the 10,000-psi design level. The maximum principal-stress theory, in which the tangential stress alone is considered to be the criterion for failure, proved to be the most suitable choice. The ASA code for pressure piping adopts this theory, and in paragraph 122b

$$tm = \frac{D}{2}\left(1 - \sqrt{\frac{S-P}{S+P}}\right) + C \ldots\ldots\ldots\ldots [1]$$

where

tm = minimum pipe-wall thickness in inches, excluding manufacturing tolerances,
P = maximum internal service pressure, psig
D = outside diameter, in.
S = allowable stress in material due to internal pressure, at the operating temperature, psi
C = allowance for threading and corrosion, in.

A study of Equation [1] reveals how wall thickness varies with allowable stress. By dropping the constant C and rearranging the equation, it becomes

$$\frac{D}{d} = \sqrt{\frac{S+P}{S-P}}$$

where D/d = theoretical ratio of outside diameter to inside diameter. Plotting D/d against allowable stress for the internal pressure of 10,300 psi, the graph shown in Fig. 1 is obtained. Several significant facts are evident from this curve. As the allowable stress approaches 10,300 psi, the D/d ratio approaches infinity. It is also apparent that at relatively low stress values, small increments cause large decreases in D/d ratio. The rate of decrease diminishes as the allowable stress increases.

Calculated data in Table 1 show an interesting comparison of

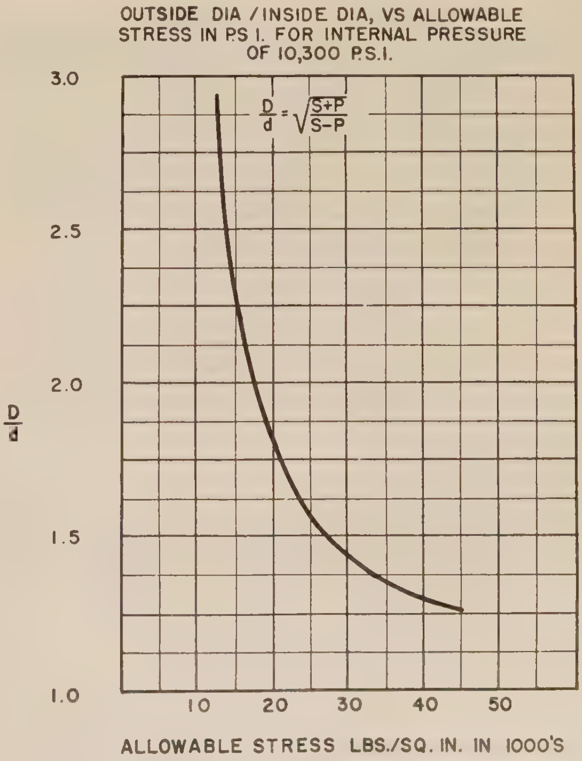

Fig. 1 Graph of Pipe Stress Versus OD/ID Ratio

---

[1] Mechanical Engineer, Coal-to-Oil Demonstration Branch, Office of Synthetic Liquid Fuels, Bureau of Mines, Louisiana, Mo.

[2] Assistant Chief, Coal-to-Oil Demonstration Branch, Office of Synthetic Liquid Fuels, Bureau of Mines.

[3] Special Engineer, Koppers Company, Inc., Louisiana, Mo.

Contributed by the Petroleum Division and presented at the Petroleum Mechanical Engineering Conference, Oklahoma City, Okla., October 2–5, 1949, of The American Society of Mechanical Engineers.

Note: Statements and opinions advanced in papers are to be understood as individual expressions of their authors and not those of the Society. Paper No. 49—PET-2.

wall thicknesses and unit weights for $2^1/_2$-in-ID pipe, both with and without manufacturing tolerances, using ASTM-A-106, grade B carbon steel for which the ASA Code for Pressure Piping stipulates an allowable stress of 18,000 psi at 375 F, and alternately API 5L, grade C for which a stress of 22,900 psi is allowed at the same temperature.

TABLE 1 CALCULATED WALL THICKNESS FOR $2^1/_2$-IN-ID 10,300-PSI PIPE

Material	Wall thickness excluding mfg. tolerances, in.	Weight lb per ft	Wall thickness including mfg. tolerances, in.	Weight lb per ft
ASTM A-106, grade B	1.25	57	1.875	88
API 5L, grade C.....	0.95	34	1.169	45

It is clear from the data that there was a distinct advantage in using API 5L for low-temperature service. Another notable fact is that manufacturing tolerances had a big influence in the final weight of the pipe. This was a factor which at the time had to be accepted as a necessary evil. Fig. 2 lists final pipe dimensions arrived at with manufacturing tolerances for seamless piping which was to be finished by hot-rolling. After completion of some tubes, manufacturing difficulty necessitated a change to cold-drawing, so that there is some slight deviation from dimensions and tolerances listed.

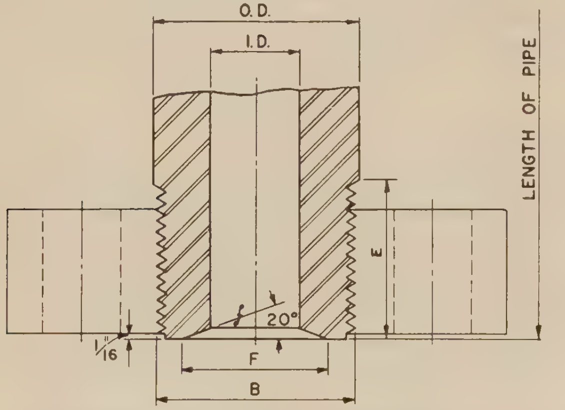

DIMENSIONS						ALLOWABLE TOLERANCE	
NOM. SIZE	O.D.	I.D.	B	E	F	ON O.D.	ON WALL THICKNESS
3/8"	1 1/32"	0.357"	1"	1 1/4"	0.75"	−1/32" +1/64"	± 15%
5/8"	1 17/32"	0.637"	1 1/2"	1 3/8"	1.125"	−1/32" +1/64"	± 12 1/2 %
1"	2 9/32"	1.039"	2 1/4"	1 3/4"	1.75"	± 1/32"	± 12 1/2 %
1 1/2"	3 1/32"	1.461"	3"	2 1/4"	2.35"	± 1/32"	± 12 1/2 %
2"	4 1/32"	2.021"	4"	2 7/8"	3.125"	± 1/32"	± 12 1/2 %
2 1/2"	4 25/32"	2.443"	4 3/4"	3 1/2"	3.75"	+1/32" −3/64"	± 12 1/2 %

NOTES: THREADS AMERICAN NATIONAL 8 THREADS PER INCH, CLASS 2 FIT.
SMOOTH MACHINE SURFACE MARKED ∫
TO BE USED ON ALL H.P. PIPING SPECS.

FIG. 2 PIPE STANDARDS

Fig. 3 shows on the left a Croloy 9M tube obtained by hot-finishing. Note the squareness of the inside circumference. On the right is a well-shaped cold-drawn tube.

Following German precedent, materials for piping were divided into four different classes based upon service, as follows:

(*a*) Low temperature, up to 375 F.

(*b*) Medium temperature, 376 F to 850 F.

(*c*) High temperature, 851 F to 1000 F.

(*d*) Miscellaneous applications in which $^3/_{16}$-in-ID × $^9/_{16}$-in-OD type 304 stainless steel or $^1/_{16}$-in-ID × $^1/_4$-in-OD, chrome-molybdenum steel tubing was used.

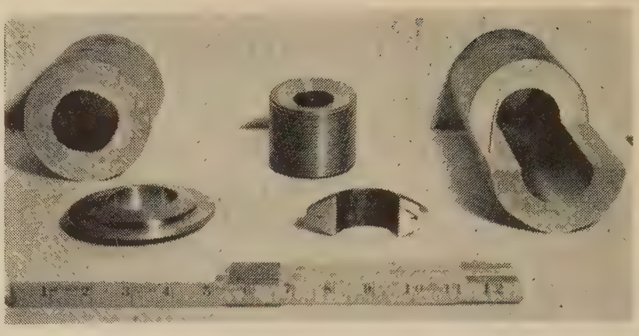

FIG. 3 PIPING AND GASKET SECTIONS

About the latter, used for instrument pressure leads, flushing-oil injection, nitrogen injection, hydrogen injection, and sampling lines, little need be said, since this type of tubing is regularly manufactured and can be obtained easily from suppliers.

The materials with their properties for the first three classes are listed in Table 2.

TABLE 2 HIGH-PRESSURE (10,300-PSI) PIPING MATERIALS

Maximum service temperature, deg F	Material	Yield point, psi	Ult. tens. strength, psi	Bhn
Low temperature:				
0 to 375 (early design)	B & W MT-1040 equal to API-5L, grade C	45000 min	75000 min	159 min
0 to 375 (later design)	SAE 4130	45000 min	75000 min	180
Medium temperature:				
376 to 850	Croloy 9M (Ref. B & W Tech. Bul. 6-D p. 49) HT-31,387 normalized and drawn at 1200 F	82000 min	103100 min	223
High temperature 851 to 1000	AISI Type 316	30000	75000	max attainable

NOTE: Creep stress for 1 per cent elongation in 10,000 hr is about 22,800 psi.

The change in the low-temperature class to SAE 4130, a low-chromium-molybdenum steel, was made during construction of the plant, primarily for improved weldability.

The dimensions given in Fig. 2 are the same for all materials, for the sake of standardization of tubing, fittings, etc. The dimensions were based on the properties of API 5L, grade C, carbon-steel seamless tubing for which, as has been noted, the allowable stress is 22,900 psi at 375 F. It would appear that a higher design stress could have been used for Croloy 9M; however, at the time it was selected, not enough was known about its behavior at temperatures near 850 F to warrant taking full advantage of its strength. In addition, such procedure would have minimized standardization. It will be noted that the dimensions chosen bring the design stress up close to the creep stress for type 316 Babcock & Wilcox 16-13-3. It was considered more desirable to design on this basis than to exceed the OD/ID ratio of 2, which was about the maximum according to German experience. Thicker walls could be expected to give trouble due to greater likelihood of internal faults and to increased temperature stresses. Temperature changes especially would have a particularly detrimental effect on stainless steel with its high coefficient of expansion and low thermal conductivity. For this reason Croloy 9M, which has better thermal-shock properties, was used in emergency let-down lines where temperature could be momentarily over 1000 F and vary widely.

FLANGED JOINTS

In a good high-pressure flanged connection, the following features are desirable:

1 Tightness must be maintained in spite of pressure and temperature fluctuations and of usual piping stresses imposed by torsion, bending, and vibration.

2 Functioning should not be affected by minor pipe misalignments in construction or by slight surface imperfections either on gaskets or faces.

3 Since it is desirable to keep the weight of the joint low, tightness should be achieved with low bolt loads. The following contribute to this end:

(*a*) A gasket pressure area as near the inside circumference of the pipe as possible.

(*b*) A design which provides high unit pressures on the gasket seat with relatively low bolt loads.

(*c*) At least a partial self-sealing at operating pressure.

4 A sufficient number of bolts should be provided so that failure of one during tightening will not cause the joint to fail completely.

With these considerations in mind, a study was made of several types of flanged joints. Fortunately, data on the lens ring joint used in Germany were available for comparison with conventional types. This was finally chosen as the one having most of the desirable characteristics. Fig. 4 illustrates an assembled connection of this type for low-temperature lines. For comparison, a Bureau of Mines pipe, flange, and lens ring was shown mated with the closest-size German pipe and flange.

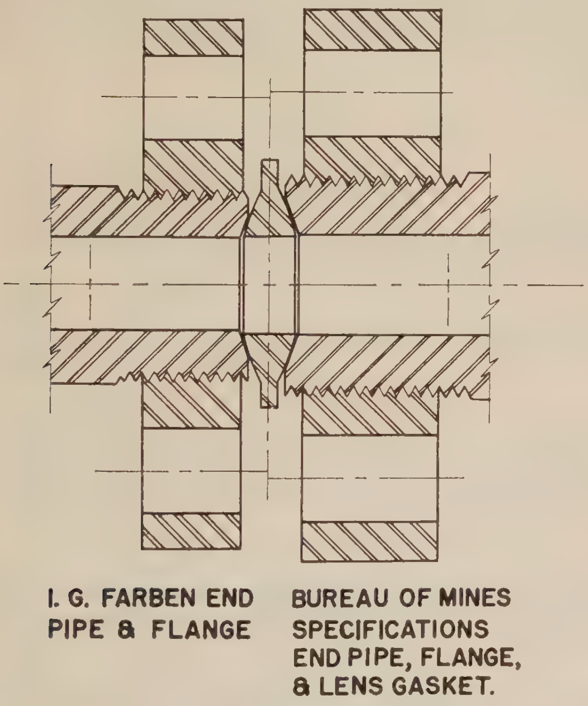

Fig. 4 Flanged-Joint Assembly

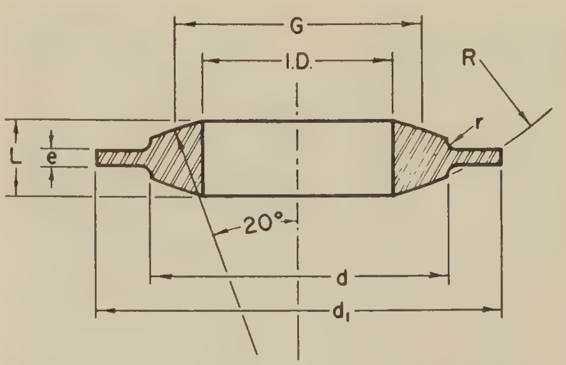

NOM SIZE	INSIDE DIA						SPHER RAD	CONTACT CIRCLE
	I D	d	d_1	L	r	e	R	G
3/8"	357"	13/16"	–	11/32"	–	–	13/16"	556"
5/8"	637	1-5/16	–	3/8"	–	–	1-11/32	.921
1"	1039"	1.75	2-1/2	17/32"	1/32	5/32	2-1/8"	1 455"
1-1/2"	1461	2 35	3-1/4	5/8"	1/32	9/64	2-15/16	2 009"
2"	2021"	3125	4-1/4	13/16"	1/16	3/16	4"	2.735
2-1/2"	2.443"	3 75	5"	31/32"	1/16	1/4"	4-13/16	3.284
5-1/2"	5.500	7-3/8	10"	2"	1/16	1-1/16	9 548	6.531"

Fig. 5 Solid-Lens Gasket Standards

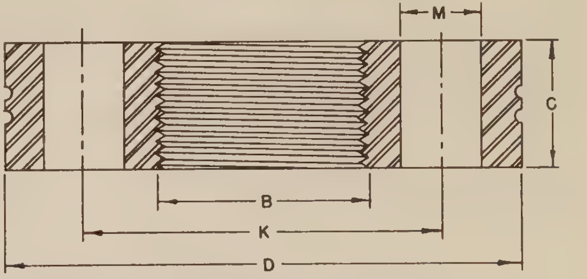

MACHINE ONE 1/16" RAD. IDENTIFICATION GROOVE
ON MEDIUM TEMPERATURE FLANGES
MACHINE TWO 1/16" RAD. IDENTIFICATION GROOVES
ON HIGH TEMPERATURE FLANGES

FLANGE DIMENSIONS				DRILLING		
NOM. SIZE	B	C	D	K	M	NO. HOLES
3/8"	1"	7/8"	3 15/16"	2 7/16"	11/16"	3
5/8"	1 1/2"	1"	4 7/16"	2 15/16"	11/16"	3
1"	2 1/4"	1 3/8"	5 9/16"	3 7/8"	7/8"	4
1 1/2"	3"	1 7/8"	6 3/4"	4 13/16"	1"	6
2"	4"	2 1/2"	8 5/8"	6 1/4"	1 1/4"	6
2 1/2"	4 3/4"	3 1/8"	10 3/16"	7 7/16"	1 1/2"	6

NOTE – TO BE USED ON ALL H.P. PIPING SPECS.

GENERAL NOTES

THREADS AMERICAN NATIONAL 8 THDS. PER INCH
CLASS 2 FIT HOLES TO BE EQUALLY SPACED AND
DRILLED ROUGH MACHINE ALL OVER

Fig. 6 Flange Standards

Fig. 5 shows the shape and dimensions of low-temperature service lens-ring gaskets, and Fig. 6 shows the dimensions of flanges used. It should be noted that a spherical gasket surface is in contact with conical surfaces on the pipe ends. It is characteristic of a metal-to-metal ball-and-cone joint that, with small bolt load, the contact area is extremely small, though very high gasket unit seating pressures are achieved. The gasket is softer than the pipe and its action under load is both plastic and elastic. Plastic deformation takes place over an almost imperceptible area and seals off against minor imperfections in machined surfaces. The greatest part of the deformation is elastic and occurs both radially and axially. Both the initial elastic deformation set up before pressure application and the internal pressure itself provide the self-sealing effect under operating conditions.

The ball-and-cone shapes allow the lens to find a seating position in spite of minor pipe misalignments. Though surface finish was specified to be very fine, it has been found that minor scratches and toolmarks do not cause leakage.

In spite of careful piping design, expansion stresses in high-temperature lines tend often to place added bending and torsion

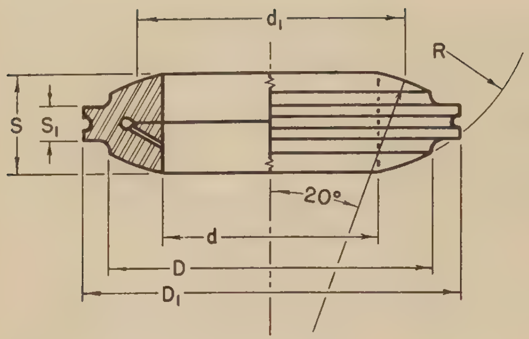

NOM. SIZE	I.D. d	O.D. D_1	CONTACT ϕ d_1	D	WIDTH S	S_1	SPHER. RAD. R	DIA. OF 20° C. SK. ON PIPE
1"	1.039"	2.04"	1.27"	1.69"	19/32	5/32	1.85"	1.75"
1-1/2	1.461"	2.75"	1.812"	2.35"	11/16"	3/16"	2.65"	2.35"
2"	2.021"	3-1/2	2.43"	3"	27/32	5/16"	3.54"	3.125"
2-1/2	2.443	4-1/4	3"	3-5/8	1-1/8"	3/8"	4-7/16	3.75"
5-1/2	5-1/2	8.82	6.5"	7.67"	2"	5/8"	9.55"	7.375"

Fig. 7 Bellows-Gasket Standards

in the flanged connections. For this reason a bellows lens as illustrated in Fig. 7, is used in medium and high-temperature lines. This type of lens ring has still greater self-sealing effect because fluid under pressure enters the annular space in the lens and acts over a greater area. Should the bending moments tend to open mating flanges, the bellows lens tends to open and to follow the seating surfaces on the pipe.

Flanging materials and their physical properties are given in Table 3.

TABLE 3 MATERIALS—HIGH-PRESSURE (10,300-PSI) FLANGED JOINTS

	Material	Yield point, psi	Ult. tens. strength psi	Bhn
	Low Temperature 0–375 F			
Flanges	Carbon steel ASTM-A-105, grade II	36000	70000	136 min
Lens-ring gaskets	Carbon steel ASTM-A-105, grade I	30000	60000	116 min 140 max
Bolts	ASTM-A-193-44, grade B-7 (SAE 4140) min draw temp. 1100 F	105000	125000	
Nuts	ASTM-A-194-40, class 2-h heavy series.			
	Medium Temperature 376–850 F			
Flanges (on tubing)	Carbon-moly ASTM-A-182-44 grade F-1	45000	70000	150 min
Flanges (on fittings and valves)	Alloy steel AISI type 304 ASTM-A-182, grade F-8	30000	75000	200 max
Lens-ring gaskets	AISI 405 chrome steel annealed	40900	64160	120 min 130 max
Bolts	Same as for low-temperature service			
Nuts	Same as for low-temperature service			
	High-Temperature 851–1000 F			
Flanges	Alloy steel AISI type 304 ASTM-A-182-44 type F-8	30000	75000	200 max
Lens-ring gaskets	AISI type 405 chrome steel annealed	40900	64160	120 min 130 max
Bolts	Same as for low-temperature service			
Nuts	Same as for low-temperature service			

The materials from which lens rings are made have in each application a Brinell number about 30-40 points below the piping materials. This follows German practice and is for the purpose of restricting plastic deformation to the lens rings, which are the elements most easily replaced. Flanges are made of materials different from tubing to avoid galling of threads.

Some idea of the weight reduction achieved by use of the 10,300-psi lens-type joint can be obtained by comparing the weights of a flange for the $2^{1}/_{2}$-in. nominal-size pipe with the weight of an ASA-2500-lb screwed flange for the same pipe size. Each weighs about 50 lb.

Results of a test[4] conducted in Germany on a 325-atm (4780-psi) working-pressure joint of this type for a pipe with an inside diameter of 4.73 in. are available. It was found that an initial total bolt load of 75,000 lb was increased to 99,000 lb by application of the design internal pressure corresponding to a total fluid force of 94,500 lb. The joint remained tight, and internal pressure had to be increased to 780 atm before signs of leakage appeared. Obviously, self-sealing took place. It is interesting to note that, at design pressure, the total bolt load exceeded the total fluid load by less than 10 per cent. Conclusions of the test report indicated that, for the joint under test, a bolt load between 1.8 and 2.5 times the total fluid load should be used in practice. The lower limit was set to avoid leakage when normal piping forces are applied, and the upper limit to avoid overstrain of bolts in service.

Lens-ring joints are used throughout except for instrument lines. These have conventional cinch joints.

Fittings

Fittings are limited to tees, 90-deg ells, and reducers, and all are forged and bored. Ells are made by bending straight forged and bored pieces. Table 4 gives materials and their physical properties.

TABLE 4 MATERIAL FOR FITTINGS

Service	Material	Ult. tensile strengh, psi	Yield point, psi	Bhn
Low temperature 0 to 375 F	SAE 1030	75000	45000	163 min
Medium temperature 376 to 850 F	Type 304 18-8 stainless steel ASTM-A-182 grade F-8	75000	30000	max attainable
High temperature 851 to 1000 F	Type 316 stainless steel ASTM-A-182-44	75000	30000	max attainable

Details and dimensions of all flanged-type tees are given in Fig. 8. Fig. 9 illustrates welding-type ells. Fig. 10 shows a typical $2^{1}/_{2}$-in. high-pressure line with flanges and fittings.

Valves

In general, shutoff, throttling, check, and relief valves are used. All bodies are forged steel. Table 5 shows materials and physical properties.

TABLE 5 MATERIALS FOR HIGH-PRESSURE (10,300-PSI) VALVE BODIES

Service	Material	Ult tens strength, psi	Yield point, psi	Bhn
Low temperature 0 to 375 F	Carbon steel SAE-1030	75000	45000	163 min
Medium temperature 376 to 850 F and high temperature 851 to 1000 F	Alloy steel AISI type 316 ASTM-A-182-44 type F-8m	75000	30000	190 max

---

[4] Report on the "Deformation of 120-Mm Sealing Rings of N5 Material Due to Internal Pressure and With Very Tightly Drawn Bolts," dated Ludwigshafen, July 12, 1936. Frames 6722-6728, inclusive of TOM Reel No. 181.

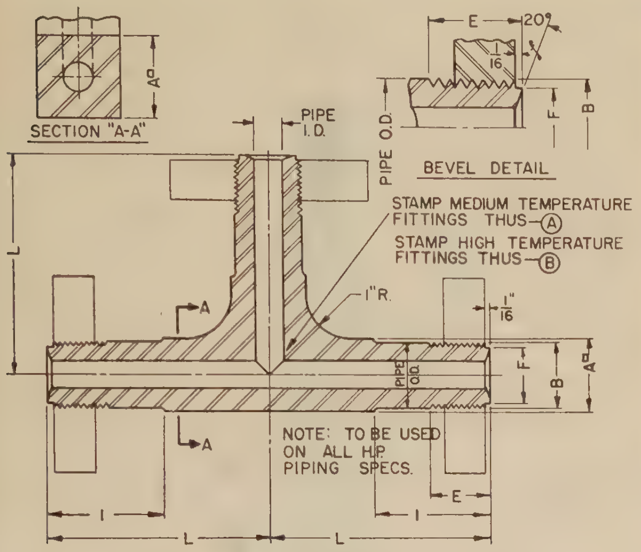

STAMP MEDIUM TEMPERATURE FITTINGS THUS—Ⓐ

STAMP HIGH TEMPERATURE FITTINGS THUS—Ⓑ

NOTE: TO BE USED ON ALL HP PIPING SPECS.

PIPE			TEE					
NOM. SIZE	I. D.	O. D.	L	I	A□	B	E	F
3/8"	0.357"	1 1/32"	4 5/8"	2 1/2"	1 1/8"	1"	1 1/4"	0.75"
5/8"	0.637"	1 17/32"	5"	2 5/8"	1 5/8	1 1/2	1 3/8"	1.125"
1"	1.039"	2 9/32"	6 3/8"	3 5/16"	2 7/16"	2 1/4"	1 3/4"	1.75"
1 1/2"	1.461"	3 1/32"	7 3/4"	4 1/16"	3 3/16"	3"	2 1/4"	2.35"
2"	2.021"	4 1/32"	9 3/4"	5 1/4"	4 1/4"	4"	2 7/8"	3.125"
2 1/2"	2.443"	4 25/32"	11 3/4"	6 7/16"	5"	4 3/4"	3 1/2"	3.75"

NOTES: THREADS AMERICAN NATIONAL 8 THDS. PER INCH. CLASS 2 FIT
SMOOTH MACHINE SURFACE MARKED ✓
A□ – THIS DIMENSION DESIGNATES SQUARE BODY

Fig. 8 Flanged Tee

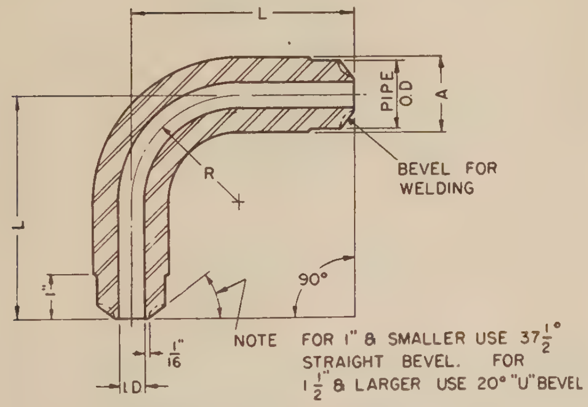

NOTE FOR 1" & SMALLER USE $37\frac{1}{2}$° STRAIGHT BEVEL. FOR $1\frac{1}{2}$" & LARGER USE 20° "U" BEVEL

PIPE			ELBOW		
NOM SIZE	I D	O D	A	L	R
3/8"	0.357"	1 1/32"	1 1/8"	4 5/8"	2 1/4"
5/8"	0 637"	1 17/32"	1 5/8"	5"	2 3/8"
1"	1 039"	2 9/32"	2 7/16"	6 3/8"	3 1/4"
1 1/2"	1 461"	3 1/32"	3 3/16"	7 3/4"	3 7/8"
2"	2 021"	4 1/32"	4 1/4"	9 3/4"	4 3/4"
2 1/2"	2 443"	4 25/32"	5"	11 3/4"	5 5/8"

NOTE TO BE USED ON H P PIPING SPEC. "AA" & "DD" ONLY

Fig. 9 Welding Ell of 90 Deg

All valves are angle type, except for a few vertical-lift check valves, which are straight-through type. The smaller sizes of shutoff and throttling valves are direct handwheel-operated and have screwed packing-gland nuts, while larger sizes, $1^1/_2$ in. and above, have bolted flanged packing glands, and are spur-gear- and handwheel-operated. Valves are so arranged that the pressure will be above the disk when closed.

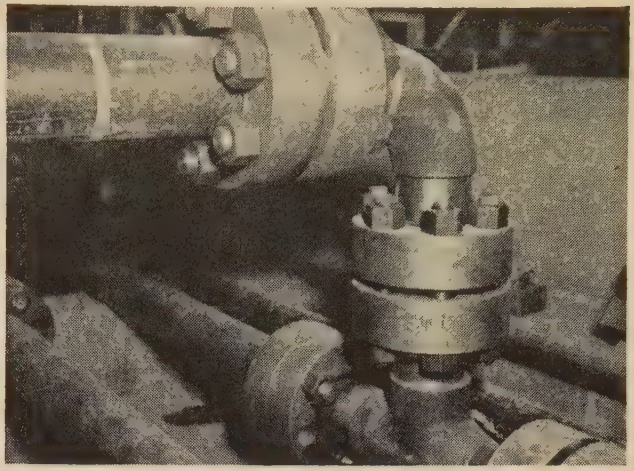

Fig. 10 Flanged Ell and Tee Assembly

High-pressure drops during opening and closing, even for mild service, are likely to cause severe erosion of disk and seat materials, unless proper precautions are taken in design. For this reason seat and disk are stellite for shutoff valves and kennametal for throttling valves. Because of the brittleness of kennametal, throttling valves cannot be used for shutoff. Provision must be made to avoid tight seating. This has been done either by providing a spring between spindle and removable disk, or by use of stop nuts on the valve spindle to limit the travel. In addition, throttling and shutoff valves must be paired and valve operations arranged so that all throttling is placed on throttling valves, while only shutoff valves are depended upon for tight shutoff.

Seat rings or bonnet closures for all valves are of the self-sealing type. This keeps down the weight of the valve and facilitates disassembly for replacement of valve internals. Valve packing, where used, is seven-ring type-220 durametallic with nitralloy base ring and gland.

Fig. 11 shows a section of a typical shutoff valve. In Fig. 12 a gear-operated 2-in. shutoff valve is compared with a 2-in. 150-psi screwed valve.

Throttling valves fall into two classes, depending upon whether service is severe or mild. Severe throttling valves are used where pressure drop would be from 10,300 psi down to about atmospheric pressure and the fluid is a mixture of liquids, gases, and solids consisting of unreacted coal, ash, and catalyst. Fig. 13 illustrates the valve used for such service. Velocities in the nozzle reach 700 to 800 fps. German experience with a similar valve indicated that a maximum service life with the best seat and disk materials available would be about 1 month. Design, therefore, had to be carried out with the object of attaining longest possible service life and of providing for the quickest and safest possible replacement of either valves or their worn elements. To minimize abrasion of the disk the valve was so designed that, with normal flow conditions, it would be fully open and all of the throttling would occur in the nozzle itself. Further, the nozzle was made with a divergent exit of 7 deg in order to prevent cavitation.

The stream leaving the nozzle enters an expansion chamber and impinges against a "target plate" made integral with the lens ring of the flanged joint on the outlet side of the valve. Flow through the plate is by means of a hole drilled eccentrically to the face which has a concave surface of stellite. The purpose of the expansion chamber and target plate is to provide for the dissipation of the energy of depressuring before entry of the fluid into the piping.

To permit rapid replacement of valve seat and disk, the con-

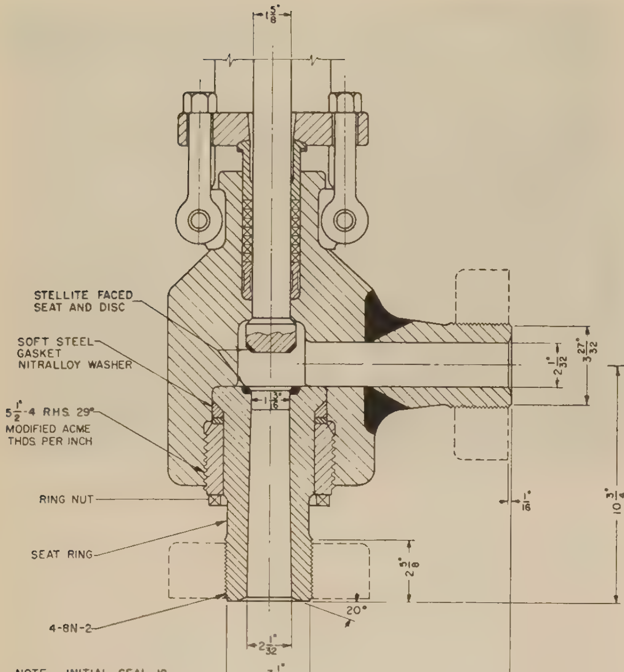

NOTE. INITIAL SEAL IS CREATED BY TIGHTENING RING NUT. INTERNAL PRESSURE ON HEAD OF SEAT RING MAINTAINS THE SEAL

Fig. 11 Shutoff-Valve Assembly

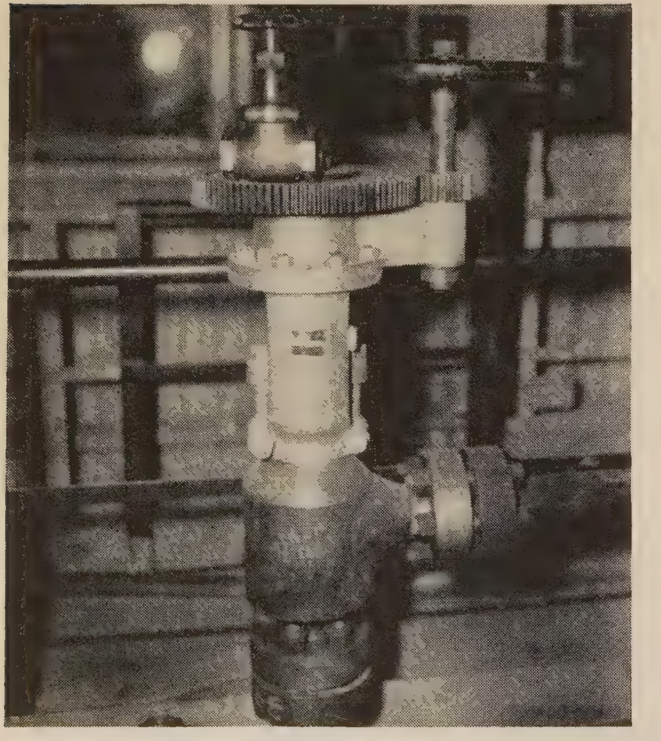

Fig. 12 2-In. Shutoff-Valve Compared With 2-In. 150-Psi Valve

struction is such that disassembly and removal of internals can be accomplished from the top without removal of the valve from the line. In the most severe service, three valves are used in parallel, two being controlled automatically and one hand-operated. One of the automatic valves and the hand-operated valve are spares.

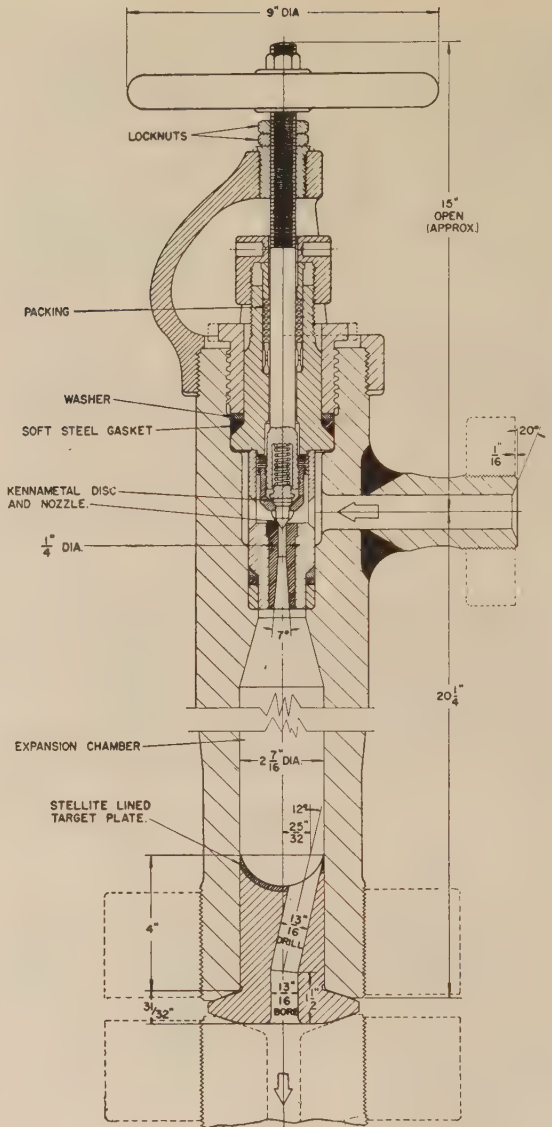

Fig. 13 Severe Throttling Valve

Each of these valves is so arranged that three stop valves are on the upstream side and one on the downstream side, in order that it may be tightly isolated from the system for either removal or repair.

The mild throttling valve is much simpler in construction. Removable seat and disk cannot be taken out without removing the valve from the line, however. Fig. 14 shows the construction of one of the smaller sizes.

Check valves used are both angle and straight-through types. The angle type illustrated in Fig. 15 is used for gases and liquids free of solids. Both seat and disk are stellite-faced, and the seat is not removable. The disk is integral with the stem, which is spring-loaded sufficiently to keep the disk seated under conditions of no pressure differential. The spring space behind the stem is connected with the pressure space by a drilled hole for pressure equalization.

The straight-through vertical-lift check valve shown in Fig. 16 is used for slurries or liquids containing solids. It functions like a ball check, but the hollow disk is shaped like a small streamlined aerial bomb. Vertical movement is guided by three stellite-faced vanes 120 deg apart. Seat, disk, and vane guides are stellite-

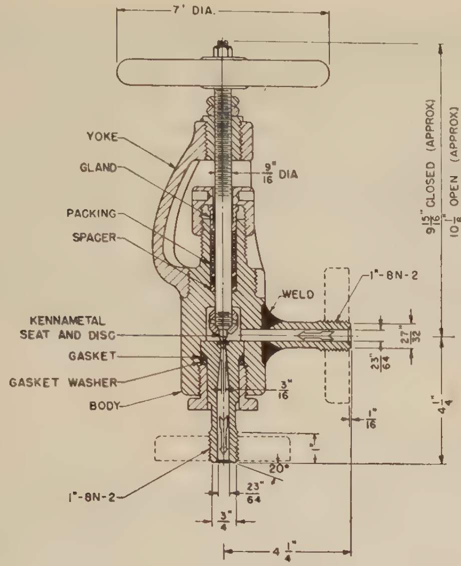

Fig. 14 Mild Throttling Angle Valve

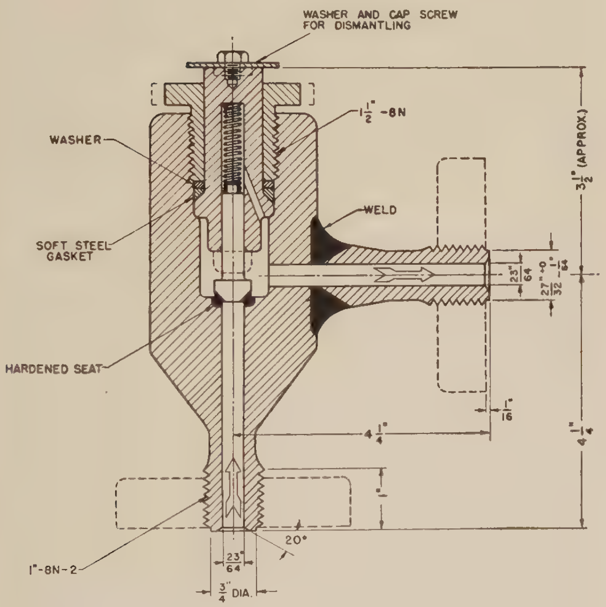

Fig. 15 Angle Check Valve

faced also, and the seat is removable. This valve must always be installed with the disk and seat downward, and flow must always be upward.

Relief valves are spring-loaded, as shown in Fig. 17. Disk and seat are stellite and the seat is removable. The disk is integral with the stem, which extends through the coiled spring and is guided near the upper and lower ends.

Control valves are diaphragm type and have the same general features as hand operated valves.

Conventional 15,000-psi straight-through needle stop and angle check valves, and 25,000-psi microregulating valves are used in high-pressure instrument lines.

Future Commercial Scale Plant Design

As it appears now, only minor changes would be made in design of fittings, flanged joints, and most valves for commercial scale plants. Possibly the severe throttling valve would be replaced by a pressure letdown engine.

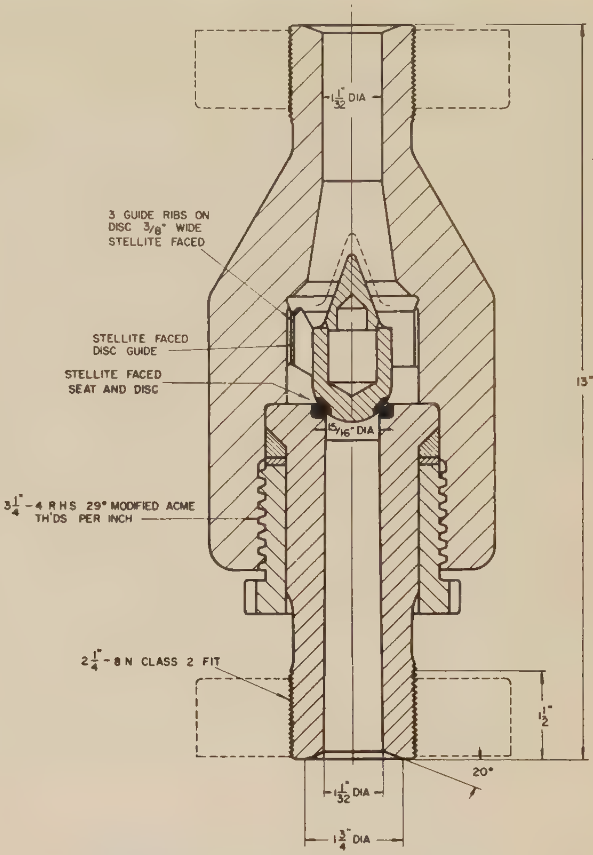
1 1/32" DIA
3 GUIDE RIBS ON DISC 3/8" WIDE STELLITE FACED
STELLITE FACED DISC GUIDE
STELLITE FACED SEAT AND DISC
15/16" DIA
13"
3 1/4"-4 RHS 29° MODIFIED ACME TH'DS PER INCH
2 1/4"-8N CLASS 2 FIT
1 1/2"
20°
1 1/32" DIA
1 3/4" DIA

Fig. 16 Vertical Check Valve

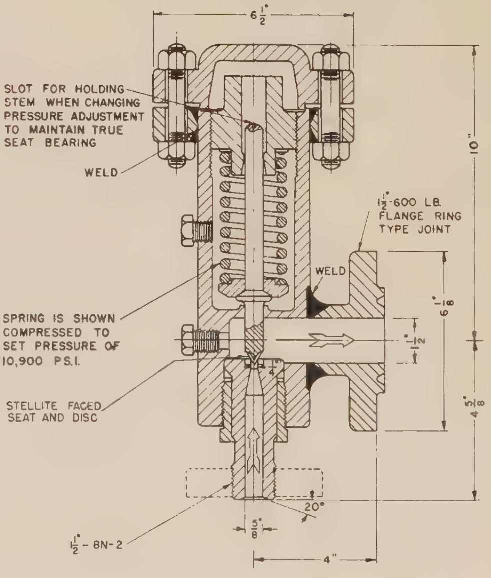
6 1/2"
SLOT FOR HOLDING STEM WHEN CHANGING PRESSURE ADJUSTMENT TO MAINTAIN TRUE SEAT BEARING
WELD
10"
1 1/2" 600 LB. FLANGE RING TYPE JOINT
WELD
6 1/8"
1/2"
SPRING IS SHOWN COMPRESSED TO SET PRESSURE OF 10,900 P.S.I.
STELLITE FACED SEAT AND DISC
4 5/8"
20°
5/8"
1/2"-8N-2
4"

Fig. 17 Relief Valve

The trend in piping, which is expected to reach a maximum size of 10 in. ID will probably be toward use of higher-strength materials in the low and medium temperature ranges, permitting higher design stresses. Possibly ends of pipe would be upset for threading so that the main body will not have excessively thick walls. The thinner walls would allow manufacture of most of the required sizes by piercing and cold-drawing rather than by forging and boring. From about 6 in. ID to the maximum of 10 in. ID, manufacture undoubtedly would be by forging and boring.

It is expected that design stresses will be of the order of magnitude of 30,000 psi. A 4-in-ID pipe would then have an OD/ID ratio of about 1.53 and weigh about 60 lb per ft. Using the old design, a 4-in-ID pipe would have an OD/ID ratio of 1.88 and weigh about 108 lb per ft.

Further, it may be possible to substitute Croloy 7 or 5 for the Croloy 9M now in use. In addition, it may be desirable to break up the present medium-temperature service range into several ranges, and to use a different material for each. Studies would have to determine whether such changes would be feasible metallurgically and if they would reduce costs appreciably.

At this time it is doubtful that a material for high-temperature service piping with a creep strength higher than AISI type 316 can be found. Heavier piping for this service will not affect the overall situation appreciably, since it represents only a small percentage of the total high-pressure piping in a coal-hydrogenation plant.

There are several super alloys in the development stage, but to date there is no evidence that any of them can be used successfully for high-temperature service tubing.

Instrumentation for Coal-Hydrogenation Service

By G. L. BRUNO,[1] F. W. GEYER,[2] and J. A. MARKOVITS[3]

The process requirements of measurement and control are described as applied to high-pressure phases of the coal-hydrogenation process. Special emphasis is given to the details of development and application of special instruments.

Introduction

THE coal-hydrogenation demonstration plant includes nearly all types of instruments found in normal refinery practice. The instrumentation is not typical of that required in a commercial plant, as many measuring devices were installed for experimental purposes to gather operating data and to accommodate changes in operation with various types of coal. The text of this paper covers only high-pressure instrumentation with emphasis given to unusual items, new developments, and adaptations; it is discussed in the order of temperature, pressure, flow, differential pressure, level, and miscellaneous instruments.

Measurement and control in high-pressure services is not new. However, when applied to coal hydrogenation, other factors complicate the problem. In addition to pressures of 700 atm, there are temperatures of 1100 F, high-viscosity erosive liquids containing up to 50 per cent solids, hydrogen, and mixed hydrocarbon vapors, as well as severe pressure drops of as much as 675 atm, and freezing weather.

In German plants, automatic control was not an economic necessity; therefore instrumentation was not highly developed for this process. It was recognized that solution of the many complex instrumentation problems would offer great possibilities for improvement over the German plants and help adapt coal hydrogenation to the economics of the United States.

The necessity for protection against the hazards of the process established the basis of design for the control center. The control house is a reinforced-concrete building, 34 ft × 90 ft, with a solid 12-in. wall on the north or stall side as further protection. Directly outside the wall are located principal control valves and by-pass valves, the handles of which extend through the wall and panel board and are located directly under their respective instruments for manual operation. The instrument board, containing 121 instruments, consists of 30 control panels and 2 annunciator panels, with 18 panels on the north wall and 7 on each wing. The instruments are either pneumatic or electric receivers, eliminating explosive gases or high-pressure liquids from the control room. High-pressure controllers are on the north wall, with miscellaneous recorders and the annunciator system on the wings. High-pressure controls operate either automatically, remote pneumatically, or manually from the center.

Temperature Instruments

The temperatures encountered in the process design range from atmospheric to 1800 F and makes the use of both iron-constantan and chromel-alumel thermocouples desirable. Twenty-gage thermal elements were used throughout the high-pressure system. This size was selected as the optimum possible, when considering thermal response in relation to thermowell ID and wall thickness, life of element, and resistance of the external instrument circuit. The thermowells used consisted of three types, skin, immersion, and vessel.

Skin-type thermocouple assemblies, as shown in Fig. 1, were required in furnaces, vessel shells, and lines containing abrasive solids. The assemblies were insulated to reduce radiation losses.

The immersion-type wells were used in all clean liquids and gas streams. The relationship of pressure to wall thickness presented the principal difficulties in the design of this type well. The design selected, illustrated in Fig. 2, afforded a minimum wall thickness at the junction of the element and incorporated the lens ring or sealing gasket which is the standard joint seal for high-pressure service.

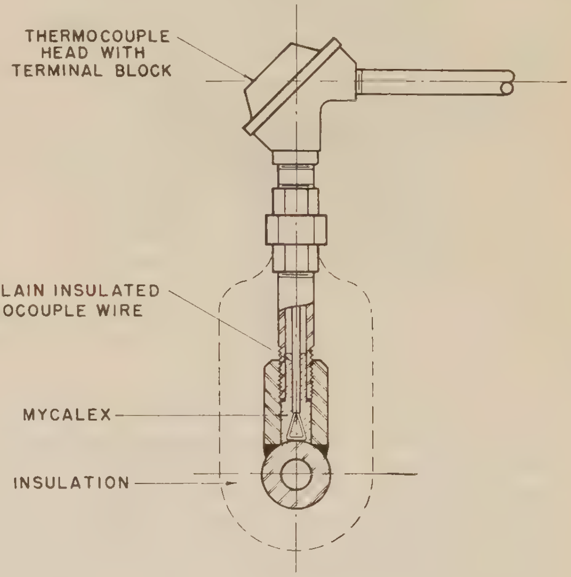
THERMOCOUPLE HEAD WITH TERMINAL BLOCK
PORCELAIN INSULATED THERMOCOUPLE WIRE
MYCALEX
INSULATION

Fig. 1 Skin-Type Thermocouple Assemblies

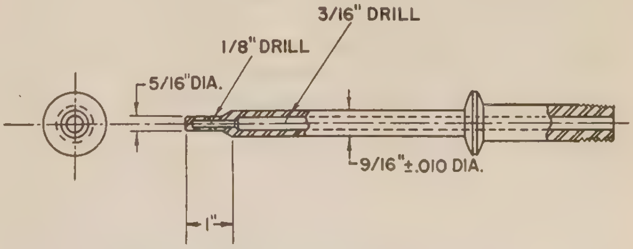

Fig. 2 Immersion-Type Thermowells

---

[1] Project Engineer, Bechtel Corporation, San Francisco, Calif.

[2] Senior Engineer, Bechtel Corporation.

[3] Assistant Chief, Coal-to-Oil Demonstration Branch, Office of Synthetic Liquid Fuels, Bureau of Mines, Louisiana, Mo.

Contributed by the Petroleum Division and presented at the Petroleum Mechanical Engineering Conference, Oklahoma City, Okla., October 2–5, 1949, of The American Society of Mechanical Engineers.

Note: Statements and opinions advanced in papers are to be understood as individual expressions of their authors and not those of the Society. Paper No. 49—PET-4.

Measurement of temperature in vessels such as converters and hot and cold catchpots was complicated by the requirement that all thermocouples enter either the top or bottom head of the vessel. The well design is identical for all vessels; however, the description of the method used is confined to the vapor-phase converter, which contained the maximum number of couples and presented the added difficulty of fixed beds of catalyst.

Due to the exothermic reaction of the process, it is necessary to introduce cooling hydrogen into the basket of the vapor-phase converter at each of the five removable grids. Hydrogen is mixed with the hot gases in the grid and flows downward through the next lower catalyst bed. A temperature point in the middle of each bed operates a diaphragm valve which controls the quantity of cooling hydrogen to the bed, maintaining the control temperature.

The pyrometer tube, as illustrated in Fig. 3, is encased in a shield which enables the tube to be removed for repairs without the catalyst falling through the grids. The shield, however, introduces a serious time lag owing to the low velocity of the gases in the converter and the devious path of heat transfer.

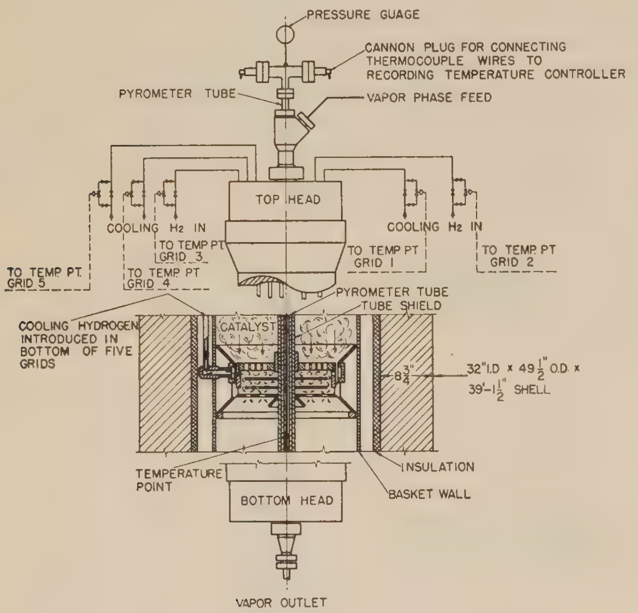

Fig. 3 Vapor-Phase Converter and Pyrometer Tube

Due to hydrogen penetration of the pyrometer tube, it was necessary to seal the outlet where the 12 pairs of thermocouple wires leave the vessel. This was done by using a drilled soapstone bushing tapered at both ends. By tightening a follower nut the soapstone crushes around each wire and tightly seals the pressure in the pyrometer tube. To indicate hydrogen penetration by increased pressure, a special fitting was installed in the pyrometer tube above the vessel with a pressure gage and vent valve.

Temperature measurement and control were obtained by using standard electronic strip-chart multipoint recorders, circular-chart recorder controllers, and multipoint, self-balancing, precision indicators with switch cabinets of 48 and 96 points.

Temperature controllers were designed with manual by-pass panels, and it was felt necessary to incorporate full throttling and automatic-reset-type control. Multipoint recorders and controllers were equipped with high-temperature alarms which actuate the annunciator system. All ranges used on these instruments were standard, except one special circular-chart controller for controlling the vapor-phase feed temperature to the converters by introducing cooling hydrogen to the stream. This instrument is unusual, in that its range is 850 to 900 F—a span and suppression not normally found in potentiometer-type instruments. This was necessary owing to the narrow span in which maximum hydrogenation efficiency is obtained.

Pressure Instruments

Static pressure measurement was made with conventional alloy-steel Bourdon tubes in ranges to 20,000 psi. These instruments include indicating pressure gages, nonindicating pressure controllers, and indicating pneumatic transmitters.

The indicating gages are 8 in. diam, with safety features such as shatterproof glass and rupture-disk backs. Connections were made by using $^{1}/_{2}$-in. straight pipe thread with annealed-copper gaskets as normally found in hydraulic work. Pressure elements installed in liquid services were equipped with a special high-pressure-design pulsation damper as normally required on services from reciprocating pumps. The measurement of static pressures in streams containing abrasive solids required special consideration, and for this purpose a diaphragm or "homogenizer" gage was used with flushing-oil connections to prevent plugging. This gage consists of a liquid-filled Bourdon tube actuated by the flexing of a flat-bulb-type diaphragm.

Nonindicating pressure controllers, ranging to 15,000 psi, were of conventional design, with special differential-cone-type high-pressure connections. As a protection against rupture of Bourdon tubes, excess-flow check valves were installed ahead of each tube. Transmission to recorders and recorder controllers was performed pneumatically by the conventional bellows system. Controllers were of the full-throttling type.

Flow Instruments

Flow measurement was made in streams consisting of hydrogen, vapors, clean liquids, and liquids containing abrasive solids by using a sharp-edged orifice in all cases except cooling hydrogen streams, where the small flow made orifice-plate measurement impractical. Orifice-plate design coefficients had to be established by extrapolation for the $^{3}/_{8}$-in. to 2-in-ID special tubing. Additional problems were presented owing to pulsation from reciprocating pumps and compressors and the necessity of using nonstandard pipe taps of 8 diameters upstream and 8 diameters downstream to meet construction requirements of the lens ring joint, the lens gasket of which is incorporated as part of the orifice plate. It is anticipated that experimental data will be collected during operations to modify the preliminary design coefficients. The materials handled also required the use of accessories, such as seal pots, flushing oil and hydrogen purges, and steam tracing of meter legs.

For streams of small volume in the range of 100 cfh at operating conditions, a second type of primary element was used. The design consists of a helical rotor suspended on instrument pivots against jeweled bearings and contained within a high-pressure housing. A small alnico magnet is mounted on the rotor and as it turns, generates an alternating-current voltage in a pair of coils placed in the assembly. These coils are in series and connect to weatherproof terminals. The output from the transmitter is of a few millivolts magnitude, with frequency and amplitude proportional to the rate of turning of the rotor. This alternating-current voltage is fed to the receiving unit. A proposed alternate method for this service was an electric transmission-type rotameter; however, it was felt that a development such as the helical rotor, if proved practical, would be more suitable for the services and would be considerably cheaper.

The receiver for the rotor-type transmitter consists of 0-100 d-c panel-mounted microammeter. As the output of the transmitter is alternating current of a small magnitude, it must be rectified and measured on a direct-current instrument. This rectification is done by a copper-oxide rectifier circuit and owing to the nonlinear characteristics of the rectifier, it is necessary to bias the rectifier with a direct-current voltage to gain linear characteristics. Due to the biased voltage on the rectifier, it is further necessary to provide an opposing bias current on the indicating meter. This biasing current is supplied from a stabilized 6-volt d-c supply common to the 12 rotor installations in the plant.

Orifice-plate differential measurements were made by two types of transmitters. One consisted of a special 200-in. high-pressure mercury-filled manometer with an inductance-type transmitter. The transmitter consists of a soft-iron armature attached to the float and moves up and down in a nonmagnetic tube surrounded by a center-tapped inductance coil. Due to changing differential pressures, the position of the armature varies with respect to the center tap of the inductance coil. This movement changes the relative inductance of the two halves, the over-all inductance remaining constant.

The receivers for the mercury-manometer-type transmitters are a special adaptation of the electronic self-balancing recorder. They contain a transformer supplying 5.0 or 6.3 volt a-c for power to the system, and a self-balancing slide-wire which repositions itself to balance the voltage changes produced by the inductance-type transmitters. In other words, an alternating-current resistance-inductance Wheatstone bridge is formed between the transmitter and receiver. The simplified wiring diagram is shown in Fig. 8. It was necessary to use the more sensitive-type receiver rather than the standard electric-inductance flow receiver, as the changes in inductance produced by the transmitter-armature movement are much smaller than in the standard transmitter. This reduction was a result of the heavy wall thickness of the nonmagnetic tube in the transmitter to withstand the higher operating pressures. These receivers are in all cases recording, full-throttling, automatic-reset, pneumatic controllers.

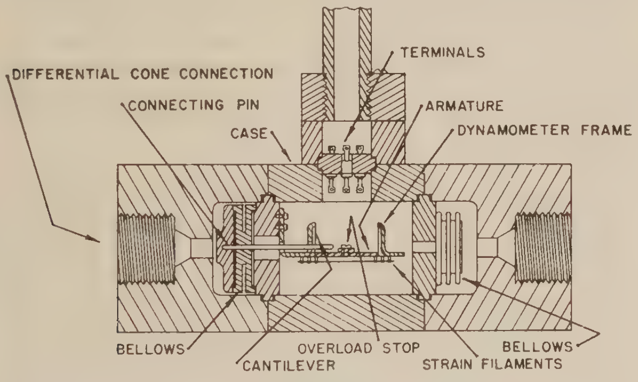

Fig. 4 Section of Differential Strain Gage

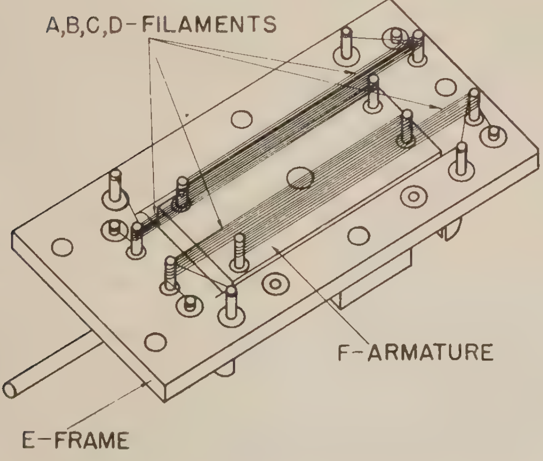

Fig. 5 Displacement Transducer Element

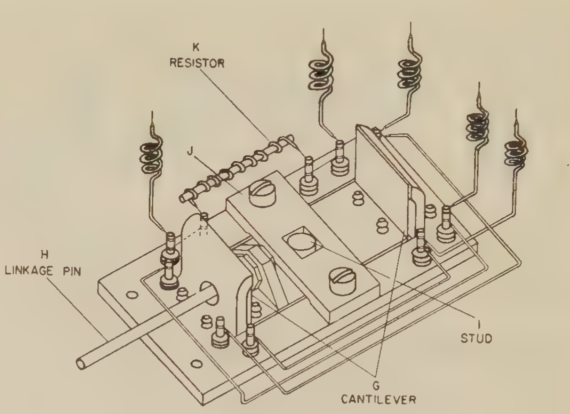

Fig. 6 Reverse Side of Transducer

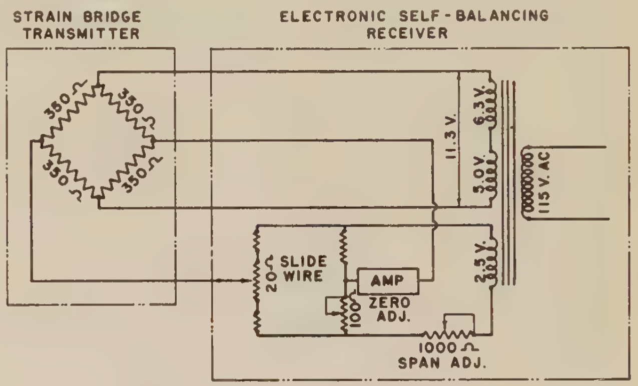

Fig. 7 Simplified Wiring Diagram of Strain Transmitter and Receiver

The second type consists of a high-pressure housing containing a measuring diaphragm and a sealing diaphragm between which is located an unbonded strain bridge or displacement transducer element immersed in a silicon liquid and connected to the measuring diaphragm, as shown in Fig. 4.

The displacement transducer element is shown in Fig. 5. It consists of a frame *E* supporting a movable armature *F* by two thin cantilever plates. Four sets of constant filaments, *A*, *B*, *C*, and *D*, are strung under initial tension between the frame and armature. When the armature is displaced longitudinally, two sets of filaments are elongated while two sets are shortened. The elongated filaments increase in resistance, and the shortened filaments decrease. The change in resistance of the filaments is proportional to their change in length. The transducer is so wired that the filaments are connected in a Wheatstone-bridge circuit. The resistance change of the filament alters the electrical balance of the bridge so that an electrical current flows in the output circuit. The reverse side of the transducer is shown in Fig. 6; *G* indicates the cantilever plates which support the armature; *H* is the linkage pin by which movement from the measuring diaphragm is transmitted to the armature; *I* is a stud attached to the armature which limits the movement of the armature to 0.0015 in. in either direction. This stop serves to protect the filaments against mechanical overload. The resistor *K* is a trimmer placed in series with one of the bridge elements. It is adjusted to equalize the resistance of the four elements of the bridge. If the bridge

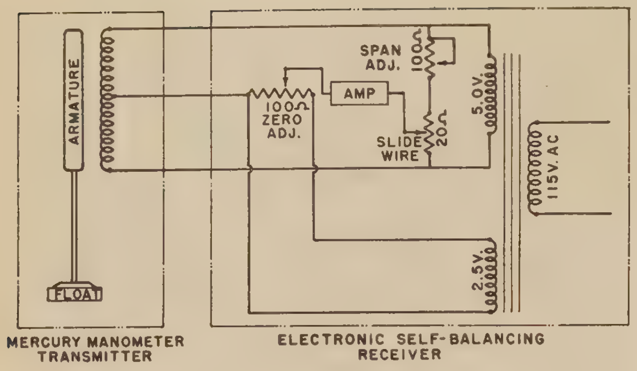

Fig. 8 Simplified Wiring Diagram for Mercury-Manometer Transmitter and Receiver

is balanced at zero output before the displacement is applied, the unbalanced electrical output of the bridge bears a linear relationship to the displacement. The complete wiring diagram, including transmitter and receiver, is shown in Fig. 7.

The receivers for the differential strain transmitters are also special, although different adaptations of the electric self-balancing potentiometer. In this case it is an alternating-current potentiometer with both the strain bridge in the transmitter and the slide-wire in the receiver being supplied power from the same transformer located in the receiver. An alternating-current potentiometer-type circuit was chosen because by connecting the four strain elements in a bridge, the largest and most easily measured output could be obtained. The output is in the order of 25 millivolts for full scale deflection of the receiver whereas, had a resistance-measurement-type circuit been used, the total resistance change for full scale deflection would have been very small with the type of unbonded strain gage used. The span and zero adjustments are accomplished by means of a potentiometer rheostat network located in the receiver and shown on the simplified wiring diagram in Fig. 7. These receivers are in all cases circular-chart recorders.

It can be noted from the foregoing description that two different types of transmitters were used for differential flow measurements. Either type could have been used throughout. The mercury-manometer type was chosen for all control applications, as it seemed to offer the best possibility of maintaining its calibration over a long period of time while the strain-element type is known to have a zero calibration shift with time. The strain type was chosen for straight flow recording on the basis that it was cheaper, and that an instrument of this type should be developed.

Differential-Pressure Instruments

Most of the differential-pressure measurements in the demonstration plant were made for collecting experimental data on such items as plastic flow of viscous fluids and exchanger fouling factors. Very few data are available, particularly at high pressures, on the plastic flow of viscous fluids such as coal paste with a viscosity of 4750 centipoises at 200 F, and a Reynolds number considerably below the range of laminar flow; and it is therefore hoped that friction factors and empirical formulas may be developed by the differential-pressure data obtained. Differential-pressure measurements are also used as an indication of changes in fouling factors of exchanger equipment due to coke, salt, and hydrates; and for process control of water-injection rates necessary to reduce the scale and salt deposits in the exchanger tubes.

The primary measuring element and transmitter for these measurements is a differential strain gage as previously described in the flow section with modifications to the diaphragms for ranges of 100, 350, 500, and 1000-lb differentials.

The receivers for these measuring elements were an adaptation of a multipoint strip-chart potentiometer recorder. The basic electric circuit for each point was the same as previously described for single-point recorders under flow measurement; however, owing to the inherent difficulties in manufacture of the strain element, the calibration factors for each transmitter were different and required a separate span and zero adjustment for each point recorded. This span-and-zero adjustment for each transmitter was located behind the receiver case.

Automatic control of differential pressure was used in only two cases—the total differential pressure across the hydrogen-recycle compressors in the vapor-phase and the liquid-phase systems. Both systems are closed and operate independently. It was necessary to by-pass part of the recycle hydrogen at a high enough pressure, to be assured at all times of a sufficient pressure differential to force a controlled flow of cooling hydrogen into the converter, while still maintaining a constant flow of process hydrogen and feed to this same converter. To accomplish this, an excess of recycle compressor capacity is maintained at all times at a pressure differential of from 500 to 750 psi. This differential-pressure-recorder controller is the most important single controller in either phase, as enough cooling hydrogen must be available to prevent a runaway condition due to the exothermic reaction. These receivers are pneumatic, full-throttling, automatic-reset, circular-chart-recorder controllers, equipped with manual by-pass panels.

Liquid-Level Instruments

Level measurement and transmission for all high-pressure vessels was accomplished by using 50-in. high-pressure mercury manometers of the type previously described in the section on flow instruments.

The receivers are circular-chart-recording, full-throttling, automatic-reset, pneumatic controllers with manual by-pass panels. The electric circuit for the receivers of the mercury manometers is the same as that used for the manometer-type flow receivers previously described.

The liquid-level measurement and control of the hot catchpot was the most difficult installation and is therefore described in detail. The hot catchpot is a vessel 24 in. ID × 38 ft high and is used in the process as the hot liquid-vapor separator. The liquid flow to the hot catchpot is intermittent, and the sudden surges must be minimized by efficient control. The heavy-oil bottoms is a liquid containing approximately 35 per cent solids, consisting of unreacted coal, ash, and catalyst, and a high percentage of absorbed gases. From the foregoing description it can be seen that this service presented many problems as to measurement, control, and maintenance; therefore three separate and distinct level systems were employed. Two were of the pneumercator or bubbler-tube type in conjunction with 50-in. mercury manometers, and the third was of the gamma-ray type described later. The pneumercator liquid-level measuring device consists of a mercury manometer connected to tubes entering the top of the vessel. One tube is terminated near the top to measure the static pressure while the other extends into the vessel to a point near the bottom. The liquid head on the second tube produces the differential on the manometer. Hydrogen is introduced into the two manometer leads through two flow recorders in one case and through capillary throttling devices in the other. The arrangement is shown in Fig. 9.

Owing to the severe service conditions of the hot catchpot, it was felt that an additional type of level measurement and transmission should be employed. This is an electronic instrument utilizing gamma radiation which is capable of measuring changes of level through the heavy wall of the vessel without the use of an access opening. The gamma rays are produced as a result of

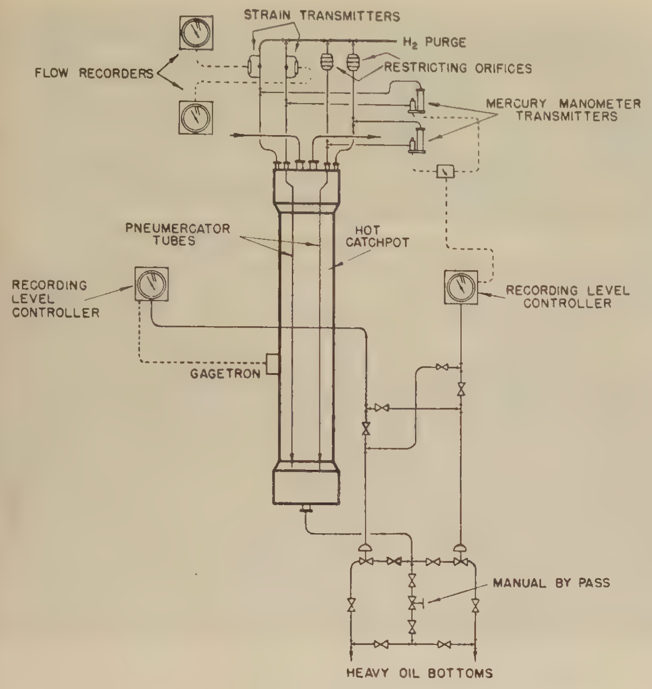

Fig. 9 Hot-Catch-Pot Level-Control System

natural disintegration of radium in a capsule located within the vessel. The number of gamma rays that penetrate a section of the vessel wall are counted and averaged by a suitable Geiger counteramplifier-integrator circuit, which supplies an output of 0-50 millivolts d c. The intensity of the radiation from the radium source varies with the distance from the source to the counter and with the densities of various materials intervening. The counter is located about 2 ft higher on the outside of the vessel than the radium sources on the inside; therefore, as the liquid rises above the source, the radiation received at the counter is progressively reduced by this intervention of a material of a higher density. The reduction of intensity continues until the liquid level is directly opposite the counter producing a 2-ft operating range.[4] The electric circuit of the receiver is a conventional self-balancing potentiometer with a range of 0–50 millivolts d c.

The manometer transmitters were wired through a switch on the control panel so that either of the two transmitters could be used on a common receiver controller. The output control air of this receiver was manifolded with that of the gamma-ray receiver controller so that either could be used to control the level in the hot catchpot. This controlled air operates either of the two diaphragm control valves of the severe throttling type, which remove the heavy-oil bottoms from the hot catchpot. A dual valve installation was required owing to the severe erosion caused by the 675-atm pressure drop of the material handled.

Special designed 15,000-psi test gage glasses also were installed on each of the vessels for manual operation and setting of control points.

Miscellaneous Equipment

Two other types of instruments deserve mention: The thermal-conductivity hydrogen-analyzer recorders, and the Ranarex specific-gravity recorders, which are used as a check on the composition of the gas streams in both the liquid and vapor phase. The instruments are of conventional design. The continuous samples to these instruments were taken from the hydrogen recycle lines through 1-mm capillary tubing which was used to partly reduce the pressure and to reduce line volume to increase speed of response of the analyzers. The final high-pressure drop was taken across double manual throttling valves into a 10-in. WC bubbler, with part of the sample vented to atmosphere and the balance going to the hydrogen-analyzing cell and the gravitometer.

Instrument piping consisted of $^{3}/_{16}$-in-ID × $^{9}/_{16}$-in-OD type 304 stainless-steel tubing, tees, connectors, and valves. Connections were made by use of a differential cone seal, as shown in Fig. 10. The connections were kept to a minimum by use of bends wherever possible.

The construction details of the diaphragm-control-valve bodies are covered in a companion paper on valves and fittings; however, some additional description covering the control operations is required. The valves are equipped with giant top works or diaphragm with 2-in. travel of the diaphragm through a linkage to give $^{3}/_{8}$-in. travel of the inner valve. To insure ample power and accurate positioning of the inner valve, all control valves are equipped with valve positioners set for the $^{3}/_{8}$-in. travel. The port sizes range from $^{1}/_{8}$ in. to $^{1}/_{2}$ in. diam, and the plugs are characterized.

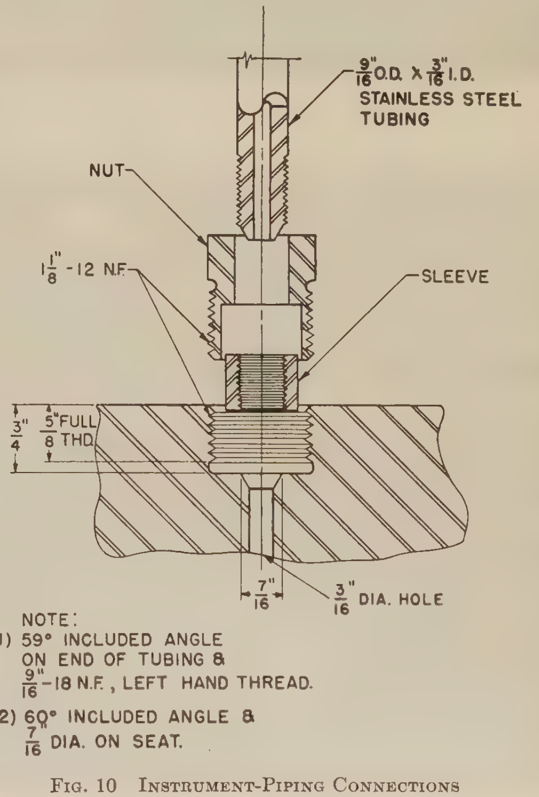
$\frac{9}{16}$" O.D. × $\frac{3}{16}$" I.D. STAINLESS STEEL TUBING
NUT
$1\frac{1}{8}$" -12 N.F.
SLEEVE
$\frac{3}{4}$"
$\frac{5}{8}$" FULL THD.
$\frac{7}{16}$"
$\frac{3}{16}$" DIA. HOLE
NOTE:
(1) 59° INCLUDED ANGLE ON END OF TUBING & $\frac{9}{16}$"-18 N.F., LEFT HAND THREAD.
(2) 60° INCLUDED ANGLE & $\frac{7}{16}$" DIA. ON SEAT.

Fig. 10 Instrument-Piping Connections

An elaborate annunciator system was installed with a normal amber light and an abnormal red light for each alarm circuit. A common howler with a reset button was used. The common-howler reset button will silence the howler for that circuit which has become abnormal, leaving the red light on and clearing the howler for operation from one of the other alarm circuits. The alarm circuits are used for high skin temperatures, thermocouple burnouts, high and low levels, low steam pressure, and low coal-paste pressure.

Conclusion

The special instruments described were developed primarily for

---

[4] For further information on the type 79D1 Gagetron refer to the Engineering Laboratories, Inc., Tulsa, Okla.

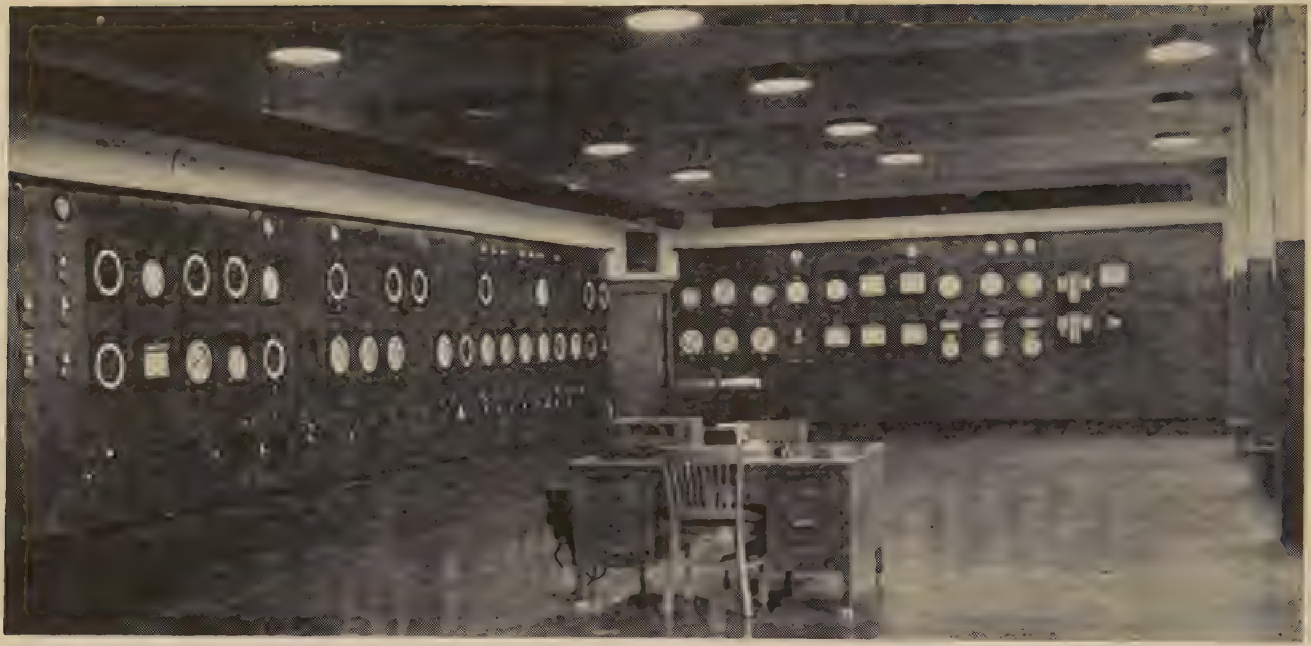

FIG. 11 INTERIOR OF HIGH-PRESSURE CONTROL HOUSE—LIQUID-PHASE INSTRUMENTS

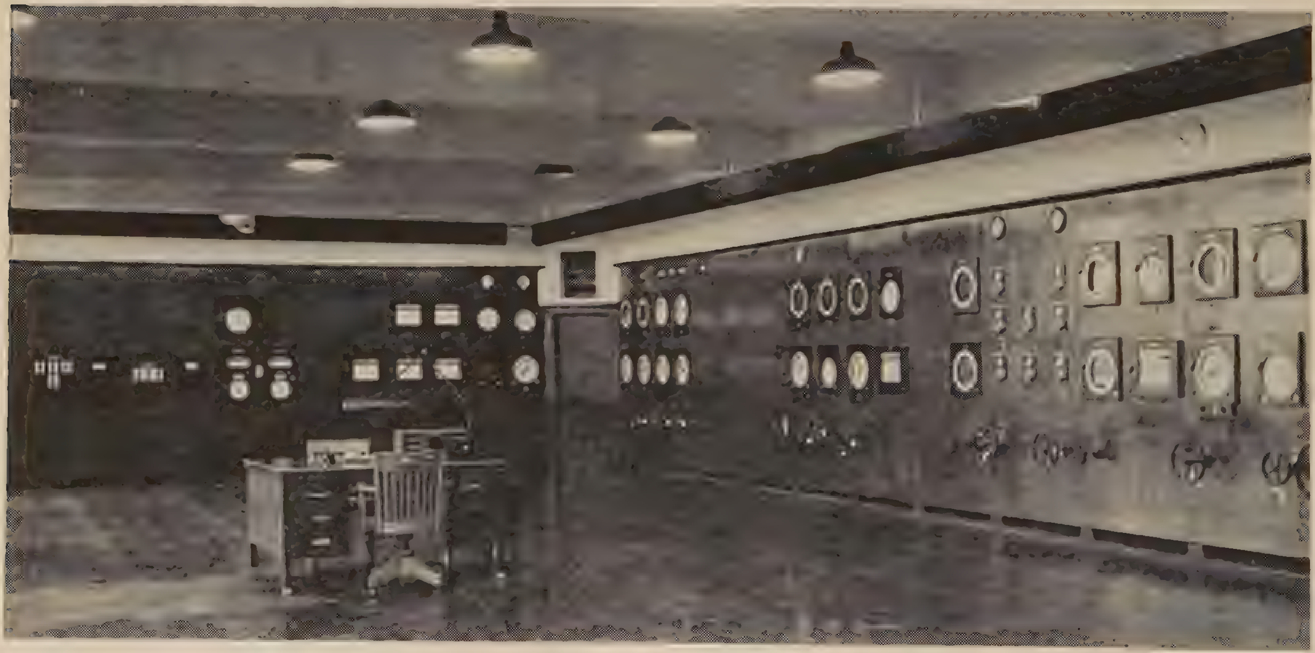

FIG. 12 INTERIOR OF HIGH-PRESSURE CONTROL HOUSE—VAPOR-PHASE INSTRUMENTS

the project through the splendid co-operation of interested manufacturers. The design of the project occurred during a period of peak demand for standard equipment; and it was therefore difficult to find suppliers to produce the equipment. Presentation of ideas to numerous manufacturers, even though they were not interested at the time, has now resulted in the development of some new equipment for high-pressure services. The instruments now in use represent the best that it was possible to develop and obtain but are by no means considered the only or final solution to the problem. It is hoped that from operating experience and continued co-operation with manufacturers, improvements and new developments may be obtained that will be applicable not only to the coal-hydrogenation process but to any future processes of comparable services. The brief operating experience obtained to date indicates that some modifications and redesign will be required; and, after further and more conclusive information is obtained, it is hoped that additional papers will be written on the subject.

Metallurgical and Fabrication Considerations in the Coal-Hydrogenation Demonstration-Plant Construction

By B. H. LEONARD, JR.,[1] G. D. GARDNER,[2] and J. A. MARKOVITS[3]

Special equipment, special steels, and heavy wall thicknesses were required to handle hydrogen and abrasive pastes at the high pressures and temperatures of coal hydrogenation. Some metallurgical and fabrication problems pertaining to this specialized process are discussed herein.

INTRODUCTION

COMPANION papers presented in this issue describe the coal-hydrogenation plant. An attempt will be made in this paper to show why certain materials were used and to point out some of the fabrication difficulties that were experienced. This discussion is necessarily limited to materials and equipment used for high pressures.

The primary consideration in the choice of materials for various services is the effect of hydrogen at different temperatures. From German and English experience in the hydrogenation field,[4] it was learned that carbon steels resisted hydrogen attack at a pressure of 10,300 psig up to a temperature of 375 F. Chromium steels in excess of approximately 6 per cent Cr were found to be hydrogen-resistant at higher temperatures.[5] At these higher temperatures, however, creep strength must also be considered. Above 800 F, straight chromium steels do not have high enough creep strength for the service conditions. These factors led to the establishment of three temperature classifications: 0 to 375 F for carbon steel, 376 to 850 F for intermediate chromium steel, and 851 to 1000 F for chromium-nickel stainless steel.

PIPING MATERIALS

To obtain materials suitable for high temperatures and high pressures, it was necessary to accept some undesirable features; one of these, common to all the metals, was hot-shortness. Seamless tubing was used throughout, with an approximate ID:OD ratio of 1:2. Because of the thick wall involved, difficulty was experienced in maintaining uniform temperatures throughout the metal, and it was possible for part of the wall to be in the hot-short range at some time during the forming operation.

Low Temperature. The service conditions in the low-temperature range closely simulate those found in normal refinery practice, except for the higher pressures. Hydrogen attack on carbon steel in this temperature range is not evident. Therefore the piping specifications were established in compliance with the ASME Pressure-Piping Code, and specifically with the API 5L, grade C, classification.[6] This specification requires a minimum yield value of 45,000 psi, and specifies a maximum allowable stress of 22,900 psi at 375 F. The most readily available material conforming to these specifications and adaptable to seamless piercing operations was MT-1040. Normal production of seamless tubing from this material employs a hot-roll finish. Due to the extremely heavy tube wall required, excessive ovality or squareness resulted from this procedure as shown in Fig. 1. Although minimum wall-thickness requirements were met, this squareness was undesirable for the following reasons: (1) Tubes of nonsymmetrical cross section will develop undeterminable stress concentrations due to internal pressure; (2) indeterminate problems would result in the calculation of bending and shear stress caused by thermal expansion, pipe supports, and anchors; (3) starting points for corrosive and erosive action, sedimentation and coke formation would be established—especially at points where the squared ID of the tubing meets the round ID of the fittings; (4) proper fluid flow and heat transmission would be impaired; (5) systematic safety inspection of irregular tubes would be impossible.

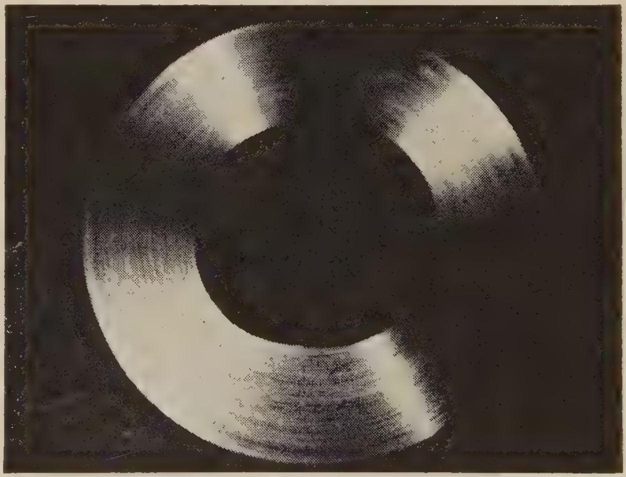

Fig. 1 Squared ID of Hot-Rolled MT-1040 Steel Tube

To eliminate squareness and give a satisfactory finish to the

---

[1] Mechanical Engineer, Coal-to-Oil Demonstration Branch, Office of Synthetic Liquid Fuels, Bureau of Mines, Louisiana, Mo. Jun. ASME.

[2] Metallurgist, Coal-to-Oil Demonstration Branch, Office of Synthetic Liquid Fuels, Bureau of Mines.

[3] Assistant Chief, Coal-to-Oil Demonstration Branch, Office of Synthetic Liquid Fuels, Bureau of Mines.

[4] "The Effect of Highly Compressed Hydrogen Upon Unalloyed Steel," by F. K. Naumann, *Stahl und Eisen*, vol. 57, 1937, p. 889. "The Effect on Various Steels of Hydrogen at High Pressure and Temperature," by N. P. Inglis and W. Andrews, *Journal of the Iron and Steel Institute*, vol. 128, 1933, pp. 383–397.

[5] "The Effect of Alloying Additions on the Resistance of Steel to Hydrogen Under High Pressure," by F. K. Naumann, *Stahl und Eisen*, vol. 58, 1938, pp. 1239–1250.

Contributed by the Petroleum Division and presented at the Petroleum Mechanical Engineering Conference, Oklahoma City, Okla., October 2–5, 1949, of The American Society of Mechanical Engineers.

Note: Statements and opinions advanced in papers are to be understood as individual expressions of their authors and not those of the Society. Paper No. 49—PET-5.

[6] ASME Code for Pressure Piping, 1942.

tubes required either boring or cold-drawing. The less expensive solution of cold-drawing was chosen. As a final step, the tubes were given a normalizing treatment for adjustment of mechanical properties.

One of the inherent properties of this steel is a hot-short range from 1400 to 1600 F. Forming should be done in a range of 1800 to 2000 F, and in no case should this material be cold-bent. Some of the tubing was found to have cracks, and it is believed that these cracks were caused by forming at too low a temperature, or in the hot-short range. A typical defect is shown in Fig. 2.

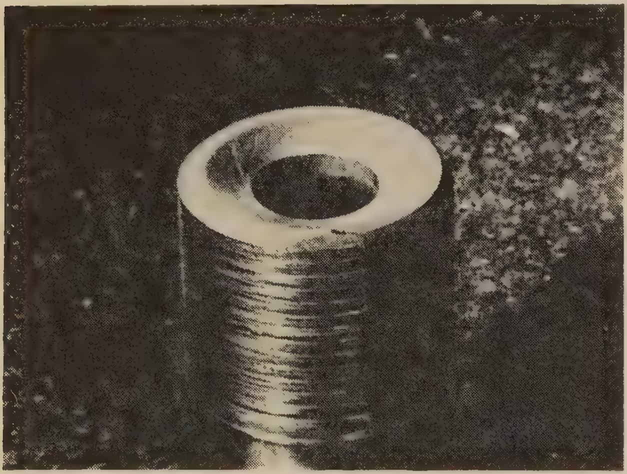

Fig. 2 Hot-Short Crack in MT-1040 Steel Tube

Intermediate Temperature. For the intermediate-temperature service, a steel with a chromium content exceeding 6 per cent was needed to resist hydrogen attack. Standardization of piping was based upon the maximum allowable stress of the low-temperature steel; 22,900 psi at 375 F. A study was made to find a material which at 850 F would have approximately this same allowable stress, and also have enough chromium to resist hydrogen attack. A stronger material would not have been economically sound; conversely, standardization would not have been possible without a material at least this strong. The most readily available material that could be heat-treated to give suitable mechanical properties and contained enough chromium to resist hydrogen was a 9 per cent chromium-molybdenum steel.

This material was found to have the same tendency to square during the customary hot-finishing operation as had been experienced on the low-temperature steel. It was necessary, therefore, to cold-draw this material also. For increased resistance to hydrogen penetration and to obtain required mechanical properties at working temperature, the chromium-molybdenum steel was normalized and drawn at 1200 F. The mechanical properties of this material could be expected to remain stable in operation because of the spread between the operating and draw temperatures. In tests on samples for 1000 hr at 800 and 900 F, only a minor loss could be found[7] in mechanical strength at room temperature or 900 F.

For the extreme deformation required in the piercing operation, 9 per cent chromium-molybdenum steel should be heated to working range of 2000 to 2250 F. Within the range of 1500 to 1800 F this metal is hot-short, and deformation may lead to cracking at the points of maximum deformation. Because of the air-hardening characteristic of this material, rapid cooling from above 1400 F could also produce cracks or checks. It is believed that the cracks found on some tubes of this material were caused by working in the hot-short range, Fig. 3.

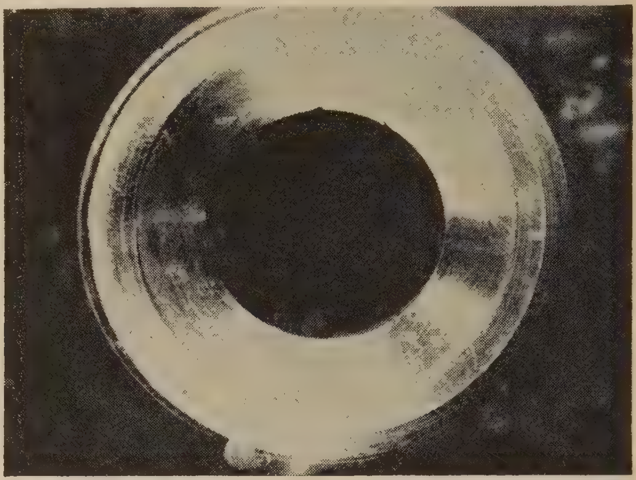

Fig. 3 Hot-Short Cracks in 9 Per Cent Chromium-Molybdenum Steel Tube

High Temperature. The high-temperature requirements were the most difficult to meet. The material had to resist hydrogen attack and have high creep strength. Again, for standardization purposes, it was necessary to find a material with a creep strength at 1000 F, close to the maximum allowable stress of the low-temperature material, 22,900 psi. The stabilized materials in common use did not have enough strength. Careful control during operation eliminates corrosion and makes possible the use of unstabilized AISI type 316 stainless steel for the high-temperature service. This steel has the highest creep strength of the heat-resisting stainless steels for which data are available.[8] Its strength for 1 per cent elongation in 10,000 hr is 23,000 psi.

AISI type 316 alloy is relatively refractory in piercing and rolling and has a tendency to surface-marking. It is therefore common practice to cold-draw this tubing to produce suitable surfaces, to eliminate notches and other stress raisers, and to save material. In addition, some cold work is applied to achieve some recrystallization on heat-treatment and to produce optimum grain size.

Fittings

The high-pressure fittings, consisting of tees, ells, and reducers, were forged from special steels required for the various temperature ranges. The tees were formed by forging solid blanks into the proper shape; these forgings were then bored to proper inside dimensions. Because of the thick walls required, it was very difficult to deform the entire mass sufficiently to modify completely the original cast structure. The ells were forged from straight bars, which were first bored eccentrically and then formed with the heavy side on the outside of the bend, in an attempt to secure uniform wall thickness.

Low Temperature. Zones of weakness in the high-pressure tees were found in the branch run. Here a minimum of work was required for the actual shaping of the forging. Fig. 4 shows a carbon-steel tee leaking at a pressure of 8000 psi during a hydrostatic test. Fig. 5 shows the cast (unworked) and the fibrous (partly worked) structures at the fractured surface of a defective tee, which had been broken to show the cause of leakage.

---

[7] Test Report from Babcock & Wilcox Tube Company, Beaver Falls, Pa., July 14, 1948.

[8] Metals and Alloys Data Book, S. L. Hoyt, Reinhold Publishing Company, New York, first edition, 1943, pp. 111 and 189–191.

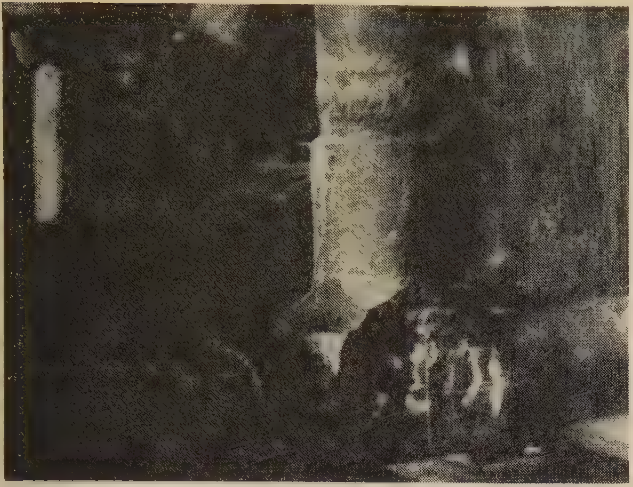

Fig. 4 Defective Carbon-Steel Tee Leaking Under Hydrostatic Test Pressure of 8000 Psi

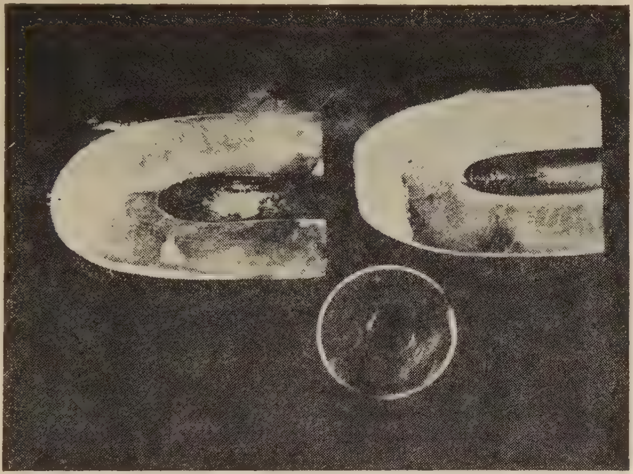

Fig. 6 Defective AISI Type 304 Stainless-Steel Ell Caused by Forging at Too Low a Temperature

Other tees exhibited forging cracks, laps, and seams at the root of the branches; ells had some checks and laps, but few of these proved to be serious.

Intermediate and High Temperature. The intermediate-temperature forgings were of AISI type 304, and the high-temperature forgings were of AISI type 316 stainless steel. The forging range of these materials is very critical and narrow; 2200 to 1800 F. Forging at temperatures either slightly above or below these limits will result in cracks and checks. More blows are required to work these materials than are required for carbon steel, and the first few blows must be light, so as to harden and toughen the surface, after which heavier blows may be applied. Because of low thermal conductivity, very rapid cooling, and longer forging time, reheating must be done quite often. It is extremely important that the hot-work finish temperature be adhered to, since this material tends to work-harden while still very hot. Fig. 6 shows a forged ell which is believed to have been cracked, owing to forging at too low a temperature.

Welding of Tubing

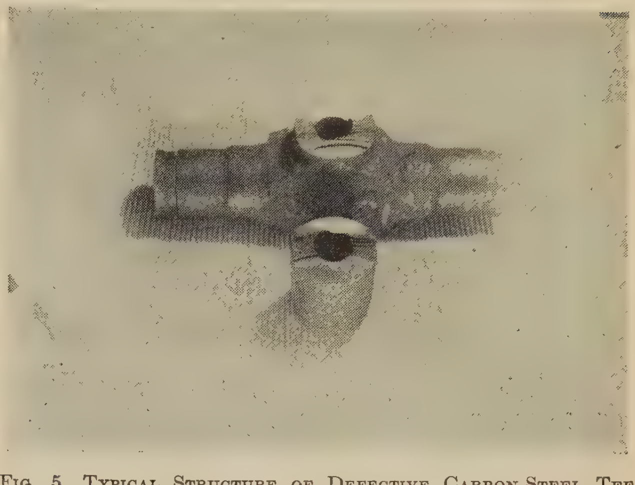

Fig. 5 Typical Structure of Defective Carbon-Steel Tee Which Leaked Under Hydrostatic Test

In the fabrication of spool pieces by welding, the metallic-arc process was used exclusively, utilizing multipass procedure. Procedures and operators were qualified on the materials and thicknesses involved. The joint design employed the conventional $37^{1}/_{2}$-deg straight bevel for wall thicknesses up to $^{3}/_{4}$ in.; above this thickness a 20-deg U-type bevel was used. Backup rings were not used for the following reasons: (1) The small ID of the tubing made it impossible to remove the rings; (2) restriction to flow caused by a ring would be undesirable; rings would establish starting points for sedimentation and coke formation; (4) damage could result to valves or pumps, were a ring to come loose; (5) it was demonstrated that 100 per cent penetration could be obtained without the use of rings.

Tube tolerances often resulted in $^{1}/_{8}$ in. eccentricity. To prevent shoulders at the joints and to assure full penetration of the weld, the eccentric ID was taper-counterbored at the time of cutting the welding bevel. This also assured alignment of the inside diameters when the outside diameters were aligned, and facilitated setup of the spool pieces before welding.

Low-Temperature Material. Welding of the MT-1040 low-temperature material was difficult because of the high carbon content. To diminish the cooling rate and hardness of the heat-affected zone, a preheat of 400 F was used and maintained during welding. The length of time the preheat was applied was governed by the wall thickness involved. Contrary to common practice of using electrodes with minimum tensile strength at least equal to that of the parent metal, E-7010 electrode was used for the low-temperature-range steel. This choice sacrificed ultimate strength for a gain in ductility; however, yield values of the filler metal exceed yield values of the parent metal. The joint and the heat-affected areas were stress-relieved immediately upon completion of the weld. The heat-affected zone was heated to 1250 F, held at this temperature for 1 hr per in. of wall thickness, and slowly cooled in still air. In no case did the heat-treatment last less than $^{1}/_{2}$ hr. No attempt was made to restore the metal to the normalized condition as it was felt that the stress-relieved weld deposit would meet the necessary tensile requirements.

Intermediate-Temperature Material. Welding of the air-hardening chromium-molybdenum steel also required care. A preheat temperature of 600 to 800 F was used to insure a minimum of 500 F, and thus prevent cracking. Upon completion of the weld, and without any loss of temperature, the joint and heat-affected zone were soaked for 2 hr at 500 F to assist martensite transformation, so that, upon heating to 1200 F (subcritical temperature), holding for 4 hr, and cooling in still air, the weld would be tempered. A filler metal of composition similar to the parent metal was used.

High-Temperature Material. The austenitic AISI type 316 stainless steel required a preheat of 400 F, because of its low thermal conductivity and because of the large mass of metal involved. To assure an austenitic weld deposit and to avoid possible sigma-phase formation, a 25 per cent chromium-20 per cent nickel electrode was used. Because of the high-temperature service condition, postheat was unnecessary.

MACHINING

Machining of the tube ends for the flanged lens joints also presented problems. To effect a seal, the tube ends had to have a smooth machine finish on a 20-deg bevel. This finish was obtained by means of a forming tool. Hard spots in the tube ends, however, would cause chatter of the tool bit and result in marks on the critical bevel face. Kerosene used as a cutting lubricant eliminated much of this trouble.

Tube and flange threads were gaged with "go" and "no-go" gages. If a tube thread were near the large limit and a flange thread near the small limit, binding would occur. This was especially troublesome with AISI type 316 material, which tended to gall. Cutting the tube thread deeper would not remedy a tight fit, but only change the thread profile. However, tube threads could be cut slightly oversize to accommodate oversize flanges. To eliminate this trouble, flanges and thread taps were supplied to the pipe-spool fabricator so that individual fitting could be achieved. These flanges were then used as thread protectors during shipping of the fabricated spool pieces. The critical bevel faces of the pipe spools had to be well protected also, for considerable time could elapse before a particular spool might be used. During this time the spool piece would lie in the pipe yard. Cosmolene was used to prevent corrosion, especially of the carbon steel, and various types of caps and plates were used to prevent damage. Even so, it was necessary to reface many tube ends before some pipe spools could be installed. This refacing was best accomplished by a tool similar to that shown in Fig. 7.[9] The collar holds the tool square with the axis of the tube, and the straight cutting edges are mounted so as to sweep an imaginary, 140-deg, included, cone angle. This arrangement produces the required 20-deg bevel on the tube end. The tool is manually operated and care is exercised to maintain uniform rotation of the cutters when they are backed off. This precaution is necessary to prevent marking of the bevel face at the termination of the cut.

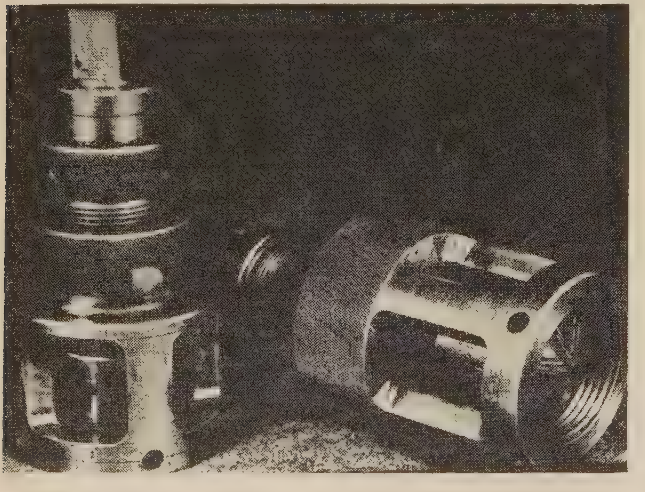

FIG. 7 TUBE-REFACING TOOL

The other critical element of the flanged joint—the lens gasket—presented no serious fabrication difficulties. In all temperature ranges, the materials used for the lens gaskets were softer than the tube ends they were to seal. In the low-temperature range, the gaskets were made of AISI-1020 steel having a maximum Brinell hardness of 140. For the intermediate and high-temperature lens gaskets, AISI type 405 chromium stainless steel was used with a maximum Brinell hardness of 130. Impurities and lack of homogeneity caused voids in the middle of a forged bar of this material which did not show up until 26 pieces, approximately $1^1/_2$ in. long, had been cut, Fig. 8. The spherical surface of the lens gasket was a polished finish; however, since manufacture was done at the job site as needed, corrosive and handling damage was minimized and refacing could be accomplished easily.

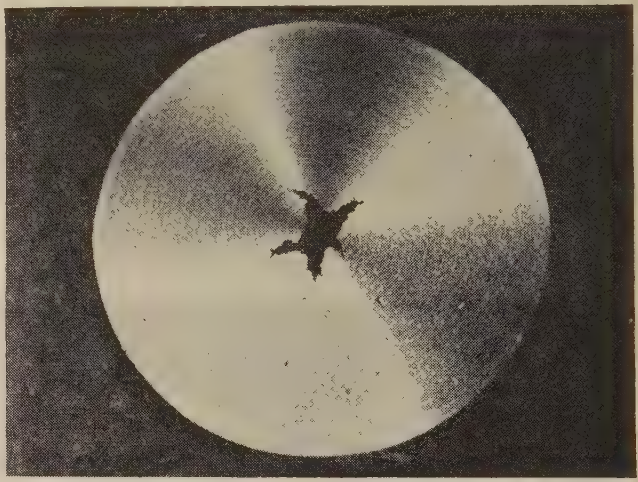

FIG. 8 PIPE IN AISI TYPE 405 STAINLESS STEEL

OTHER PROBLEMS

The process equipment, including valves, pumps, heat exchangers, instruments, and vessels, is subjected to the same operating conditions as the tubing. Special steels and careful fabrication were required on these elements also. Hence special problems pertaining to each arose.

Materials. Cemented carbide is used for disks and seats of throttling valves and control valves. This material is very hard, but also very brittle, and slight pressure will cause fracture. It is therefore inadvisable to close these valves completely. Where both control and complete stoppage of flow are required, it is necessary to install throttling and stop valves in series. In some cases the cemented-carbide disks were replaced with stellite or hardened stainless steel, having less abrasive resistance but more toughness.

Two materials used for Bourdon tubes are straight 12 to 14 per cent chromium stainless steel and chromium-vanadium steel. Several chromium tubes failed after 5 days under hydrogen pressure. Tubes of similar material have been known to fail after short service in refinery operation because of corrosive attack of a deep cellular nature which causes excessive stress concentrations at tube corners. Fractures of the tubes in question also originated at corners of the cross section, and it is believed that similar attack occurred. Two of the chromium-vanadium tubes failed after 24 hr under hydrogen pressure. Fig. 9 illustrates a typical failure, in this case caused by corrosion fatigue. As a solution to this problem, tube-material specifications have been changed to a corrosion-resistant material, AISI type 316 stainless steel.

Welding. Welded pressure parts of equipment have to withstand the same service as welded tube joints. The proper preheat and postheat must be used regardless of how small the pressure

---

[9] Tool designed by the Bureau of Mines, patent applied for.

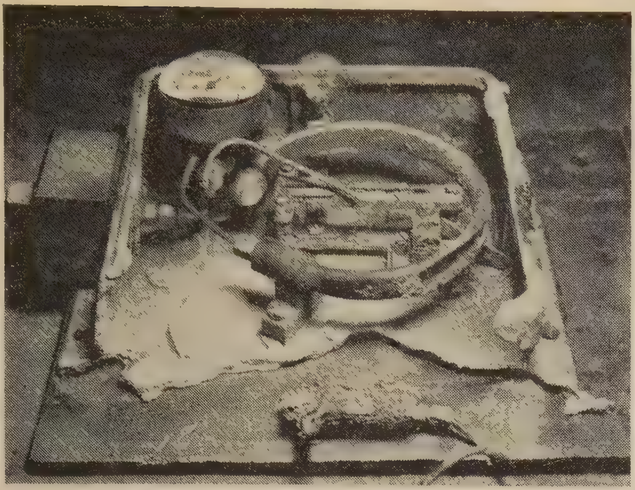

FIG. 9 BOURDON-TUBE ASSEMBLY AFTER RUPTURE FROM HYDROGEN PRESSURE OF 12,000 PSIG

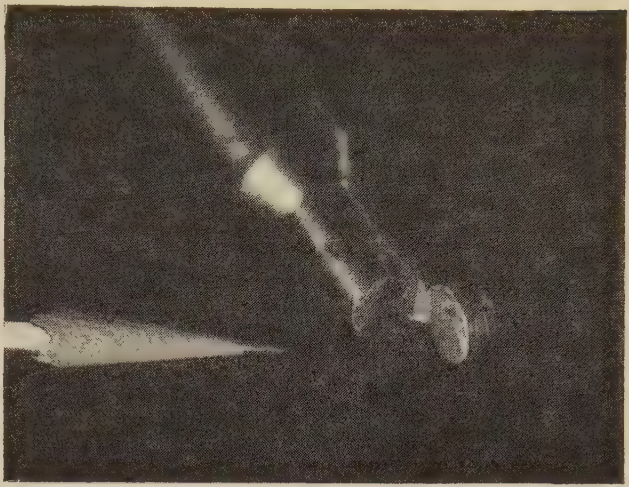

FIG. 11 COLLAPSED THERMOCOUPLE WELL

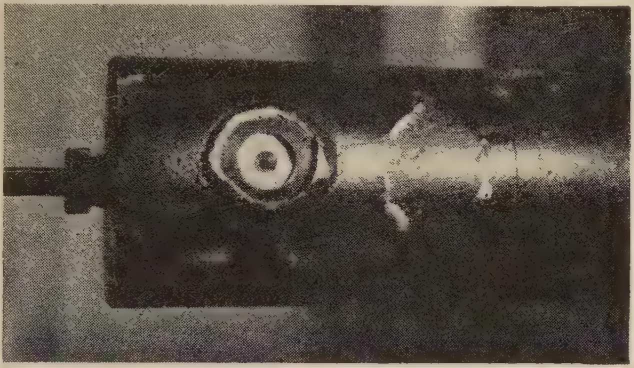

FIG. 10 FAILURE OF WELD ON AISI-1025 CARBON STEEL

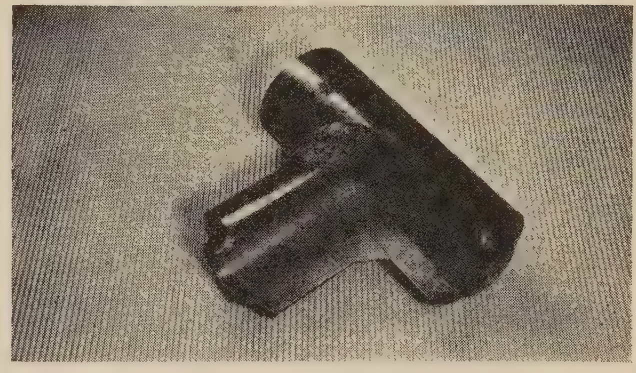

FIG. 12 WELDED TEE

part might be; the electrode and welding bevel must be suitable for the materials and the thicknesses involved. One of the most important requirements is qualification of the welding operator.

Fig. 10 shows the weld failure of a plug connection of a sample bomb made of AISI-1025 steel which possesses good weldability. When joining light sections to heavy sections, the heavier section must be preheated to obtain good fusion and to avoid quenching the weld. The single-bead-weld fracture displayed a very brittle structure which would indicate insufficient preheat.

Seal welds were one of the most frequent weld failures. Several plugs in heat-exchanger header blocks leaked after a short time under pressure, and numerous pump-block plugs leaked during the pump break-in period. In both cases the weld was too small. Regardless of the tightness of a mechanical seal, the heat of the seal weld will in most cases destroy the fit. A good practice is to employ a seal-weld design capable of withstanding full pressure and to disregard any advantage that may be derived by mechanical means.

Machining. Thermocouple wells of stainless steel were difficult to machine. Two sizes are required: $11^1/_4$ in. long × $^9/_{16}$ in. OD × $^3/_{16}$ in. ID and $9^5/_8$ in. long × $^9/_{16}$ in. OD × $^3/_{16}$ in. ID. Both sizes reduce down near the tip to $^5/_{16}$ in. OD × $^1/_8$ in. ID with a wall thickness of $^3/_{32}$ in. which is subjected to a collapsing pressure of 10,300 psig. The wells are turned from solid bars which are then drilled for the thermocouple leads. Drill drift resulted in eccentricity, thin walls, and subsequent failure as shown in Fig. 11. To eliminate the trouble, tips of all the wells were cut. Eccentric wells were rejected and concentric wells were reclaimed by welding repair. Replacements were made in two sections and welded together.

CONCLUSIONS

Experience gained in the construction of the hydrogenation demonstration plant evinces many possible improvements.

Some changes in materials and fabrication methods were made during the latter stages of construction. Most of these were effected because of a particular problem and have already been discussed. However, one change that was made to obtain better weldability and to lessen heat-treatment requirements was the use of AISI-4130, chromium-molybdenum steel for low-temperature tubing.

Investigation is being continued to find the most suitable materials to be used in contact with hydrogen at high pressures and temperatures.

One particular development in fabrication procedure is a welded-tee connection. This type of construction could be used to replace forged tees and thus eliminate two joints. An additional advantage is a close control of the material involved, Fig. 12.

Because of the seriousness of failures, one of the most stringent requirements in the construction of high-pressure and high-temperature plants is careful inspection. Materials must be thoroughly checked as to quality and suitability. Design must be commensurate with service conditions. Fabrication must be in accordance with the highest standards of workmanship.

Design of Preheaters and Heat Exchangers for Coal-Hydrogenation Plants

By P. W. LAUGHREY,[1] W. I. GWILLIM,[1] H. SCHAPPERT,[2] AND J. A. MARKOVITS[3]

The preheater and the heat-exchanger possibilities of the coal-hydrogenation process are described. Comparison has been made between the demonstration and the German plant equipment. Emphasis has been placed on the importance of developing applicable high-pressure heat exchangers for commercial-size plants, in order to eliminate the preheaters and increase the thermal efficiency of the process.

INTRODUCTION

An important step toward improving the economic aspect of the coal-hydrogenation process is to achieve high thermal efficiency. Various means have been suggested for a high thermal efficiency. Full utilization of the exothermic heat of reaction through an efficient heat-recovery system and proper preheater design become important in achieving this goal. Possible improvements in design and heat recovery are discussed herein.

PURPOSE OF PASTE PREHEATER

The function of the liquid-phase preheater is to raise the temperature of the coal paste-hydrogen mixture at 10,300 psi pressure from 250 F inlet temperature to about 815 F, before the mixture enters the converters. The reaction in the converters is highly exothermic. The amount of heat developed in the converters compares favorably with that necessary for preheating the paste to the reaction temperature. A summation of all of the reactions occurring in the converter during operations gives a mean heat of reaction of 800 Btu per lb of moisture and ash-free coal converted. This paste has about 40 per cent moisture and ash-free coal content (see Table 1), which means that 1 lb of moisture and ash-free coal makes 2.5 lb of paste. Gas is added to the paste in a ratio of about 16 standard cu ft per lb of paste. Therefore the preheating of this paste and gas requires the following heat quantities per pound of moisture and ash-free coal input:

$$\begin{aligned} 2.5 \times 0.54 \times (815\text{–}250) &= 770 \text{ Btu} \\ 40 \times 0.02 \times (815\text{–}100) &= 570 \text{ Btu} \\ \text{Total} &= 1340 \text{ Btu} \end{aligned}$$

From this computation it can be seen that the amount of heat needed for preheating the paste proper is approximately the same as the amount of the heat of reaction. It is obvious that with good heat exchange between feed and product, not only is no external heat needed, but a surplus of the major portion of the reaction heat must be removed. Consequently, with a good product-feed heat exchange, there would be no need of a preheater. A small preheater would be needed only for start-up, and the size of this preheater would depend entirely on the length of time to reach full operating conditions. However, it is known that in the German plants, the preheater, especially for subbituminous-coal operation, was a very large and expensive piece of equipment which transmitted a large quantity of heat to the paste. The reason for this fact is to be found, for the most part, in the properties of the coal paste.

PROPERTIES OF THE PASTE

The main property of the coal paste which may determine the design and size of the coal-paste preheater is the viscosity. The change of viscosity of paste with temperature is shown in Fig. 1. An analysis of coal paste is presented in Table 1.

TABLE 1 ANALYSIS OF ROCK SPRINGS COAL PASTE

	Weight per cent
Moisture and ash-free coal	36.4
Pasting oil (solids free)	55.4
Solids in pasting oil	6.5
Water	.3
Ash and catalyst	1.4
Total	100.0

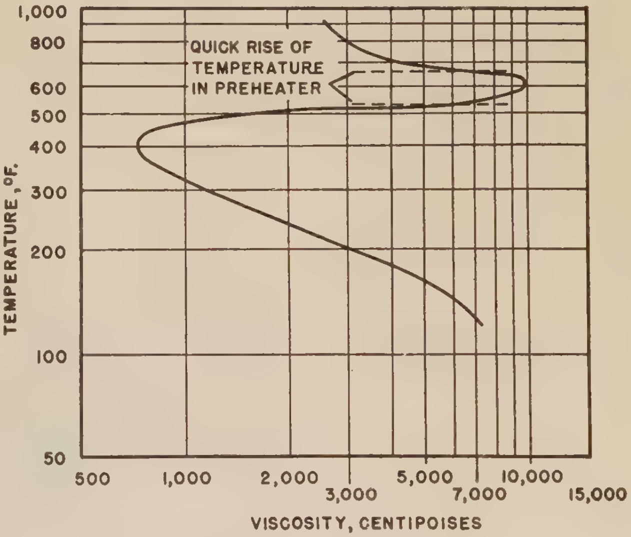

FIG. 1 VISCOSITY OF COAL-PASTE FEED

The products of hydrogenation, such as gasoline, Diesel oil, and the intermediate heavy-oil products, do not deviate from the ordinary behavior of natural hydrocarbons in regard to viscosity; but the coal paste has a singular behavior concerning viscosity, and this is caused by the swelling properties of the coal. The pulverized coal and the pasting oil are mixed, thereby surrounding each particle of coal with oil. The thickness of the oil film on the coal particles is determined by the ratio of pasting oil to coal and the sum of the entire surfaces of these coal particles. As long as the oil film has a certain thickness, the viscosity of the paste is determined mainly by the viscosity of the pasting oil; but within a certain range, the coal swells, and consequently the viscosity increases markedly. This happens even in the presence of hydrogen, because at the beginning of the heating cycle the temperature is too low for hydrogenation of the coal. At higher temperatures hydrogenation and liquefaction take place, and the viscosity begins to decrease. The factors affecting this peculiar behavior of the paste are: Origin of the coal, solids content of the paste, fineness of the coal particles, and asphalt content of the pasting oil. In general, younger coals do not exhibit as marked a viscosity change in the swelling range. Increase of all the other factors mentioned tends to promote an increased viscosity of the paste in the swelling range.

---

[1] Chemical Engineer, Coal-to-Oil Demonstration Branch, Office of Synthetic Liquid Fuels, Bureau of Mines, Louisiana, Mo.

[2] Special Engineer, Koppers Company, Inc., Louisiana, Mo.

[3] Assistant Chief, Coal-to-Oil Demonstration Branch, Office of Synthetic Liquid Fuels, Bureau of Mines.

Contributed by the Petroleum Division and presented at the Petroleum Mechanical Engineering Conference, Oklahoma City, Okla., October 2–5, 1949, of THE AMERICAN SOCIETY OF MECHANICAL ENGINEERS.

NOTE: Statements and opinions advanced in papers are to be understood as individual expressions of their authors and not those of the Society. Paper No. 49—PET-1.

Obviously, at a high viscosity of the paste, the heat transfer in the preheater is poor, and at a low viscosity it is good. Translating this viscosity effect into a more usable term, that of paste-film coefficient, the curve shown in Fig. 2 results. In the swelling-temperature range the paste-film coefficient reaches a minimum, and it improves with the beginning of the liquefaction. Since the tube-wall temperatures of the preheater are calculated by means of the paste-film coefficient, a knowledge of the values of this coefficient is very important. Characteristics of pastes derived from the various types of U. S. coals will be investigated in the preheater of the demonstration plant.

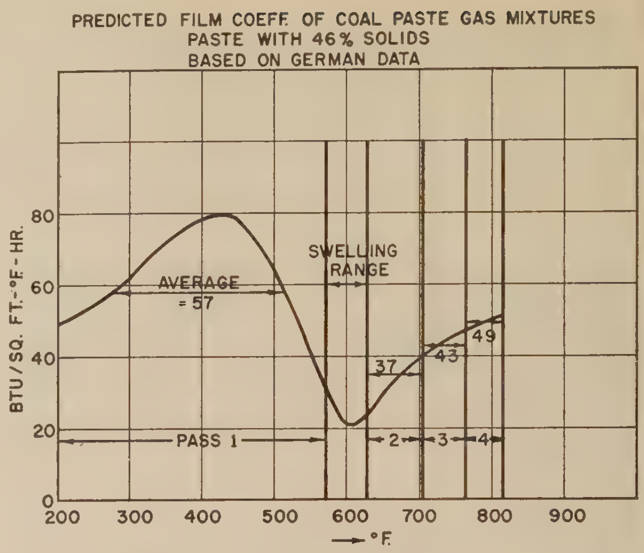

Fig. 2 Predicted Film Coefficients of Coal Paste

Description of Paste Preheater

An isometric drawing of the paste preheater is shown in Fig. 3. Because of the unusual viscosity and heat-transfer characteristics of the paste, which have been described, the paste preheater was designed with four separate cells, which are fired independently for optimum temperature control. It will be noted from the drawing that eight vertical hairpins are contained in each cell. The $2^1/_2$-in-ID hairpins are surrounded with a 5-in-ID steam jacket, and the steam-jacket tube is exposed to radiant heat. The high-pressure tube is made of type-316 stainless steel, and the steam tube is made of 4 to 6 per cent chrome, and $^1/_2$ per cent molybdenum steel with dimensions as shown. The steam jacket promotes equal distribution of heat throughout the circumference of the high-pressure tube and aids in controlling the tube-metal temperatures.

Design data for the paste preheater applicable to operation on Rock Springs coal are given in Table 2.

Operation of Paste Preheater

The paste, with a small amount of gas, enters the first cell of the preheater. Addition of the gas improves the flow conditions, and therefore, the heat transmission. Between the first and second cells of the preheater, at about 570 F paste temperature, two outside streams are introduced into the paste. One is a hot stream of hydrogen at 710 F. The other stream is a heavy solids-containing oil, called "heavy-oil letdown" (HOLD). This latter stream flows hot (775 F) directly from the bottom of the hot

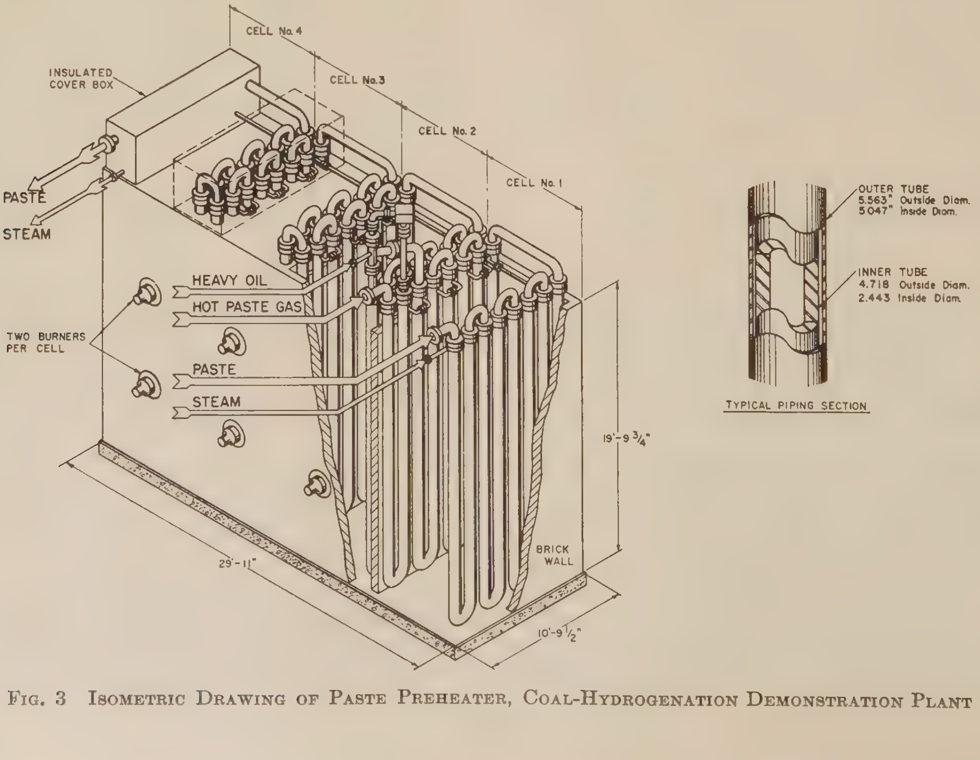

Fig. 3 Isometric Drawing of Paste Preheater, Coal-Hydrogenation Demonstration Plant

TABLE 2 DESIGN DATA FOR PASTE PREHEATER (ROCK SPRINGS COAL)

	Maximum design conditions
Heat duty, Btu per hr:	
Paste	6560000
Gas	180000
Total	6740000
Quantity input, lb per hr:	
Coal paste at 250 F	20183
Heavy oil letdown at 775 F	2500
Hot paste gas at 710 F	3500
Total	26183
Steam into jacket (400 psig at 700 F), lb per hr	550
Inlet pressure, psig	10000
Maximum working pressure, psig	10300
Pressure drop, steam, psig	200–220
Firebox temperature, deg F	1400
Flue-gas temperature leaving furnace, deg F	1200
Heat fired, Btu per hr	10400000
Furnace efficiency, per cent	65

catchpot and is boosted with a surge-type pump. The injection of these two hot streams produces a sharp temperature rise in the paste to about 630 F, thereby causing the paste to pass over the swelling range of the coal quickly. Also, enough hydrogen is introduced into the paste to start the liquefaction of the coal.

The velocity in the coal-paste preheater is an important design factor. For the foregoing design conditions the velocities are cell No. 1, 3 fps; cell No. 2, 8.5 fps; cell No. 3, 9 fps; cell No. 4, 9.5 fps.

The velocity in the last three cells is increased owing to the addition of the hot gas and heavy-oil let-down. In the German plants, experience showed that a velocity of 15-20 fps was quite suitable for 4-in-ID preheater tubes. This velocity range assured a uniform flow of paste throughout the preheater, was under the erosion limit of approximately 25 fps, and did not cause an excessive pressure drop across the preheater.

Operating conditions for Rock Springs coal have been established, and various temperatures in the preheater under these conditions have been calculated as shown in Fig. 4. Fig. 5 shows that even if some coking of the tubes should occur, only a slight decrease in throughput is required to maintain tube-metal temperatures below the maximum allowable, 1000 F.

The throughput of various coals in the demonstration plant will vary according to the ease of hydrogenation, and therefore the design velocities in the paste preheater are purposely rather low, in order to accommodate coals that hydrogenate easily. The demonstration-plant preheater is, therefore, suitably designed to solve all the problems involved in experimentation with all varieties of American coals.

Large-Scale Paste-Preheater Installations

All German preheaters were of the convection type. Tubes were arranged vertically in the form of hairpins in narrow cells in which flue gas was circulated at fairly high velocity. These hairpins were finned tubes with an outside:inside surface ratio of 20:1, to compensate for the low film heat-transfer coefficient on the flue-gas side. Tube-metal temperatures were controlled by regulating the quantity and temperature of the circulated flue gas.

A plan view of such a preheater is shown in Fig. 6. The inlet connections for heavy-oil and hot paste gas, shown in this drawing, indicate that the swelling range of the coal in this preheater was bridged in a similar manner to that in the preheater of the demonstration plant.

All things being equal, such as duty and maximum allowable tube-metal temperature, the total heating-surface requirement, based on inside area of the high-pressure tube is approximately the same for the finned-tube convection-type, the radiant-type, or the steam-jacketed radiant-type preheater of the demonstration plant. The reason for this fact is that the paste film represents 80 to 90 per cent of the total resistance to heat flow; therefore it is the determining factor in calculating the total surface requirement. The resistance to heat flow on the outside of the high-pressure tubes is lowered by the compensatory highly finned surface in the convection type, and the high-velocity steam flow in the steam-jacketed radiant type. A proper selection of a preheater for large-scale installations, therefore, must discard the convection type because of the added capital cost of fabricating the finned surfaces and the auxiliary equipment such as ducts and blowers. In comparing the conventional radiant type with the steam-jacketed radiant-type preheater, the operational features of the latter such as uniformity of heat distribution, prevention of coking, and optimum process control, must outweigh its slightly greater cost. It is conceivable that in the plant of the future a

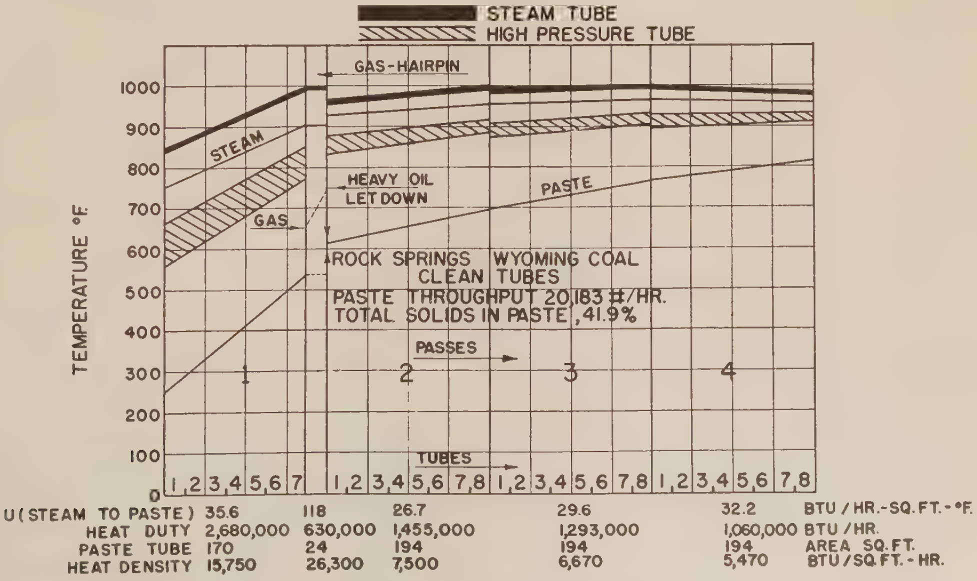

Fig. 4 Calculated Temperature Gradient With Clean Tubes, Paste Preheater, Coal-Hydrogenation Demonstration Plant

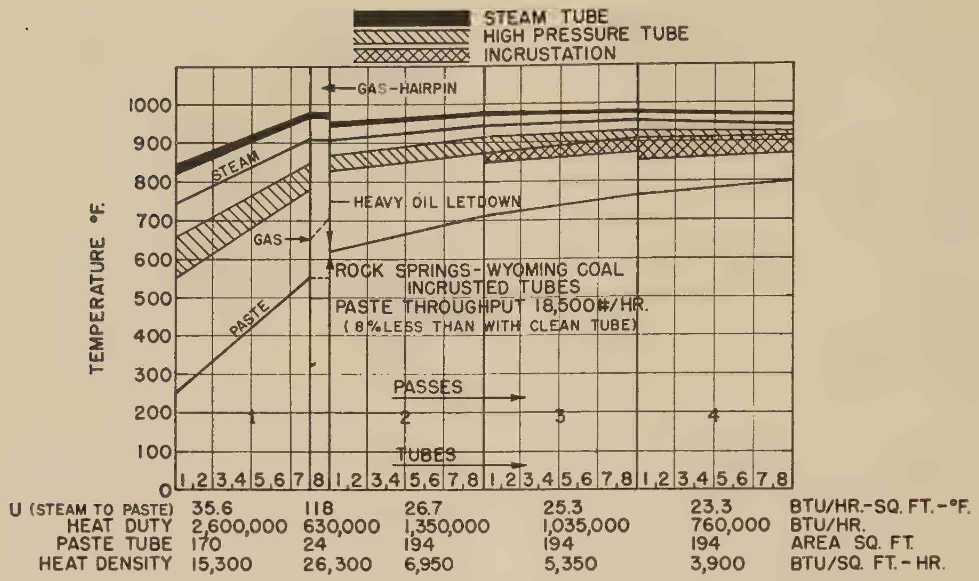

Fig. 5 Calculated Temperature Gradient With Incrusted Tubes, Paste Preheater, Coal-Hydrogenation Demonstration Plant

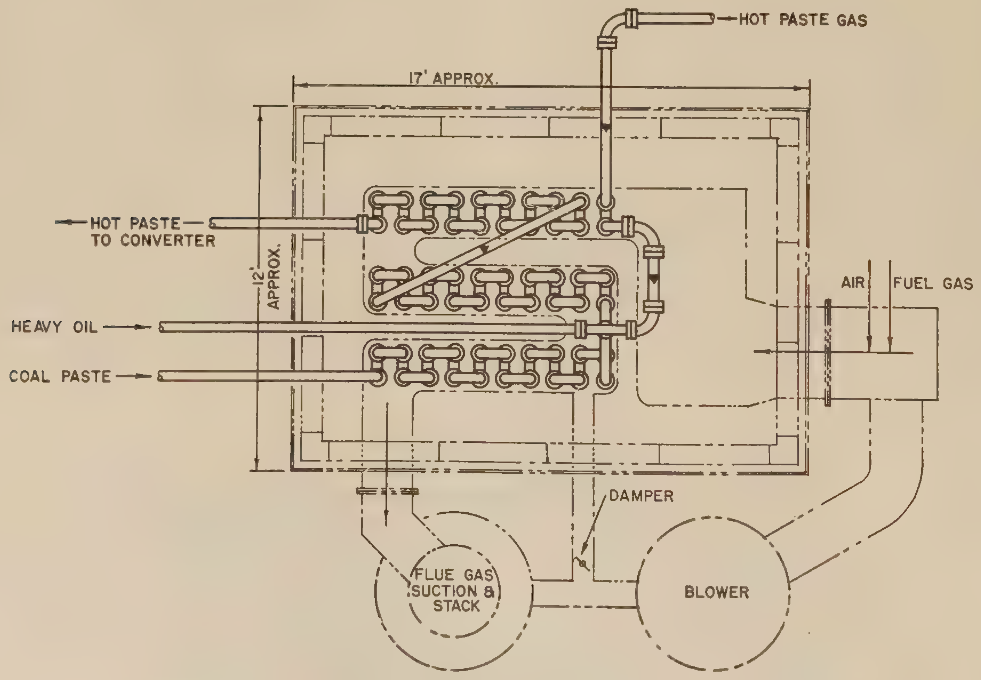

Fig. 6 Plan View of Convection-Type Preheater

conventional radiant-type preheater with low heat densities would be feasible. It can be designed along the following lines: The multicelled setting would take the form of a long, rectilinear box with hairpin tubes suspended from the roof in the center of the box. Firing would take place on each side of the box with short-flame burners and good burning characteristics, permitting wide variations in firing rate, with minimum percentages of excess air.

Vapor-Phase Preheater

For the first time in coal hydrogenation at 10,000 psig, a radiant-type preheater is used in the vapor-phase hydrogenation demonstration plant. This preheater is gas-fired, contains thirty $1^1/_4$-in-ID type 316, stainless-steel horizontal tubes arranged in two parallel streams, and has a design duty of 1,890,000 Btu per hr. Feed to the preheater consists of middle oil from the liquid-phase operation (620 F end point), and recycle oil from the vapor-phase distillation, which, together with hydrogen, comes from the product-feed exchanger with a temperature of about 780 F to the preheater. The preheater superheats the oil vapors to reaction temperature or to about 900 F.

Design data for the vapor-phase preheater are given in Table 3.

TABLE 3 DESIGN DATA FOR VAPOR-PHASE PREHEATER

	Maximum design conditions
Heat duty, Btu per hr	1890000
Quantity input, lb per hr—vapor	15650
Inlet pressure, psig	10300
Maximum working pressure, psig	10300
Pressure drop (estimated), psig	430
Firebox temperature, deg F	1450
Flue-gas temperature leaving furnace, deg F	1200
Heat fired, Btu per hr (max)	2910000
Furnace efficiency, per cent	65

Both the liquid- and vapor-phase preheaters were furnished by Alcorn Combustion Company, Philadelphia, Pa.

Heat Exchangers

The foregoing discussion shows how important it is to provide good heat exchange and how necessary it is to utilize fully the heat of reaction in the converters. The demonstration plant, however, was purposely not designed for maximum heat recovery, since the additional expense could not be justified in such a small plant. There are 40 heat exchangers in the plant. Thirty-one exchangers are designed for low-pressure service in the distillation and storage areas. Nine exchangers are designed for 700-atm operation in the liquid- and vapor-phase hydrogenation. All except the HOLD cooler are double-pipe exchangers, and only two of these high-pressure exchangers service process streams with the full 10,300 psi in both tubes. The wall thickness of the inside tube in these two exchangers is only 8 gage. It is designed for a differential pressure of 2000 psi so that testing and starting has to be done with both tubes under pressure. The other high-pressure exchangers are designed with full 10,300 psi operating pressure on the inside tube, the outside tube consisting of a low-pressure tube jacket in which either cooling water or low-pressure oil is flowing. The tube jackets are constructed of carbon steel, and the high-pressure tubes of 8-10 per cent chrome and $^1/_2$ per cent molybdenum alloy. The HOLD cooler is a forced-draft air cooler with eight hairpins, made with Croloy-9M tubes, 30 ft long and 1 in. ID, connected in series flow. The cooling air passes downward at 58 fps through a 64-in. × 10-in. rectangular duct enclosing the hairpins. All exchangers in high-pressure service were supplied by Industrial Engineers, Inc., Los Angeles, Calif.

The demonstration plant was designed in order that the following information may be obtained: (1) Heat balances to determine where the different heat quantities occur and in what relationship they occur; (2) the type of heat-exchange equipment most suitable for a particular heat-exchange job; and (3) determination of film heat-transfer coefficients and fouling factors. This information will be obtained on only the high-pressure equipment, since heat-exchange design in the low-pressure area follows conventional petroleum-refinery practice. All of the points mentioned must be investigated with the view of obtaining design data for commercial plants. As an example of the type of information to be obtained, a heat balance around the liquid-phase stall of the demonstration plant has been calculated as shown in Table 4 and summarized in Fig. 7.

Although this heat balance is applicable to the demonstration plant, the heat ratio of the top and bottom products will be maintained in commercial plants. This ratio is approximately 12,000,000 : 3,000,000 Btu per hr or 4 to 1. Heat exchange can best be carried out on the top product. The heat balance shows that the heat contained in the top product is sufficient to supply the following requirement:

Heat required:	
3793 lb per hr hydrogen	2,750,000
20,183 lb per hr paste (preheater)	6,740,000
Total	9,490,000
Heat available from top product of the hot catchpot, Btu per hr	12,280,000

It can be seen that the heat required is only about 75 per cent of the heat available. The problem is how to utilize fully this heat, and one answer to the problem may again be found in later German developments. These developments introduced a heat-exchange procedure in which two paste streams of different solids content were used. Thick paste with a total solids content of 53 per cent was heated in an exchanger train up to its swelling tem-

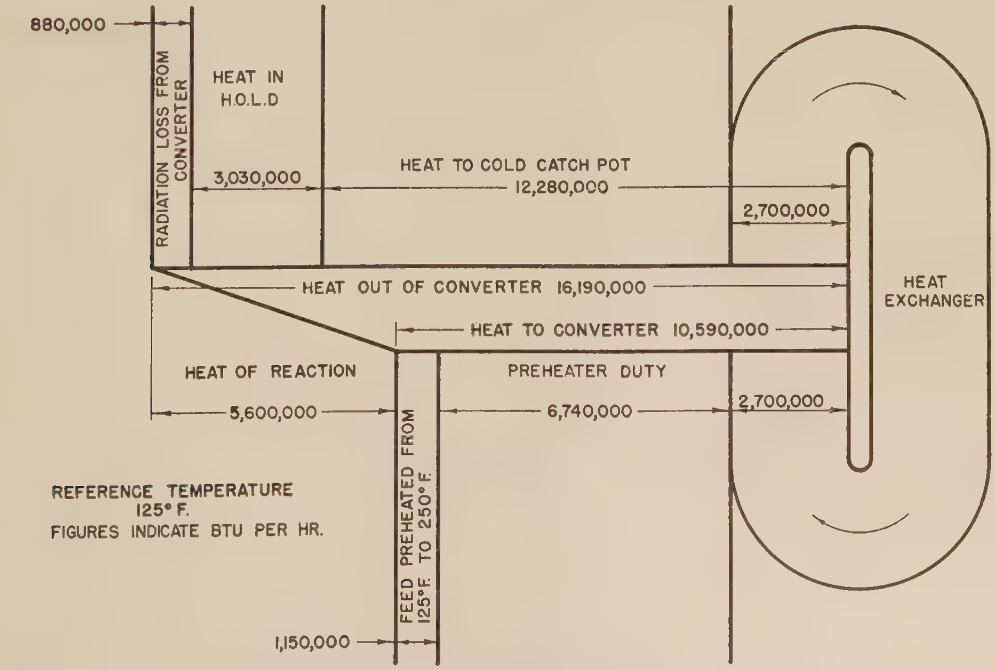
880,000
RADIATION LOSS FROM CONVERTER
HEAT IN H.O.L.D
3,030,000
HEAT TO COLD CATCH POT
12,280,000
2,700,000
HEAT OUT OF CONVERTER 16,190,000
HEAT EXCHANGER
HEAT TO CONVERTER 10,590,000
HEAT OF REACTION
5,600,000
PREHEATER DUTY
6,740,000
2,700,000
REFERENCE TEMPERATURE 125° F.
FIGURES INDICATE BTU PER HR.
FEED PREHEATED FROM 125°F. TO 250°F.
1,150,000

Fig. 7 Heat Balance Around Liquid-Phase Stall

TABLE 4 HEAT BALANCE—LIQUID-PHASE STALL COAL-HYDROGENATION DEMONSTRATION PLANT, ROCK SPRINGS COAL

(Reference temperature, 125 F)

Heat in				
	lb per hr	spec. heat	Δt deg F	M Btu per hr
Feed preheat:				
Paste.	20183	0.44	(250–125)	1100
Paste gas (H_2).	293	1.31	(250–125)	50
Recirculated gas (H_2 by heat exchange. .	3500	1.31	(710–125)	2700
Preheater duty.	. . . .	. . . .	(800–250)	6740
Cooling gas (H_2).	2220	1.31	(125–125)	. . .
Total heat into converter.				10590
Heat of reaction.	. . .	. . .	. . .	5600
Total.	26196			16190

Heat out				
Heat to cold catchpot (hot catchpot overhead)	lb per hr	Spec. heat	Δt deg F	M Btu/hr
Liquid-oil product.	10775	0.62	(880–125)	5080
Hydrogen-gas product.	1297	0.76	(880–125)	750
Unreacted H_2 gas.	3375	1.31	(880–125)	3400
Water formed in reaction.	660	1300 Btu per lb		860
Cooling gas (H_2).	2220	1.31	(880–125)	2190
Total.	18327			12280
Heat in HOLD (Hot catchpot bottoms).	7869	0.57	(800–125)	3030
Total.	26196			15310
Radiation loss.				880
Total.	26196			16190

perature of 570 F. A thin paste with 42 per cent solids content made by diluting the thick paste with pasting oil, was heated in another exchanger train up to full reaction temperature with no difficulty. These two streams were then combined, and the remaining heat supplied in a small preheater. This procedure was not as advantageous as it should have been because of wide fluctuations in solids content of the various paste batches due to poor mixing technique.

It is anticipated in a projected 30,000-bbl per day coal-hydrogenation plant that a nearly perfect heat exchange can be achieved using a single paste with 47 per cent total-solids content. To do this, however, improved mixing controls must be introduced in order to insure a constant quality of paste. The preparation of the coal must also be such that all fines are eliminated from the process coal. These may be burned in the power plant. The heat-exchange system for the 30,000-bbl per day plant is shown in Fig. 8. The paste flow is divided into two streams, in such a manner that the larger stream (approximately 75 per cent), is heated up in exchangers to the reaction temperature without a preheater. The smaller stream is heated in exchangers to as high a temperature as the remaining heat will allow, and further heat requirement is supplied with a small preheater. The extent of improvement by carrying out the foregoing procedure can be shown by comparison with conventional German design, that is, 3 times the German throughput can be obtained with the same number of preheaters of smaller duty.

Since the total heat requirement of the process can be supplied from the top products of the hot catchpot, the question arises as to how the heat from the bottom products can be used economically. There are several considerations as follows:

1 In the demonstration plant, the feasibility of a flash distillation of the heavy-oil let-down (HOLD) will be determined. Therefore it may be possible that in larger plants the bottom product of the hot catchpot may be flash-distilled without cooling.

2 If it becomes necessary to cool the HOLD for other treatment, such as centrifuging, steam can be produced by jacketing the HOLD lines.

3 If there is no need or demand for steam, the temperature can be lowered by a combination of air-and-water cooling.

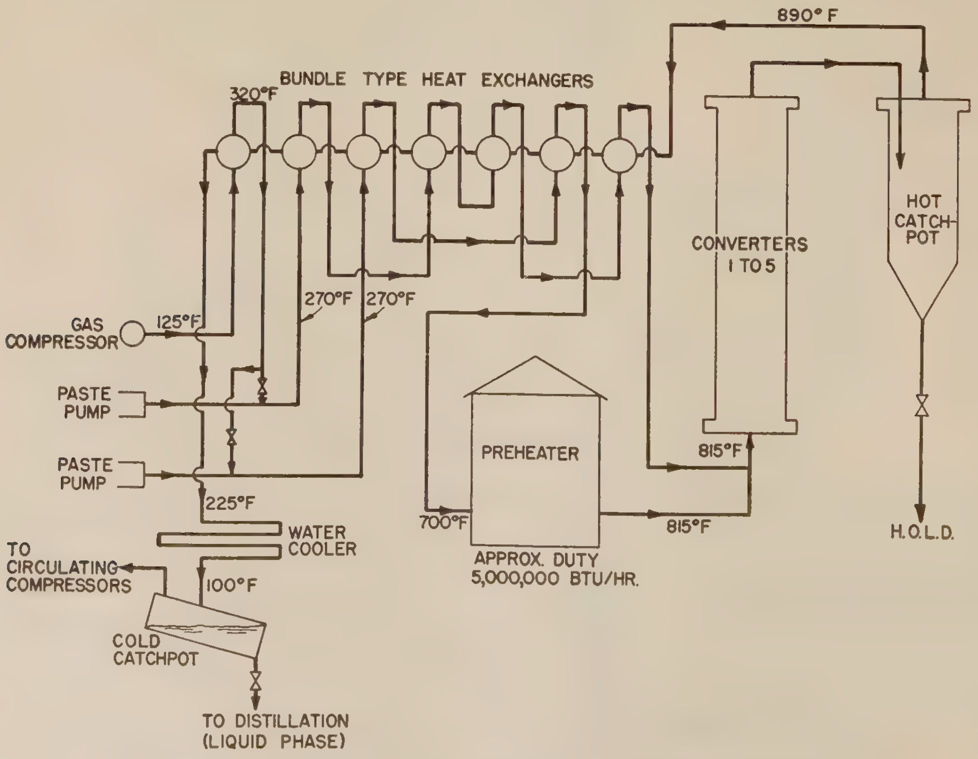

Fig. 8 Proposed Heat-Exchange System for Commercial Plant

There is no hot catchpot in the vapor-phase hydrogenation plant, and the heat of reaction is very high. Therefore a better heat exchange can be established in the vapor phase than in the liquid phase. The vapor-phase section can be operated without any external heat supply. Only a small preheater is necessary for starting-up operations.

The heat exchangers which were used in Germany were the shell-and-tube type designed for 10,000 psig operating pressure and placed in a vertical position. The bundle was inserted in a high-pressure internally insulated vessel and connected outside by means of a stuffing box on the top of the heat exchanger. The paste-feed stream flowed outside the tubes from bottom to top, and the product inside the tubes from top to bottom. The center-to-center distance of the tubes was determined by fabricating limitations and by the composition of the paste feed, that is to say, by the clogging tendency of the paste to form bridges between the tubes. A single design and size were used in both liquid-phase and vapor-phase operation. The tubes of this exchanger were designed for the full operating pressure of 10,000 psig. The bundle was designed with 199 tubes, (0.55 in. ID × 0.91 in. OD), about 57 ft long, for use in a high-pressure vessel of 22 in. ID. The average heating surface was 2150 sq ft. Originally, forged shells were used, but later designs were based upon wrapped or spiral-wound construction.

In designing high-pressure heat exchangers for commercial plants, consideration has to be given to: (1) The thickness and material of the tube walls; (2) the minimum distance between center to center of the tubes; (3) pressure difference of the gas-recycle compressors, in order to determine the cross section of the heat-exchanger bundle; and (4) equal distribution of the product and the feed through the heat exchanger.

In special cases, for instance, with the heavy-oil letdown, double-pipe exchangers are quite effective. The HOLD stream flows through the tubes and the medium to be heated through the annular space. These double-pipe exchangers for 700-atm design pressure are cumbersome, owing to the extreme wall thickness.

Film Heat-Transfer Coefficients

Film heat-transfer coefficients of all gases increase greatly with pressure at constant linear velocity, as shown in the calculated example for pure hydrogen in Table 5. This, combined with the fact that the thermal conductivity of hydrogen is about 10 times that of other gases such as nitrogen, carbon monoxide, and carbon dioxide, makes for high film coefficients in coal-hydrogenation heat-exchange equipment.

TABLE 5 EFFECT OF PRESSURE ON FILM HEAT-TRANSFER COEFFICIENT OF PURE HYDROGEN

	Pressure		
	1 atm	20 atm	700 atm
Standard cu ft per hr at 60 F	1000000	1000000	1000000
Cu ft per hr at flow	1000000	56000	2250
Pounds per hour	5320	5320	5320
Density, lb per cu ft	0.00532	0.095	2.36
Pipe ID, in.	32.0	7.5	1.5
Linear velocity, fps	50	50	50
Mass velocity, lb per sec-ft^2	0.266	4.75	118
Calculated film heat-transfer coefficient, Btu per hr-ft^2-deg F	9	115	2100

The principal consideration in determination of the film coefficient of the gas streams is the hydrogen purity, due to the effect of the high thermal conductivity of hydrogen on the film-transfer coefficient. Since the film coefficient for hydrogen-containing gases is high, especially at 700 atm, the use of the correct fouling factor also becomes very important. Fouling is quite rapid on new exchangers; therefore a film coefficient of about 110 Btu/hr-ft^2-deg F for hydrogen of 80-90 per cent purity flowing at a velocity of about 15 fps, is a reasonable design figure.

Since coal paste is always heated up in the presence of hydrogen, its high thermal conductivity increases the film coefficient of the paste. The film coefficient is highly dependent on the solid concentration of the paste, and also on the fineness of the pulverized coal, but the fact was established in Germany that the film coefficient for the same paste was higher in the heat exchangers than in the preheater within the same temperature range. This effect was contributed to a better flow distribution through the heat-exchanger bundle. The film-coefficient values varied from 80-120 Btu/hr-ft^2-deg F in the paste heat exchangers with a paste velocity of 8 fps.

Film coefficients range from 130-160 Btu/hr-ft^2-deg F for middle oil and hydrogen in the relative portions used in vapor-phase hydrogenation where 15 to 30 cu ft of hydrogen is used per lb of oil at velocities from 6 to 15 fps. This range applies after a few months of operation.

The film coefficients for heavy-oil letdown (HOLD) have been determined from German data on air coolers. This coefficient varies with solids and asphalt content of the HOLD, but an average figure for this coefficient is 90 Btu/hr-ft^2-deg F at velocities ranging from 9 to 15 fps and at temperatures above 400 F.

The German data quoted in this report were useful in designing the demonstration plant, and it is hoped that the operation of the plant will furnish the necessary information on all varieties of American coals. When these data are determined, perhaps an ideal heat-exchange system for future big-scale plants can be designed in both phases, and the use of both preheaters will become obsolete.

A Simple Hydrodynamic Thrust Bearing

By F. R. ARCHIBALD,[1] PRINCETON, N. J.

Considerable mathematical difficulty has handicapped the designer in the application of the hydrodynamic theory of lubrication. This difficulty arises essentially from the shapes assumed by the oil films. In 1918 Lord Rayleigh gave a detailed analysis of the simple slider bearing, neglecting the side-leakage effect, in which he determined that the greatest load capacity occurs when the slider element gives a stepped convergence to the oil film. From the simple geometry of this oil film, a solution, taking account of side leakage, might be obtained fairly easily. The author proves this to be so, and gives solutions for the case of rectilinear motion with finite bearing width, and also the more practical sectorial case of a thrust bearing.

APPLICATIONS of the theory of lubrication have been handicapped by the considerable mathematical difficulties encountered in the solution of practical problems. Even in the elementary case of a flat inclined plate of finite width, the solution, given by A. G. M. Michell, is so difficult as to discourage much hope for the solution of many other practical problems.

Much of the mathematical difficulty arises from the shapes taken by oil films. Therefore, if a bearing can be devised in which the oil film has a simple shape there is a good prospect that an analytical solution can be given for its performance.

It might be thought impossible to obtain an oil-film shape simpler than that given by the inclined flat plate, but there is such a shape. At least there is a configuration much simpler to deal with in the lubrication problem.

In 1918 Lord Rayleigh[2] gave a detailed analysis of the simple slider bearing neglecting the side-leakage effect. He considered various shapes for the surface of the slider element. After showing very slight improvement in the load capacity when the slider surface was curved instead of being flat, he then set the variational problem to find the best possible shape from the point of view of load capacity. The result of this analysis was to show that greatest load capacity occurs if the slider element is made as shown in Fig. 1, giving a stepped convergence to the oil film.

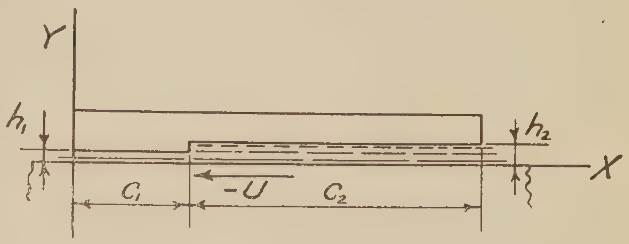

FIG. 1

The results of the flat inclined slider-bearing calculation, when side leakage is neglected, are well known. For a given viscosity, speed, length of slider, and minimum film thickness, μ, U, c, and h_1, respectively, the maximum load per unit width is given by

$$W_{\max} = \frac{0.160\mu U c^2}{h_1^2}$$

With the shape given by Rayleigh it is possible to have a maximum load per unit width of

$$W_{\max} = \frac{0.206\mu U c^2}{h_1^2}$$

This is about 29 per cent greater than for the inclined flat-plate bearing.

It would appear that with the simple geometry of this oil film, a solution, taking account of side leakage, might be fairly easy to obtain. This turns out to be so and solutions are given both for the case of rectilinear motion with finite bearing width and also the more practical sectorial case of a thrust bearing.

CASE WITH NO SIDE LEAKAGE

Before proceeding to the more complicated three-dimensional problem the case with no side leakage might be considered to advantage. The "calculus of variations" is perhaps not familiar to many who may be interested in the problem, and in any event this method of solution is available in Rayleigh's more elegant paper. Therefore the results will be obtained by the usual methods, but starting with the stepped-film shape. The notation will be the same as in Rayleigh's paper.[2]

From a consideration of the shear stress and velocity gradient in the film it is easily shown that

$$\frac{\partial^2 u}{\partial y^2} = \frac{1}{\mu}\frac{dp}{dx} \quad \ldots\ldots\ldots\ldots [1]$$

Upon integrating this equation twice with respect to y and substituting the boundary conditions; $u = -U$ when $y = 0$, and $u = 0$ when $y = h$, the following expression for u is obtained

$$u = \frac{y^2 - hy}{2\mu} - \left(1 - \frac{y}{h}\right)U \quad \ldots\ldots\ldots\ldots [2]$$

By integrating this expression over the film thickness the flow per unit width is obtained as

$$-Q = -\frac{1}{12}\frac{h^3}{\mu}\frac{dp}{dx} - \frac{1}{2}Uh \quad \ldots\ldots\ldots\ldots [3]$$

This same expression for flow in the X-direction is obtained in the side-leakage problem, but in this case it is the rate of flow at a point rather than over a unit width. A partial derivative of p with respect to x is also necessary in this case. Because this relation is needed in the three-dimensional problem it will be given here

$$-q_x = -\frac{1}{12}\frac{h^3}{\mu}\frac{\partial p}{\partial x} - \frac{1}{2}Uh \quad \ldots\ldots\ldots\ldots [3a]$$

From Equation [3]

$$\frac{dp}{dx} = \frac{6\mu U}{h^3}\left(\frac{2Q}{U} - h\right)$$

---

[1] School of Engineering, Princeton University.

[2] "Notes on the Theory of Lubrication," by Lord Rayleigh, *Philosophical Magazine*, vol. 35, 1918, pp. 1–12.

Contributed by the Research Committee on Lubrication and the Petroleum Division and presented at the Annual Meeting, New York, N. Y., November 27–December 2, 1949, of THE AMERICAN SOCIETY OF MECHANICAL ENGINEERS.

NOTE: Statements and opinions advanced in papers are to be understood as individual expressions of their authors and not those of the Society. Paper No. 49—A-29.

Call

$$\frac{2Q}{U} = H$$

Then

$$\frac{dp}{dx} = \frac{6\mu U}{h^3}(H - h) \qquad [4]$$

If h is constant this equation can be integrated to give the pressure as follows

$$p = \frac{6\mu U}{h^3}(H - h)x + A \qquad [5]$$

The evaluation of A depends on the boundary conditions. It is convenient here (and more so in the three-dimensional problem) to consider the problem for each stepped region separately. The co-ordinate axis being left as in Fig. 1 for region (1) and being moved forward by $(c_1 + c_2)$, i.e., to the leading edge, for region (2).

For region (1) when $x = 0$, $p = 0$ and $A = 0$

$$\therefore p = \frac{6\mu U}{h_1^3}(H - h_1)x \qquad [6]$$

For region (2), when $x = 0$, $p = 0$, and $A = 0$

$$\therefore p = \frac{6\mu U}{h_2^3}(H - h_2)x \qquad [7]$$

The pressure given by Equation [6] when $x = c_1$ is the same as that given by Equation [7], when $x = -c_2$

$$\frac{6\mu U}{h_1^3}(H - h_1)c_1 = -\frac{6\mu U}{h^3_2}(H - h_2)c_2$$

which upon solving for H gives

$$H = \frac{h_1h_2(c_1h_2^2 + c_2h_1^2)}{c_1h_2^3 + c_2h_1^3} \qquad [8]$$

The load for each region is obtained by integrating the pressure over the areas as follows:

For region (1)

$$W_1 = \int_0^{c_1} pdx = \frac{6\mu U}{h_1^3}(H - h_1)\int_0^{c_1} xdx = \frac{3\mu U}{h_1^3}(H - h_1)c_1^2 \qquad [9]$$

For region (2)

$$W_2 = \int_{-c_2}^{0} pdx = \frac{6\mu U}{h_2^3}(H - h_2)\int_{-c_2}^{0} xdx = \frac{3\mu U}{h_2^3}(h_2 - H)c_2^2 \qquad [10]$$

The total load, $W = W_1 + W_2$

$$\therefore W = 3\mu U\left[\left(\frac{H - h_1}{h_1^3}\right)c_1^2 + \left(\frac{h_2 - H}{h_2^3}\right)c_2^2\right]$$

$$= 3\mu U\left[H\left(\frac{c_1^2}{h_1^3} - \frac{c_2^2}{h_2^3}\right) + \frac{c_2^2}{h_2^2} - \frac{c_1^2}{h_1^2}\right] \qquad [11]$$

If H from Equation [8] is now placed in Equation [11] the load is obtained as a function of the parameters

$$W = 3\mu U\left[\frac{h_1h_2(c_1h_2^2 + c_2h_1^2)}{c_1h_2^3 + c_2h_1^3}\left(\frac{c_1^2h_2^3 - c_2^2h_1^3}{h_1^3h_2^3}\right) + \frac{c_2^2h_1^2 - c_1^2h_2^2}{h_1^2h_2^2}\right]$$

This expression for W will simplify to

$$W = 3\mu U\, c_1c_2(c_1 + c_2)\frac{h_2 - h_1}{c_1h_2^3 + c_2h_1^3} \qquad [12]$$

If the total length of the bearing $c = (c_1 + c_2)$, and the minimum film thickness h_1, are prescribed, the proportions for maximum load capacity can be found as follows

$$c_2 = c - c_1, \quad \text{and let} \quad h_2 = kh_1$$

Then

$$W = \frac{3\mu U\, cc_1(c - c_1)(k - 1)}{h_1^2[c_1(k^3 - 1) + c]}$$

$W = f(c_1, k)$ and will have a maximum when $\partial W/\partial c_1 = 0$ and $\partial W/\partial k = 0$

$$\frac{\partial W}{\partial c_1} = \frac{3\mu U\, c(k - 1)}{h_1^2} \times \left\{\frac{[c_1(k^3 - 1) + c](c - 2c_1) - c_1(c - c_1)(k^3 - 1)}{[c_1(k^3 - 1) + c]^2}\right\} \qquad [13]$$

For $\partial W/\partial c_1 = 0$ it is sufficient that

$$[c_1(k^3 - 1) + c](c - 2c_1) - c_1(c - c_1)(k^3 - 1) = 0$$

which will reduce to

$$k^3 = \left(\frac{c - c_1}{c_1}\right)^2 \qquad [14]$$

$$\frac{\partial W}{\partial k} = \frac{3\mu U\, c_1c(c - c_1)}{h_1^2}\left\{\frac{c_1(k^3 - 1) + c - 3(k - 1)c_1k^2}{[c_1(k^3 - 1) + c]^2}\right\}$$

For $\partial W/\partial k = 0$ it is sufficient that

$$c_1(k^3 - 1) + c - 3(k - 1)c_1k^2 = 0$$

which will reduce to

$$c_1 = \frac{c}{1 - 3k^2 + 2k^3} \qquad [15]$$

From Equation [14]

$$c = c_1(k^{3/2} + 1)$$

Substituting in Equation [15]

$$c_1 = \frac{c_1(k^{3/2} + 1)}{1 - 3k^2 + 2k^3}$$

which will reduce to

$$4k^3 - 12k^2 + 9k - 1 = 0$$

The three roots of this equation are

$$k = 1 \text{ and } k = 1 \pm \sqrt{3}/2$$

Obviously, the required value for maximum load is $k = 1 + \sqrt{3}/2 = 1.866$

Now $(c_1 + c_2) = c$, and from Equation [14]

$$c_1(1 - 3k^2 + 2k^3) = c$$

With $k = 1.866$ these relations make $c_2 = 2.549c_1$

The maximum load from Equation [12] is now found as

$$W = 0.2062\frac{\mu Uc^2}{h_1^2} \qquad [16]$$

These results are the same as given by Rayleigh.

STEPPED SHAPED SLIDER

The problem of the stepped shaped slider of finite width will next be considered. In this case a flow perpendicular to the direction of motion, i.e., a side-leakage effect, has to be included and recourse is had to Reynolds partial differential equation for pressure in a lubricating film

$$\frac{\partial}{\partial x}\left(h^3\frac{\partial p}{\partial x}\right)+\frac{\partial}{\partial z}\left(h^3\frac{\partial p}{\partial z}\right)=6\mu U\frac{dh}{dx}\ldots\ldots\ldots[17]$$

The scheme of the bearing is as shown in Fig. 2.

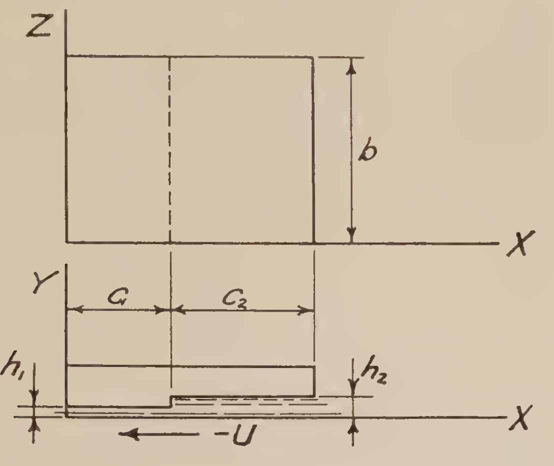

FIG. 2

The region in which h is constant at h_1 is called region (1), and the region in which h is constant at h_2 is called region (2). The X–Z plane is taken as the flat moving element having a velocity $-U$ as shown. It will again be found convenient to use two co-ordinate systems. For region (1) the co-ordinates are as shown, but for region (2) they will be moved forward so that the Z axis is on the leading edge of region (2).

If h is constant, the right-hand side of Reynolds equation is zero, and h^3 can be divided from the left-hand side leaving

$$\frac{\partial^2 p}{\partial x^2}+\frac{\partial^2 p}{\partial z^2}=0\ldots\ldots\ldots\ldots\ldots\ldots[18]$$

This is the Laplace partial differential equation.

An interesting incidental result can be obtained at this stage. Consider a rectangular flat plate being moved parallel to another flat plate and separated from it by a fluid film of thickness h, Fig. 3.

In this case Equation [18] applies. However, if Laplace's equation applies to a region, on the boundaries of which the function is everywhere zero, the only solution is zero, i.e., $p = 0$ is the solution to the pressure equation in this case. This is a well-known result and is not of course restricted to a rectangular shape.

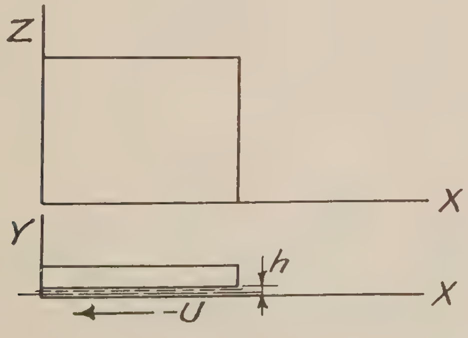

FIG. 3

To return to the problem of the stepped slider. The pressure on the exterior boundaries of regions (1) and (2) is zero, but on the common boundary the pressure is not known. It is assumed that the pressure on this common boundary is given by the following Fourier sine series

$$p=\sum_{n=1,3,5\cdots}^{\infty}P_n\sin\frac{n\pi z}{b}\ldots\ldots\ldots\ldots[19]$$

The summation is over the odd values because of the symmetry. P_n is the Fourier coefficient to be evaluated later.

The general solution for p can be put in the following form

$$p=\sum_{n=1,3,5\cdots}^{\infty}\left(A_n\cos\frac{n\pi z}{b}+B_n\sin\frac{n\pi z}{b}\right)\left(C_n\cosh\frac{n\pi x}{b}+D_n\sinh\frac{n\pi x}{b}\right)\ldots\ldots\ldots[20]$$

The boundary conditions for region (1) are

$p = 0$ at $x = 0$ for all values of z.....I

$p = 0$ at $z = 0$ for all values of x.....II

$p = 0$ at $z = b$ for all values of x.....III

$$p=\sum_{n=1,3,5\cdots}^{\infty}P_n\sin\frac{n\pi z}{b}\text{ at }x=c_1\ldots\ldots\text{IV}$$

From conditions I and II, $A_n = C_n = 0$

From condition IV

$$\sum_{n=1,3,5\cdots}^{\infty}P_n\sin\frac{n\pi z}{b}=\sum_{n=1,3,5\cdots}^{\infty}B_nD_n\sin\frac{n\pi z}{b}\sinh\frac{n\pi c_1}{b}$$

$$\therefore B_nD_n=\frac{P_n}{\sinh\frac{n\pi c_1}{b}}$$

$$\therefore p=\sum_{n=1,3,5\cdots}^{\infty}\frac{P_n}{\sinh\frac{n\pi c_1}{b}}\sin\frac{n\pi z}{b}\sinh\frac{n\pi x}{b}\ldots\ldots[21]$$

For region (2) a solution of the same form as Equation [20] is taken

$$p=\sum_{n=1,3,5\cdots}^{\infty}\left(E_n\cos\frac{n\pi z}{b}+F_n\sin\frac{n\pi z}{b}\right)\left(G_n\cosh\frac{n\pi x}{b}+H_n\sinh\frac{n\pi x}{b}\right)\ldots\ldots\ldots[22]$$

The boundary conditions are

$p = 0$ at $x = 0$ for all values of z......I

$p = 0$ at $z = 0$ for all values of x.....II

$p = 0$ at $z = b$ for all values of x.....III

$$p=\sum_{n=1,3,5\cdots}^{\infty}P_n\sin\frac{n\pi z}{b}\text{ at }x=-c_2\ldots\text{IV}$$

From conditions I and II, $E_n = G_n = 0$

From condition IV

$$\sum_{n=1,3,5\cdots}^{\infty} P_n \sin\frac{n\pi z}{b} = -\sum_{n=1,3,5\cdots}^{\infty} F_nH_n \sin\frac{n\pi z}{b}\sinh\frac{n\pi c_2}{b}$$

$$\therefore F_nH_n = -\frac{P_n}{\sinh\dfrac{n\pi c_2}{b}}$$

$$\therefore p = -\sum_{n=1,3,5\cdots}^{\infty} \frac{P_n}{\sinh\dfrac{n\pi c_2}{b}} \sin\frac{n\pi z}{b}\sinh\frac{n\pi x}{b} \ldots. [23]$$

In order that the pressure be calculable the Fourier coefficient, P_n, must now be evaluated. This is done by making use of the principle of continuity. At any point on the common boundary it will be seen that the rate of flow out of region (2) is the same as the rate of flow into region (1). The rate of flow in the X-direction is given by Equation [3a]

$$-q_x = -\frac{Uh}{2} - \frac{h^3}{12\mu}\frac{\partial p}{\partial x} \ldots\ldots\ldots\ldots. [3a]$$

The equality of the rate of flow for both regions at the common boundary is expressed as follows

$$\frac{Uh_1}{2} + \frac{h_1^3}{12\mu}\left(\frac{\partial p}{\partial x}\right)_{c_1} = \frac{Uh_2}{2} + \frac{h_2^3}{12\mu}\left(\frac{\partial p}{\partial x}\right)_{-c_2} \ldots\ldots. [24]$$

The partial derivative, $\partial p/\partial x$, for regions (1) and (2) must now be evaluated at $x = c_1$ for region (1), and at $x = -c_2$ for region (2).

For region (1)

$$\frac{\partial p}{\partial x} = \sum_{n=1,3,5\cdots}^{\infty} \frac{\dfrac{n\pi}{b}P_n}{\sinh\dfrac{n\pi c_1}{b}} \sin\frac{n\pi z}{b}\cosh\frac{n\pi x}{b}$$

$$\therefore \left(\frac{\partial p}{\partial x}\right)_{c_1} = \sum_{n=1,3,5\cdots}^{\infty} \frac{n\pi}{b} P_n \coth\frac{n\pi c_1}{b}\sin\frac{n\pi z}{b} \ldots. [25]$$

For region (2)

$$\frac{\partial p}{\partial x} = -\sum_{n=1,3,5\cdots}^{\infty} \frac{\dfrac{n\pi}{b}P_n}{\sinh\dfrac{n\pi c_2}{b}} \sin\frac{n\pi z}{b}\cosh\frac{n\pi x}{b}$$

$$\therefore \left(\frac{\partial p}{\partial x}\right)_{-c_2} = -\sum_{n=1,3,5\cdots}^{\infty} \frac{n\pi P_n}{b} \coth\frac{n\pi c_2}{b}\sin\frac{n\pi z}{b} \ldots [26]$$

Equation [24] is rewritten using the values of $\partial p/\partial x$ from Equations [25] and [26]

$$\frac{Uh_1}{2} + \frac{h_1^3}{12\mu}\sum_{n=1,3,5\cdots}^{\infty} \frac{n\pi}{b} P_n \coth\frac{n\pi c_1}{b}\sin\frac{n\pi z}{b} = \frac{Uh_2}{2}$$
$$-\frac{h_2^3}{12\mu}\sum_{n=1,3,5\cdots}^{\infty} \frac{\pi n}{b} P_n \coth\frac{n\pi c_2}{b}\sin\frac{n\pi z}{b} \ldots\ldots\ldots [27]$$

which can be rearranged as follows

$$\sum_{n=1,3,5\cdots}^{\infty} \frac{n\pi}{b} P_n \left(h_1^3\coth\frac{n\pi c_1}{b} + h_2^3\coth\frac{n\pi c_2}{b}\right)\sin\frac{n\pi z}{b}$$
$$= 6\mu U(h_2 - h_1) \ldots\ldots. [28]$$

The right-hand side of Equation [28] is expanded in a Fourier sine series by use of the standard sine series for $\pi/4$

$$\sum_{n=1,3,5\cdots}^{\infty} \frac{n\pi}{b} P_n \left(h_1^3\coth\frac{n\pi c_1}{b} + h_2^3\coth\frac{n\pi c_2}{b}\right)\sin\frac{n\pi z}{b}$$
$$= \sum_{n=1,3,5\cdots}^{\infty} 6\mu U(h_2 - h_1)\frac{4}{n\pi}\sin\frac{n\pi z}{b}$$

The Fourier coefficient, P_n is thus

$$P_n = \frac{24\mu\, Ub(h_2 - h_1)}{n^2\pi^2\left(h_1^3\coth\dfrac{n\pi c_1}{b} + h_2^3\coth\dfrac{n\pi c_2}{b}\right)} \ldots\ldots [29]$$

The pressure can now be calculated at any point by placing this value of P_n in the pressure Equations [21] and [23]. However, the total load on the bearing is of more interest, and this is easily found. The load supported by region (1) is called W_1 and the load supported by region (2) is called W_2

Evidently $$W_1 = \int_0^b\int_0^{c_1} p\, dxdz$$

$$\therefore W_1 = \int_0^b\int_0^{c_1}\sum_{n=1,3,5\cdots}^{\infty} \frac{P_n}{\sinh\dfrac{n\pi c_1}{b}}\sin\frac{n\pi z}{b}\sinh\frac{n\pi x}{b}\,dxdz$$

$$= \int_0^b \sum_{n=1,3,5\cdots}^{\infty} \frac{b}{n\pi}\frac{P_n}{\sinh\dfrac{n\pi c_1}{b}}\left(\cosh\frac{n\pi c_1}{b} - 1\right)\sin\frac{n\pi z}{b}dz$$

$$\therefore W_1 = \sum_{n=1,3,5\cdots}^{\infty} \frac{2b^2P_n}{n^2\pi^2\sinh\dfrac{n\pi c_1}{b}}\left(\cosh\frac{n\pi c_1}{b} - 1\right) \ldots [30]$$

Again, for region (2)

$$W_2 = \int_0^b\int_{-c_2}^{0} -\sum_{n=1,3,5\cdots}^{\infty} \frac{P_n}{\sinh\dfrac{n\pi c_2}{b}}\sin\frac{n\pi z}{b}\sinh\frac{n\pi x}{b}\,dxdz$$

$$= \int_0^b \sum_{n=1,3,5\cdots}^{\infty} \frac{b}{n\pi}\frac{P_n}{\sinh\dfrac{n\pi c_2}{b}}\left(\cosh\frac{n\pi c_2}{b} - 1\right)\sin\frac{n\pi z}{b}dz$$

$$\therefore W_2 = \sum_{n=1,3,5\cdots}^{\infty} \frac{2b^2P_n}{n^2\pi^2\sinh\dfrac{n\pi c_2}{b}}\left(\cosh\frac{n\pi c_2}{b} - 1\right) .. [31]$$

The total load, $W = W_1 + W_2$

Then

$$W = \sum_{n=1,3,5\cdots}^{\infty} \frac{2b^2P_n}{n^2\pi^2}\left(\frac{\cosh\dfrac{n\pi c_1}{b} - 1}{\sinh\dfrac{n\pi c_1}{b}} + \frac{\cosh\dfrac{n\pi c_2}{b} - 1}{\sinh\dfrac{n\pi c_2}{b}}\right)$$

By use of standard relations for the hyperbolic functions, W can be rewritten as

$$W = \sum_{n=1,3,5\cdots}^{\infty} \frac{2b^2P_n}{n^2\pi^2}\left(\tanh\frac{n\pi c_1}{2b} + \tanh\frac{n\pi c_2}{2b}\right)$$

If P_n from Equation [29] is substituted, the load is obtained as

$$W = \frac{48\mu U b^3(h_2 - h_1)}{\pi^4} \sum_{n=1,3,5\cdots}^{\infty} \frac{1}{n^4} \frac{\tanh\frac{n\pi c_1}{2b} + \tanh\frac{n\pi c_2}{2b}}{h_1^3\coth\frac{n\pi c_1}{b} + h_2^3\coth\frac{n\pi c_2}{b}} \ldots\ldots [32]$$

The foregoing solution applies to a rectangular slider having uniform rectilinear motion. This simplified problem is a logical first step because the mathematical work is more likely to be soluble. The result is also useful for comparison with the results of Michell's solution for the inclined flat-plate bearing. However, a more practical solution is possible, and this will be given before discussing the implications of Equation [32].

STEPPED SECTORIAL SLIDER

Instead of the stepped rectangular slider consider a stepped sectorial slider as shown in Fig. 4.

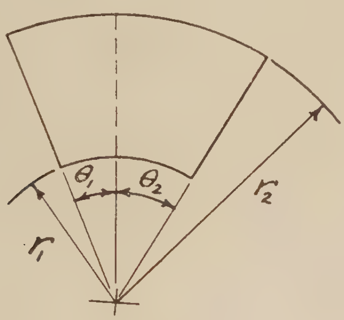

FIG. 4

With such a configuration, it is natural to adopt plane polar co-ordinates. Laplace's equation, that is Equation [18], in polar co-ordinates becomes

$$\frac{\partial^2 p}{\partial r^2} + \frac{1}{r^2}\frac{\partial^2 p}{\partial\theta^2} + \frac{1}{r}\frac{\partial p}{\partial r} = 0 \ldots\ldots\ldots\ldots [33]$$

A new variable is introduced by letting $r = r_1e^\rho$, where r_1 is the inner radius of the sector and ρ is the new variable. Clearly, when

$$r = r_1,\ \rho = 0, \text{ and when } r = r_2,\ \rho = \rho_2 = \log r_2/r_1$$

If the new variable ρ is substituted, Equation [33] becomes

$$\frac{\partial^2 p}{\partial\rho^2} + \frac{\partial^2 p}{\partial\theta^2} = 0 \ldots\ldots\ldots\ldots\ldots\ldots [34]$$

The solution now proceeds on almost exactly similar lines to the rectangular case. It is assumed that the pressure on the common boundary is given by

$$p = \sum_{n}^{\infty} P_n \sin\frac{n\pi\rho}{\rho_2} \ldots\ldots\ldots\ldots\ldots [35]$$

The question of what values of n are to be used in the summation is left open at this stage. It is fairly evident from the physical situation that the curve will not be symmetrical.

As in the previous cases, it is convenient to use two co-ordinate systems. For region (1) the zero of θ is taken through the trailing edge of the slider. For region (2) the zero of θ is moved forward to the leading edge of region (2). The equations for pressure in regions (1) and (2) are obtained by the same methods as for the rectangular case and are identical in form. They are as follows:

For region (1)

$$p = \sum_{n}^{\infty} \frac{P_n}{\sinh\frac{n\pi\theta_1}{\rho_2}} \sin\frac{n\pi\rho}{\rho_2} \sinh\frac{n\pi\theta}{\rho_2} \ldots\ldots [36]$$

For region (2)

$$p = -\sum_{n}^{\infty} \frac{P_n}{\sinh\frac{n\pi\theta_2}{\rho_2}} \sin\frac{n\pi\rho}{\rho_2} \sinh\frac{n\pi\theta}{\rho_2} \ldots\ldots [37]$$

To calculate the Fourier coefficient P_n, it is necessary to use the rate-of-flow relation given by Equation [3*a*]. But now this must be expressed in polar co-ordinates. The rate of flow in the tangential direction is then

$$-q_\theta = -\frac{r\omega h}{2} - \frac{h^3}{12\mu r}\frac{\partial p}{\partial\theta} \ldots\ldots\ldots\ldots [38]$$

where $-\omega$ is the rotational speed of the moving element.

On making the substitution $r = r_1e^\rho$ this equation for flow becomes

$$-q_\theta = -\frac{\omega r_1 e^\rho h}{2} - \frac{h^3}{12\mu r_1 e^\rho}\frac{\partial p}{\partial\theta} \qquad [39]$$

The evaluation of $\partial p/\partial\theta$ at the common boundary is exactly the same as for the rectangular case and need not be repeated. The equality of the rate of flow out of region (2) into region (1) at any point on the common boundary, therefore, can be written down directly from Equation [39] and by analogy with Equation [27]

$$-\frac{\omega r_1 e^\rho h_1}{2} - \frac{h_1^3}{12\mu r_1 e^\rho}\sum_{n}^{\infty}\frac{n\pi}{\rho_2}P_n\coth\frac{n\pi\theta_1}{\rho_2}\sin\frac{n\pi\rho}{\rho_2} = -\frac{\omega r_1 e^\rho h_2}{2}$$
$$+\frac{h_2^3}{12\mu r_1 e\rho}\sum_{n}^{\infty}\frac{n\pi}{\rho_2}P_n\coth\frac{n\pi\theta_2}{\rho_2}\sin\frac{n\pi\rho}{\rho_2}$$

which can be rewritten as

$$\sum_{n}^{\infty}\frac{n\pi}{\rho_2}P_n\left(h_1^3\coth\frac{n\pi\theta_1}{\rho_2} + h_2^3\coth\frac{n\pi\theta_2}{\rho_2}\right)\sin\frac{n\pi\rho}{\rho_2}$$
$$= 6\mu\omega r_1^2 e^{2\rho}(h_2 - h_1) \ldots\ldots [40]$$

The factor $e^{2\rho}$ can be expanded in a Fourier series as follows

$$e^{2\rho} = \sum_{n}^{\infty} K_n \sin\frac{n\pi\rho}{\rho_2}$$

$$K_n = \frac{2}{\rho_2}\int_0^{2\rho} e^{2\rho}\sin\frac{n\pi\rho}{\rho_2}\,d\rho$$

Upon evaluation of this integral, K_n is given for all integral values of n as

$$K_n = \frac{2n\pi[(-1)^{n+1}e^{2\rho_2} + 1]}{n^2\pi^2 + 4\rho_2^2} \qquad \text{[41]}$$

Equation [40] can be written

$$\sum_n^\infty \frac{n\pi}{\rho_2} P_n \left(h_1^3 \coth \frac{n\pi\theta_1}{\rho_2} + h_2^3 \coth \frac{n\pi\theta_2}{\rho_2}\right) \sin \frac{n\pi\rho}{\rho_2}$$

$$= \sum_n^\infty 6\mu\omega r_1^2(h_2 - h_1)K_n \sin \frac{n\pi\rho}{\rho_2} \qquad \text{[42]}$$

This can be solved for P_n and gives, when K_n is substituted from Equation [41]

$$P_n = \frac{12\mu\omega r_1^2\rho_2[(-1)^{n+1}e^{2\rho_2} + 1](h_2 - h_1)}{(n^2\pi^2 + 4\rho_2^2)\left[h_1^3 \coth \frac{n\pi\theta_1}{\rho_2} + h_2^3 \coth \frac{n\pi\theta_2}{\rho_2}\right]} \qquad \text{[43]}$$

The pressure can now be found at any point of region (1) or (2) by use of Equations [36] and [37]. But, as in the rectangular case, the load is of more interest and is readily obtained by integrating over the areas. As before, W_1 will refer to the load supported by region (1), and W_2 will refer to the load supported by region (2). Then

$$W_1 = \int_{r_1}^{r_2} \int_0^{\theta_1} p r d\theta dr$$

$$= \int_0^{\rho_2} \int_0^{\theta_1} p r_1 e^\rho d\theta r_1 e^\rho d\rho$$

$$\therefore W_1 = \int_0^{\rho_2} \int_0^{\theta_1} \sum_n^\infty \frac{r_1^2 P_n}{\sinh \frac{n\pi\theta_1}{\rho_2}} e^{2\rho} \sin \frac{n\pi\rho}{\rho_2} \sinh \frac{n\pi\theta}{\rho_2} d\rho d\theta$$

$$= \int_0^{\rho_2} \sum_n^\infty \frac{r_1^2 P_n}{\sinh \frac{n\pi\theta_1}{\rho_2}} \frac{\rho_2}{n\pi} \left(\cosh \frac{n\pi\theta_1}{\rho_2} - 1\right) e^{2\rho} \sin \frac{n\pi\rho}{\rho_2} d\rho$$

$$= \sum_n^\infty \frac{r_1^2 P_n}{\sinh \frac{n\pi\theta_1}{\rho_2}} \frac{\rho_2}{n\pi} \left[\frac{e^{2\rho}\left(-\frac{n\pi}{\rho_2} \cos n\pi\right) + \frac{n\pi}{\rho_2}}{\left(\frac{n^2\pi^2}{\rho_2^2} + 4\right)}\right] \left(\cosh \frac{n\pi\theta_1}{\rho_2} - 1\right)$$

Since n may be even or odd, this can be written as

$$W_1 = \sum_n^\infty \frac{r_1^2 P_n[(-1)^{n+1}e^{2\rho_2} + 1]}{\left(\frac{n^2\pi^2}{\rho_2^2} + 4\right) \sinh \frac{n\pi\theta_1}{\rho_2}} \left(\cosh \frac{n\pi\theta_1}{\rho_2} - 1\right) \qquad \text{[44]}$$

In the same way W_2 is given as follows

$$W_2 = \int_0^{\rho_2} \int_{-\theta_2}^0 - \sum_n^\infty \frac{P_n}{\sinh \frac{n\pi\theta_2}{\rho_2}} e^{2\rho} \sin \frac{n\pi\rho}{\rho_2} \sinh \frac{n\pi\theta}{\rho_2} d\rho d\theta$$

$$\therefore W_2 = \sum_n^\infty \frac{r_1^2 P_n [(-1)^{n+1} e^{2\rho_2} + 1]}{\left(\frac{n^2\pi^2}{\rho_2^2} + 4\right) \sinh \frac{n\pi\theta_2}{\rho_2}} \left(\cosh \frac{n\pi\theta_2}{\rho_2} - 1\right) \qquad \text{[45]}$$

$$\therefore W = \sum_n^\infty \frac{r_1^2 P_n[(-1)^{n+1} e^{2\rho_2} + 1]}{\left(\frac{n^2\pi^2}{\rho_2^2} + 4\right)} \left(\frac{\cosh \frac{n\pi\theta_1}{\rho_2} - 1}{\sinh \frac{n\pi\theta_1}{\rho_2}} + \frac{\cosh \frac{n\pi\theta_2}{\rho_2} - 1}{\sinh \frac{n\pi\theta_2}{\rho_2}}\right)$$

Placing in the value of P_n from Equation [43] and making use of the standard hyperbolic relations, W can be written as

$$W = 12\mu\omega r_1^4\rho_2^3(h_2 - h_1) \sum_n^\infty \left[\frac{(-1)^{n+1} e^{2\rho_2} + 1}{n^2\pi^2 + 4\rho_2^2}\right]^2 \left[\frac{\tanh \frac{n\pi\theta_1}{2\rho_2} + \tanh \frac{n\pi\theta_2}{2\rho_2}}{h_1^3 \coth \frac{n\pi\theta_1}{\rho_2} + h_2^3 \coth \frac{n\pi\theta_2}{\rho_2}}\right]$$

But $\epsilon^{2\rho_2} = (r_2/r_1)^2$, and $\rho_2 = \log r_2/r_1$

$$\therefore W = 12\mu\omega \left(\log \frac{r_2}{r_1}\right)^3 (h_2 - h_1) \sum_n^\infty \left[\frac{(-1)^{n+1}r_2^2 + r_1^2}{n^2\pi^2 + 4\left(\log \frac{r_2}{r_1}\right)^2}\right]^2$$

$$\times \left[\frac{\tanh \frac{n\pi\theta_1}{\log\left(\frac{r_2}{r_1}\right)^2} + \tanh \frac{n\pi\theta_2}{\log\left(\frac{r_2}{r_1}\right)^2}}{h_1^3 \coth \frac{n\pi\theta_1}{\log \frac{r_2}{r_1}} + h_2^3 \coth \frac{n\pi\theta_2}{\log \frac{r_2}{r_1}}}\right] \qquad \text{[46]}$$

It is now a fairly easy matter to obtain the relations for the quantity of lubricant passing through the bearing and also to find the force and torque on the bearings. Since these are matters of secondary importance only the final formulas will be given.

FORCE REQUIRED TO MOVE FLAT ELEMENT IN RECTANGULAR BEARING

For the rectangular bearing, the force required to move the flat element is given by

$$F = \mu U b \left(\frac{c_1}{h_1} + \frac{c_2}{h_2}\right) + \frac{24\, \mu U b^2(h_2 - h_1)^2}{\pi^3} \sum_{n=1,3,5\cdots}^\infty \frac{1}{n^3\left(h_1^3 \coth \frac{n\pi c_1}{b} + h_2^3 \coth \frac{n\pi c_2}{b}\right)} \qquad \text{[47]}$$

The quantity entering at the leading edge is

$$Q_2 = \frac{U h_2 b}{2} - \frac{4 U b h_2^3(h_2 - h_1)}{\pi^2} \sum_{n=1,3,5\cdots}^\infty \frac{1}{n^2 \sinh \frac{n\pi c_2}{b}} \left(\frac{1}{h_1^3 \coth \frac{n\pi c_1}{b} + h_2^3 \coth \frac{n\pi c_2}{b}}\right) \qquad \text{[48]}$$

The quantity leaving at the trailing edge is

$$Q_1 = \frac{Uh_1b}{2} + \frac{4Ubh_1^3(h_2 - h_1)}{\pi^2} \sum_{n=1,3,5\cdots}^{\infty} \frac{1}{n^2 \sinh \dfrac{n\pi c_1}{b}} \left(\frac{1}{h_1^3 \coth \dfrac{n\pi c_1}{b} + h_2^3 \coth \dfrac{n\pi c_2}{b}} \right) \quad \ldots\ldots\ldots [49]$$

The side leakage can be obtained by difference.

For the sector bearing the corresponding quantities are as follows:

The torque required to turn the bearing is given by

$$T = \frac{\mu\omega(r_2^4 - r_1^4)}{4} \left(\frac{\theta_1}{h_1} + \frac{\theta_2}{h_2} \right) + 6\pi(h_2 - h_1)^2 \mu\omega \left(\log \frac{r_2}{r_1} \right)^2 \sum_{n}^{\infty} \left[\frac{(-1)^{n+1} r_2^2 + r_1^2}{n^2\pi^2 + 4\left(\log \dfrac{r_2}{r_1} \right)^2} \right]^2 \left(\frac{1}{h_1^3 \coth \dfrac{n\pi\theta_1}{\log \frac{r_2}{r_1}} + h_2^3 \coth \dfrac{n\pi\theta_2}{\log \frac{r_2}{r_1}}} \right) \quad \ldots\ldots [50]$$

The lubricant entering at the leading edge is given by

$$Q_2 = \frac{\omega h_2(r_2^2 - r_1^2)}{4} - 2\omega \left(\log \frac{r_2}{r_1} \right) h_2^3(h_2 - h_1)(r_2^2 - r_1^2)$$

$$\sum_{n=1,3,5\cdots}^{\infty} \frac{1}{\left[n^2\pi^2 + 4\left(\log \dfrac{r_2}{r_1} \right)^2 \right] \sinh \dfrac{n\pi\theta_2}{\log \frac{r_2}{r_1}} \left(h_1^3 \coth \dfrac{n\pi\theta_1}{\log \frac{r_2}{r_1}} + h_2^3 \coth \dfrac{n\pi\theta_2}{\log \frac{r_2}{r_1}} \right)} \quad \ldots\ldots\ldots [51]$$

The lubricant leaving at the trailing edge is given by

$$Q_1 = \frac{\omega h_1 (r_2^2 - r_1^2)}{4} + 2\omega \left(\log \frac{r_2}{r_1} \right) h_1^3(h_2 - h_1)(r_2^2 - r_1^2) \times$$

$$\sum_{n=1,3,5\cdots}^{\infty} \frac{1}{\left[n^2\pi^2 + 4\left(\log \dfrac{r_2}{r_1} \right)^2 \right] \sinh \dfrac{n\pi\theta_1}{\log \frac{r_2}{r_1}} \left(h_1^3 \coth \dfrac{n\pi\theta_1}{\log \frac{r_2}{r_1}} + h_2^3 \coth \dfrac{n\pi\theta_2}{\log \frac{r_2}{r_1}} \right)} \quad \ldots\ldots\ldots [52]$$

The side leakage can be obtained by difference.

It will be observed that the series in Equations [32] and [46] converge very rapidly. For a square bearing a single term gives a result within 1 or 2 per cent of the actual value. The series for the sectorial bearing will converge somewhat less rapidly. For a "square" shape (i.e., the mean arc length equal to the radial depth), a satisfactory value can be obtained with 3 or 4 terms. In both cases the convergence becomes less rapid as the bearing becomes wider with respect to its length.

Equations [12], [32], and [46] give the load that can be supported on a bearing having the stepped-film shape. The conditions for a maximum of Equation [12] are fairly easily found, and this maximum is given in Equation [16]. The same device if applied to Equations [32] and [46] leads to great complication, and the method of trial is easier. It is found that the proportions for maximum load when side leakage is neglected are not the best proportions for a bearing of finite width. The values for the case of no side leakage were, $h_2 = 1.866 h_1$ and $c_2 = 2.549\, c_1$. For a square bearing, it is found that the best values are, approximately, $h_2 = 1.7h_1$ and $c_2 = 1.2c_1$ However, the load capacity is not very sensitive to changes in the vicinity of these values.

Comparison of Loads With Michell Flat-Plate Bearing Loads

It is interesting to compare the load given by Equation [32] for a square bearing to that given by Michell for an inclined flat plate. If the proportions given in the foregoing for the case of no side leakage are used, the bearing is about 6 per cent less effective than the inclined-plane bearing. But if the best proportions are used it is about 3 per cent more effective. The 29 per cent improvement, obtained when side leakage is neglected, is reduced so that the bearing is only slightly better than the inclined-plane bearing in this respect. The side-leakage effect is no doubt aggravated because the large film thickness extends into the highest-pressure region, and thus offers an easier means of escape for the lubricant. If the bearing is made wider it gradually gains on the inclined-plane bearing and tends to approach the value given by Equation [16]. If it is made narrower it gradually gets less than the inclined-plane bearing.

A way in which the bearing could be improved to some extent would be to make the stepped element as shown in Fig. 5. Such a shape would add to the mathematical difficulties and would be somewhat harder to produce unless it were etched. Probably the matter of increasing the capacity is not very important in practice as the loads that arise are already being taken by tilting-block bearings of reasonable size, and it has been shown that these bearings are not quite as effective as the stepped arrangement.

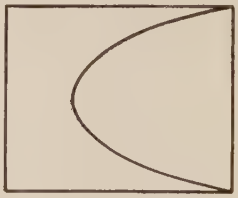

Fig. 5

An interesting conclusion can be drawn from Equations [32] and [46] by inspection. It will be recalled that the hyperbolic tangent approaches unity for quite small values of its argument. For example, tanh 3 = 0.99505 and tanh 5 = 0.9991. It is clear that if all other conditions are held constant, the load capacity is not increased appreciably by an increase in the length of the bearing beyond a certain point. This has particular significance in the case of a sector bearing because here there is a limit to the angle that can be subtended by a sector, viz., 360-deg. Thus if the ratio of outer to inner radii is 2, a pair of 180-deg sectors would support almost exactly twice the load that could be carried by a single 360-deg bearing, other conditions being held constant. Also, three 120-deg sectors would be almost exactly 3 times as effective as a single 360-deg bearing (oil passages are neglected for simplicity in discussion; their influence would be small for large sectors). Obviously, there is a point at which this process of division would start to give a diminishing return. This could be fairly easily determined if the sector radii and oil-passage space were prescribed as well as the conditions of speed and viscosity. The matter is a little complicated by the fact that for each new angular condition the ratios of θ_2 to θ_1 and h_2 to h_1 will change for best conditions. However, a very good result would be obtained by holding these ratios constant at some reasonable value until the best number of sectors was found, and then making a more careful calculation in this vicinity to find best conditions.

Conclusion

The stepped-bearing arrangement has a good deal to recommend it in practice although there are two matters which are not especially in its favor. The bearing does not have any great advantage in load capacity over the inclined-plane bearing, and it is restricted to one direction of rotation. Offsetting these matters is its great constructional simplification over the tilting-block bearing, or even over those bearings in which the taper is machined into one of the elements. In addition, the fairly simple explicit equations for the load offer some advantage in design where the influence of each parameter is fairly easy to see and can be checked quite readily. It is true that viscosity has been taken as constant, and this can be quite misleading. However, there are ways of estimating the change in viscosity through the bearing, and a mean value seems to give fairly good results. In this respect the solution is no worse than others. It should be possible to apply this bearing to a great many thrust problems and in particular to those cases where space considerations are of importance.

Some experiments of a semiquantitative nature have been made with bearing models. It is well known that precise results by this means are rather difficult to obtain. However, reasonable agreement was found. An air-lubricated model in which the step height, i.e., $(h_2 - h_1)$, is about 0.00005 in. has been made and is entirely successful. Lord Rayleigh describes a simple test he made of the scheme in his paper.[2]

Discussion

J. R. Menke.[3] The author has presented a useful extension of Lord Rayleigh's calculations and has done a service in calling more general attention to this relatively unappreciated paper.[4] The writer's attention was drawn to the paper in 1943–1944 by John E. Viscardi and Mayo D. Hersey with a practical result.

The author remarks in his discussion upon the behavior of the hyperbolic tangent terms in Equations [32] and [46]. This behavior is hardly surprising in the physical sense, indicating only that side leakage as usual reduces the advantage of increasing length in long, "thin" (i.e., not wide) bearings.

Fig. 5 of the paper indicates an interesting improvement, and one wonders about the estimated extent of this improvement. Is a large part of the potential 29 per cent gain over inclined-plate bearings feasible? Tests on this point should prove worth while.

The bearing examined is evidently simple in two respects; it can be readily understood and it can be manufactured cheaply. With such advantages and its indicated performance one might expect some industrial acceptance after these thirty-odd years since Lord Rayleigh's paper.

---

[3] Nuclear Development Associates, Inc., New York, N. Y. Jun. ASME.

[4] Author's reference (2).

Density-Pressure Relationships for Two Low-Viscosity Dimethyl Siloxanes

By S. B. GUNST,[1] PITTSBURGH, PA.

An instrument used to determine liquid compressibilities is described[2] as is its use in the determination of density versus pressure for hexamethyldisiloxane and octamethyltrisiloxane. Results at pressures to 10,000 psi, and at temperatures to 200 F for the hexamethyldisiloxane and to 300 F for the octamethyltrisiloxane are shown. The densities are precise within 0.3 per cent.

Introduction

THE dimethyl siloxanes are members of the group frequently called silicone liquids (1, 2, 3).[3] They are heat-stable, chemically inert compounds (4). Their stability and small viscosity change with temperature suggest their potential excellence as viscometer-calibration standards, the objective which prompted this investigation.

In the rolling-ball viscometer (5), an instrument used for the determination of absolute viscosities of fluids at elevated pressures, the densities of the fluids under test conditions must be ascertained. This investigation was undertaken to determine the density-pressure relationships for two dimethyl siloxanes.

For mineral oils the density-pressure equation of Dow and Fink (6) has given satisfactory results; but for silicone liquids, in so far as is known, little experimental work from which such relations may be derived has been published (7, 8). Although the results of this investigation on only two silicone liquids are insufficient to yield a density-pressure equation for all silicones, they should be useful for the liquids tested, and subsequent work may lead to a density-pressure equation for silicones corresponding to that of Dow and Fink for mineral oils.

Description of Apparatus

For this investigation it was necessary to design and build an instrument for making measurements from which the compressibility of a liquid could be computed. A search of the literature (9, 10, 11) showed the many difficulties and attendant uncertainties experienced by the early investigators, and it is believed the instrument embraces the best principles of design known at this time. The pressure joints are self-sealing; the expansion of the pressure vessel is irrelevant; the test liquid is contained in a thin-walled, commercially available brass bellows, whose spring constant and bulk compression are negligibly small, and whose free end is unhampered by any sliding surfaces with their attendant friction; the instrument demands no calibration with a liquid whose compressibility is known; and it is continuously reading so that a single charge of sample liquid within the bellows suffices for all pressures and temperatures encountered in this investigation.

A cross-sectional sketch of the instrument, hereafter referred to as the "compressibility meter," is shown in Fig. 1. The brass bellows 1, soldered to brass plugs 2 and 3, is filled with the test-liquid sample. The sample is trapped in the bellows by a steel taper pin 4, and a steel contact plate 5, which seals by compressing an aluminum gasket 6. The upper end of the bellows is held fixed by threading the upper plug 2 into the steel end plate 7, which is positioned in the steel pressure housing 8 by a steel end screw 9. A bakelite bushing 10, electrically insulates the brass bellows housing 11, with its brass micrometer spider 12, and steel micrometer screw 13, from the bellows. Adjustment of the micrometer screw is accomplished by turning the graduated brass knob 14. This turns a steel shaft 15, whose three steel fingers 16, engage the bakelite fluted coupling 17, attached to the micrometer screw. A steel spring 18, takes up the micrometer-screw backlash, and a thrust bearing 19, takes the load on the head of the shaft 15, resulting from internal pressure applied hydraulically inside the

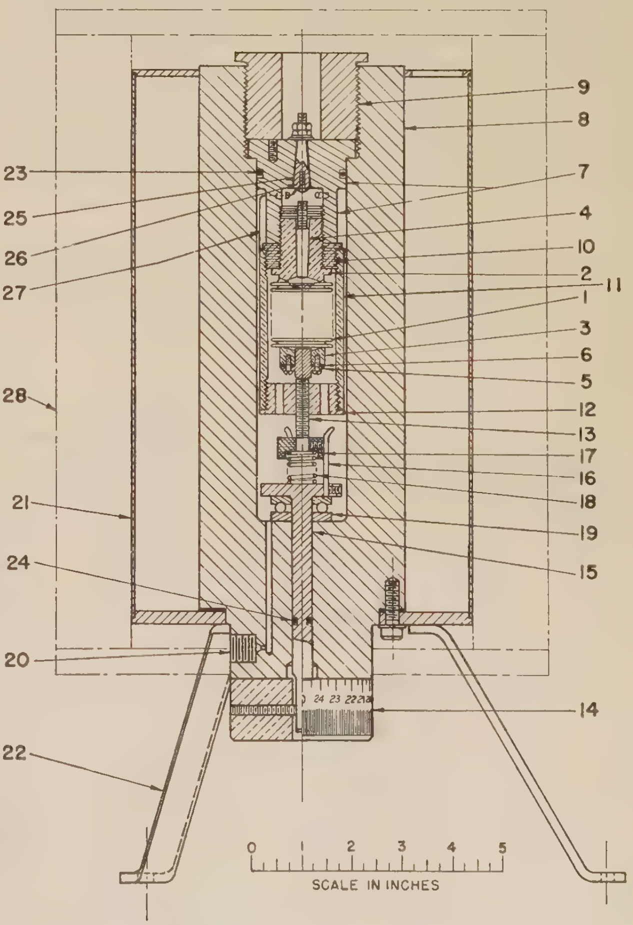

Fig. 1 Sectional Diagram of Compressibility Meter

---

[1] Gulf Research and Development Company, and University of Pittsburgh.

[2] Additional details can be found in a University of Pittsburgh thesis by the author.

[3] Numbers in parentheses refer to the Bibliography at the end of the paper.

Contributed by the Research Committee on Lubrication and the Petroleum Division and presented at the Annual Meeting, New York, N.Y., November 27–December 2, 1949, of The American Society of Mechanical Engineers.

Note: Statements and opinions advanced in papers are to be understood as individual expressions of their authors, and not those of the Society. Paper No. 49—A-91.

pressure housing through the inlet 20. Three equally spaced annular slots in the top plate of the jacket 21, permit the admission of liquid into the jacket, and the immersion in this liquid of a strip heater, a stirrer, a thermoregulator, and a thermometer. Three steel legs 22, support the compressibility meter on a suitable workbench. Synthetic-rubber O-rings 23 and 24, serve as self-sealing gasket and packer, respectively, and a nylon bushing 25, serves both as a self-sealing gasket and an electrical insulator for the contact pin 26. A fiberglas-insulated wire 27, connects the contact pin to the bellows housing 11.

When the micrometer screw 13, is made to contact the contact plate 5, electrical connection is effected from the contact pin 26, to the bellows housing to the micrometer screw to the bellows to the pressure housing. Thus a suitable electrical indicator connected between the contact pin and the pressure housing will indicate contact between the contact plate and the micrometer screw. The micrometer screw has a major diameter of $^1/_4$ in. and 40 threads per inch. One turn advances the screw 0.025 in. Fifty graduations on the circumference of the knob 14, permit direct readings corresponding to a micrometer-screw advance of 0.0005 in. and estimations to 0.0001 in. With a suitably sensitive indicator, therefore, the variation in bellows length can be measured to 0.0001 in.

Hydraulic pressure, applied by means of a free-piston gage (12), commonly called a "dead-weight tester," is transmitted to all parts inside the pressure housing—to the bellows via six axial holes in the micrometer spider 12, and four axial slots (not shown in Fig. 1) in the bellows housing 11, and to the top of the taper pin 4, sealing the top of the bellows via four radial holes in the collar of the end plate 7. The application of pressure to the outside of the bellows compresses the test-liquid sample within the bellows and results in a decrease in bellows length, which can be measured as previously indicated.

In order to decrease heat loss, asbestos steam-pipe insulation 28, $1^1/_2$ in. thick, blankets the compressibility meter so that only the legs, the knob, the pressure inlet, and parts of the thermometer and temperature-control apparatus are exposed.

Analytical Considerations

Measurements of a variation in bellows length can be used to calculate the change in density of a test-liquid sample. For a mass m of liquid occupying a volume V the liquid density is given by

$$\rho = m/V \quad \text{[1]}$$

With atmospheric-pressure conditions denoted by a subscript 0, an isothermal change in density because of a change in pressure is given by

$$\Delta\rho = \rho - \rho_0 = (m/V) - (m/V_0) = \frac{m(V_0 - V)}{VV_0} \quad \text{[2]}$$

Let $V = V_0 + \Delta V$ and Equation [2] becomes

$$\Delta\rho = -\frac{m\Delta V}{V_0(V_0 + \Delta V)} = -\frac{\rho_0}{(V_0/\Delta V) + 1}$$

$$= -\frac{\rho_0}{(m/\rho_0 \Delta V) + 1} \quad \text{[3]}$$

Tests to determine the change in bellows volume with change in bellows length at constant temperature and pressure showed that $\Delta V = A\,\Delta L$, where ΔL is the change in bellows length and A is a constant, obviously the effective cross-sectional area of the inside of the bellows. Equation [3] can therefore be written

$$\Delta\rho = -\frac{\rho_0}{(m/\rho_0 A\,\Delta L) + 1} \quad \text{[4]}$$

from which the isothermal change in density resulting from a change in pressure can be calculated if all quantities on the right are known.

A graph of $\Delta\rho$ or ρ versus pressure p can be used to calculate the isothermal compressibility k of a liquid if desired. With isothermal conditions designated by a subscript T, k is given by

$$k = -\frac{1}{V}\left(\frac{\partial V}{\partial p}\right)_T = -\frac{1}{V}\left(\frac{\partial \rho}{\partial p}\right)_T\left(\frac{\partial V}{\partial \rho}\right)_T = \frac{1}{\rho}\left(\frac{\partial \rho}{\partial p}\right)_T$$

$$= \frac{1}{(\rho_0 + \Delta\rho)}\left(\frac{\partial \rho}{\partial p}\right)_T \quad \text{[5]}$$

Since the slope of the graph of $\Delta\rho$ or ρ versus pressure at any pressure is $(\partial\rho/\partial p)_T$, readily obtainable by graphical differentiation, k can be calculated.

Test Methods and Results

Preliminary investigations were made in order to establish methods for temperature measurement and control, to determine the effective cross-sectional area of the bellows, and to ascertain the effect of cubic compression of the various parts of the compressibility meter on bellows length measurements. The latter was found to be negligible.

The two liquids investigated were hexamethyldisiloxane and octamethyltrisiloxane, referred to by one manufacturer, the Dow-Corning Corporation, as DC-200 silicone fluid, viscosity 0.65 centistoke at 25 C, and DC-200 silicone fluid, viscosity 1.0 centistoke at 25 C, respectively. Equation [4] was used to calculate change in density $\Delta\rho$ for various temperatures and pressures.

1 *The density* ρ_0*:*

The density ρ_0 at atmospheric pressure and test temperature was obtained from hydrometer tests by chemists at the author's laboratory and checked with the results of Hurd (3).

2 *Effective bellows cross-sectional area A:*

The cross-sectional area A of the bellows was found to be essentially independent of bellows length and pressure. The value of A of 0.764 sq in. determined by test at 75 F was used and corrected for thermal expansion, using a handbook value for the expansivity of brass.

3 *The mass m of liquid filling the bellows:*

Anticipated difficulties in filling the bellows with a test sample of liquid to the essential exclusion of air were easily overcome. The bellows assembly, with the taper pin removed, was immersed in an oil bath until only $^1/_8$ in. of the bellows taper-pin plug was exposed. The bath was maintained at a temperature above the maximum test temperature of a specific test liquid. A long-necked eyedropper inserted through the taper-pin hole was used to fill the bellows with test liquid. A glass stirring rod was used to agitate the bellows convolutions in order to rid them of air bubbles. The bellows was kept constantly filled by means of the eyedropper. After all evidence of bubbling through the taper-pin hole had ceased, the taper pin was driven into the taper-pin hole, thus sealing the test liquid within the bellows.

The mass m of test-sample liquid is the difference between the filled-bellows mass and empty-bellows mass obtained by the double massing method (13) with appropriate corrections for air buoyancy. The bellows assembly was carefully cleaned and dried prior to all mass determinations.

Only one filling of the bellows was necessary for all tests made on each of the liquids and their corresponding masses were as follows:

Hexamethyldisiloxane mass m = 13.630 grams
Octamethyltrisiloxane mass m = 13.575 grams

4 *Isothermal change in bellows length ΔL versus pressure:* Measurements of variation in bellows length at pressure intervals of 100 psi from 0 to 500 psi (gage), and at intervals of 500 psi from 500 to 10,000 psi (gage) were made for the two liquids at the following temperatures:

Hexamethyldisiloxane 76.0, 100.0, 149.9, 200.0 F
Octamethyltrisiloxane 77.5, 100.0, 150.0, 200.0, 250.0, 300.0 F

(At an absolute pressure of 760 mm Hg, the liquids have the following approximate boiling points: Hexamethyldisiloxane, 211 F; octamethyltrisiloxane, 306 F).

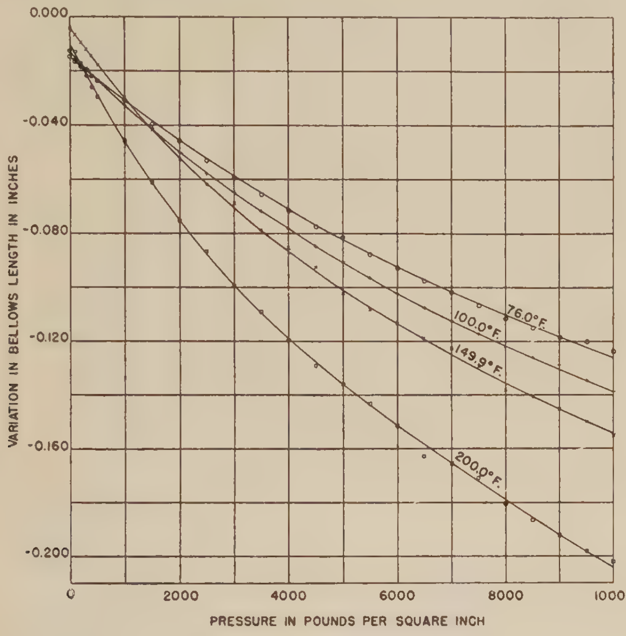

FIG. 2 MEASURED VARIATION IN BELLOWS LENGTH FROM ARBITRARY ZERO AT EACH TEMPERATURE VERSUS GAGE PRESSURE FOR HEXAMETHYLDISILOXANE

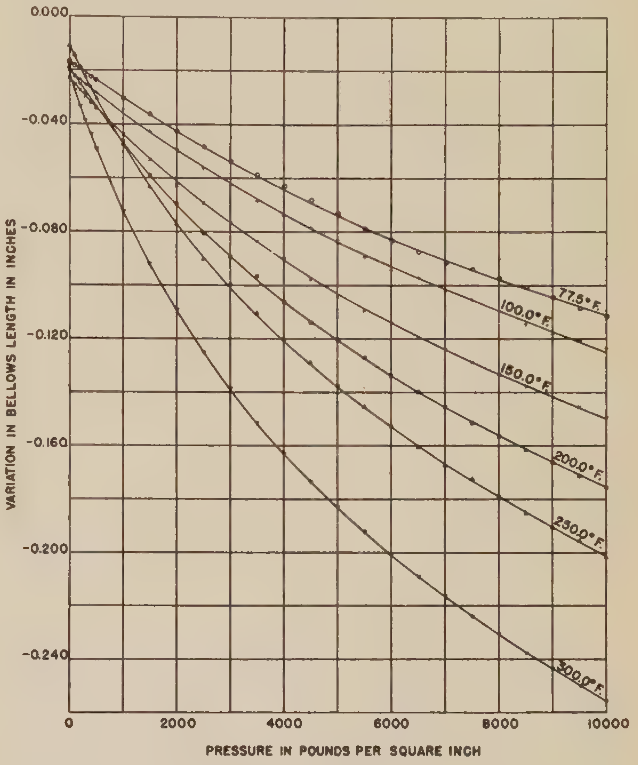

FIG. 3 MEASURED VARIATION IN BELLOWS LENGTH FROM ARBITRARY ZERO AT EACH TEMPERATURE VERSUS GAGE PRESSURE FOR OCTAMETHYLTRISILOXANE

TABLE 1 CHANGE IN DENSITY VERSUS PRESSURE FOR HEXAMETHYLDISILOXANE

mass m = 13.630 grams

Temp, F	76.0		100.0		149.9		200.0	
A, sq in	0.764		0.764		0.765		0.766	
ρ_0, gram per cu cm	0.7634		0.7496		0.7194		0.6883	
Gage pressure, psi	ΔL in.	$\Delta\rho$ gram per cu cm	ΔL in.	$\Delta\rho$ gram per cu cm	ΔL in.	$\Delta\rho$ gram per cu cm	ΔL in.	$\Delta\rho$ gram per cu cm
0	0.0000	0.0000	0.0000	0.0000	0.0000	0.0000	0.0000	0.0000
500	−0.0085	0.0046	−0.0105	0.0055	−0.0130	0.0062	−0.0190	0.0084
1000	−0.0160	0.0087	−0.0200	0.0105	−0.0255	0.0123	−0.0365	0.0163
2000	−0.0310	0.0169	−0.0370	0.0196	−0.0480	0.0236	−0.0655	0.0298
3000	−0.0440	0.0243	−0.0520	0.0279	−0.0665	0.0331	−0.0895	0.0414
4000	−0.0560	0.0312	−0.0655	0.0354	−0.0825	0.0415	−0.1090	0.0511
5000	−0.0675	0.0379	−0.0780	0.0426	−0.0965	0.0491	−0.1260	0.0597
6000	−0.0775	0.0438	−0.0895	0.0493	−0.1090	0.0559	−0.1410	0.0676
7000	−0.0865	0.0492	−0.0995	0.0552	−0.1205	0.0623	−0.1555	0.0753
8000	−0.0950	0.0544	−0.1090	0.0609	−0.1310	0.0683	−0.1690	0.0826
9000	−0.1035	0.0597	−0.1175	0.0660	−0.1405	0.0738	−0.1820	0.0898
10000	−0.1110	0.0643	−0.1255	0.0709	−0.1495	0.0790	−0.1940	0.0965

TABLE 2 CHANGE IN DENSITY VERSUS PRESSURE FOR OCTAMETHYLTRISILOXANE

mass m = 13.575 grams

Temp, F	77.5		100.0		150.0		200.0		250.0		300.0	
A, sq in	0.764		0.764		0.765		0.766		0.767		0.768	
ρ_0, gram per cu cm	0.8171		0.8046		0.7767		0.7479		0.7188		0.6900	
Gage pressure, psi	ΔL in.	$\Delta\rho$ gram per cu cm	ΔL in.	$\Delta\rho$ gram per cu cm	ΔL in.	$\Delta\rho$ gram per cu cm	ΔL in.	$\Delta\rho$ gram per cu cm	ΔL in.	$\Delta\rho$ gram per cu cm	ΔL in.	$\Delta\rho$ gram per cu cm
0	0.0000	0.0000	0.0000	0.0000	0.0000	0.0000	0.0000	0.0000	0.0000	0.0000	0.0000	0.0000
500	−0.0065	0.0040	−0.0080	0.0048	−0.0110	0.0062	−0.0140	0.0073	−0.0195	0.0094	−0.0275	0.0123
1000	−0.0130	0.0081	−0.0155	0.0094	−0.0210	0.0119	−0.0275	0.0145	−0.0365	0.0179	−0.0510	0.0233
2000	−0.0255	0.0160	−0.0295	0.0180	−0.0385	0.0221	−0.0505	0.0271	−0.0660	0.0330	−0.0875	0.0409
3000	−0.0370	0.0234	−0.0415	0.0256	−0.0540	0.0313	−0.0700	0.0380	−0.0900	0.0458	−0.1175	0.0560
4000	−0.0475	0.0303	−0.0530	0.0330	−0.0675	0.0395	−0.0865	0.0476	−0.1100	0.0568	−0.1415	0.0686
5000	−0.0570	0.0367	−0.0635	0.0398	−0.0800	0.0473	−0.1010	0.0562	−0.1270	0.0663	−0.1615	0.0794
6000	−0.0660	0.0428	−0.0725	0.0458	−0.0910	0.0543	−0.1145	0.0643	−0.1420	0.0750	−0.1795	0.0894
7000	−0.0735	0.0479	−0.0810	0.0515	−0.1010	0.0607	−0.1260	0.0714	−0.1560	0.0833	−0.1950	0.0983
8000	−0.0810	0.0531	−0.0895	0.0573	−0.1100	0.0665	−0.1370	0.0783	−0.1680	0.0905	−0.2095	0.1067
9000	−0.0880	0.0580	−0.0970	0.0624	−0.1185	0.0722	−0.1465	0.0843	−0.1795	0.0975	−0.2220	0.1141
10000	−0.0940	0.0623	−0.1045	0.0677	−0.1270	0.0779	−0.1560	0.0904	−0.1905	0.1043	−0.2345	0.1217

The results of the tests for hexamethyldisiloxane, the dimer, are graphed in Fig. 2, and for octamethyltrisiloxane, the trimer, in Fig. 3.

Computed Results

Smoothed values of change in bellows length ΔL versus gage pressure, taken from the graphs in Figs. 2 and 3, are shown in Tables 1 and 2, as are the corresponding values of change in test-liquid density $\Delta\rho$ calculated from Equation [4]. The box headings of the tables bear appropriate values of the test-liquid temperature, the bellows cross-sectional area A, and the test-liquid density ρ_0 at atmospheric pressure. Graphs of test-liquid density ρ as a function of gage pressure are presented in Figs. 4 and 5, from which the density for any pressure can be read. Moreover, isobaric graphs of ρ versus temperature can readily be constructed from the graphs in Fig. 4 or 5, with which the density at any temperature from 75 to 200 F for the dimer, and from 75 to 300 F for the trimer and at any gage pressure from 0 to 10,000 psi for either can be determined.

Check tests confirmed results within experimental error.

The isothermal compressibilities, computed according to Equation [5], are shown in Figs. 6 and 7.

Conclusion

Calculations showed that the densities of the two dimethyl siloxanes were determined with a probable error no greater than 0.0018 gram per cu cm over a pressure range of 10,000 psi and at various temperatures.

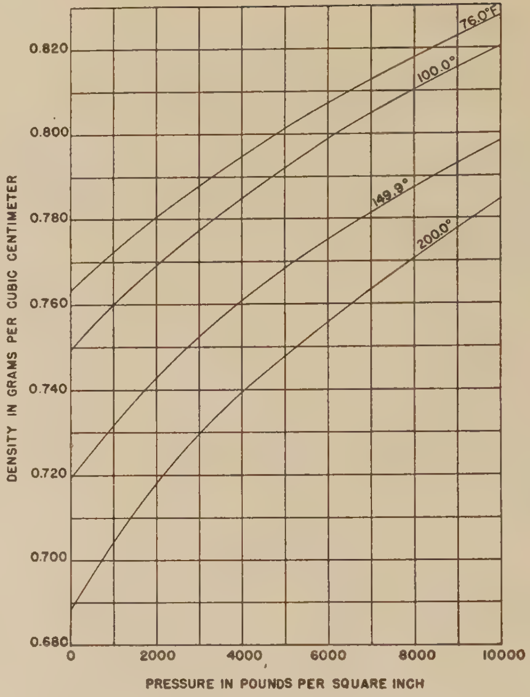

FIG. 4 DENSITY VERSUS GAGE PRESSURE FOR HEXAMETHYLDISILOXANE

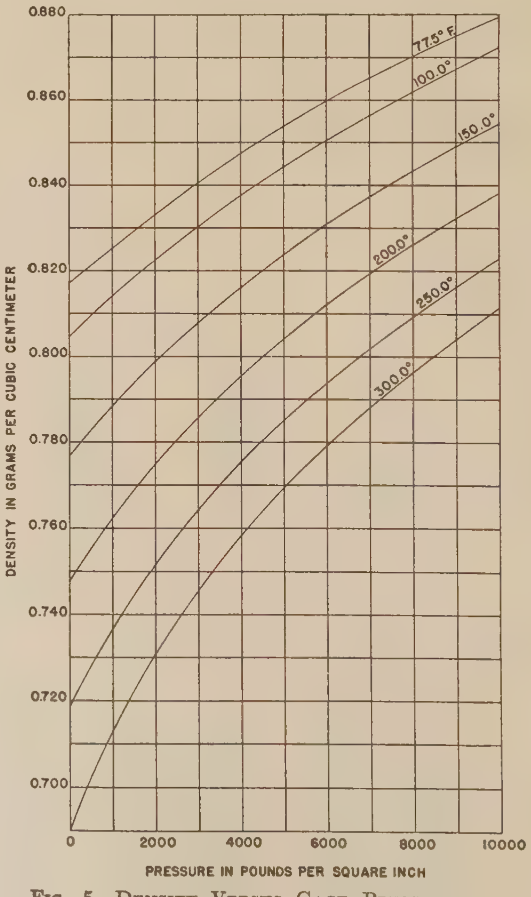

FIG. 5 DENSITY VERSUS GAGE PRESSURE FOR OCTAMETHYLTRISILOXANE

Acknowledgment

The author is indebted to Mr. Paul G. Exline, formerly Section Engineer of Gulf Research and Development Company, for early suggestions concerning the problem and equipment design features; to Dr. David Halliday of the University of Pittsburgh, and to Mr. R. J. S. Pigott, Director of Engineering of Gulf Research and Development Company, for sponsoring this investigation; and to Dr. Paul D. Foote, Executive Vice-President and Director of Gulf Research and Development Company, for permission to disclose the results.

BIBLIOGRAPHY

1 "Nomenclature of Organosilicon Compounds," by R. O. Sauer, *Journal of Chemical Education*, vol. 21, 1944, pp. 303–305.

2 "Methylpolysiloxanes," by Winton Patnode and D. F. Wilcock, *Journal of the American Chemical Society*, vol. 68, 1946, pp. 358–363.

3 "Studies on Siloxanes: I. The Specific Volume and Viscosity in Relation to Temperature and Constitution," by C. B. Hurd, *Journal of the American Chemical Society*, vol. 68, 1946, p. 364.

4 "Dielectric Constants of Dimethyl Siloxane Polymers," by E. B. Baker, A. J. Barry, and M. J. Hunter, *Industrial and Engineering Chemistry*, vol. 38, 1946, pp. 1117–1120.

5 "Viscosity Determination of Subsurface Samples of Crude Oil," by P. G. Exline and H. J. EnDean, *Drilling and Production Practice*, 1939, pp. 659–665 (American Petroleum Institute), 1940.

6 "Computation of Some Physical Properties of Lubricating Oils at High Pressures," by R. B. Dow and C. E. Fink, *Journal of Applied Physics*, vol. 11, 1940, pp. 353–357.

7 "Further Rough Compressions to 40,000 Kg/cm^2, Especially Certain Liquids," by P. W. Bridgman, Proceedings of the American Academy of Arts and Sciences, vol. 77, 1949, pp. 129–145.

8 "Ultrasonic Investigation of Molecular Properties of Liquids. III. Linear Polymethylsiloxanes," by Alfred Weissler, *Journal of the American Chemical Society*, vol. 71, 1949, p. 93.

9 "The Physics of High Pressure," by P. W. Bridgman, The MacMillan Company, New York, N. Y., 1931; pertinent bibliographies on pp. 17–29, 147–148.

10 "The Design of High Pressure Plant and the Properties of Fluids at High Pressures," by D. M. Newitt, The Clarendon Press, Oxford, England, 1940; pertinent bibliography on p. 466.

11 "Recent Work in the Field of High Pressures," by P. W. Bridgman, *Review of Modern Physics*, vol. 18, 1946, pp. 1–93; pertinent

bibliography on pp. 15–16; and *Journal of the Institute of Petroleum*, vol. 32, 1946, p. 254A.

12 "Pressure-Responsive Elements," by P. G. Exline, Trans. ASME, vol. 60, 1938, pp. 625–632.

13 "Heat," by A. G. Worthing and David Halliday, John Wiley & Sons, Inc., New York, N.Y., 1948, pp. 6–8.

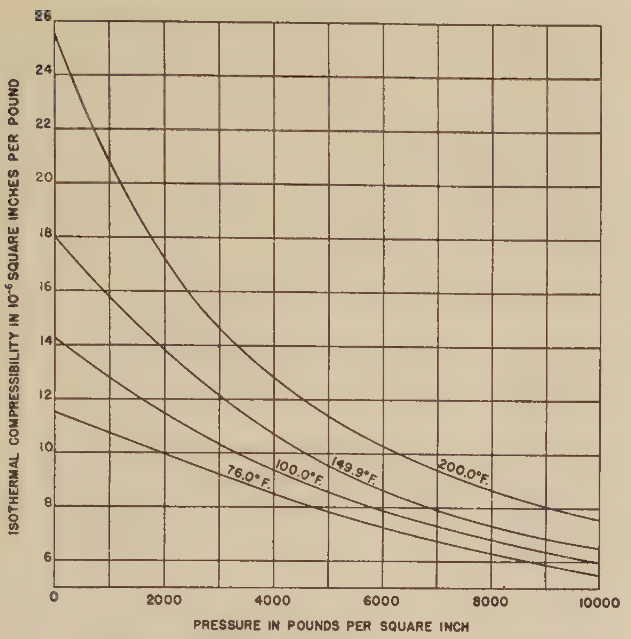

FIG. 6 ISOTHERMAL COMPRESSIBILITY VERSUS GAGE PRESSURE FOR HEXAMETHYLDISILOXANE
(Precision is limited by graphical differentiation of Fig. 4.)

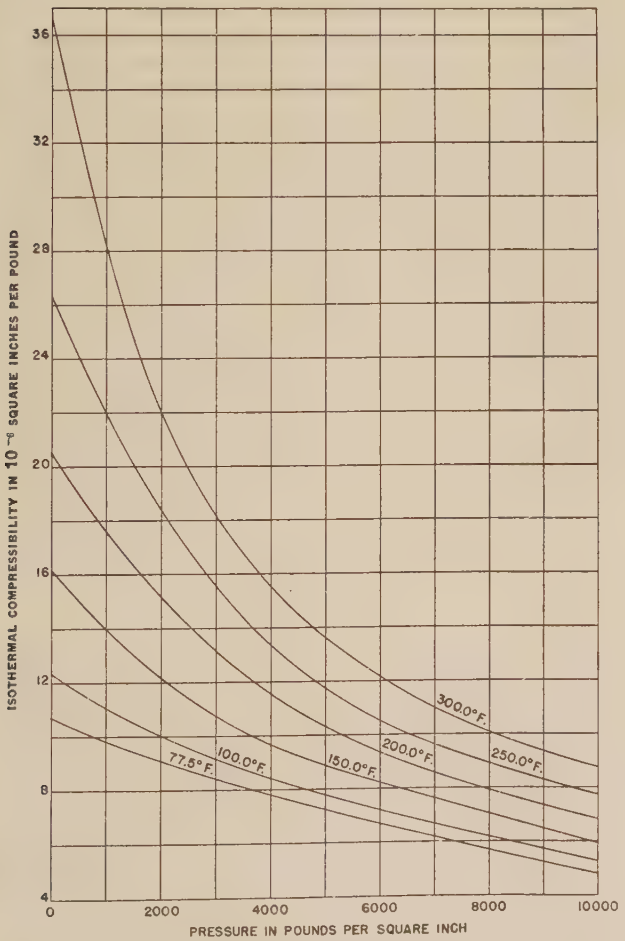

FIG. 7 ISOTHERMAL COMPRESSIBILITY VERSUS GAGE PRESSURE FOR OCTAMETHYLTRISILOXANE
(Precision limited by graphical differentiation of Fig. 5.)

Discussion

P. W. BRIDGMAN.[4] This is an interesting and ingenious adaptation of the sylphon method of measuring compressibilities which the writer developed a number of years ago[5] for use over a wider pressure range. For the purpose at present in view (determination of the density correction in rolling-ball viscometers used under pressure), and within the range of accuracy claimed (0.3 per cent on the densities), the apparatus seems entirely adequate. A check on this is afforded by comparing the author's results with those of the writer[6] for the same two liquids at room temperature. After making corrections for slight differences of temperature, and expressing the results as fractional changes of initial volume instead of initial density, the writer finds for the author's value of $\Delta V/V_0$ at approximately 24 C at a pressure of 7110 psi (500 kg per sq cm) for hexamethyldisiloxane and octamethyltrisiloxane, respectively, 0.0552 and 0.0597. These values may be compared with the writer's of 0.0568 and 0.0586, respectively. The agreement is thus well within the claimed error, which would correspond to 0.003.

It would seem that the method should be capable of considerably greater accuracy than claimed, for 0.3 per cent on the absolute density is not high. It is to be regretted that the author did not take the opportunity to find the probable limits of accuracy. To do this, comparison with measurements by other methods is necessary, because there can be no question but there are intrinsic sources of error in the sylphon method owing to internal strains in the metal of the sylphon, which has been subject to very great deformations in the forming process. It may well be that the accuracy would prove great enough to justify use of the apparatus in making measurements of the compression of liquids for their own sake, as demanded in work on the equation of state of liquids. This apparatus has an especial advantage for such use in the wide temperature range that can be covered easily.

R. B. DOW.[7] This paper represents a valuable contribution to the means available for calibrating high-pressure viscometers over the moderate pressure range of 10,000 psi. The writer and his collaborators have previously used a series of carefully chosen lubricating oils of such densities and viscosities as required to give suitable calibration curves for the rolling-ball type of viscometer. The present choice of silicone liquids is to be preferred chiefly because of the ready availability of a standard product, although the stability and small temperature coefficients of viscosity are valid reasons for considering them more suitable than oils. The author's results should be useful for all workers in this field who will welcome all advances toward standardization.

The compressibility meter is a well-designed and simple device which has been adapted from the sylphon piezometer of Prof. P. W. Bridgman. The techniques of measurement differ only in the method of measuring changes of length, Bridgman using changes of resistance of a fine manganin slide wire attached directly to the top of the sylphon instead of direct readings on a micrometer screw. The sylphon piezometer has several obvious points of superiority over the old type of piston displacement in a pressure cylinder containing the test liquid. For the present pressure range the use of a micrometer is both direct and convenient since it can be used with a simple pressure seal which would not suffice at much higher pressures.

---

[4] Lyman Laboratory of Physics, Harvard University, Cambridge, Mass.

[5] "The Volume of 18 Liquids as a Function of Pressure and Temperature," by P. W. Bridgman, Proceedings of the American Academy of Arts and Sciences, vol. 66, 1931, pp. 185–233.

[6] See p. 143 of reference (7) in Bibliography of paper.

[7] Bureau of Ordnance, Re9a, Navy Department, Washington, D. C.

In respect to the corrections employed in the present work, it appears that the length of the screw was not corrected for possible changes due to changes of pressure and temperature. The correction for pressure would be negligible except at the highest pressure used, at which it would be of a magnitude about comparable with the accuracy of measurement. The correction for temperature, on the other hand, appears to be well within the accuracy of measurement between the limits of 76 and 200 F.

The value of the results are enhanced by the fact that several temperatures were used. It is suggested that, in addition to the value of 100 F, it would be desirable to have data at 130 and 210 F since the viscosities of oils are commonly measured at these temperatures.

P. G. Exline.[8] This paper describes an instrument capable of determining liquid densities and compressibilities with a higher order of accuracy and with much greater convenience than has hitherto been obtainable. A single filling of the instrument suffices for all determinations over the allowable temperature and pressure range of the instrument. The pressure and temperature ranges covered by the author were rather arbitrarily limited by the materials tested and by the pressure-measuring instruments used. It would add to the value of the paper if a reasonable estimate could be given of the pressure and temperature limits to which the instrument could be used.

Although the author reports unusually high accuracy for determinations of this nature, the writer believes that an additional correction could well have been made. In determining liquid compressibilities in a vessel in which the internal pressure equals the external pressure, the direct observations yield the difference between the compressibility of the liquid and that of the material of the vessel.[9] The fact that in the author's instrument the liquid is contained in a vessel capable of free axial elongation does not alter the situation, as the radius of the bellows is reduced by the pressure, and the brass bellows housing carrying the micrometer nut will be shortened. At the most, this correction would alter the reported values of $\Delta\rho$ by slightly under 1 per cent.

In calculating compressibilities from the density data the author has selected a definition of K which does not yield easily usable values, a mistake of which the writer has also been guilty.[10] If the compressibility is defined as

$$K = \frac{1}{V_0} \frac{(V_0 - V)}{P}$$

where V is the volume at pressure P and V_0 is the volume at zero pressure, it is much more easily applied to numerical computations. In this case the compressibility can be expressed as a function of ρ as follows

$$K = \frac{\Delta\rho}{(\rho_0 + \Delta\rho)P}$$

and the computations can be made directly from Tables 1 and 2 of the paper.

The initial values of K, computed this way, will be the same as in Figs. 6 and 7 of the paper, but the values at 10,000 psi will be 50 to 70 per cent higher.

The writer has had occasion to reduce the data reported in the paper to analytical expressions of the form $\rho = \rho_0(1 + aP + bP^2 + cP^3)$. The values of the coefficients thus obtained are given in the following table:

Temp, deg F	ρ_0 gram per cu cm	a in.^{2}/lb	b in.^{4}/lb^2	c in.^{6}/lb^3
		HEXAMETHYLDISILOXANE		
76	0.7634	1.196×10^{-5}	-4.65×10^{-10}	1.13×10^{-14}
100	0.7496	1.440	-7.13	2.28
149.9	0.7194	1.868	-12.3	4.63
200	0.6883	2.539	-20.5	9.13
		OCTAMETHYLTRISILOXANE		
77.5	0.8171	1.038×10^{-5}	-2.95×10^{-10}	0.344×10^{-14}
100	0.8046	1.227	-5.80	1.94
150	0.7767	1.588	-8.85	3.00
200	0.7479	2.060	-13.35	4.84
250	0.7188	2.674	-20.60	8.38
300	0.6900	3.364	-26.0	10.0

Alfred Weissler.[11] This interesting paper introduces a greatly improved instrument for the determination of isothermal compressibility. The measurement of sound velocity by means of the ultrasonic interferometer is an attractive, precise method for the determination of adiabatic compressibility, from which the isothermal compressibility may be computed if the heat capacity and thermal expansion coefficient are known.[12]

The latter method was utilized[13] to measure the compressibilities (at atmospheric pressure and 86 F) of 16 methylsiloxane liquids, including the two studied in the present work. It is interesting to note that the values obtained from ultrasonic propagation are about 20 per cent higher than those found in the paper. This difference may be understood in terms of the rapid decrease in compressibility with increasing pressure, as shown in Figs. 6 and 7 of the paper. Inasmuch as the excess pressure attained in our ultrasonic interferometer is 0.1 psi or less, the compressibilities obtained thereby are valid for the range of 0 to 0.1 psi (gage). By contrast, the first measurement at each temperature in the present work gives the "average" compressibility over the range 0 to 100 psi (gage), from which it is not possible to extrapolate to zero pressure with any great accuracy. In the same connection, the isothermal compressibilities of these liquids determined at Dow Corning are considerably lower than those found in the present work, presumably because an even larger pressure interval was used.

It appears, therefore, that the ultrasonic interferometer is particularly valuable for the measurement of compressibility of fluids at zero gage pressure.

AUTHOR'S CLOSURE

The author gratefully acknowledges the stimulating discussion submitted by Professor Bridgman, Dr. Dow, and Messrs. Exline and Weissler, each of whom has made valuable contributions in the field of compressibility.

The corrections for changes in length of the micrometer screw because of temperature and pressure changes and for compression of the material of the vessel, suggested by Dr. Dow and Mr. Exline, respectively, are well within the reported probable error on the density ρ of 0.3 per cent. That the results could be improved by these and other corrections[14] is true, although in many cases it is questionable if the increased accuracy obtained would justify the additional labor in computation.

---

[8] President, Exline Engineering Company, Tulsa, Okla. Mem. ASME.

[9] "A Text-Book of Physics—'Properties of Matter,'" by V. H. Poynting and J. J. Thomson, 11th edition Charles Griffin & Company, Ltd., London, England, pp. 116–119.

[10] "Leakage in Capillary Seals of Hydraulic Valves and Pumps," by P. G. Exline, *Product Engineering*, vol. 17, April, 1946, p. 292.

[11] Naval Research Laboratory, Washington, D. C.

[12] "Ultrasonics," by L. Bergmann, John Wiley & Sons, Inc., New York, N. Y., 1944, chapt. 3.

[13] See reference (8) in Bibliography of paper.

The instrument described was designed as an engineering instrument with which results sufficiently accurate for most engineering uses could be obtained rapidly by a semiskilled technician with little supervision. The direct readings on the micrometer screw, the facility of testing at various temperatures, the single filling of the bellows for all temperatures and pressures investigated, and the omission of higher-order corrections to simplify the computations are considered important features in the use of the instrument for engineering purposes.

The maximum possible precision obtainable with the instrument has not been investigated. Professor Bridgman's suggestion of comparison with measurements by other methods, and the application of corrections, such as those suggested by Dr. Dow and Mr. Exline, would be necessary in an investigation to determine the limits of accuracy obtainable with the instrument.

The maximum pressure and temperature to which the instrument could be used are limited primarily by the materials incorporated in the design. Synthetic-rubber O-ring seals in similar applications have been subjected to 40,000 psi at room temperature and to 12,000 psi at 400 F without failure in either case. The maximum temperature, however, is limited to approximately 350 F because a soft solder was used to join the bellows to the bellows plugs.

The isothermal compressibility K, defined by Mr. Exline, is approximately the integrated average between atmospheric and pressure p of the isothermal compressibility k shown in Figs. 6 and 7 of the paper. That Mr. Exline obtained results at 10,000 psi 50 to 70 per cent higher than those presented in Figs. 6 and 7, is therefore to be expected. In the opinion of the author, the isothermal compressibility defined by Equation [5] of the paper is more useful than that defined by Mr. Exline for theoretical analyses leading to calculations of such quantities as adiabatic compressibility and velocity of sound.

Mr. Exline's empirical equation for the density results should be useful, provided the user bears in mind that such expressions cannot safely be extrapolated nor differentiated. Since the labor involved in the evaluation of coefficients is considerable, Mr. Exline's contribution is especially appreciated.

Mr. Weissler's work[15] on the adiabatic compressibility of methyl-siloxane liquids permitted him to calculate the isothermal compressibility at atmospheric pressure. His discussion unquestionably explains part of the difference between his results and those of this paper. Some of the difference, however, probably lies in the uncertainties in the quantities used in his calculations, notably the thermal expansivity and the specific heat at constant pressure.

---

[14] See appendixes to the University of Pittsburgh thesis (MS) by the author (reference 2 of paper).

[15] See reference (8) in Bibliography of paper.

A Mathematical Evaluation of Pressures in a Grease-Lubricated Bearing[1]

By K. B. LAWRENCE,[2] STATE COLLEGE, PA.

Of the various methods proposed in the past for the numerical evaluation of pressures developed in a film of lubricant, perhaps the best method, in general, consists of the application of a finite-difference formula developed from the fundamental differential equation. Such a formula has been developed by Derman G. Christopherson (1),[3] who also has shown that the formula gives accurate results when applied to calculations involving oil-lubricated bearings. The author herein applies the finite-difference formula to calculations of the pressure distribution existing in a grease-lubricated bearing and compares the results obtained with the results of a recent experimental investigation by Cohn and Oren (2), which was conducted under similar conditions of operation.

NOMENCLATURE

The following nomenclature is used in the paper:

$a = r/L$ = dimensionless radius of a circle constructed about a central node o, which includes the surrounding nodes n upon its circumference
A_o, A_{o-n} = influence coefficients
C = eccentricity factor
E = eccentricity of journal, in.
F_o, F_{o-n} = residuals
h = radial clearance or film thickness at point in film, in.
h_0 = radial clearance at point of closest approach
$H = h/h_0$ = dimensionless ratio of radial clearance to radial clearance at point of closest approach
L = length of bearing surface in direction of relative motion, in.
$M = Z/Z_e$ = dimensionless ratio of absolute viscosity at points in film to viscosity at inlet to convergent section of channel
n = subscript denoting points on circles of radius a or $2a$
o = subscript denoting centers of circles
p = pressure $\left[\dfrac{6Z_eUL}{(h_0)^2}\right]P$, psi
P = dimensionless pressure
U = rate of shear of viscous lubricant at point in film, ips
x = distance measured in direction of relative motion, in.
y = distance measured in the plane of, and at right angles to relative motion, in.
Z = absolute viscosity at point in film, poise
Z_e = absolute viscosity at inlet to convergent section of channel, poise
η = radial clearance, in.
$\xi = x/L$ = dimensionless ratio of lengths measured along bearing arc from inlet position, to total length of bearing arc

INTRODUCTION

A method is to be shown herein for the solution of the pressure distribution in bearings lubricated with a copious supply of a non-Newtonian substance such as a grease or a polymer-laden oil. This subject is of considerable interest at the moment and has presented a problem of some difficulty because of the viscosity characteristics of the lubricants mentioned.

It has been shown by M. H. Arveson (3) and others that the apparent viscosity of greases varies as some function of the rate of shear, indicating an infinite value at zero rate of shear, with the viscosity approaching a constant value at extremely high rates of shear, such as indicated in Fig. 1. This effect is important in any analytical consideration of grease as well as of other non-Newtonian substances used as a lubricant, inasmuch as the rate of shear is a variable under the conditions of thick-film lubrication of journal bearings.

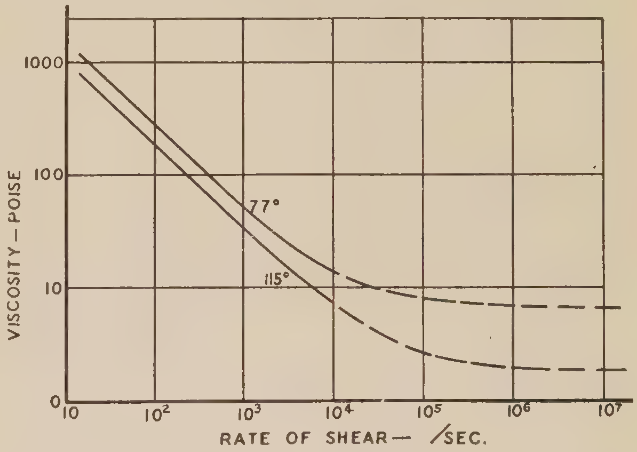

FIG. 1 VISCOSITY CURVES

It has been shown in hydrodynamic theory that the following equation formulated by Osborne Reynolds (4) applies in conditions of journal-bearing operation utilizing a copious supply of a viscous lubricant

$$\frac{\partial}{\partial x}\left(\frac{h^3}{Z}\frac{\partial p}{\partial x}\right)+\frac{\partial}{\partial y}\left(\frac{h^3}{Z}\frac{\partial p}{\partial y}\right)=6U\frac{dh}{dx}$$

This equation, although admitting certain simplifications, remains general in so far as the viscosity characteristics of the lubricant are concerned, allowing viscosity changes in both

---

[1] This paper is an abstract of a thesis submitted to The Pennsylvania State College, June, 1948, in partial fulfillment of the requirements for a Master of Science degree in Mechanical Engineering.

[2] Instructor, Department of Mechanical Engineering, Pennsylvania State College.

[3] Numbers in parentheses refer to the Bibliography at the end of the paper.

Contributed by the Research Committee on Lubrication and the Petroleum Division and presented at the Annual Meeting, New York, N. Y., November 27–December 2, 1949, of THE AMERICAN SOCIETY OF MECHANICAL ENGINEERS.

NOTE: Statements and opinions advanced in papers are to be understood as individual expressions of their authors and not those of the Society. Paper No. 49—A-69.

the X and Y-directions for any cause whatsoever. Considerable difficulty has been experienced, however, in the determination of a general, easily understood, and readily workable method for the solution of this equation. Much important work has been done in this respect by Reissner (5), Vogelpohl (6, 7, 8), Skinner (9), Kingsbury (10), and Christopherson (1). It is the last-named to whom we are indebted for the finite-difference formula which is to be used in this work.

In its very simplest elements, the solution of a differential equation in finite-difference form consists of the substitution of finite quantities in the place of the infinitely small differentials existing in the original. On this basis then, the equation containing the finite differences lends itself to numerical computations—however, at the sacrifice of accuracy. On the other hand, a satisfactory degree of accuracy can be obtained by limiting the finite differences to suitably small intervals simply as one approximates the slope of a graph by considering differences in the ordinates over suitably small intervals.

Christopherson (1) has determined the following finite-difference expressions as solutions of Reynolds equation

$$\sum_{n=1}^{4}{}_{a}\left[\left(\frac{H^3}{M}\right)_n+\left(\frac{H^3}{M}\right)_o\right]P_n - P_o\sum_{n=1}^{4}{}_{a}\left[\left(\frac{H^3}{M}\right)_n+\left(\frac{H^3}{M}\right)_o\right] = 2a^2\frac{\partial H}{\partial \xi}$$

which is accurate to the order of a^2, or

$$16\sum_{n=1}^{4}{}_{a}\left[\left(\frac{H^3}{M}\right)_n+\left(\frac{H^3}{M}\right)_o\right]P_n - \sum_{n=5}^{8}{}_{2a}\left[\left(\frac{H^3}{M}\right)_n+\left(\frac{H^3}{M}\right)_o\right]P_n - P_o\left\{16\sum_{n=1}^{4}{}_{a}\left[\left(\frac{H^3}{M}\right)_n+\left(\frac{H^3}{M}\right)_o\right] - \sum_{n=5}^{8}{}_{2a}\left[\left(\frac{H^3}{M}\right)_n+\left(\frac{H^3}{M}\right)_o\right]\right\} = 24a^2\frac{\partial H}{\partial \xi}$$

which is accurate to the order of a^4.

The summations in the foregoing equation apply to points equally spaced on the circumference (n-points) and at the center (o-points) of circles of radius a or $2a$ such as shown in Fig. 2, situated in the hydrodynamic field in the plane of relative motion. These points are thought of as nodes formed by a grid of equally spaced lines covering the field which is transformed into the X,Y-plane as is shown in Figs. 2 and 3, where the latter shows the fine-grid node construction.

It is necessary also to apply the relaxation method of Southwell (11) to the results determined by the foregoing formulas, since these results will be in error due to the necessity of using a coarse grid, Fig. 2, at the starting points.

Viscosity Analysis

Data are given in Table 1 for the reference grease which is to be used in the calculations. These data are for the same grease tested and reported by Cohn and Oren (2).

TABLE 1 CAPILLARY VISCOSITY DATA

U/h (rate of shear in reciprocal seconds)	—Z (viscosity in poise)—	
	77 deg F	115 deg F
15.6	1132.4	717.3
47.0	547.4	345.2
108.9	262.1	183.0
203.1	161.3	107.8
434.0	89.1	59.9
678.7	63.2	42.6
2737.0	26.4	16.4
8200.0	15.0	8.3

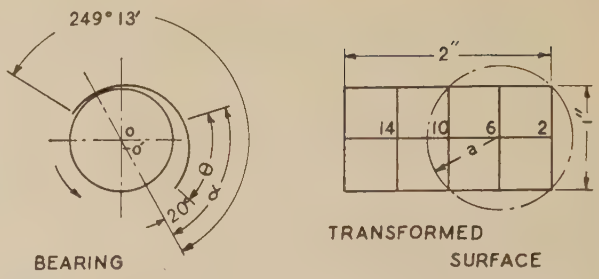

Fig. 2 Initial Node Arrangement

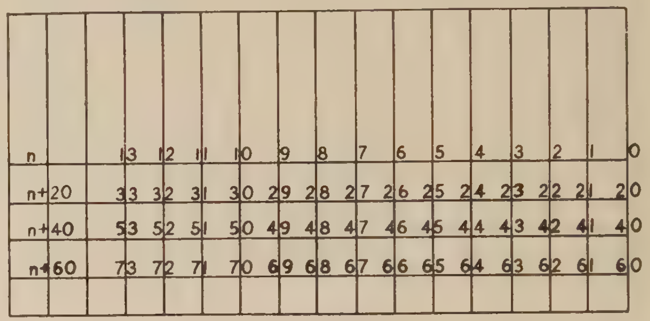
n 13 12 11 10 9 8 7 6 5 4 3 2 1 0
n+20 33 32 31 30 29 28 27 26 25 24 23 22 21 20
n+40 53 52 51 50 49 48 47 46 45 44 43 42 41 40
n+60 73 72 71 70 69 68 67 66 65 64 63 62 61 60

Fig. 3 Fine-Grid Node Arrangement

A mathematical formula is fitted to each of the viscosity sets of values by a standard textbook method (12) which results in the following

$$Z(\text{at 77 deg F}) = 10{,}960\left(\frac{U}{h}\right)^{-0.8016} + 6.8$$

$$Z\ (\text{at 115 deg F}) = 6377\left(\frac{U}{h}\right)^{-0.7690} + 1.82$$

This is done in order to extrapolate the existing data in the direction shown dotted in Fig. 1.

Solution of Finite-Difference Formula

A cylindrical 1-in. × 1-in. bearing is selected for investigation. The bearing surface is transformed as in Fig. 2, and an area as indicated is selected for investigation in which positive hydrodynamic pressures are anticipated. Furthermore, the area, consisting of 2 in. of the bearing arc, is selected in particular to enable initial calculations to be made for pressures at nodes 6, 10, and 14, involving only pressures at nodes on the boundaries where the values for P_n are known to be zero.

The appropriate physical values are determined in the following calculations:

C = eccentricity factor = 0.46 (assumed)
η = radial clearance of bearing and journal = 0.0082 in.
E = eccentricity of bearing and journal centers
= 0.46 × 0.0082 = 0.00377 in.
Mean film temperature 115 F (assumed)
Journal speed 250 rpm
h_0 = minimum film thickness = 0.0082 — 0.00377 = 0.0044 in.
h_e = film thickness at entrance = 0.0082 — 0.00377 cos 20 deg
= 0.0117 in.

$$\frac{U}{h_e} = \text{rate of shear at entrance} = \frac{\pi \times 1 \times 250}{60 \times 0.0177} = \frac{13.1}{0.0177}$$

= 1119 reciprocal sec

$$Z_e = 6376\ (1119)^{-0.769} + 1.82 = 30.6 \text{ poises}$$

$$\xi = \frac{x}{L} = \frac{r\,\theta}{L} = \frac{0.5\,\theta}{2} = \frac{\theta}{4}$$

$$\alpha = \theta + 20 \text{ deg}$$

$$H = \frac{h}{h_e} = \frac{\eta + E \times \cos \alpha}{h_e} = \frac{\eta}{h_e} + \frac{E}{h_e} \cos (4\xi + 20)$$

$$\frac{\partial H}{\partial \xi} = \frac{-4E}{h_e} \sin (4\xi + 20) = \frac{-4 \times 0.00377}{0.0044} \sin \alpha$$

$$= -3.425 \sin \alpha$$

TABLE 2

Node	α	h	H	U/h	Z	$M = Z/Z_e$	H^3/M	$\frac{\partial H}{\partial \xi}$
2	20	0.0177	2.66	1119	30.6	1.000	18.90	...
6	77°18′	0.0090	2.042	1457	25.4	0.830	10.28	—1.932
10	134°36′	0.0056	1.272	2340	18.2	0.595	3.46	—2.442

It is to be noted in Table 2 that the viscosity of the grease calculated at each of the nodes is based upon the circumferential rate of shear which is assumed to be constant across the thickness of the film. This involves two cases in point. The one case involves the assumption just mentioned, and amounts to the neglect of the second-order effect of pressure on the velocity distribution across the film thickness. Further, it may be reasoned that the rate of shear as a function of x and y should be determined correctly in the direction of the flow at the points under consideration. However, since the flow in the X-(or circumferential) direction is of such a higher order of magnitude than the flow endwise at any point, it is reasoned that the circumferential rate of shear will be a satisfactory approximation and most especially so in this, the case of the highly viscous grease where the end flow is exceedingly low.

The dimensionless pressure at node 6 is now calculated as a sample

$$a = \frac{0.5}{2 \times 0.707} = 0.3535$$

$$P_6 = \frac{2(0.3535)^2 \times 3.345}{2\,(18.9) + 2\,(3.46) + 4\,(10.28)} = 0.00974$$

The pressures at nodes of progressively finer grids are calculated in a similar manner, using values at nodes previously determined.

Since the formula gives accurate results only for fine grids and the foregoing values were based upon values determined initially for an exceedingly coarse grid, it is necessary now to reduce the error by the relaxation technique.

Application of Relaxation Method

Numerical values called residuals are calculated by the reapplication of the finite-difference formula. The residuals defined by

$$F_o = \sum_{n=1}^{4} a \left[\left(\frac{H^3}{M}\right)_n + \left(\frac{H^3}{M}\right)_o\right] P_n -$$
$$P_o \sum_{n=1}^{4} a \left[\left(\frac{H^3}{M}\right)_n + \left(\frac{H^3}{M}\right)_o\right] - 2a^2 \frac{\partial H}{\partial \xi}$$

are in effect the numerical inequalities existing in the equation due to errors in the pressures. It is seen from the formula that a change in the residual may be made by effecting a change in the P_o; in addition, a change in P_o results in an accompanying change in the residual at the neighboring nodes. To facilitate making these changes the quantities

$$\left[\left(\frac{H^3}{M}\right)_n + \left(\frac{H^3}{M}\right)_o\right]$$

and

$$\sum_{n=1}^{4} a \left[\left(\frac{H^3}{M}\right)_n + \left(\frac{H^3}{M}\right)_o\right]$$

are given symbols A_{o-n} and A_o, respectively, and are called influence coefficients. Then at the center

$$\Delta P_o = -\frac{\Delta F_o}{A_o}$$

and at the n-nodes

$$\Delta F_n = \Delta P_o \times A_{o-n} = -\Delta F_o \frac{A_{o-n}}{A_o}$$

The ratios A_{o-n}/A_o are calculated in advance and serve as multipliers.

In the manner then of reducing the residuals at each of the nodes successively according to the formulas given, values of corrected dimensionless pressures are obtained.

In this, the first case, an additional series of calculations are necessary to extend the area under consideration throughout the convergent section of the channel. The results obtained thereby are given in Table 3 and plotted in Figs. 4, 5, 6, and 7, as the No. 1 set of curves.

In a similar manner the values for the No. 2 set which were taken at the lower temperature, are determined, with the exception, however, that instead of determining initially approximate pressures by means of the formula, a rather arbitrary pressure distribution is assumed and corrections are made thereto by the relaxation method.

The No. 3 set of curves shows the results at the conditions of a higher temperature and increased eccentricity factor. These curves result from the application of the second and more accurate finite-difference formula in the determination of the residuals.

Summary

The reader's attention is invited first to the consideration of the viscosity curves in Fig. 1. It is here noted that the apparent viscosity levels off asymptotically at high values of rate of shear, which phenomenon has been reported by M. H. Arveson (3) and others, based upon experimental evidence. The term apparent viscosity is here used advisedly since the data given were determined by the capillary-tube method, and there is some question as to its applicability because of the possible coring effect in the capillary, which may be attributed to the non-Newtonian characteristic of the grease. However, these data are of sufficient accuracy to demonstrate the general behavior of the lubricant.

The curves in Figs. 4, 5, 6, and 7 are qualitatively similiar to those of the oil family; however, no quantitative comparison is attempted here because of the basic differences in the two types of lubricants and the impracticability of establishing the conditions for a rational basis of comparison.

Finally, the curves in Fig. 8 are to be noted. Here the curves for the No. 2 set of conditions are compared with those determined by an experimental investigation by Cohn and Oren (2) on a bearing of similar dimensions. The latter are shown dotted. Rather good conformity is therein noted, although it should be emphasized that there is considerable uncertainty concerning the comparableness of some of the corresponding physical conditions existing in the two cases. Possibly the most notable deviation is the diversity in the unit radial clearance. In this work the value of 0.0164 in. per in. was used, while Cohn and Oren report for their bearing a value of 0.0071 in. per in. Of similar importance

TABLE 3 CORRECTED PRESSURES FOR CURVES NO. 1 PSI

n	$n+0$	$n+20$	$n+40$	$n+60$
1	0	0	0	0
2	7.74	6.95	5.50	4.20
3	13.88	12.77	9.42	6.10
4	20.99	19.85	16.12	9.77
5	26.39	24.88	20.52	13.43
6	32.62	30.66	24.97	15.08
7	39.6	37.0	29.9	17.5
8	46.1	42.6	34.6	20.7
9	50.8	47.0	39.6	23.8
10	51.1	45.0	38.4	23.8
11	47.2	43.1	35.6	21.4
12	35.1	32.0	26.0	16.0
13	17.7	14.1	13.2	7.4
14	0	0	0	0

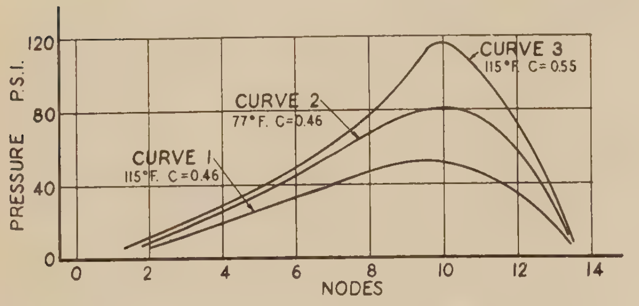

Fig. 4 Pressure Distribution at n-Nodes (Center)

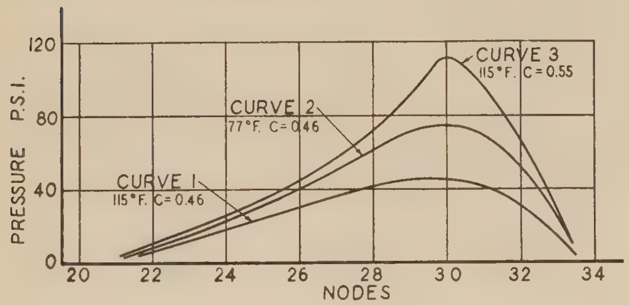

Fig. 5 Pressure Distribution at $n + 20$ Nodes

is the matter of the running position of the shaft, since there is no reported value of eccentricity in the experimental investigation. The constant mean film temperature, as assumed herein for the lower (77 deg F) cases, roughly approximates the bearing shell temperatures observed by Cohn and Oren, and, although the finite-difference formula is adaptable to temperature variations in the film, no allowance was made for this occurrence in this work.

It is also to be noted that although the curves were plotted to the same scale on the abscissa, their relative location was chosen arbitrarily, since this mathematical treatment does not determine directly the angular position of the application of the load.

Conclusions

This work is presented as an illustration of the use of the finite-difference formula as applied to determining the pressure distribution in a journal bearing using grease as a lubricant. In a similar manner, this same method can be used equally as well where other non-Newtonian substances are used, as well as Newtonian substances. This method may be considered as valid in so far as the assumptions made herein apply, and presents the possibility of the establishment of a simpler method which can be applied to everyday lubrication problems involving non-Newtonian lubricants. This can be accomplished through the analytical survey of the whole field of application by this method. Then the evolution of a semianalytical method can be brought about, constructed on a rational basis.

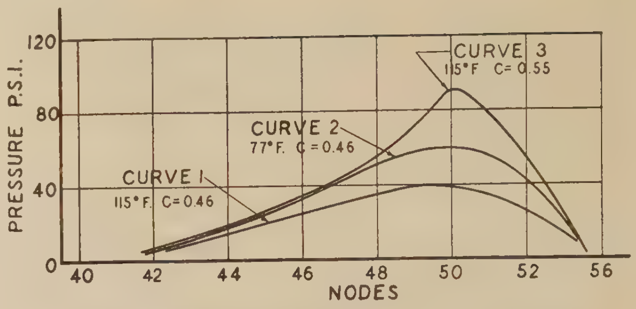

Fig. 6 Pressure Distribution at $n + 40$ Nodes

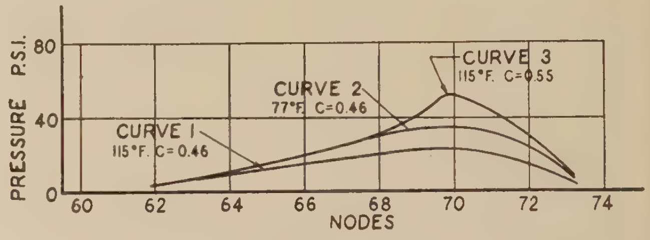

Fig. 7 Pressure Distribution at $n + 60$ Nodes

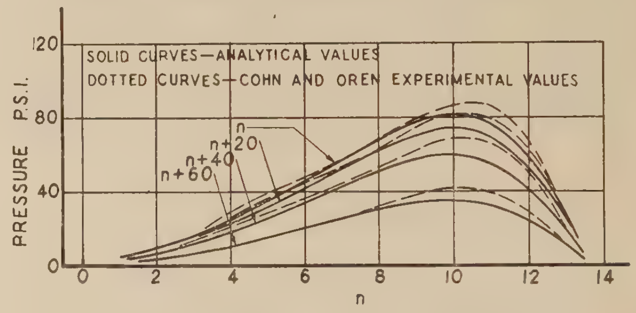

Fig. 8 Comparison of Analytical and Experimental Pressures

Acknowledgments

The author wishes to express his appreciation for the aid given in the preparation of the original thesis by Prof. L. J. Bradford, formerly of The Pennsylvania State College, and for the many helpful suggestions given in the preparation of this paper by E. M. Barber, F. J. Villforth, Jr., and J. R. Muenger of The Texas Company.

BIBLIOGRAPHY

1 "A New Mathematical Method for the Solution of Film Lubrication Problems," by D. G. Christopherson, The Institution of Mechanical Engineers, Journal and Proceedings, vol. 146, 1941, pp. 126–135.

2 "Film-Pressure Distribution in Grease-Lubricated Journal Bearings," by Gunther Cohn and Jess W. Oren, Trans. ASME, vol. 71, July, 1949, p. 555.

3 "Flow of Petroleum Lubricating Greases," by M. H. Arveson, *Industrial and Engineering Chemistry*, vol. 24, 1932, p. 71.

4 "On the Theory of Lubrication and Its Application to Mr. Beauchamp Tower's Experiments . . . (*a*), by O. Reynolds, *Philosophical Transactions*, Royal Society, vol. 177, part 1, 1886, pp. 157–234; (*b*) Papers on Mechanical and Physical Subjects, The Macmillan Company, New York, N. Y., vol. 2, 1901, pp. 228–310.

5 "Ebene und räumliche Strömung zäher inkompressibler trägheitsfreier Flüssigkeiten zwischen excentrischen, relative zu einander rotierenden Zylinderflachen. Beitrag zur Theorie der Schmierung," by H. Reissner, *Zeitschrift für angewandte Mathematik und Mechanik*, vol. 15, 1935, pp. 81–87; vol. 16, 1936, pp. 275–286, and 384.

6 "Zur hydrodynamischen Theorie der Lagerreibung," by G. Vogelpohl, *Zeitschrift für angewandte Mathematik und Mechanik*, vol. 15, 1935, pp. 278–285.

7 "Hydrodynamisch Lagertheorie und halbflüssige Reibung,"

by G. Vogelpohl, *Zeitschrift für angewandte Mathematik und Mechanik*, vol. 16, 1936, pp. 371–372.

8 "Beitrage zur Kenntrisder Gleitlagerreibung," by G. Vogelpohl, *Forschungsheft* 386, 1937, p. 28.

9 "Film Lubrication of Non-Planer Surfaces of Finite Width," by S. M. Skinner, Bulletin, American Physical Society vol. 12, 1937, p. 7.

10 "On Problems in the Theory of Fluid Film Lubrication, With an Experimental Method of Solution," by A. Kingsbury, *Journal of Applied Mechanics*, Trans. ASME, vol. 53, paper no. APM-53-5, 1931, p. A-59.

11 "Relaxation Methods in Engineering Science," by R. V. Southwell, The Clarendon Press, Oxford, England, 1940.

12 "Empirical Equations and Nomography," by D. S. Davis, McGraw-Hill Book Company, Inc., New York, N. Y., 1943, pp. 11–14.

Investigation of Lubricants for Power Circuit Breakers

By R. R. BUSH,[1] PHILADELPHIA, PA.

This paper describes a technique for the selection of proper lubricants for power circuit breakers. The circuit breaker is described briefly, and its lubrication requirements for dependable operation are discussed. The laboratory methods set up to determine the performance of the grease best suited for this application are outlined. Results of the laboratory test data are shown and evaluated with reference to circuit-breaker requirements. Properties of some typical greases are compared with their performance for this particular application. Because performance depends not only upon grease properties, but also upon the process of manufacture, the greases tested are referred to only in code. Life tests on actual circuit breakers have checked laboratory results. Therefore it is concluded that tests may be set up to determine the suitability of a lubricant for any particular application and especially for power circuit breakers.

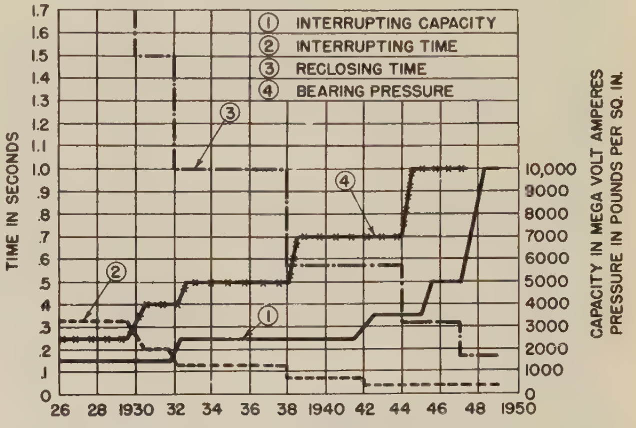

Fig. 1 General Chronological Development of Allowable Bearing Pressures Compared to Other Power-Circuit-Breaker Characteristics

Introduction

PROPER lubrication of power circuit breakers is a problem of considerable importance because the operation of the entire power system depends so completely on the reliable operation of the breakers under any emergency. When a short circuit occurs on a power line, the portion in which the disturbance originated must be isolated quickly to prevent damage to associated apparatus and to restore service to the rest of the system. Its entire operation must be completed in less than $^1/_{10}$ sec. To obtain this high-speed operation, friction of all moving parts must be held to a minimum. The better the lubrication of all friction points, the lower the friction which will be encountered. This means higher speed of operation and longer life of all moving parts.

The lubrication problem in power-circuit-breaker bearings and other friction points is peculiar in that the motion is extremely intermittent, generally oscillatory, and generally heavily loaded. The contacts of the power circuit breaker are opened in response to the operation of a high-speed relay by means of a powerful driving force properly connected through cranks, cams, and rollers. The driving force is generally obtained from energy stored in compressed springs, or compressed air. Quick opening is accomplished by suddenly releasing this stored energy. Each passing year has seen the size and speed of circuit breakers increase. With each such increase, the duty on bearings has also increased, as indicated in Fig. 1. To keep friction and maintenance to a minimum, better and better lubricants have been required. Hand in hand with this development went the choice of the proper lubricant for the bearings depending on the duty they perform.

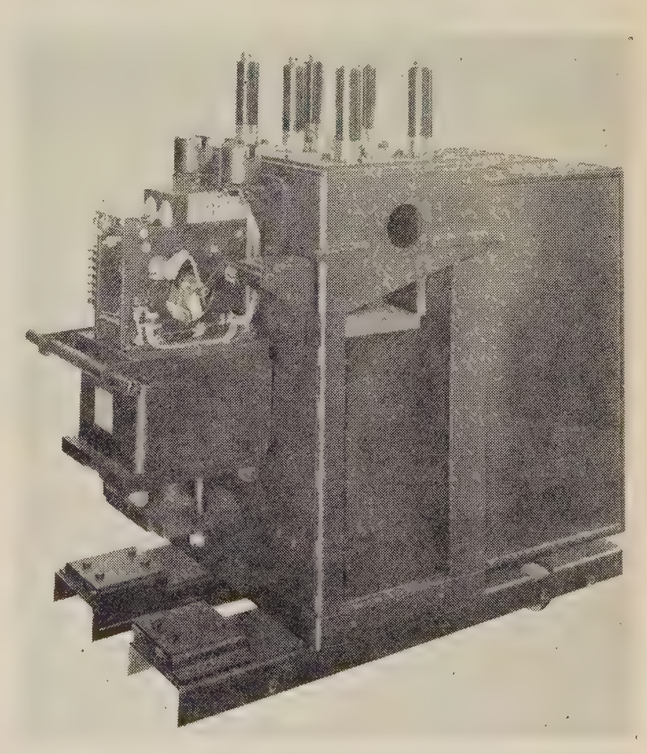

Fig. 2 Magne-Blast Power Circuit Breaker Rated 500,000 Kva at 13,800 Volts

(Bearings must operate instantly but intermittently at medium speed and relatively heavy loading.)

Fig. 2 is a magne-blast circuit breaker rated at 13,800 volts and 500,000 kva interrupting capacity, which represents one of the smaller types of modern circuit breakers. Fig. 3 is a 360,000-volt circuit breaker with an interrupting capacity of 10,000,000 kva, which represents the highest-capacity circuit breaker yet developed

---

[1] Development Engineer, Switchgear Divisions, General Electric Company. Mem. ASME.

Contributed by the Research Committee on Lubrication and the Petroleum Division and presented at the Annual Meeting, New York, N. Y., November 27–December 2, 1949, of The American Society of Mechanical Engineers.

Note: Statements and opinions advanced in papers are to be understood as individual expressions of their authors and not those of the Society. Paper No. 49—A-17.

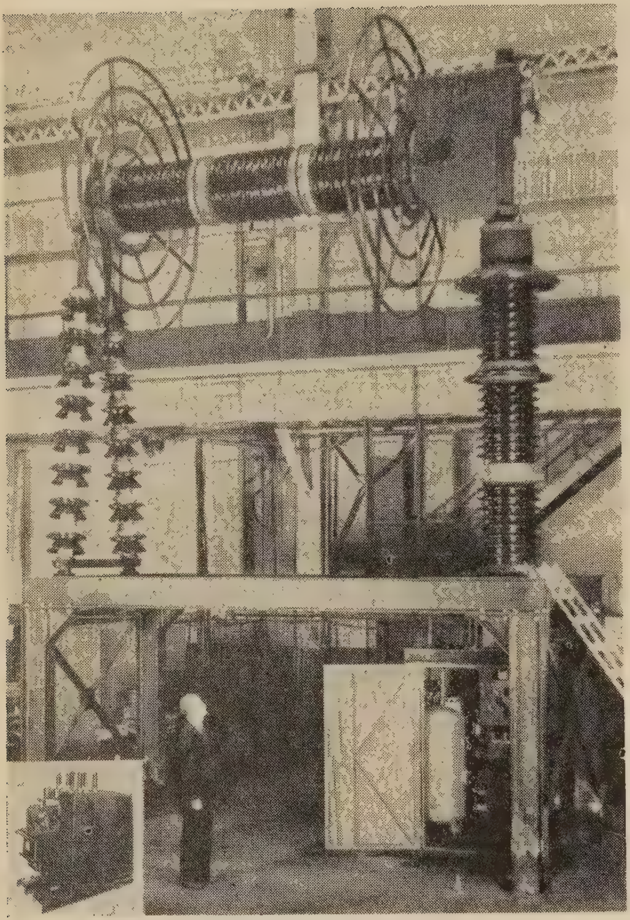

FIG. 3 LOW-OIL-CONTENT IMPULSE-TYPE OIL CIRCUIT BREAKER RATED 10,000,000 KVA AT 360,000 VOLTS
(Interrupting time 0.05 sec; reclosing time 0.167 sec. Inset of breaker from Fig. 2 compares sizes.)

Its 6 sets of contacts are designed to carry 1000 amp continuously, to open in 0.05 sec and reclose in 0.16 sec. For comparison of size, the inset at the lower left-hand corner shows the breaker from Fig. 2 to the same scale as this breaker. The development of most modern breakers would not have been possible without corresponding development in bearings and lubricants to keep friction to a minimum.

LUBRICATION REQUIREMENTS OF MODERN BREAKERS

It is well known that greases provide better lubrication than oils for power circuit breakers because they stay in the bearings better than oils under high pressures. They also exclude dirt to a greater degree than oils. This is especially true on textolite bearings,[2] and open antifriction or rolling-friction bearings. However, grease lubricants tend to stiffen up with time because of oxidation. In bearings in circuit-breaker mechanisms, where the available torque for initiating operation is low, this added friction may be serious because it may prevent the circuit breaker from opening. Some breaker bearings have been found in service in which the grease was practically solid around the rollers of trip latches. In cases when such breakers opened, it was found that the opening time had increased 3 to 5 times. This may be very serious under short-circuit conditions. Further investigation of these cases showed the torque required to operate the trip latch had increased several times over the normal torque required for tripping, because of hardened grease. The only assurance users have had of proper operation of circuit breakers has been periodic checking with a time-travel recorder to see that they have the proper speed. On outdoor breakers, located in cold climates, the increase in consistency, or decrease in penetration, with temperature is also a problem with many greases.

Another duty that greases must perform in power circuit breakers is protection from corrosion and rusting of bearings and other sliding metal parts, both during storage before placing in service, and after being placed in service. Humidity or corrosive atmospheres are particularly severe on roller bearings unless they are properly protected with a film of lubricant.

In sleeve bearings, the coefficient of friction varies widely with the type and condition of the lubricant. This is critical because of the high bearing pressures used in circuit breakers. With older metallic-bushing bearings, the grease film must persist at pressures around 7000 psi and in the modern textolite-bushing bearings at around 10,000 psi. Many greases may be found to satisfy one or more of the requirements just outlined, but to find one which will satisfy all these requirements is much more difficult.

The dependable and trouble-free operation of power circuit breakers under all conditions, however, dictates that the lubricant used meet all these requirements. Preferably a single lubricant should be used in all locations of a given circuit breaker to avoid the necessity of selection on the part of the maintenance crew and to avoid the stocking of several types of greases. Hence this investigation was initiated to determine the best type of lubricant for use in modern power circuit breakers. It must be realized that the best grease from an over-all standpoint will not necessarily be the best grease from all standpoints. This review, therefore, is presented more to point out the method of investigation rather than as a grease recommendation; and, accordingly, all greases are referred to by number only.

METHOD OF ATTACKING THE PROBLEM

Engineers from a number of lubricating companies were asked to review the problem. All agreed it was worth while to look for one grease, although the possibilities of finding one suitable for all operating conditions were doubtful. Accordingly, the following specifications were set down for the grease:

1 High resistance to oxidation.
2 Operating temperature range from —30 F to +150 F.
3 Good lubricating qualities.
4 Good corrosion protection.
5 Must not be forced out of bearing under high pressure.

With these points in mind, some thirty different greases were recommended for investigation.

The first check was on oxidation. The shelf life of the grease was considered the criterion for grease in antifriction bearings, because of the short working life and intermittent oscillatory motion imposed on them in circuit breakers. The Norma-Hoffman bomb test gave the best laboratory measure of this property, but the test was time-consuming.

For textolite sleeve bearings, it was considered that the oxidation of a thin film would be more indicative of the lasting qualities of the grease. In order to produce thin films for oxidation tests, a tool, shown in Fig. 4, was devised, the knife-edge of which spread an even thin film of grease on a chromium-plated steel plate measuring 1 in. × 5 in. × 12 in. This plate was lapped to a flatness of about 15 microinches before flash-plating with chromium about 0.0002 in. thick. The 0.001-in. thickness of

---

[2] "Heavy-Duty Bearings With Intermittent Oscillatory Motion," by R. R. Bush, presented at the Fall Meeting, Erie, Pa., September 28–30, 1949, of THE AMERICAN SOCIETY OF MECHANICAL ENGINEERS.

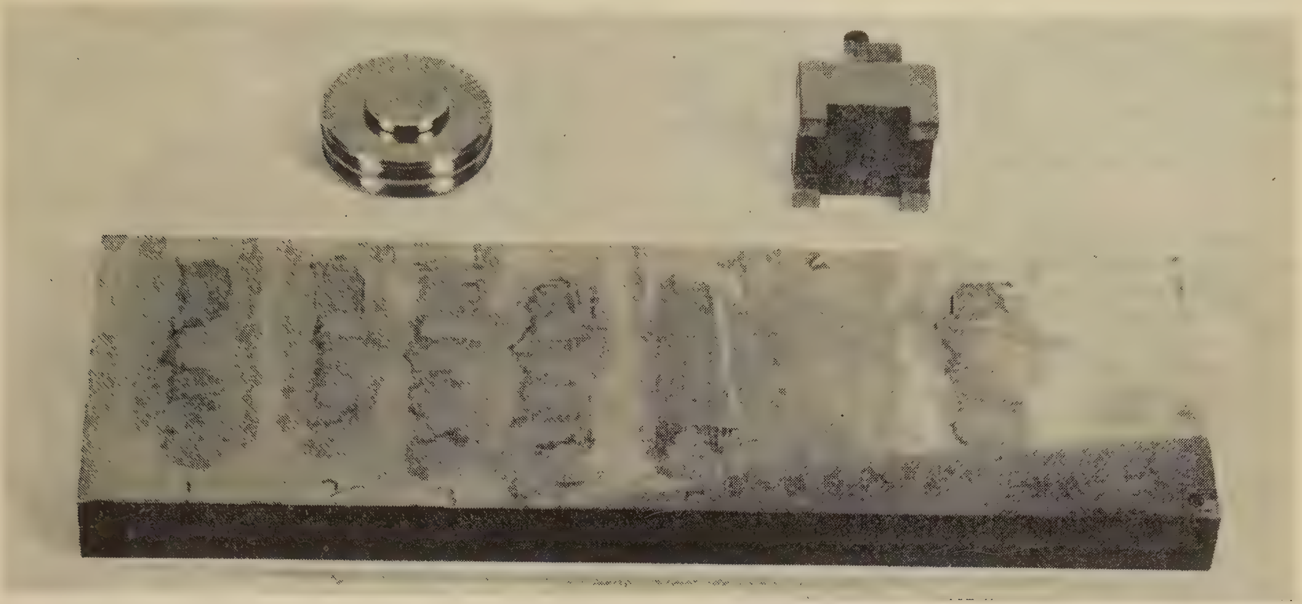

FIG. 4 APPARATUS FOR THIN-FILM OXIDATION TESTS

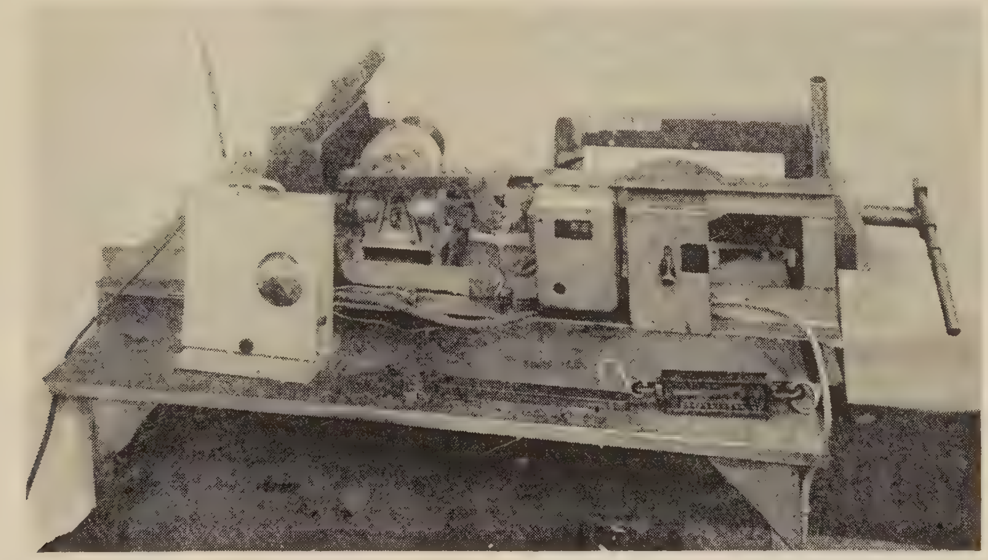

FIG. 5 BEARING TEST MACHINE FOR LIFE TEST AND FRICTION MEASUREMENTS

the film of grease as laid down was checked to within 0.0001 in. by a Gardner interchemical thickness gage.

Several greases were put on the plate at the same time and then placed in a circulating oven at 100 C. It was considered that any grease used for this purpose should remain relatively intact at this temperature and that the oxidation would be accelerated to give a comparative answer in a reasonable time. Greases which were not acceptable lost their lubricating properties in as short a time as 24 hr while many of the more acceptable ones lasted at least 120 hr. Some of the best greases retained their lubricating properties for even longer periods.

As soon as a grease indicated it might pass the thin-film oxidation test, it was checked in an ordinary refrigerator for 48 hr to see if it showed stiffening as lowered temperatures occurred. If it indicated satisfactory performance under these conditions, the grease was put on friction test in textolite bearings on the test machine shown in Fig. 5. Corrosion tests also were run at this time in both salt-spray and humidity chambers.

The friction test was run 100 operations at 8000 psi of projected area, 100 operations at 10,000 psi of projected area, and 100 at 12,000 psi. Starting and running friction were measured after each of the steps and if everything appeared satisfactory, a 14,000 operation life test was run at 12,000 psi. Starting and moving friction were determined at intervals during the run. Also, the machine was left standing overnight and over week ends and the starting friction measured just before resuming the run. The frictional values for both starting and running were compared because both are equally important in circuit breakers which must trip instantly and open at high speed. When a grease had passed the friction test, the thin-film test, the refrigerator cold test, and appeared to be satisfactory on the corrosion tests, then a Norma-Hoffman oxygen-bomb[3] test, and a torque-temperature test in a ball bearing were run. To check with types of sliding bearings other than textolite, friction runs were also taken on bronze bearings. Evaporation tests were also made on those greases which showed promise.

---

[3] "Some Applications of an Accelerated Test for Determining the Chemical Stability of Lubricating Greases," by F. L. Wright and H. A. Mills, Proceedings of the ASTM, vol. 38, part 2, 1938, pp. 525–538.

With the laboratory tests all satisfactory, the grease was then put in actual circuit breakers as a final check.

Results of Tests

Following will be a review of the results of tests made on a representative number of the greases investigated. It must be realized that any statement given applies only to the peculiar application investigated under the conditions outlined and is not a criterion for that grease under conditions different from those under consideration. Also, for the purpose of avoiding any possible undesirable reflection on any product, the greases are coded with only number reference. Table 1 is a tabulation of general performance as determined by test. Since readings were comparative, designations are listed as "acceptable" or "unacceptable." If any grease approaches acceptable in any given requirement, it is marked unacceptable and starred to indicate that further investigation is warranted. Table 2 lists general properties of several representative types of these greases together with general performance. Space does not permit listing all greases tested. Again, it is realized that the properties do not tell the whole story as to how a grease may perform. They are given merely to show any relation they might have to their performances under the conditions tested.[4] For better understanding of these tables, the following curves show typical detailed test data.

Fig. 6 shows the performance of two greases acceptable for friction. Fig. 7 shows the performance of two greases unacceptable for bearing friction. No grease was considered acceptable which showed a marked tendency to exceed 0.10 coefficient of starting friction during a run. Starting friction after a long period of rest might exceed this figure but would not be desirable. The maximum reached when grease 21 was used was 0.128 in one case. With grease 14, the coefficient of friction never exceeded 0.11 when the grease was new. However, when quite old, it would permit scoring of the bearings and pin after a short run at the high pressures involved. Fig. 8 illustrates oxygen-pressure loss with time in the Norma-Hoffman bomb. These curves give relative resistance to oxidation of four different greases.

Fig. 9 shows torque-temperature properties of two greases of widely different composition. Both of the greases illustrated were acceptable on this test as it indicates low torque on ball bearings in cold weather. Fig. 10 illustrates the loss by evaporation of 5-g samples of different greases placed in an oven at 210 F.

Examination of the tables and charts will reveal that grease 21, when compared with others, performed most consistently acceptable in all tests to which it was submitted. It also will be noted that while its average performance is good all around for the purpose investigated, other greases exceeded it on some points, but fell down on others.

TABLE 1 RESULTS OF PERFORMANCE TESTS AS CONDUCTED ON GREASES BY LABORATORY METHODS

GREASE NO.	OXIDATION		FRICTION MACH.	COLD REFRIG.	CORROSION TESTS
	FILM	BOMB			
1	U				
2	A	A	U	A	U
3	A		U	A	U
4	U				
5	U				
6	U				
7	U				
8	U				
9	U	U	U	U	
10	U*	U	U*	A	U
11	A		U		
12	U				
13	U				
14	U		A		A
15	U	U			
16	A	A	U	A	A
17	U				
18	A		U	U	
19	U			U	
20	U			U	
21	A	A	A	A	A
22	A		U	A	
23	A		U*		U
24	U				
25	U				

A = Acceptable
U = Unacceptable
* = Warrants further investigation

TABLE 2 CHARACTERISTIC PROPERTIES OF SEVERAL GREASES LISTED AGAINST RESULTS OF PERFORMANCE TESTS AS CONDUCTED BY LABORATORY METHODS

PROPERTIES							PERFORMANCE			
GREASE NO.	SOAP BASE	OIL		INHIBITORS		CONSIST. UNWORKED	THIN FILM	FRICTION MACH.	COLD REFRIG.	CORROSION TESTS
		TYPE	VISC. 100°F	OXY.	RUST					
21	Na	Pet.	200	Yes	Yes	300	A_b	A	A_c	A
11	Na	Pet.	125	Yes	No	300	A	U	U	-
14	Ca	Pet.	300	Yes	-	250	U	A	U	A
10	Ca	Pet.	285	No	No	350	U	U	U	-
23	Li	Pet.	300	Yes	Yes	275	A	U*	-	U
16	Li	Syn. & Pet.	72	Yes	-	265	A	U	A	A
2	Li	Syn.	70	Yes	Yes	250	A	U	A	U
3	Li	Syn.	70	Yes	Yes	250	A	U	A	U

A = Acceptable
U = Unacceptable
* = Warrants further investigation
b = Also bomb test—induction period exceeds 1000 hr
c = Also torque test —900 gm cm to start at —30 F

It appears that inhibitors against oxidation are mandatory. Rust inhibitors are a help against corrosion, but other ingredients may accomplish this protection. The sodium soap base appears to perform better on resistance to oxidation than calcium soap base, but either is good on friction when formulated with petroleum oil having in the neighborhood of 275 SUS viscosity at 100 F, and showing a consistency of around 275 penetration. The lithium soap base with a 300 SUS viscosity performed much better on the friction machine than those with lighter oils, although the test results did not show up good enough. Generally, they gave the least protection in corrosion tests but showed very good resistance to oxidation.

It may be of interest here to mention that dry lubrication was tried on textolite bearings and stainless-steel shafts without success at any pressures in the ranges considered.

After the laboratory tests, grease 21 was put on life tests on large and small-sized breakers. Its performance met expectations in all cases except on high-speed open gearing. It lacked the ability to stick fast on these fast-rotating parts. Circuit breakers have few such applications in their design.

Conclusions

Review of the data reveals that much investigation is necessary to determine the suitability of a lubricant for any particular apparatus. It was possible to find a grease that fulfilled most of the

---

[4] "Functional Tests for Lubricants and Their Interpretation," by T. G. Roehner and E. S. Carmichael, *Lubrication Engineering*, vol. 5 February, 1949, pp. 15–18 and 47.

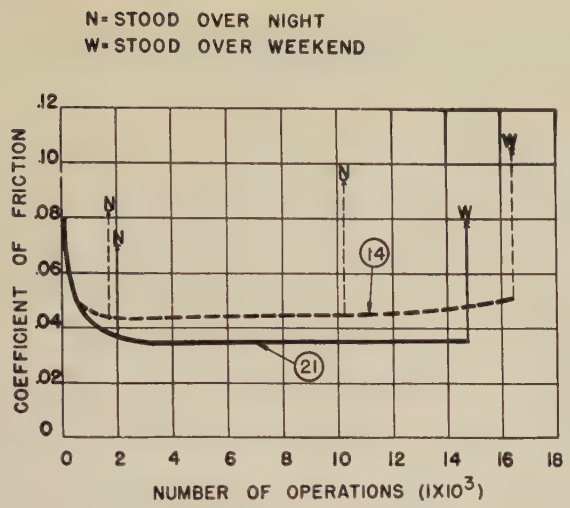

FIG. 6 CURVE SHEET SHOWING COEFFICIENT OF FRICTION OF BEARINGS WITH TWO ACCEPTABLE GREASES

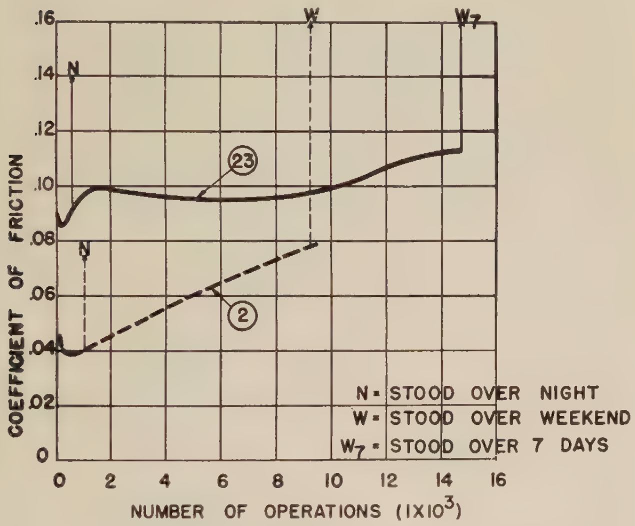

FIG. 7 CURVE SHEET SHOWING COEFFICIENT OF FRICTION OF BEARINGS WITH TWO UNACCEPTABLE GREASES

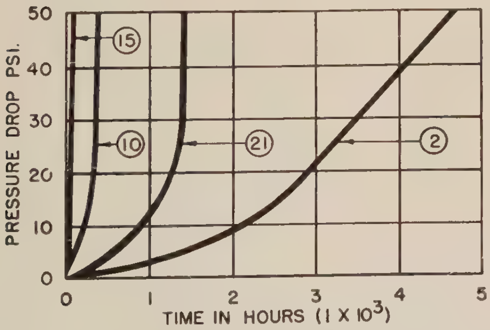

FIG. 8 CURVE SHEET SHOWING OXYGEN-BOMB TESTS AT 210 F OF SEVERAL GREASES

requirements set down for the particular application. For a few very special considerations a special lubricant is necessary. Investigation shows that laboratory tests are the quickest and the most reliable way to check a large number of possible greases for a specific application. Results obtained in an actual circuit breaker gave performance far superior to any of the standard greases previously used for this application. Each application, however, will require its own peculiar tests of several lubricants, and different weights will be given to each characteristic to arrive at an acceptable solution for that application. Life tests then must be made on the apparatus itself to insure that performance on all points is satisfactory. In circuit breakers, such a lubrication investigation has yielded results far better than could have been obtained in any other way.

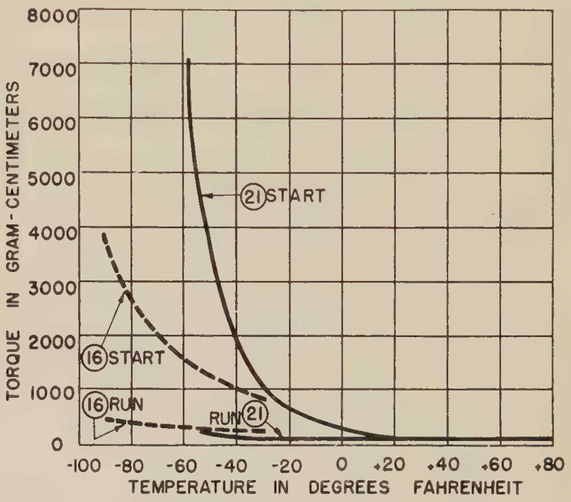

FIG. 9 CURVE SHEET SHOWING TEMPERATURE-TORQUE CHARACTERISTICS OF TWO GREASES

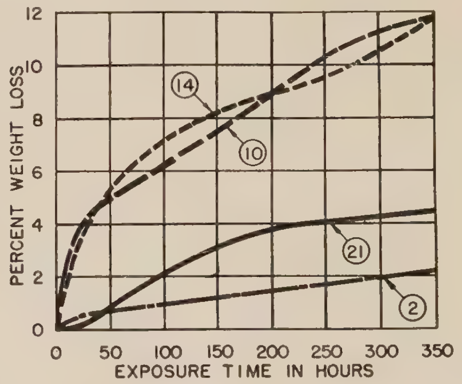

FIG. 10 CURVE SHEET SHOWING EVAPORATION LOSSES OF SEVERAL GREASES AT 210 F

Discussion

V. L. BARR.[5] One very important point which needs restressing is that this work was conducted to find a suitable lubricant for sleeve-type bearings, primarily textolite. The bearing pressures shown in Fig. 1 of the paper, for instance, are for this type bearing and not antifriction bearings. Successful applications of needle-type bearings under similar service conditions operate at much higher loading on a projected-area basis.

The data presented are applicable to antifriction bearings, but not in the same order of importance as shown in this paper. For ball and roller bearings, we would list the requirements in the following order:

---

[5] Director of Engineering, Roller Bearing Company of America, Trenton, N. J. Jun. ASME.

1 Resistance to oxidation.
2 Wide temperature range of operation.
3 Corrosion protection.
4 Good lubricating qualities.

The author's last requirement has no particular interest for antifriction bearings.

For the particular service required in circuit breakers, we are not too concerned with the lubrication properties of a grease. For continuous-rotating applications, however, this is not true.

With these points in mind and reviewing Table 1 of the paper, it is the writer's opinion that grease No. 16 would be very satisfactory for the antifriction bearings used in circuit breakers. Assuming corrosion conditions are not too severe, grease No. 2 would be highly satisfactory. Grease No. 11 we feel should be investigated further since it may be satisfactory for antifriction bearings.

Perhaps from Table 2 some of the greases may be recognized in terms of governmental specifications. In this respect, it is our opinion that service received from various manufacturers' products, meeting a particular specification, is quite varied. We believe any specifications for lubricants should include more performance-test requirements.

To stress further the difference in requirements between sleeve bearings and antifriction bearings, the variation between greases Nos. 21 and 16 from Fig. 9 will be noted. Grease No. 16 is much more desirable at the extreme low temperatures, yet, on the friction machine, grease No. 16 is unsatisfactory, while No. 21 was acceptable.

This last point suggests that for sensitive tripping mechanisms in extreme cold it may be absolutely necessary to use a grease such as No. 16 in the antifriction bearings.

Author's Closure

Mr. Barr has ably pointed out the difference between the requirements of an antifriction bearing used in a power circuit breaker and those of the same bearing working under what might be termed the usual running conditions. It must be remembered, however, that the grease selected for this application operates successfully in both the antifriction bearings and the textolite sleeve bearings working under the intermittent oscillatory motion encountered in circuit breakers.

Had the problem been restricted entirely to antifriction bearings, both greases No. 16 and No. 2 would have given better operation at lower temperatures than was required. Grease No. 11, however, was not as good in this respect as grease No. 21 which was chosen. The need for one all-purpose grease was imperative for this application and the selection was made on this basis.

The suggestion that specifications for lubricants should include more performance-test requirements is very timely. These requirements should be such that they can be checked in the laboratory with reasonable facility. The time required to work out a suitable set of tests as a procedure for screening the lubricants before final life tests will yield dividends. Each application will require its own peculiar tests of several lubricants, and different weights will be given to each characteristic to arrive at an acceptable solution for the application being considered.

Heat Transfer to Superheated Steam at High Pressures

By W. H. McADAMS,[1] W. E. KENNEL,[2] and J. N. ADDOMS[3]

Local coefficients of heat transfer from a 12.3-in. length of 0.252-in. tubing to steam flowing upward in a vertical annulus were measured for pressures from 115 to 3500 psia, for temperatures from 430 to 1000 F, and for temperature differences from 100 to 620 F. All results are correlated in Fig. 8 in terms of the local Nusselt number, the Reynolds number, the Prandtl number, and the geometrical ratio L/D_e, with the physical properties evaluated at the film temperature. An improved correlation, employing new data on thermal conductivity, is presented in Fig. 10 of the Addendum.

Nomenclature

The following nomenclature is used in the paper:

A = area of heat-transfer surface, sq ft
a = constant, dimensionless
c = specific heat of fluid at constant pressure, Btu/(lb) (deg F)
D = diameter, ft
D_e = equivalent diameter, equal to 4 times the hydraulic radius based on total wetted perimeter, ft
d = prefix, indicating first derivative, dimensionless
f_m = mean value of friction factor, dimensionless
G = mass velocity of fluid, lb/(hr) (sq ft of cross section)
h = local coefficient of heat transfer, Btu/(hr) (sq ft) (deg F); h_m for mean value
I^2R = rate of electrical generation of heat in wall of heater, Btu/hr
K = function of L/D_e, defined by Equation [9]
k = thermal conductivity of fluid, Btu/(hr) (ft) (deg F); k_h for wall of heater
L = length of heat-transfer surface, ft
m = exponent, dimensionless
q = rate of heat transfer, Btu/hr
q/A = density of heat flux, Btu/(hr) (sq ft)
r = radius of wall of heater, ft
S = cross section for fluid flow, sq ft; $\pi D^2/4$ inside tubes; $\pi(D_2^2 - D_1^2)/4$ in annuli
t = bulk temperature of fluid, deg F
V = average velocity of fluid, based on density at bulk-stream temperature, ft/hr
X, X', X'' = abscissas of Figs. 4, 5, 6, dimensionless
x_h = thickness of wall of heater
Y, Y', Y'', Y''' = ordinates of Figs. 4, 5, 6, 8
Δt = temperature potential, deg F
μ = viscosity of fluid, lb/(hr) (ft), equal to 2.42 × viscosity in centipoises
π = 3.1416
ρ = density of fluid, lb/cu ft

Subscripts:

1, 2 = entering and leaving
c = conduction and convection
f = physical property evaluated at film temperature; t_f equals $(t + t_w)/2$
i = inside wall of heater
m = mean
o = outside wall of heater
r = by radiation
t = total by conduction, convection, and radiation
w = physical property evaluated at wall temperature t_w
wi, wo = inside wall, outside wall, of heater

Dimensionless Moduli:

$c\mu/k$ = Prandtl number
DG/μ = Reynolds number based on inside diameter tube
D_eG/μ = Reynolds number based on equivalent diameter D_e
$DV\rho_w/\mu_w$ = modified Reynolds number
hD_e/k = Nusselt number, local
h_mD/k, h_mD_e/k = Nusselt number, mean
μ_w/μ = ratio of viscosities
L/D, L/D_e = geometrical ratios

Introduction

The object of this investigation was to determine local or point coefficients of heat transfer from metal to superheated steam at pressures up to 3500 psia, for a heater having an outside diameter of 0.25 in., concentrically located in an unheated vertical jacket having an inside diameter of 0.382 in. Mass velocities in the annulus were to be restricted to the range from 55,000 to 165,000 lb per hr per sq ft of cross section. Heater temperatures were to be as high as possible.

Review of the Literature on Heating and Cooling

Turbulent Flow Inside Tubes. Various mathematical analogies between the transfer of heat and momentum lead to quantitative relations among four dimensionless moduli as follows:

h_mD/k, mean Nusselt number, based on heated length

$c\mu/k$, Prandtl number, which is ratio of molecular diffusivity of momentum (μ/ρ) to molecular diffusivity of heat $(k/\rho c)$

$$\frac{DV}{\mu/\rho} = \frac{DG}{\mu}, \text{ “diameter” Reynolds}$$

number, which is a ratio of acceleration forces to viscous forces.

f_m, mean friction factor, equal to shear stress at wall, divided by $\rho V^2/2g_c$.

In deriving the analogies, various simplifying assumptions are made, such as, the flow is fully developed and incompressible, the physical properties are independent of temperature, and

---

[1] Professor of Chemical Engineering, Massachusetts Institute of Technology, Cambridge, Mass. Mem. ASME.

[2] Research Department, Standard Oil Co. of Indiana, Whiting, Ind.

[3] Assistant Professor of Chemical Engineering, Massachusetts Institute of Technology.

Contributed by the Special Research Committee on High Temperature Steam Generation, Joint Committee on Effect of Temperature on Properties of Metals, Heat Transfer, and Power Divisions, and presented at the Annual Meeting, New York, N. Y., November 27–December 2, 1949, of The American Society of Mechanical Engineers.

Note: Statements and opinions advanced in papers are to be understood as individual expressions of their authors and not those of the Society. Paper No. 49—A-32.

the velocity distribution is known and is independent of Δt.

Owing to lack of fundamental information on temperature and velocity profiles, experimental data on mean heat-transfer coefficients are usually correlated empirically in terms of the first three of the dimensionless numbers just listed, or their equivalent. The empirical equations differ as to the temperatures at which the physical properties are evaluated. To allow for variation in properties with temperature, ratios such as μ/μ_w, ρ/ρ_w, and k/k_w are sometimes introduced.

In the last 16 years three types of equations have been accepted generally for predicting coefficients for heating fluids flowing inside tubes:

All physical properties are based on bulk-stream temperature t

$$\frac{h_m D/k}{(c\mu/k)^m} = a\left(\frac{DG}{\mu}\right)^{0.8} \qquad [1]$$

Reference:[4]	a	m	Equation
(6), (12)	0.024	0.4	[1a]
(10), (11)	0.023	0.4	[1b]
(7)	0.021	1/3	[1c]

All physical properties are based on bulk-stream temperature, except μ_f is taken at $t_f = (t + t_w)/2$

Reference:	a	m	
(4)	0.023	1/3	[2]

All physical properties are based on bulk-stream temperature, except μ_w

$$\frac{(h_m D/k)}{(c\mu/k)^m}\left(\frac{\mu_w}{\mu}\right)^{0.14} = a\left(\frac{DG}{\mu}\right)^{0.8} \qquad [3]$$

Reference:	a	m	Equation
(13)	0.027	1/3	[3a]
(2)	0.023	1/3	[3b]

The foregoing equations are based on experimental data for relatively small values of Δt; at moderate Δt, they predict approximately the same values of h_m for water.

A recent paper (8) reports data on heating air at Δt up to 940 F and at DG/μ from 10,000 to 230,000. Regardless of whether the physical properties were evaluated at the bulk-stream temperature or at the wall temperature, the data fell on curves of changing slope, and the data were lower than predicted by Equations [1a] and [1b]. The data were brought into close agreement (8) by the equation

$$\frac{h_m D/k_w}{(c\mu/k)_w^{0.4}} = a\left(\frac{DV\rho_w}{\mu_w}\right)^{0.8} \qquad [4]$$

wherein all physical properties are evaluated at the wall temperature, and a modified Reynolds number

$$\frac{DV\rho_w}{\mu_w} = \left(\frac{DV\rho}{\mu}\right)\left(\frac{\mu}{\rho}\right)\left(\frac{\rho_w}{\mu_w}\right) \qquad [4a]$$

was employed. With a bellmouth entry (8), and for L/D of 60, the constant a was 0.022

$$\frac{h_m D/k_w}{(c\mu/k)_w^{0.4}} = 0.022\left(\frac{DV\rho_w}{\mu_w}\right)^{0.8} \qquad [4b]$$

Alternatively, $(c\mu/k)_w$ could be omitted (8) giving

$$\frac{h_m D}{k_w} = 0.018\left(\frac{DV\rho_w}{\mu_w}\right)^{0.8} \qquad [4c]$$

No other data at high Δt are available for heating gases. The literature contains no reliable data on heat transfer to steam under conditions of high pressure and high Δt.

Reference (1) shows curves of the local coefficient for air versus L/D for the entrance section of a tube at values of DG/μ from 17,000 to 56,000, for a number of entrance conditions. For flow in a tube following a sudden contraction, the initial value of h (for the first 0.56 diam) was roughly twice that at L/D of 10. Reference (3) reports results for DG/μ from 18,000 to 8000, which indicate that the local heat-transfer coefficient varies as the minus 0.15 power of L/D, for the first 31.5 diam.

Turbulent Flow in Annuli. While several equations have been proposed, the latest is that of reference (2)

$$\frac{hD_e/k}{(c\mu/k)^{1/3}}\left(\frac{\mu_w}{\mu}\right)^{0.14} = 0.023\left(\frac{D_e G}{\mu}\right)^{0.8} \qquad [5]$$

wherein all physical properties, except μ_w, are evaluated at the bulk-stream temperature; D_e is equal to 4 times the hydraulic radius based on total wetted perimeter, and is equal to $D_2 - D_1$.

Further support of the use of D_e is given by the results of reference (5) for rectangular passages; as shown in reference (11),[5] these data ran 10 to 25 per cent below Equation [1b].

EXPERIMENTAL

Introduction. To accomplish the objectives, an apparatus capable of withstanding pressures of 3500 psia at 1000 F and per-

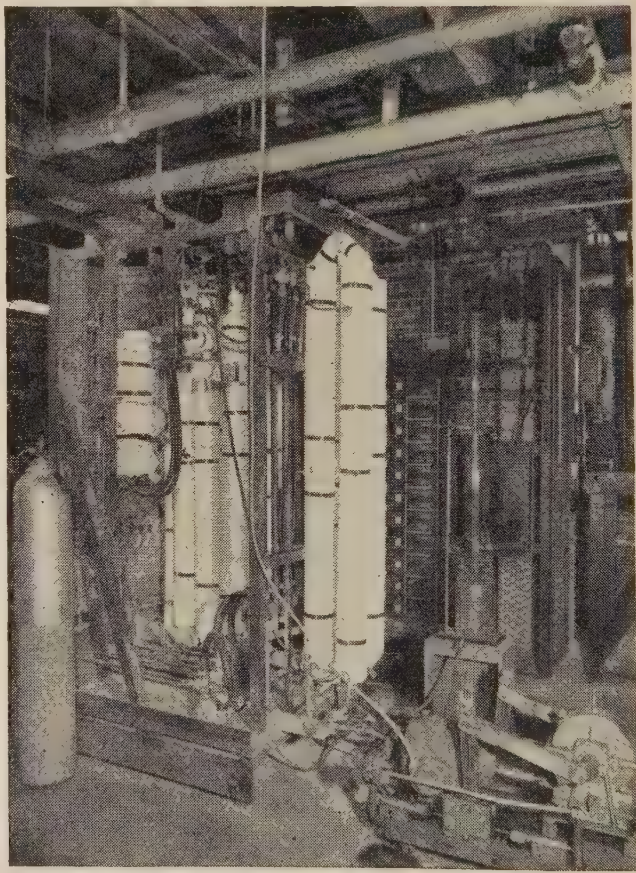

FIG. 1 HIGH-PRESSURE APPARATUS, WITH STEEL SAFETY BOOTH REMOVED

(Right foreground, adjustable-stroke 4-cylinder pump, feed reservoir, and condensate-measuring tube. Heavily insulated 13-pass electrically heated series boiler is located in front of the a-c switchboard, and condenser and cooler are visible. Heavily insulated test section, and the d-c busbars, are mounted just behind control panel near nitrogen cylinder.)

---

[4] Numbers in parentheses refer to the Bibliography at the end of the paper.

[5] Reference (11), p. 198.

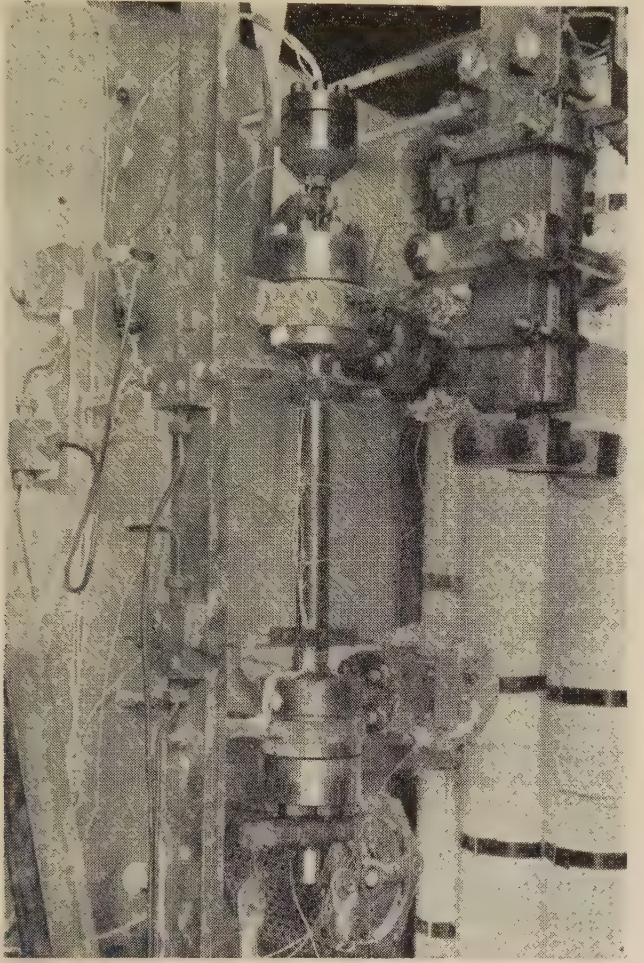

Fig. 2 Test Section Before Insulating

(Leads to thermocouples installed inside heating tube are brought out through nitrogen-pressurized fitting at top. The d-c power connections and potential taps can be seen. Further details shown in Fig. 3.)

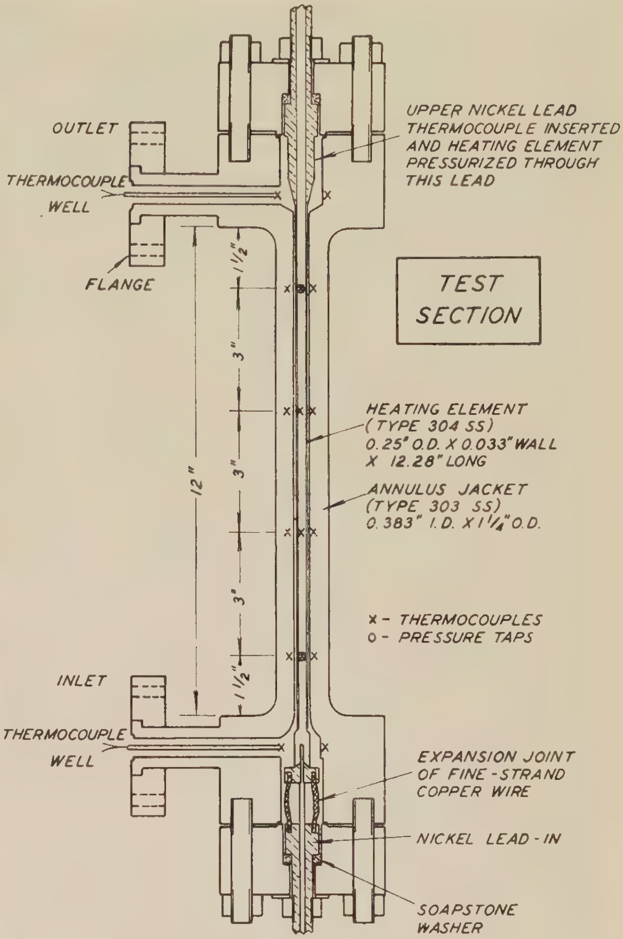
OUTLET
THERMOCOUPLE WELL
FLANGE
UPPER NICKEL LEAD THERMOCOUPLE INSERTED AND HEATING ELEMENT PRESSURIZED THROUGH THIS LEAD
TEST SECTION
1 1/2"
3"
3"
3"
1 1/2"
12"
HEATING ELEMENT (TYPE 304 SS) 0.25" O.D. X 0.033" WALL X 12.28" LONG
ANNULUS JACKET (TYPE 303 SS) 0.383" I.D. X 1 1/4" O.D.
x - THERMOCOUPLES
o - PRESSURE TAPS
INLET
THERMOCOUPLE WELL
EXPANSION JOINT OF FINE-STRAND COPPER WIRE
NICKEL LEAD-IN
SOAPSTONE WASHER

Fig. 3 Detailed Drawing of Test Section

mitting accurate measurement of the local heat flow and local temperature driving force was required. Condensing mercury vapor, molten metals, and fused salts were considered as sources of heat but were discarded in favor of electric heat generated in the wall of a metal tube. Because the wall of the electrically heated tube had to be thin to avoid use of excessive current and to minimize longitudinal conduction of heat, it was impossible to use the tube itself as the pressure vessel. Consequently, the electrically heated tube was pressurized internally with nitrogen, and was located concentrically in a high-pressure jacket, thus forming an annular passage for flow of steam.

The procedure was to heat superheated steam as it flowed upward at a measured rate through the annular space. The heat dissipated by the heating element was calculated from electrical measurements; the corresponding temperature of the heating element was determined by measuring the inside temperature and correcting for the radial temperature gradient in the wall. The temperature of the steam was measured at the entrance and exit of the test section and was corrected for heat losses. The point coefficient of heat transfer could be calculated from the data for given flow conditions.

Apparatus. The apparatus was a flow system in which water was drawn from a reservoir and pumped through a preheater, a test section, throttle valves, a condenser and condensate cooler, and back to the reservoir. Views of the apparatus are shown in Figs. 1 and 2. Stainless steel, which has good corrosion resistance and strength at high temperatures, was used as the material of construction. Safety devices included a movable steel booth enclosing the entire apparatus, two rupture disks calibrated to blow at 4400 psia, and an automatic device to shut off electrical power whenever the pressure decreased substantially.

A four-cylinder pump of the positive-displacement type drew water from the reservoir at atmospheric pressure and injected it into the high-pressure system. The flow rate was measured volumetrically at the inlet of the pump.

The preheater, seen in Fig. 1, took cold water from the pump and produced superheated steam at any desired temperature up to 900 F at flow rates up to 75 lb per hr. It consisted of 80 ft of $^3/_8$-in. extra-heavy stainless-steel pipe covered with insulation and electrical windings capable of dissipating 35 kw at 110 alternating current. Power to the preheater was controlled by switches on each of 12 electrical windings and by a Variac on the last winding. Total preheater power was indicated by a wattmeter. A spiral strip of stainless steel was inserted in the last two 6-ft lengths of the preheater to impart a centrifugal motion to the fluid, so that any entrained liquid would contact the heated wall and thus be vaporized.

The test section (Figs. 2 and 3), consisted of a vertical annulus in which a stainless-steel heating element was mounted coaxially inside a pressure jacket which had an inside diameter of 0.382-in. Removable end closures on the pressure jacket were equipped with insulated nickel leads which supplied electrical power. The heating element was a stainless-steel tube having an outside diameter of 0.252 in., a length of 12.28 in., and a wall thickness of

0.0332 in. At the lower end it was silver-soldered to an adapter on a flexible connection which served as an expansion joint and electrical lead. At the upper end, the element was silver-soldered to a hollow nickel electrical lead through which were inserted four chromel-alumel thermocouples, spaced at 3-in. intervals. By means of a special fitting on the open end of the upper nickel lead, nitrogen pressure was applied to the inside of the heating element to prevent collapse under the external pressure of the steam.

Iron-constantan thermocouples were installed in wells at the entrance and exit of the test section to measure steam temperatures. Ten thermocouples were installed in small radial holes in the wall of the pressure jacket to permit estimates of temperature at the inner surface.

Power to the test section was supplied by a 15-volt 1000-amp direct-current generator. To measure voltage drop across the heating element a voltage-divider circuit, consisting of a 10-ohm resistor and a 1000-ohm resistor, was connected across the heating element. A calibrated 0.00005-ohm resistor was connected in series with the heating element to determine the current. The voltage drop across the 10-ohm resistor and the 0.00005-ohm resistor, and the potential generated by the thermocouples, were measured by means of a portable precision potentiometer.

Following the test section, $^1/_8$-in. and $^3/_8$-in. needle valves were installed in parallel to throttle the steam from operating pressure to that at the entrance to the condenser and cooler.

Operating Procedure. Before mounting a heating element in the test section, the resistances of its component parts were determined. The thermocouple assembly was then inserted in the heating element, which was mounted in the test section. The end closures were secured, and the system was pressure-tested.

The throttle valves were opened, the pump was started, and the desired flow rate was set by adjusting the stroke of the pump. The power to the preheater was then turned on and adjusted to approximately the desired value, and the temperature of the system was allowed to rise. The desired operating conditions were approached by adjusting the throttle valves and the power to the preheater. After a final adjustment of the pump to the desired flow rate, the system was allowed to come to a steady-state condition.

The approach to steady-state condition was determined by plotting the difference between the millivolt readings of the thermocouples measuring inlet and outlet steam temperature versus time. When this temperature rise became substantially constant, a run was begun. Each run was made with constant flow rate, pressure, and temperature of the inlet steam.

The first one or two data points in each run were taken with no power to the heating element, in order to determine the heat loss. Data points were then taken at various settings of power input to the test section. Most of the runs were concluded at power inputs such that the temperature inside the heating element did not exceed 1300 F, because early runs showed that operation at higher temperatures caused warping and discoloration.

Method of Calculation. For each setting of power to the test section, the total density of heat flux, the heat transferred by radiation (see Appendix), the temperature of the outside wall of the heating element, the bulk temperature of the steam, the Δt, and the local coefficient of heat transfer were calculated. Each of these factors was evaluated at four positions corresponding to the locations of the thermocouples inside the heating element.

The power dissipated by the heating element was calculated by using the product I^2R where I is the current through the heating element and R is the resistance at the average wall temperature. The density of heat flux was then calculated from the power dissipated and the dimensions of the heating element. The temperature of the outer wall of the heating element was determined from the temperature of the inside wall by subtracting the temperature drop through the wall

$$t_{wi} - t_{wo} = \left(\frac{dq_t}{dA_o}\right)\frac{r_o}{k_h}\left(\frac{1}{2} - \frac{r_i^2}{r_o^2 - r_i^2}\ln\frac{r_o}{r_i}\right) \quad \ldots\ldots [6]$$

$$(\Delta t)_w = \left(\frac{dq_t}{dA_o}\right)\frac{x_h}{k_h}\left(\frac{1}{2} + \frac{x_h}{6\,D_o}\right) \quad \ldots\ldots\ldots [6a]$$

Equation [6] was derived by assuming uniform generation of heat per unit volume of the wall and constant thermal conductivity at the average wall temperature; Equation [6a] follows upon expansion of the logarithmic term. For the densities of heat flux employed, the $(\Delta t)_w$ calculated from Equation [6a] was sufficiently close to that calculated by allowing for variation of thermal conductivity and electrical resistivity with temperature.

Since the temperature of the steam was measured only at the entrance and exit of the last section, it was necessary to calculate the temperature of the steam at the positions corresponding to the four thermocouples. The heat lost by the steam while it flowed from the entrance to any point in the test section was determined from data at zero heat input. The heat generated by the heating element up to the same position was calculated. The increase in the temperature of the steam from the entrance to the desired location was calculated by difference.

The local rate of heat transfer by the combined mechanisms of conduction and convection (dq_c/dA_o) was obtained by deducting an estimate for radiation (dq_r/dA_o) from the total local flux (dq_t/dA_o). Since the emissivity and absorptivity of water vapor for radiation have not been investigated at high pressure, it was necessary to extrapolate the values from atmospheric pressure (see Appendix). The radiation correction never exceeded 12 per cent and usually was less than 10 per cent.

The local Δt and the local density of heat flux dq_c/dA_o were used to calculate the local coefficient of heat transfer

$$h = \frac{\dfrac{dq_t}{dA_o} - \dfrac{dq_r}{dA_o}}{t_{wo} - t} = \frac{\dfrac{dq_c}{dA_o}}{\Delta t} \quad \ldots\ldots\ldots\ldots [7]$$

Results

Twenty-seven runs were made, of which twenty-five were successful. The ranges of pressure, temperature, and mass velocity are given in Table 1. Over-all heat balances were good, allowing for heat losses. Points of two kinds were eliminated; those for outer wall temperatures above 1300 F, and those with Δt less than 100 F. The points in the former category were discarded because there was the probability of distortion and oxidation of the heater. All data with Δt of less than 100 F were eliminated, since slight changes in line voltage to the preheater made precise control of the steam temperature difficult; a change of 1 per cent in the preheater power resulted in 10 to 12 F change in steam temperature.

The local Nusselt numbers, Prandtl numbers, Reynolds numbers, length-diameter ratios, and viscosity ratios were tabulated for all the data to be correlated. Local Nusselt numbers at L/D_e of 57 are plotted in Figs. 4, 5, and 6.

Plots similar to Figs. 4, 5, and 6 were made for local Nusselt numbers at L/D_e of 11.4; the trends were similar to those shown in Figs. 4, 5, and 6. In addition, plots similar to Figs. 4 and 6 were constructed for the local Nusselt numbers at L/D_e of 37 and 80.

The effect of L/D_e was determined from Fig. 6 and similar plots. The best straight line was drawn through each set of points, and the constant K in the equation

$$Y'' = K\,(X'')^{0.89} \quad \ldots\ldots\ldots\ldots [8]$$

TABLE 1 RANGES OF VARIABLES

Pressure, psia	Run no.	$\frac{G}{1000}$	$\frac{q_e/A_o}{1000}$	t, deg F	Δt, deg F
115	27	55	30–53	477–735	267–540
	26	110	38–93	441–668	198–564
	24	165	44–110	429–591	178–513
	25	165	48–103	639–790	177–442
500	1	56	11–61	569–821	107–624
	2	110	26–48	541–643	130–291
	8	110	33–85	606–791	170–487
	9	110	33–56	617–729	168–357
	16	110	22–48	913–948	110–242
	3	165	47–108	544–673	167–507
1000	6	55	27–44	612–755	223–481
	4	110	27–74	590–705	120–444
	14	110	24–47	915–1000	116–250
	5	165	35–107	602–713	114–465
2000	7	55	24–40	711–812	166–425
	18	55	23–28	922–1011	171–258
	11	106	35–69	713–789	148–405
	15	110	23–48	934–1012	105–248
	12	164	57–98	730–808	193–402
	19	153	30–65	924–1012	104–238
3000	17	110	24–47	924–970	100–225
	22	97	29–51	886–967	130–284
	20	160	29–72	932–980	100–271
3500	23	96	27–52	891–964	112–293
	21	156	72–72	960–1000	226–238

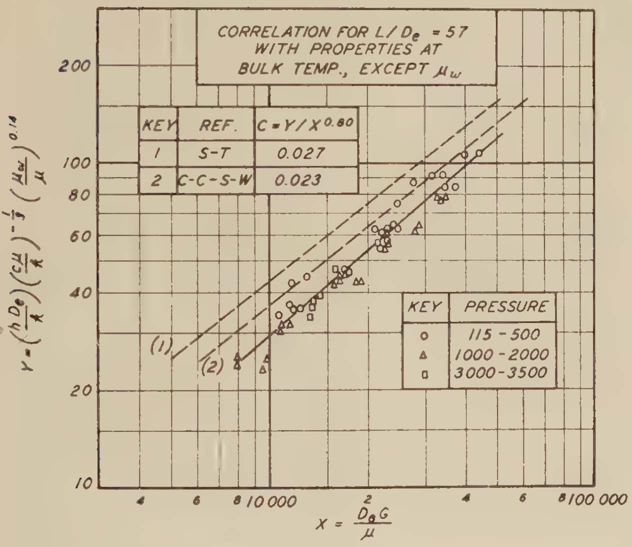

FIG. 4 CORRELATION OF DATA AT L/D_e OF 57
(Using co-ordinates of references 2 and 13.)

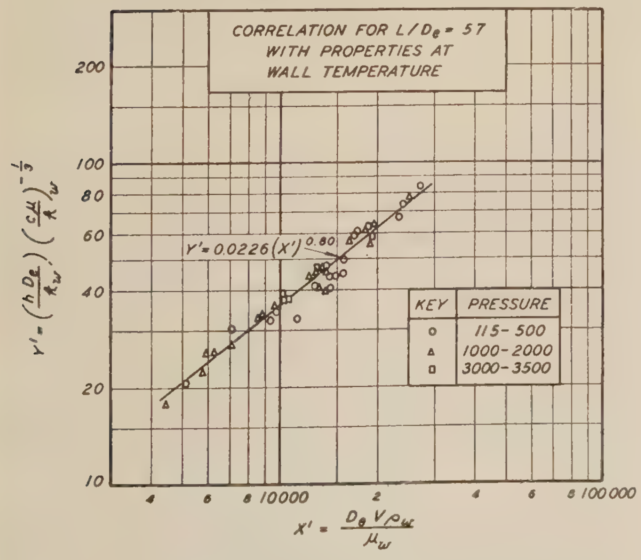

FIG. 5 DATA OF FIG. 4 REPLOTTED WITH CO-ORDINATES OF REFERENCE (8)

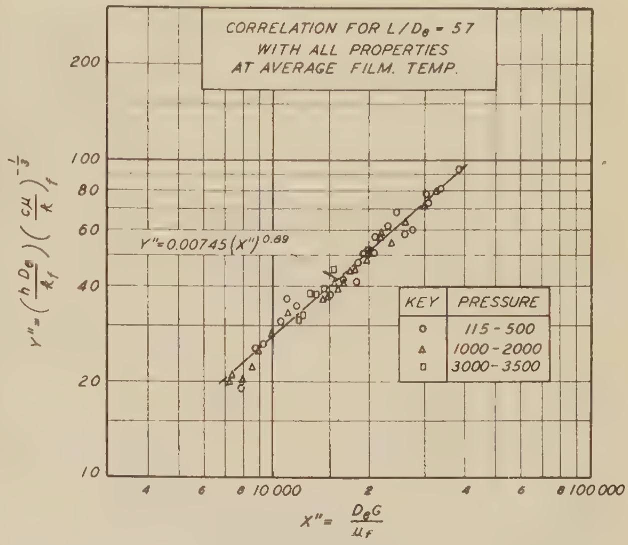

FIG. 6 DATA OF FIG. 4 REPLOTTED WITH ALL PROPERTIES EVALUATED AT FILM TEMPERATURE: $t_f = (t_w + t)/2$

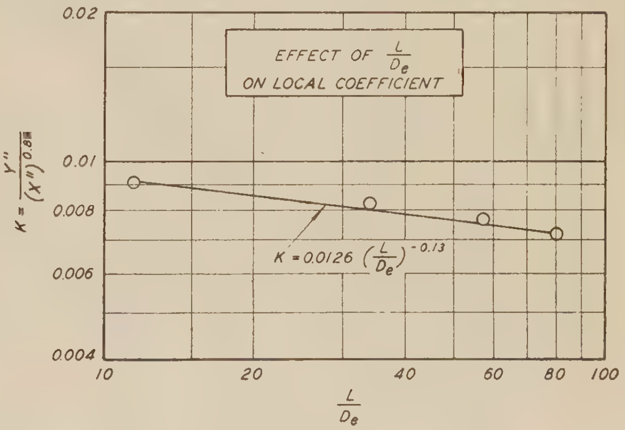

FIG. 7 CROSS-PLOT OF RESULTS FROM FIG. 6, AND SIMILAR GRAPHS FOR VARIOUS VALUES OF L/D_e

was evaluated for each L/D_e. Fig. 7 shows these values of K plotted against L/D_e, yielding

$$K = 0.0126\,(L/D_e)^{-0.13}\ldots\ldots\ldots\ldots\ldots\ldots[9]$$

The final correlation, involving local coefficients at four different values of L/D_e, is given in Fig. 8

$$\frac{(h\,D_e/k_f)}{(c\mu/k)_f{}^{1/3}}\left(\frac{L}{D_e}\right)^{0.13} = 0.0126\left(\frac{DG}{\mu_f}\right)^{0.89}\ldots\ldots\ldots[10]$$

Since the simplified dimensional equation

$$\frac{h}{cG} = \frac{S}{A}\,\frac{(t_2 - t_1)}{(t_w - t)} = \frac{0.0144}{(DG)^{0.2}}\ldots\ldots\ldots\ldots[11]$$

correlates data for certain common gases at moderate Δt, this type of correlation was tried for the present data on steam at one L/D_e. A plot of h/c versus G gave a slope of 0.87, but the maximum deviation from the main line was ±40 per cent. The term $h/cG^{0.87}$ was plotted versus film temperature, but separate curves were obtained for the several pressures.

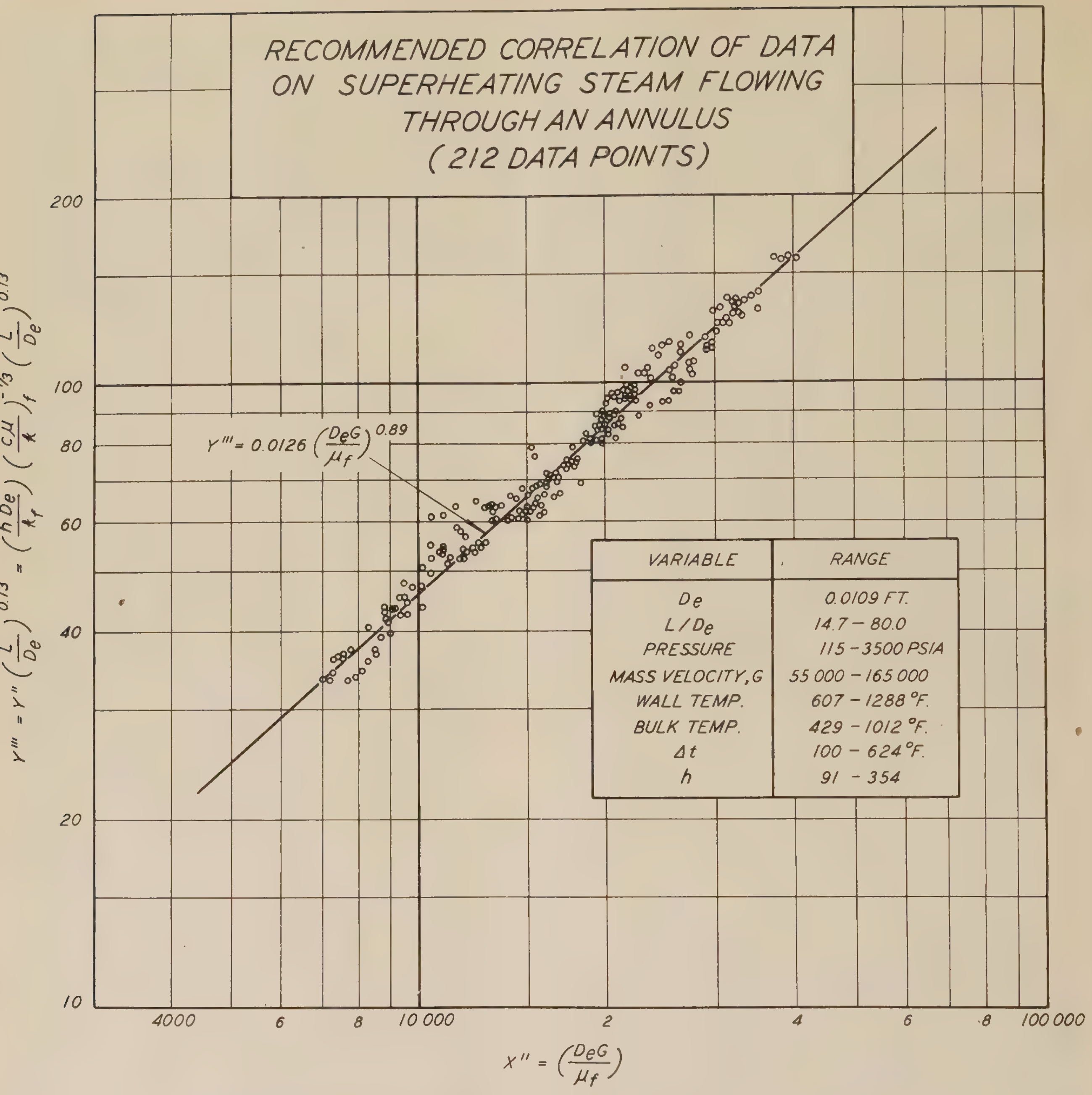

VARIABLE	RANGE
De	0.0109 FT.
L/De	14.7 – 80.0
PRESSURE	115 – 3500 PSIA
MASS VELOCITY, G	55 000 – 165 000
WALL TEMP.	607 – 1288 °F.
BULK TEMP.	429 – 1012 °F.
Δt	100 – 624 °F.
h	91 – 354

Fig. 8 Recommended Correlation of All Results

Discussion of Results

In Fig. 4 all of the local Nusselt numbers lie below the dotted line of reference (13) for mean Nusselt numbers, and most of the data fall below the dotted line of reference (2). The solid line represents an average of the data. The points at pressures of 3000 to 3500 psia are close to the line, most of those for 115 to 500 psia are above, and most of those for 1000 to 2000 psia are below.

In Fig. 5 the correlation is better than in Fig. 4. The slope of the curve is the conventional value of 0.8, the same as that reported (8) for air flowing in a tube, with Δt up to 940 F. The ordinate contains an exponent of $^1/_3$ on the Prandtl number, in place of 0.4. For the pressures and temperatures involved, the ordinate would be changed but little by using $(c\mu/k)_w^{0.4}$ instead of $(c\mu/k)_w^{1/3}$. Consequently, it is interesting to note that Fig. 5 gives a constant of 0.0226 for the local Nusselt number at L/D_e of 57, as compared with 0.022 for the mean Nusselt number for L/D_e of 60, Equation [4b]. At a given pressure, the thermal conductivity of steam may either decrease or increase with increase in temperature, while for low-pressure air, k always increases with increase in temperature. Furthermore, as temperature increases, the Prandtl number decreases more rapidly for steam than for low-pressure air.

The plot (not shown) of Y' versus X', at L/D_e of 11.4, gives a constant of 0.0267, which is higher than the constant of 0.0226 at L/D_e of 57.

In Fig. 6 the correlation is distinctly better than that in Fig. 4, and is somewhat better than that in Fig. 5; the same was true for L/D_e of 11.4. Consequently, the co-ordinates Y'' and X'' were employed for the final correlation. Fig. 7 shows that

L/D_e entered to the minus 0.13 power. The recommended correlation of the local Nusselt numbers at the four values of L/D_e is given in Fig. 8. The equation of the line is given by Equation [10], in which all physical properties are evaluated at the film temperature, t_f equals $(t_w + t)/2$. This equation correlates all the data, but should not be extrapolated outside the range of the data. At lower Reynolds numbers, modified streamline flow would prevail, and other dimensionless groups would be involved; at higher Reynolds numbers, the slope might decrease. At L/D_e above 80, h may become asymptotic.

Values of viscosities were taken from reference (15), thermal conductivities were taken from reference (16), and the other properties were taken from steam tables (9). The range of values of μ_f, k_f and $c_p\mu/k_f$ for each pressure is shown in Table 2.

TABLE 2 RANGES OF PHYSICAL PROPERTIES

Pressure	t_f	μ_f	k_f	$(c\mu/k)_f$
115	518	0.0443	0.0240	0.95
	1011	0.0726	0.0525	0.79
500	606	0.0503	0.0294	1.01
	1132	0.0820	0.0646	0.77
1000	650	0.0535	0.0338	1.18
	1134	0.0830	0.0656	0.76
2000	787	0.0639	0.0441	1.21
	1140	0.0859	0.0673	0.82
3000	951	0.0765	0.0551	1.03
	1116	0.0874	0.0665	0.88
3500	947	0.0774	0.0580	1.13
	1120	0.0893	0.0675	0.92

Conclusions

1 The use of electric heat developed in a thin-walled tube minimizes longitudinal conduction and permits measurement of local coefficients of heat transfer to steam flowing upward through a vertical annulus.

2 For a given Reynolds number and Prandtl number, the local Nusselt number always decreases as L/D_e increases, regardless of the temperature at which the physical properties are evaluated.

3 For a given L/D_e, the method of plotting used in Fig. 6, with all physical properties evaluated at the film temperature, is distinctly better than that in Fig. 4, and is somewhat better than that in Fig. 5; the quantitative effect of L/D_e from 11.4 to 80 is shown in Fig. 7.

4 The recommended correlation of all the data is shown in Fig. 8 and is given by Equation [10], which should not be extrapolated outside the range of data shown in Fig. 8. For a given Reynolds number the maximum deviation in the ordinate is 28 per cent, and the average deviation is 7 per cent.

BIBLIOGRAPHY

1 "An Investigation of Aircraft Heaters, XXVII, Distribution of Heat Transfer Rate in the Entrance Section of a Circular Tube," by L. M. K. Boelter, G. Young, and H. W. Iversen, Technical Note 1451, Washington, D. C., July, 1948.

2 "Heat Transfer and Friction of Water in an Annular Space," by F. G. Carpenter, A. P. Colburn, E. M. Schoenborn, and A. Wurster, Trans. AIChE, vol. 42, 1946, pp. 165–187.

3 "Heat Transfer: Local and Average Coefficients for Air Flowing Inside Tubes," by A. Cholette, *Chemical Engineering Progress*, vol. 44, 1948, pp. 81–88.

4 "A Method of Correlating Forced Convection Heat Transfer Data and a Comparison With Fluid Friction," by A. P. Colburn, Trans. AIChE, vol. 29, 1933, pp. 174–210.

5 "The Friction and Heat Transfer Coefficients of Rough Pipes," by W. F. Cope, Proceedings of The Institution of Mechanical Engineers, London, England, vol. 137, 1941, pp. 99–105.

6 "Heat Transfer in Automobile Radiators," by F. W. Dittus and L. M. K. Boelter, University of California Publication in Engineering, vol. 2, 1930, pp. 443–461.

7 "Heat Transfer Coefficients for Air Flowing in Round Tubes, Rectangular Ducts, and the Finned Passages of Blower-Cooled Cylinders," by R. E. Drexel and W. H. McAdams, Wartime Report W-108, National Advisory Committee for Aeronautics, Washington, D. C. 1945.

8 "Heat Transfer From High Temperature Surfaces to Fluids I—Preliminary Investigation With Air in an Inconel Tube With a Rounded Entrance, Inside Diameter of 0.4 Inch and a Length of 24 Inches," by L. V. Humble, W. H. Lowdermilk, and M. Grele, Research Memorandum, No. E7L31, National Advisory Committee for Aeronautics, Washington, D. C., May, 1948.

9 "Thermodynamic Properties of Steam," by J. H. Keenan and F. G. Keyes, John Wiley & Sons, Inc., New York, N. Y., 1936.

10 "Heat Transmission," by W. H. McAdams, McGraw-Hill Book Company, Inc., New York, N. Y., first edition, 1933, p. 169.

11 "Heat Transmission," by W. H. McAdams, McGraw-Hill Book Company, Inc., New York, N. Y., second edition, 1942, pp. 168, 174.

12 "Heat Transmission to Liquids Flowing in Pipes," by T. K. Sherwood and J. M. Petrie, *Industrial and Engineering Chemistry*, vol. 24, 1932, pp. 736–745.

13 "Heat Transfer and Pressure Drop of Liquids in Tubes," by E. N. Sieder and G. E. Tate, *Industrial and Engineering Chemistry*, vol. 28, 1936, pp. 1429–1435.

14 "Thesis in Chemical Engineering," by H. S. Rice, Massachusetts Institute of Technology, Cambridge, Mass., 1931.

15 "The Determination of the Viscosity of Steam and Water at High Temperatures and Pressures," by D. L. Timroth, *Journal Physics* (USSR), vol. 2, 1940, p. 419.

16 "The Viscosity and Heat Conduction of Steam at High Temperatures and Pressures," by D. Timroth and N. Vargaftik, *Journal of Technical Physics* (USSR), vol. 9, 1939, pp. 461–469; 963–970; vol. 10, 1940, p. 1063.

Appendix

Heat Transferred by Radiation

Since the present data were obtained for steam flowing in an annulus with an outer jacket that was colder than the flowing steam, an estimate was made of the net radiation from the heating element to the flowing steam and the outer jacket.

Professor H. C. Hottel of the Chemical Engineering Department at the Massachusetts Institute of Technology, derived an exact general solution of the problem by the method outlined by Hottel and Egbert (11). The result, a multiple-series equation, was too complex. A simplification, similar to the one used by Hottel and Egbert, gave the following equation

$$(q/A)_r = 0.173\,\epsilon'_w \left\{ \left(\frac{T_w}{100}\right)^4 [\alpha_{L1} + (1 - \alpha_{L1})]\epsilon_j - \left(\frac{T_j}{100}\right)^4 \epsilon_j\,(1 - \alpha_{L2}) - \left(\frac{T_g}{100}\right)^4 \epsilon_{gL2} \right\} \ldots\ldots\ldots [12]$$

where

α = gas absorptivity for specified beam length and pressure
ϵ_g = emissivity of steam for specified beam length and pressure
ϵ_j = emissivity[6] of stainless jacket
ϵ_w = emissivity[6] of stainless heater at T_w
ϵ'_w = effective emissivity of heating element equal to $(1 + \epsilon_w)/2$
T_w, T_j, T_g = absolute temperatures of heating element, jacket, and steam, respectively, in deg Rankine
$L1$ = effective beam length for gas radiation from heating element to gas
$L2$ = effective beam length for gas radiation from gas to heating element

Note: Beam lengths $L1$ and $L2$ were assumed equal to 1.4 times clearance between heating element and jacket.

Since the present work was done at pressures far in excess of any for which gas-radiation data are available, the evaluation of the gas emissivities and absorptivities required an extrapolation of the existing data. Emissivities and absorptivities for gas radiation (extrapolated to zero pressure were taken from Fig. 29 of reference (11), and were multiplied by the correction factor C_1 from Table 3, extrapolated from Fig. 30 of reference (11).

---

[6] The emissivity of stainless steel (14) was taken as a linear function of temperature, based upon 0.44 at 420 F and 0.36 at 914 F.

TABLE 3 VALUES OF C_1

P', psia........	115	500	1000	2000	3000	3500
P, atm.........	7.82	34.0	68.0	136	204	238
PL, atm-ft.....	0.119	0.515	1.03	2.06	3.09	3.60
C_1..............	1.85	1.75	1.65	1.50	1.45	1.42

As pressure increases C_1 decreases, but the emissivity at zero pressure increases faster than C_1 decreases; consequently the emissivity ($C_1\epsilon_{pw=0}$) increases. For example, at 1000 F, the emissivity increases from 0.156 at 115 psia to 0.568 at 3500 psia.

The simplified Equation [12] was shown to agree within 3 per cent of the exact equation for a typical case which was computed by both methods.

Addendum

Subsequent to the submission of this paper, new data on the thermal conductivity of steam became available through the courtesy of Prof. F. G. Keyes of the Department of Chemistry, M.I.T. The new data of Keyes and Sandell[7] are shown in Fig. 9 of this addendum, for comparison with the earlier data of Timroth and Vargaftik (16) which were employed in the original correlation of Fig. 8. The new data have been extrapolated beyond a temperature of 660 F and pressure of 2200 psia by means of the correlating equation developed by Keyes and Sandell. The per cent deviation of the new data from the old becomes acute at high temperature, but is practically independent of pressure.

The new values of thermal conductivitiy were employed to recalculate all of the present data at L/D_e of 57. Plots of the recalculated data were made utilizing the parameters of Figs. 4, 5, and 6; the correlation of the type shown in Fig. 4 was very poor, that similar to Fig. 5 was fairly good, although the exponent on the Reynolds number was 0.71, and the best one was again the correlation employing film temperature similar to Fig. 6.

All the present data were then recomputed using the parameters of Fig. 6, and the effect of L/D_e was redetermined. The final revised equation, correlating all of the heat-transfer data and based upon the thermal conductivities extrapolated from the data of Keyes and Sandell is

$$\frac{hD_e}{k_f} = 0.0214\left(1+\frac{2.3}{L/D_e}\right)\left(\frac{D_eG}{\mu_f}\right)^{0.8}\left(\frac{c\mu}{k}\right)_f^{1/3} \quad \text{. . [13]}$$

As shown in Fig. 10 of the addendum, the maximum error is 17 per cent, as compared with 28 per cent for the correlation in Fig. 8.

Advantages of the revised correlation are (a) retention of conventional 0.8 power on the Reynolds modulus; (b) adoption of the fadeaway function for L/D_e, and (c) adoption of a value of 0.0214 for the constant in close agreement with established values at high L/D_e. It is worth noting that the fadeaway type of L/D_e correction could not have been obtained with the earlier value of thermal conductivity. The revised correlation is expected to be considerably better than the original one for purposes of extrapolation.

Further work remains to be done in extending the range of physical properties. Viscosities are still in question.

The authors desire to acknowledge the co-operation of Prof. F. G. Keyes in making his data available.

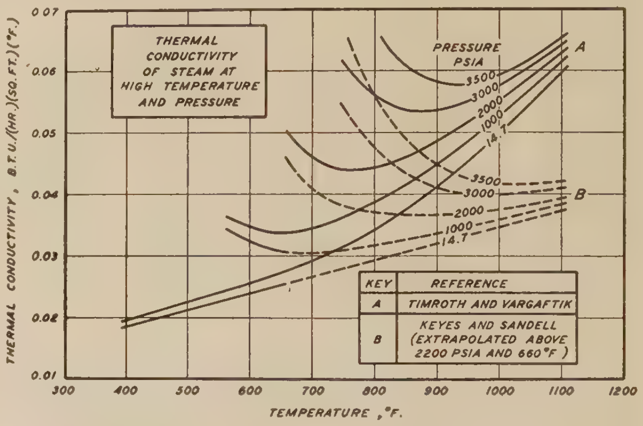

Fig. 9

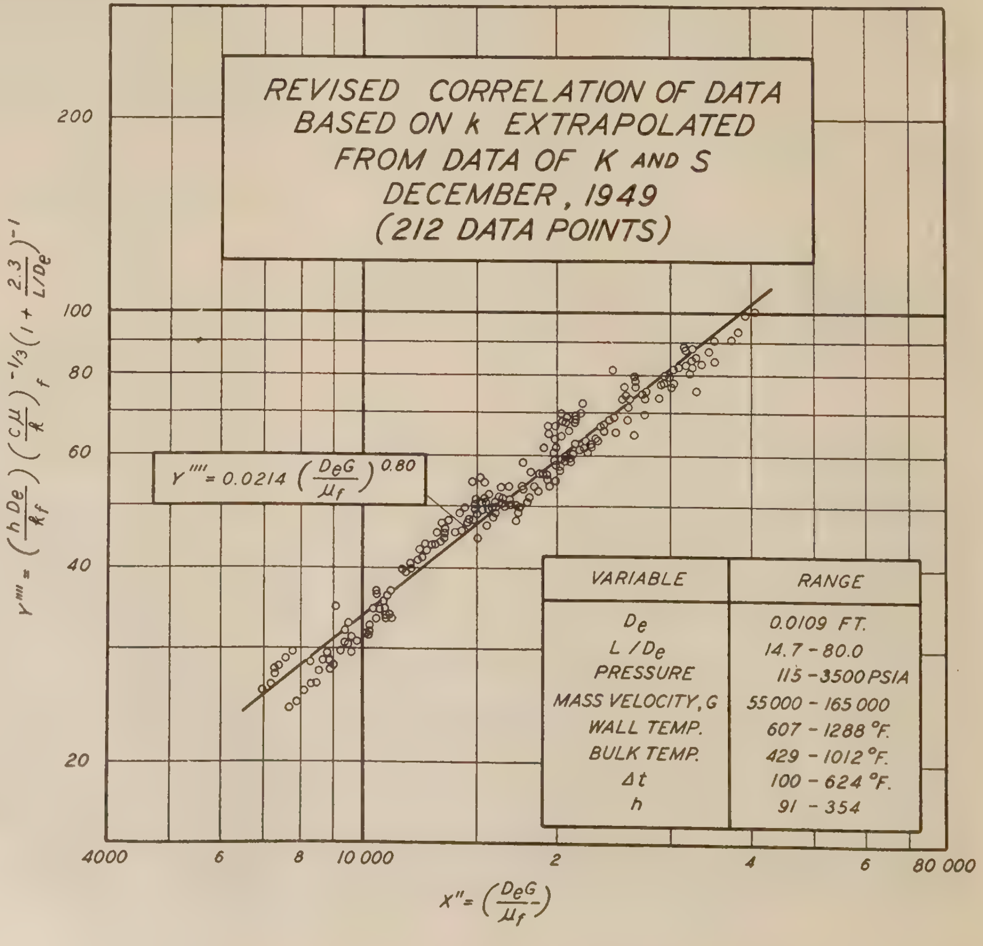

Fig. 10

---

[7] "New Measurements of the Heat Conductivity of Steam and Nitrogen," by F. G. Keyes and D. J. Sandell, presented at the Annual Meeting, New York, N. Y., November 27–December 2, 1949, of The American Society of Mechanical Engineers.

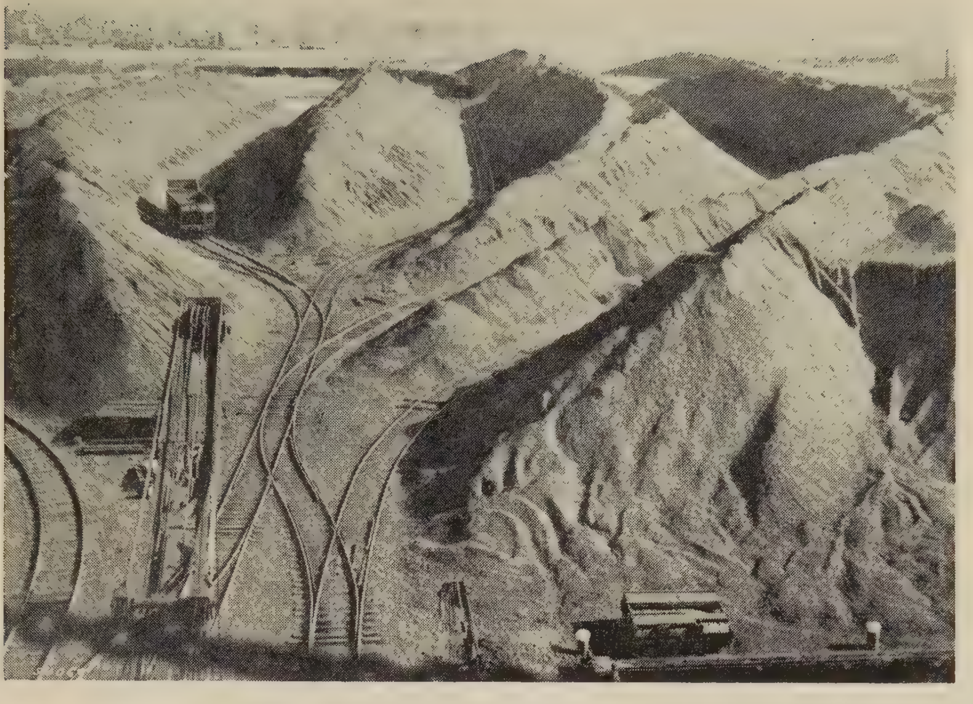

FIG. 1 PETTY ISLAND STOCK PILES PRIOR TO 1946

Philadelphia Electric Company Adopts Mobile Coal-Handling Equipment

By E. C. RUSSELL,[1] PHILADELPHIA, PA.

The paper covers the change from storing and reclaiming coal by cranes and locomotives to the use of standard self-propelled earth-moving equipment. The size and type of equipment are described, as well as its use. The change in design of storage piles is also considered. Description of new storage systems designed for the use of mobile equipment is presented. An analysis of operating costs and capacities is made with a comparison of the two methods.

THE Philadelphia Electric Company in 1946 began to make a complete change in its method of handling coal into and out of coal-storage piles. Coal stock piles are maintained for emergency use only and are reclaimed only when there is an interruption of the regular supply.

Coal is delivered normally to all but one of the six generating stations by barge, where it is unloaded by coal-tower clamshell-bucket installations. At the sixth station, barge facilities are not available and rail coal is unloaded into track hoppers.

Prior to 1946 the company's method of coal storage was in piles between a system of parallel tracks. Fig. 1 shows the Petty Island coal-storage-plant stock piles prior to 1946. Fig. 2 is a recent view of the same location. These tracks were laid out on approximately 110-ft centers to give maximum height and width to the piles, using locomotive clam-shell cranes with 60-ft booms. This arrangement resulted in piles 100 ft wide and 30 to 35 ft high. On reclaiming, the cranes loaded into company-owned hopper cars. A locomotive switched these cars over track hoppers with a conveyer system which transported the coal to the normal bunker conveying system, or in the case of the Petty Island coal-storage plant, to a coal barge for transportation to a generating station. For storing coal, these same hopper cars were loaded at the coal tower by chutes fed by the coal-tower conveying system. A locomotive switched the cars to the storage yard, and the locomotive clamshell crane unloaded them.

CHANGE TO MOBILE EQUIPMENT

In March, 1946, we received the first piece of mobile coal-handling equipment on our initial order of three units. The other two units followed a short time later, and, by the end of the year we had acquired four more. Two more were put into operation early in 1949. These units are heavy earth-moving machines designed for construction work, self-propelled, bottom-loading, scraper type with four pneumatic tires. They have sufficient power to move their loads at relatively high speeds up

---

[1] Supervisor, Coal Bureau and Steam Heating Division, Philadelphia Electric Company.

Contributed by the Power, Fuels, and Materials Handling Divisions and presented at the Annual Meeting, New York, N. Y., November 27–December 2, 1949, of THE AMERICAN SOCIETY OF MECHANICAL ENGINEERS.

NOTE: Statements and opinions advanced in papers are to be understood as individual expressions of their authors and not those of the Society. Paper No. 49—A-63.

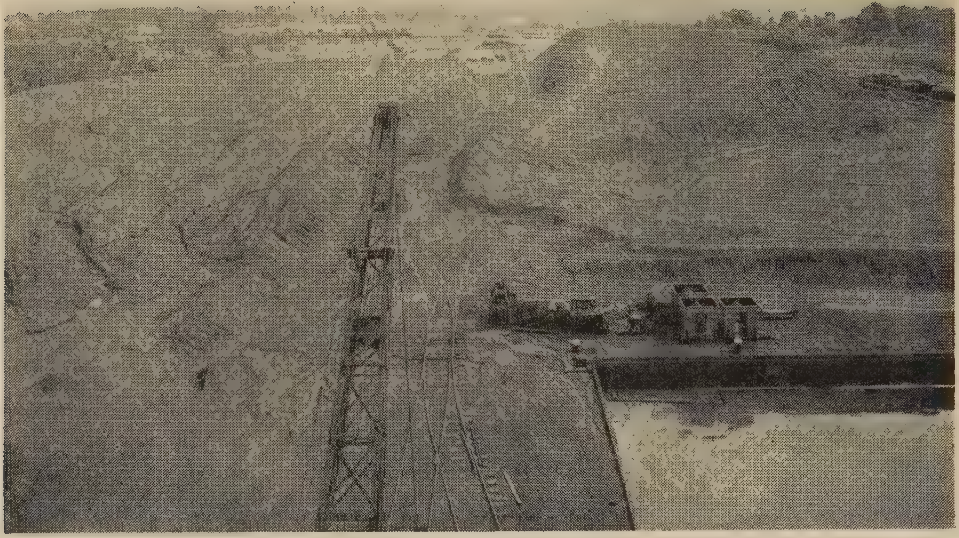

Fig. 2 Petty Island Stock Piles for Mobile Equipment

10 per cent grades and unload while moving, but need assistance in loading.

They are all Super "C" Tournapulls with Model LP Carryall scrapers, manufactured by R. G. LeTourneau, Inc., Peoria, Ill. The engines are 4-cycle 6-cylinder Diesel engines. Five of the nine are 150-hp Cummins engines, while the other four are 124-hp Hercules engines. The maximum speed of these units is 14.3 mph. The scraper capacity is 12.1 cu yd; heaped it has a 15-cu-yd capacity.

On the reclaiming cycle, we average $8^1/_2$ to 9 tons per load. On the storing cycle, since they are loaded by an overhead chute, a pant-leg-type hopper had to be designed to straddle the operating mechanism directly over the center line of the bowl of the scraper. This increases the tonnage per load on storing to 11 tons. Fig. 3 shows one of the units.

Self-propelled units have the advantage of the greater speed on the longer hauls and are usually more economical than the crawler-tractor-drawn scrapers on hauls over 600 or 800 ft on earth-moving work. However, the self-propelled units are favored even on the shorter hauls, for unlike most earth-moving work they are mechanically loaded when storing coal which theoretically is 50 per cent of their operation.

Self-propelled units being rubber-tired vehicles have the added advantage of being better-suited for use around paved station yards. They are also readily transferred over the road under their own power to another location. At times it is advantageous to be able to transfer a unit from one station to another to assist in the movement of coal.

Track-Type Bulldozers Used

Since the inception of mobile coal-handling equipment we have purchased four track-type bulldozer tractors. They are all Oliver Cle-Trac Model FDE with 130-hp Hercules Diesel engines. This is the largest tractor Oliver Cle-Trac make and is comparable in size to the International TD 18 or the Caterpillar D8. All four tractors are equipped with bulldozer blades as well as a power control unit on the rear. The power control unit is used to cable-operate a drawbar for towing the scrapers to assist loading on the reclaiming cycle.

The scrapers are equipped with a pusher pad on the rear for pusher-loading by a bulldozer. However, we have established a definite policy of not using this method of loading because our self-propelled scrapers are clutch-steered on the driving wheels. This presents the possible hazard of jackknifing if the bulldozer

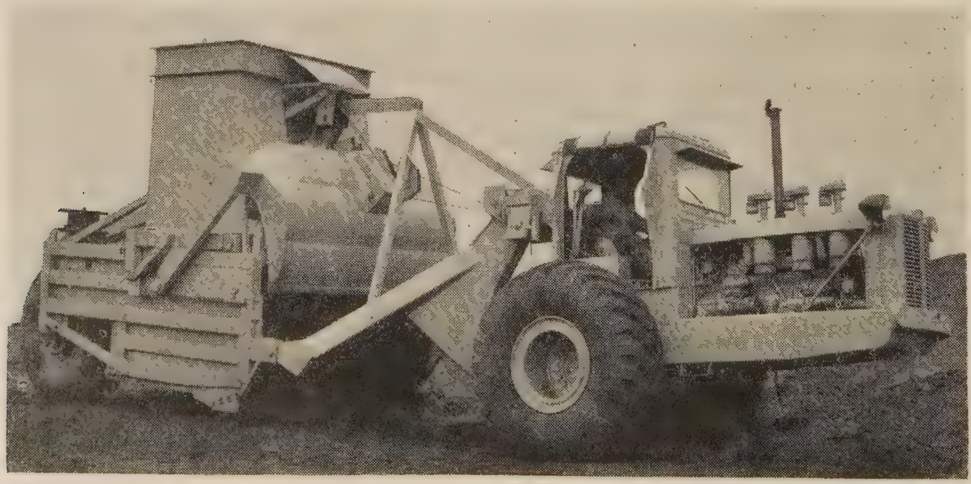

Fig. 3 Scraper Showing Pant-Leg Hopper

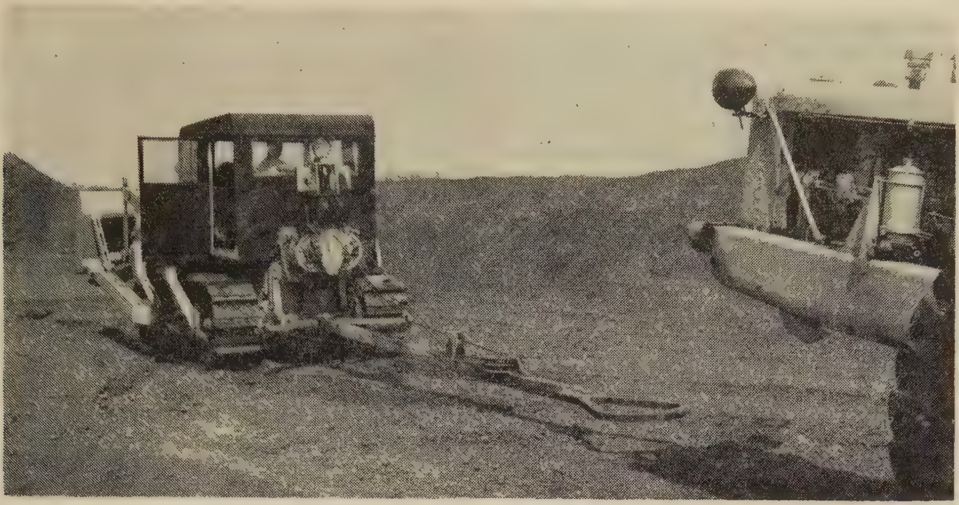

Fig. 4 Tractor Drawbar Engaging Scraper Hook

is pushing faster than the scraper engine is driving it. Also there is some possibility of the bulldozer blade cutting a rear tire of the scraper if proper contact is not made. It is felt that our method of loading has the added advantage of leaving the scraper operator's hands free to operate the power control unit, and his attention therefore can be directed toward the loading of his machine, since the tractor is towing, and thus guiding its direction. Later models of Tournapulls have positive steering, and likely there are advantages in push-loading them.

One other point in connection with the clutch-steering model is that the ramps or inclines on the storage piles should be straight if possible, especially if the change is being made to this method of storage, and men are being trained in the operation of this equipment. This is mentioned because it is necessary to have power on the driving wheels for steerage; if the practice is to coast down the incline with the engine idling, it is necessary to reverse clutch or "cross-steer." This of course is no problem for experienced operators.

The drawbars used for towing or snatch-loading are approximately 16 ft long with a 24-in. eye in a horizontal plane on the outboard end to engage a hook, mounted point down on the front end of the engine frame at the bottom. Fig. 4 shows a bulldozer preparing to snatch-load a scraper. The oil pan of the engine crankcase is protected with heavy plates so the eye can slide onto the hook. The drawbar is raised and lowered through a series of cables and sheaves by the power control unit on the rear of the tractor. Thus the scraper to be loaded drives up to the rear of the tractor in line with the drawbar. The drawbar is raised by the tractor operator, and upon engagement the tractor starts its tow. The operator of the scraper then concentrates upon the operation of the power control unit which raises the gate and lowers the bowl of the machine. When loaded, he lowers the gate, raises the bowl, speeds up, and turns to avoid the tractor, at the same time the tractor operator is lowering the drawbar.

Method of Storing Coal With Mobile Equipment

The method of storing coal with mobile equipment is entirely different from old methods with locomotive cranes. The Philadelphia Electric Company made the change-over to mobile equipment at an opportune time. Due to mine strikes, the coal stocks in 1946 were reduced to the lowest level at any time in the preceding 12 years. Thus we were able to remove the parallel tracks and relocate essential trackage where necessary, so that stock piles could be laid to the best advantage for this type of equipment.

It is readily apparent that one of the advantages of this method of storage is the increased quantity that can be stored on the same area. The parallel piles with the tracks between reduce the volume by approximately 50 per cent.

Figs. 1 and 2 show a very good comparison of the two methods of storing coal. The piles in Fig. 1 total approximately 150,000 tons of coal. The three piles shown in Fig. 2 total approximately 180,000 tons. It is quite apparent they have not even approached their maximum height. Close study of the two illustrations also will reveal that the piles in Fig. 2 extend possibly only one half the distance in the background compared with the piles in Fig. 1.

Furthermore, with mobile equipment, piles of much greater height are possible. Scraper-type equipment is ideal for storing coal, since this method of unloading allows the coal to be laid down in thin layers. Rolling or any other method of compaction as a fire preventive is not necessary as the mobile equipment with its large pneumatic tires has increased the density in our piles from 60 to 69 lb per cu ft. The old method of packing was to run a small crawler tractor, dragging a section of railroad rail on a bridle over the pile constantly while storing coal. We still follow this practice with the large tractors, but to a much lesser extent, and then only to maintain a fairly level surface, and to pack and spread the extreme edges of the pile where a self-propelled unit might encounter difficulties from its outside wheels sinking in the soft edges.

On the reclaiming cycle, the top of the pile is scraped off as evenly as possible, leaving the pile in shape for the time when coal is restocked again. One tractor will take care of the loading of two scrapers on the shorter hauls, while on the longer hauls three machines can be used.

Where possible, piles should be laid out with the ultimate tonnage desired in mind; so that the top of the completed pile will be as small as possible and still allow sufficient maneuverability for mobile equipment. This is essential because, in any case, there is a relatively large area of hard-packed coal, and the run-off of rain water resulting from a heavy downpour may be quite large. Provisions for handling this run-off should be made. If the top of the pile is made saucer-shaped, then the end result may be a small lake. At times of reclaiming, obviously, this is not desirable. The difficulties of handling wet coal in the usual chutes and conveyer systems, as well as the problems of burning extremely wet coal are well known. We have had some success in grading the top toward one or more wooden chutes to lead the water down the side of the pile. These chutes require attention occasionally, especially after a heavy rain. It is interesting to note that it has been found necessary to calk all cracks and keep the chute absolutely watertight or a serious washout beneath the chute may result.

In changing to mobile equipment the weight of the loaded unit must be considered if there are light paving slabs, manhole structure, or underground facilities too close to the surface. Also, in locations of limited area, minimum maneuvering space should be studied. The scrapers on our system will turn in a space 40 ft wide; however, we prefer a minimum width of 60 ft to improve maneuvering time.

The reclaiming of finer sizes of coal from the highly compacted piles made by mobile equipment has at times given some trouble with poor flow of coal in the pipes from bunkers to pulverizing mills and stokers. Former troubles in the stoker hoppers have been eliminated by the installation of agitators.

Coal-Handling Facilities

The Philadelphia Electric Company has stock piles at four generating stations, and a coal-storage plant on an island in the Delaware River. Petty Island—the coal-storage plant—serves the two stations without storage facilities by barge, and supplements the reclaiming at the other stations when necessary.

The change-over to mobile equipment required very little change in coal-handling facilities. The track hoppers in all locations had to be covered with some form of heavy steel grating designed to carry the load of a scraper. With the large-diameter wheels this grating can be made quite open.

On new installations, facilities are designed for the use of mobile equipment. At our Barbadoes Island Station where additional generating capacity was recently added, completely new coal-handling facilities were designed and installed for mobile-equipment use. This is the one station which must rely on rail coal delivery. The coal-unloading shed and track hoppers are laid out for the reclamation of coal by mobile equipment. The average haul distance is approximately 500 ft.

For storing coal, a scraper loading hopper was included in the design. This is a hopper of 20 tons capacity fed from the bunker conveying system so that a scraper can be loaded quickly without waiting for the normal flow of the 250 tons per hr of the conveying system, which would require approximately 3 min for loading. The haul distance for storing coal is approximately 400 ft.

A new coal-storage yard with an ultimate capacity of 1,000,000 tons is now in the planning stage. It is being designed to have a scraper loading hopper of 250 tons capacity and an ultimate rate of 500 tons per hr stocking by mobile equipment. For reclaiming, it is planned to have two unloading hoppers of 50 and 25 tons capacity, respectively, and a reclaiming rate by mobile equipment of 700 tons per hr.

ANALYSIS OF OPERATING EXPENSE

An analysis of the various accounts involving the storing and reclaiming of coal, and the operation and maintenance of cranes, locomotives, and mobile equipment reveals some interesting figures. However, these figures must be analyzed in the light of our operating conditions and accounting methods.

Three accounts were analyzed for the years 1944, 1945, 1947, and 1948. The year 1946 was excluded since that year involved the transition period from the old method of handling coal to the present method. The three accounts analyzed were (1) crane expense, (2) storing coal, (3) reclaiming coal.

It should be noted that the operating and maintenance expenses of a locomotive or locomotive crane is charged to the crane account regardless of its use. Some are regularly used by the Gas Department for handling coke, coal, and ashes, while others are digging ashes and slag as well as handling coal at the various generating stations—or making occasional lifts of heavy equipment.

The crane account was analyzed in order to establish an average actual cost per hour of use for operating and maintenance expenses.

The storing and reclaiming coal accounts were studied to determine the hours of equipment operation and the tons of coal handled.

One year of the maintenance account on the cranes was analyzed completely to determine the ratio between material and maintenance labor so that the various years could be adjusted to 1948 costs by material and labor indexes. It was found that approximately 40 per cent of the account was material, and the remaining 60 per cent was maintenance labor. This agrees favorably with studies that have been made on generating-station maintenance accounts. Therefore it was assumed these figures would hold true for all years.

The maintenance labor costs of the various years were adjusted to 1948 costs by labor factors which have been established on actual conditions in the company. Materials in the maintenance account were also adjusted to 1948 costs by a materials index. A cost per hour of operation adjusted to 1948 costs was then derived for the cranes and locomotives for 1944 and 1945, and for the scrapers and tractors for 1947 and 1948.

These costs per hour of equipment use were then applied to the respective year's hours of equipment use on reclaiming and storing coal at two different locations. The two years for each method of operation were then combined to give weighted average costs.

Table 1 gives the comparison between the old method of using cranes and locomotives and the new, using scrapers and tractors for both reclaiming and storing coal at the Petty Island coal storage plant. Table 2 is a similar tabulation for handling storage coal at Richmond Station.

TABLE 1 COMPARISON OF OLD AND NEW METHODS AT PETTY ISLAND PLANT

	Tons (1)	Tons per hr (2)	Equipment cost, dollars per hr (3)	Equipment cost, cents per ton (4)
		Reclaiming Coal		
Cranes and locomotives......	87519	48.0	3.38	7.0
Mobile equipment...........	26066	60.2	3.50	5.8
		Storing Coal		
Cranes and locomotives......	63399	47.9	3.39	7.1
Mobile equipment...........	210009	74.2	3.43	4.6

TABLE 2 COMPARISON OF OLD AND NEW METHODS AT RICHMOND STATION

		Reclaiming Coal		
Cranes and locomotives......	85856	43.6	3.33	7.6
Mobile equipment...........	140176	43.3	3.35	7.7
		Storing Coal		
Cranes and locomotives......	90839	35.1	3.36	9.6
Mobile equipment...........	186825	69.8	3.39	4.9

Referring to the tables, column (1) is the tons of coal handled. Column (2) is the tons per hour handled. Column (3) is the weighted average cost per hour of equipment use. Column (4) is equipment cost per ton of coal handled. All figures are a weighted average for the two-year period for the respective equipment.

To be explicit, the 87,519 tons in column (1), Table 1, are the total tons of coal reclaimed during 1944 and 1945, at Petty Island. Column (2) is the tons in column (1) divided by the hours of operation in the two years. The 3.38 dollars in column (3) are the result of dividing the total of 1944 and 1945 equipment expense by the total hours of operation for the two years. Column (4) is the total equipment expense divided by the tons of column

(1). Column (3) divided by column (2) will of course also produce column (4).

The same procedure was followed for the scrapers and tractors for the years 1947 and 1948.

It is apparent from column 3 of either table that the equipment cost per hour is practically the same for the two types of equipment. This was also found to be the case when the total 1944 and 1945 crane and locomotive account for the 28 pieces of equipment on the entire system was averaged and compared with a similar 1947 and 1948 figure for the 7 scrapers and 4 tractors. The two figures were 3.39 and 3.38 dollars, respectively, or so close that it would appear to have been intentional.

However, on comparing the results in either table for the two types of equipment, it is seen that the tons per hour handled are 25 per cent to 100 per cent greater than with the old method, with one exception, that is, reclaiming coal by mobile equipment at the Richmond Station.

It must be understood that the tons per hour in column (2) for either reclaiming or storing coal are per equipment-hour including tractors as well as the scrapers. For instance, on the reclaiming cycle we will have to assume that the normal method of operation was one tractor and two scrapers. To find the approximate scraper tons per hour the 60.2 tons on the second line of column 2 of Table 1 will be three pieces of equipment times 60.2 divided by two scrapers, or an average of 90.3 tons per hr reclaimed per scraper. However, on the storing cycle, the tractor is not usually used full time, hence the same ratio does not hold.

The foregoing partially explains the greater tonnage per hour moved on the storing cycle compared with the reclaiming cycle. Another factor is the 2 to $2^1/_2$ tons or approximately 25 per cent greater capacity of the scrapers when storing coal. On the reclaiming cycle, too, a little more time is consumed on the pile loading the scrapers than in loading them to haul to the storage pile. Likewise, in discharging their load in the hoppers when reclaiming, the machine must come to a complete stop, but, when storing, the discharging is done on the move, and the machine continues on its route back to reload. The advantages of the self-propelled unit on storing are quite obvious regardless of the length of haul.

The low tons per hour reclaiming rate at Richmond Station as compared to the Petty Island operation is due to several factors, as follows:

1 The reclaiming hoppers at Richmond Station are not of sufficient capacity for mobile-equipment use. They are track hoppers for unloading railroad hopper cars and are now in the process of being rebuilt with a greater capacity.

2 Operating conditions at the two locations are not the same. Petty Island is strictly a coal-storage plant and, when reclaiming, loads barges of as much as 2400 tons capacity. Richmond, being a generating station, reclaims the coal demands of the station. This station also burns two kinds of coal—stoker and pulverized—and has two bunker belts in each bunker. Thus many times during a day of reclaiming there are short delays due to changing over bunker belts, changing from one bunker to the other, which also means changing from one storage pile to another. Furthermore, reclaiming stock coal, especially if wet, always causes some operating difficulties with conveyer systems. It cannot be expected under those conditions to deduct these short interruptions from the over-all equipment operating time. Hour meters installed on each machine would of course give the actual hours of operation.

It must also be pointed out that the total equipment-hours for either reclaiming or storing which were used to arrive at the hourly rate figure may include some nonproductive hours in so far as tons moved into or out of stock are concerned; since it is necessary at times to use the equipment to regrade a pile after considerable coal has been removed, or to clean up after a heavy rain may have damaged a pile. This time would be charged to one or the other accounts. Thus the data in the two tables are over-all figures for the two-year period and include all the equipment time relative to stock piles.

We know from several spot checks for periods ranging from 1 hr to a full day's work that a scraper is capable of reclaiming 70 to 90 tons per hr and will store better than 100 tons per hr.

A real saving in the use of mobile equipment is the resulting laborsaving. Formerly at Richmond Station it was necessary to use two cranes and a locomotive, and work longer hours at overtime rates to supply the demands of the station. This would require two engineers and two firemen for the cranes, an engineer for the locomotive and a brakeman, a total of six men. Stocking coal, one additional man would be required to pack and spread the coal with a tractor. Today, with mobile equipment more coal is reclaimed or stocked with but three men, namely, two scraper operators and one tractor operator. Furthermore, it takes far less time to train a scraper operator than a crane operator.

Conclusion

In conclusion, we feel that mobile coal-handling equipment is ideal for our conditions and methods of operation. For the first two full years of operation it has proved to be sound from an economy standpoint. We feel that the equipment is much more versatile than our former equipment for handling storage coal. If we find it necessary to store or reclaim coal on short notice it doesn't seem like the major operation that it appeared to be previously

Finally, it must be remembered that mobile equipment is built primarily for earth moving and not for coal handling. Since coal is approximately one half the density of earth, it means that scrapers should be able to carry a considerably greater volume of coal than they are capable of handling. Therefore, from the standpoint of the buyer of equipment for coal-handling, improvements could be made.

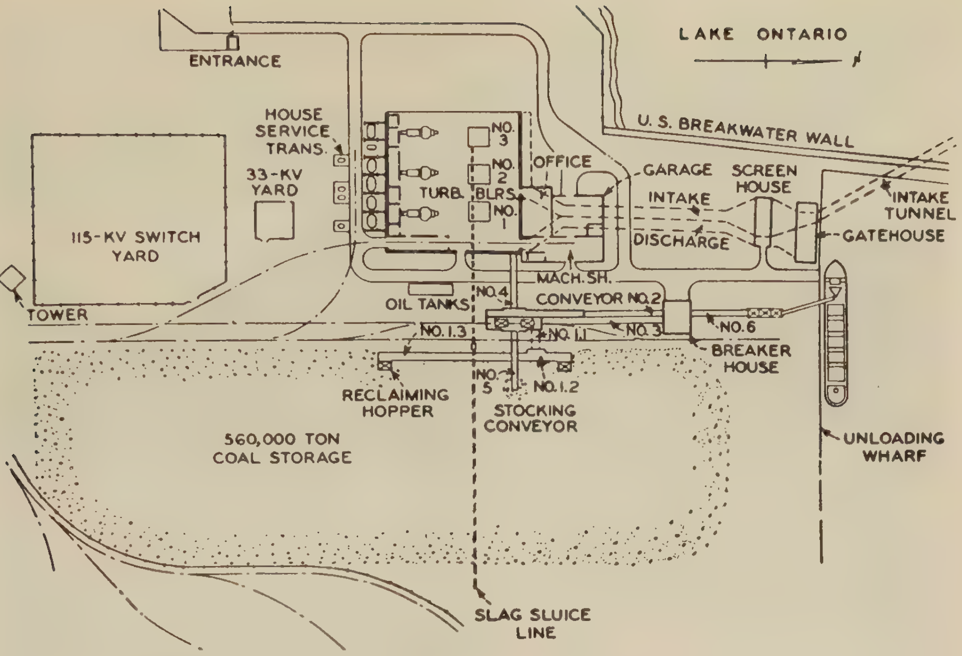

Fig. 1 Plan of Coal-Handling System, Oswego Steam Station

Storing and Reclaiming Coal With Earth-Moving Equipment at the Oswego Steam Station

By J. N. Ewart,[1] Buffalo, N. Y.

Earth-moving equipment at the Oswego Steam Station of the Central New York Power Corporation has handled in excess of 3 billion ton-feet of coal during its first 9 years of operation. Coal is stored in a single pile 100 ft high with no danger of spontaneous combustion. The paper describes the operation of bulldozer-carryall units and presents operating and maintenance costs.

General Description

The coal-handling system of the Oswego Steam Station of the Central New York Power Corporation is a simple one and lends itself readily to expansion of the station. Fig. 1 is a plan of the coal-handling system, showing the location of the storage pile and its relation to the receiving and reclaiming points. It also shows the arrangement of belt conveyers which permit movement of coal to the house coal bunkers or to and from storage from either track hoppers or self-unloading lake boats.

Although provision is made for either rail or lake delivery of coal, all coal is received by self-unloading boats which discharge directly to either a receiving hopper or to one end of a 1400-ft-long × 400-ft-wide stocking pile. This pile often reaches a height of 100 ft on the high end and has contained as much as 560,000 tons of coal, Fig. 2. From the receiving hopper the coal is carried through a Bradford breaker direct to the house coal bunkers or to a stocking conveyer, equipped with a telescopic chute which discharges to the stocking pile about 300 ft from the wharf end.

Stocking and Reclaiming Operation

The coal is moved into storage from the discharge of the self-unloader or from the stocking pile entirely by means of bulldozer-carryall units. During the stocking operation a bulldozer-carryall unit makes a round trip of approximately 2000 ft every 10 min. This trip starts at the stocking pile where the carryall picks up its load of 13 tons, carries it an average of 700 ft to the spreading area, and lays it down in a ribbon approximately 13 ft wide, 40 ft long and 10 in. thick, and then completes the circuit by returning for another load. Subsequent trips pack this ribbon of coal and integrate it with the rest of the pile to produce a section which is nearly impervious to air and water. Test pits have

---

[1] Chief Mechanical Engineer, Buffalo Niagara Electric Corporation. Mem. ASME.

Contributed by the Power, Fuels, and Materials Handling Divisions and presented at the Annual Meeting, New York, N. Y., November 27–December 2, 1949, of The American Society of Mechanical Engineers.

Note: Statements and opinions advanced in papers are to be understood as individual expressions of their authors and not those of the Society. Manuscript received at ASME Headquarters, October 8, 1949. Paper No. 49—A-98.

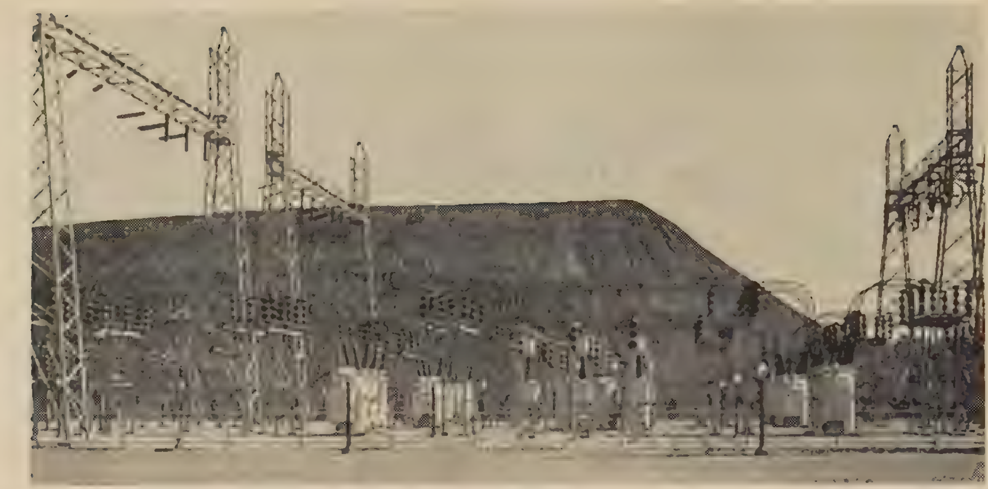

Fig. 2 Coal Storage Pile 100 Ft High Looking East From Gate House

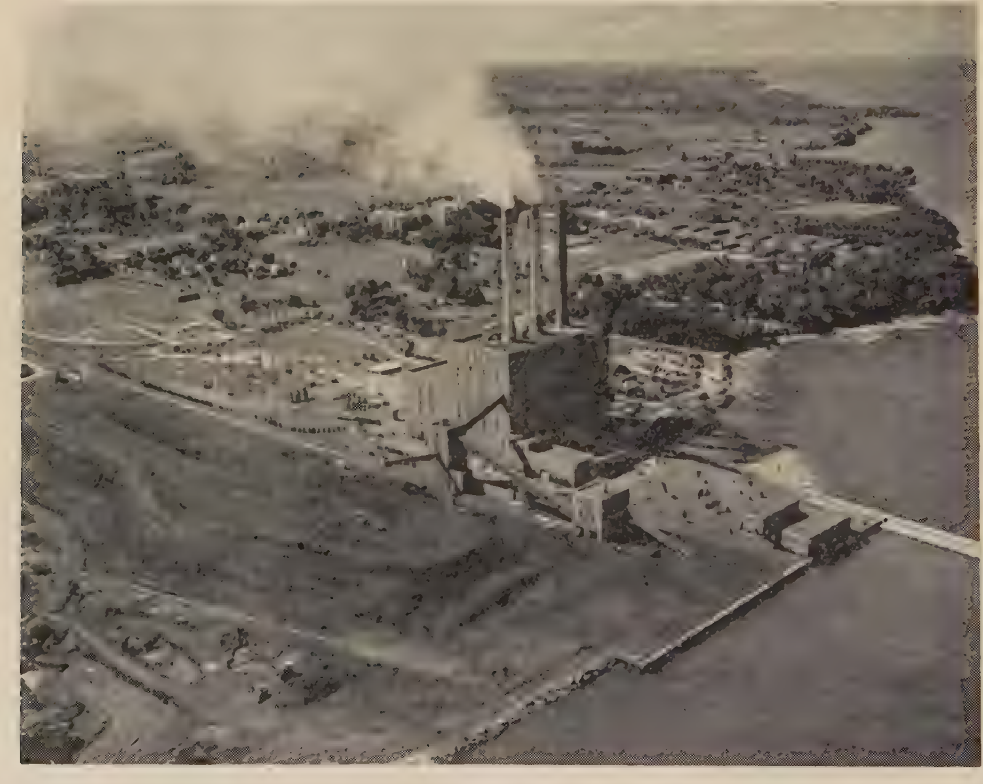

Fig. 3 Aerial View of Top of Storage Pile During a Stocking Operation

indicated that this coal is packed to densities of 80 lb per cu ft.

Fig. 3 shows the operation on the top of the pile during stocking. There have been no fires in this coal pile to date and sections of it have stood untouched for as long as 3 years.

Oswego's experience would indicate that many of the usual rules for successful storage of coal can be violated if coal is laid down in thin layers and adequately compacted. For example, no effort is made to avoid segregation though coal may be purchased from 60 mines varying in volatile matter from 17 to 37 per cent and sized from fine slack to double-screened and run of mine. Sulphur varies from 1 to 3 per cent. No particular effort has been made to provide a hard base or adequate drainage for the foundation, and there is no limit to the height of the pile.

Coal is reclaimed entirely by means of the bulldozer-carryall units. Two reclaiming hoppers are located along the lengthwise toe of the storage pile, 300 ft apart. Additional hoppers can be provided if necessary to reduce the reclaim hauling distance. In reclaiming coal from the stock pile the coal is removed, in so far as possible, by working it off in vertical layers starting from one end of the pile. In this way the top surface of the pile is disturbed the least, and the nearly vertical surfaces which are exposed will absorb practically no water or snow. The coal is packed well enough that nearly vertical sides have been formed 40 ft high with no experience of a cave-in.

Since all of the coal is received by boat and, therefore, a year's supply must be obtained during the favorable navigation season of approximately 6 months, there is necessarily considerable movement of coal in and out of the storage pile over the period

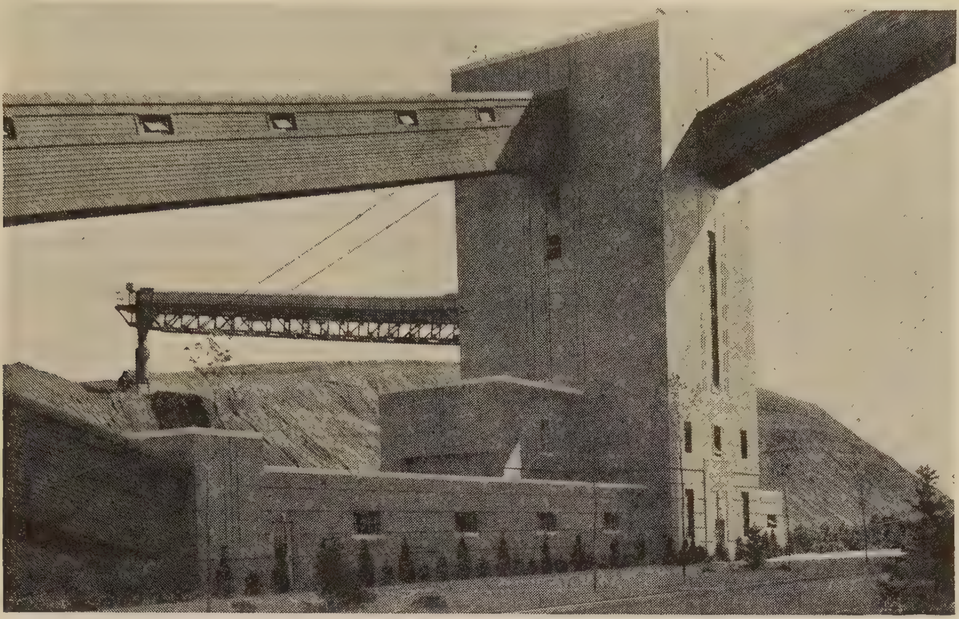

FIG. 4 TRACK HOPPER BUILDING AND JUNCTION TOWER, OSWEGO STEAM STATION

of a year. For example, the total movement of coal in and out of storage for the 9-year period was 5,225,000 tons, compared with an amount burned during this period of 3,600,000 tons.

OPERATING DATA

Table 1 shows the operating and maintenance cost of the bulldozer-carryall equipment in dollars per 1000 ton-feet by years, covering the period 1945 to 1948, inclusive. Comparable information prior to these years is not available.

TABLE 1 BULLDOZER-CARRYALL OPERATING AND MAINTENANCE COST DATA AT OSWEGO STEAM STATION

		Dollars per 1000 ton-feet				
		Operation		Maintenance		
Year	Total coal handled, tons	Labor	Fuel	Labor	Material	Total
1945	614080	0.046	0.006	0.026	0.020	0.098
1946	444894	0.067	0.006	0.035	0.011	0.119
1947	700986	0.063	0.006	0.026	0.010	0.105
1948	828985	0.064	0.008	0.032	0.021	0.125
Average		0.060	0.006	0.030	0.016	0.112

Figures are shown in Table 1 on the basis of ton-feet in order to consider the length of the haul as well as the tonnage in arriving at the unit costs. It is recognized that there is not necessarily a straight-line relationship between cost and hauling distance. The incremental cost for distance, once the carryall is loaded and under way, may be relatively small. Using the average total value of 0.112 per 1000 ton-feet for the 4 years, it may be seen that Oswego's 700-ft out-haul cost was 7.8 cents per ton, and the 500-ft reclaiming cost, 5.6 cents per ton. It is believed that the the maintenance cost of this equipment has reached its leveling-off value, except for possible increase in labor rates and material, since, at the end of 1948, the average life of the bulldozer-carryall units was 7 years, and a continuing program of replacing the older units has been developed.

It is interesting to note that one bulldozer handled approximately 500 million ton-feet before retirement.

INVESTMENT COST

The foregoing operating costs are exclusive of fixed charges on the capital investment. One of the advantages of mobile equipment, as compared with permanently installed machinery for handling storage coal, is that the initial investment can be small, and only that which is required for the initial installation. As and if the station expands, the storage area and coal-storage equipment can be expanded as required and always with modern equipment. Much in the way of improved and more efficient mobile equipment for handling coal has been developed in the last 5 years, and further improvements are inevitable.

Table 2 shows the capital investment in mobile equipment by years for the Oswego Station. Note that the initial investment was very small for the first few years of two-unit operation and increased as additional units were added. The original installation at Oswego consisted of two 80,000-kw rated, 100,000-kw maximum turbogenerator units with steam conditions of 1250 psi, 900 F. Each unit is supplied by a single boiler rated at 900,000 lb per hr. The third unit, essentially a duplicate of the first two, went into service in December, 1948. Installation of the fourth unit is now in progress and scheduled to be in service in 1951.

TABLE 2 CAPITAL INVESTMENT IN MOBILE EQUIPMENT AT OSWEGO STATION

Year	Station capacity, kw	Capital investment	Bulldozer units	Carryall units
1940	80000	$54780	3	2
1941	160000	54780	3	2
1942–1947	160000	65544	4	2
1948	240000	73143	4	3

Fig. 4 is shown to emphasize that the coal-handling structures and even the coal pile itself can become not too unsightly if proper consideration is given to architectural lines and landscaping, followed by a desire on the part of the station operators to maintain a good appearance of the buildings and grounds.

Vibration of Marine-Turbine Blading

By R. W. Nolan,[1] Newport News, Va.

The purpose of this paper is to give a general explanation of the vibration phenomena encountered in turbine design. Detailed methods have been omitted. The behavior of a vibrating cantilever is expressed in terms of the exciting force and damping factor. The sources of damping and excitation are discussed. Impulse excitation is briefly considered and the reasons for its devastating effects are shown. The procedure of tuning low-pressure blading, to avoid resonance at the lower harmonics of the turbine speed, is explained in considerable detail. An apparatus for determining the natural frequency of blading, and another for applying both tensile and alternating bending stresses simultaneously, are described. The direct tensile stress in the test is plotted versus the alternating bending stress which causes failure, thus obtaining a curve which shows the resistance of the blade to any combination of these stresses. The designed stresses for certain turbine blades and the stresses involved in several blade failures have been plotted on this diagram for purposes of comparison.

General

In recent years there has been a demand for decreased fuel consumption and a decrease in weight and space requirements for marine machinery. This of course had to be accomplished with no sacrifice in reliability because machinery failure can, on some occasions, endanger the life of the ship. The result of this demand has been a trend toward small high-speed turbines.

In the case of the high-pressure turbine, little difficulty was encountered in increasing speeds and a very rugged machine has been obtained. The low-pressure turbine, on the other hand, presents a complicated problem. The volume of steam passing through the last rows of blading is determined mainly by the horsepower and vacuum. This in turn approximately determines the diameter for the last blade row. With the diameter determined, the speed in revolutions per minute is then governed by stress considerations. The blade is made as long as possible to obtain maximum area for the steam passages, but its height is limited by considerations of stress and vibration. The blading in the last few stages is a compromise governed by steam flow, vacuum, efficiency, wheel stress, blade stress, and vibration.

At this point it should be mentioned that the last few rows of blading are not the only ones which can give vibration trouble. They are, however, the most susceptible to it and are the ones on which most vibration studies are concentrated. It is usually assumed that turbine blades are subjected to steady forces. Actually, this is not entirely true. All turbine blades are subject to certain variations in force. In the great majority of cases these force variations do no harm. Occasionally, however, the vibration characteristics of the blade might be such that a dangerous vibration could be set up by the exciting force variations which are always present in the turbine. It is the duty of the designer to see that this does not happen.

Behavior of Bodies Subjected to Vibratory Forces

Before proceeding with specific turbine problems, it is desirable to review briefly the behavior of a simple vibrating structure, and to define the terms which will be used. For this purpose, consider a steel cantilever beam of constant rectangular cross section 2 in. × $^1/_2$ in. and 12 in. in length. These scantlings have been chosen because they give characteristics which are not too far from those of a low-pressure exhaust blade. Assume further, that this beam is subjected to a force which varies sinusoidally with a maximum value of 0.6 lb uniformly distributed over the broad side.

The behavior of the beam subjected to this force is shown in Fig. 1 in which the amplitude of vibration at the end of the blade is plotted as a function of the frequency of the applied force. At frequencies approaching zero, the amplitude of vibration is 0.000208 in. which is equal to the static deflection produced by a force of 0.6 lb. As the frequency of the exciting force is increased, the amplitude increases until it theoretically reaches infinity at 6800 cycles per minute (cpm) (following the solid curve). Above this frequency the amplitude drops sharply. If the frequency of the exciting force were increased sufficiently, the amplitude would be found to approach infinity again at 42,600 and 119,500 (cpm) and at still higher values.

The frequencies at which the amplitude reaches infinity are the natural frequencies of this blade. The natural frequency at 6800 cycles is the first critical or first mode and that at 42,600 cycles is the second critical or second mode. The turbine designer is usually interested only in the first mode. The term "resonance" is used to describe the action which takes place when the frequency of the applied force coincides with a natural frequency. The terms "resonant" frequency and "critical" frequency are frequently used for natural frequency.

The curve under consideration is based on the assumption that there are no losses of energy in the vibrating system. Such a condition would be the equivalent of perpetual motion. Actually, frictional forces are always present, and it is fortunate that they are. Otherwise all turbines would strip out their blades in a relatively short time.

In vibration problems the frictional resistance to vibration is expressed frequently as a damping coefficient.[2] The dotted curve in Fig. 1 shows the behavior of this same blade with a damping coefficient of 0.10. At resonance, the amplitude of the first

---

[1] Engineering Technical Department, Newport News Shipbuilding & Dry Dock Company.

Contributed by the Power Division and the Society of Naval Architects and Marine Engineers and presented at the Annual Meeting, New York, N. Y., November 27–December 2, 1949, of The American Society of Mechanical Engineers.

Note: Statements and opinions advanced in papers are to be understood as individual expressions of their authors and not those of the Society. Paper No. 49—A-76.

[2] "Vibration Problems in Engineering," by S. Timoshenko, D. Van Nostrand Company, Inc., New York, N. Y., second edition, 1937, chapt. 1, sects. 8 and 9:

Damping force $= c\,\dfrac{dy}{dx}$ (Damping is proportional to velocity):

$$2n = c\,\frac{g}{w}$$

$$\gamma = \frac{2n}{p} = \frac{c\,g}{pw}$$

γ = damping coefficient
g = acceleration of gravity
p = 2π × natural frequency
$\dfrac{W}{g}$ = mass

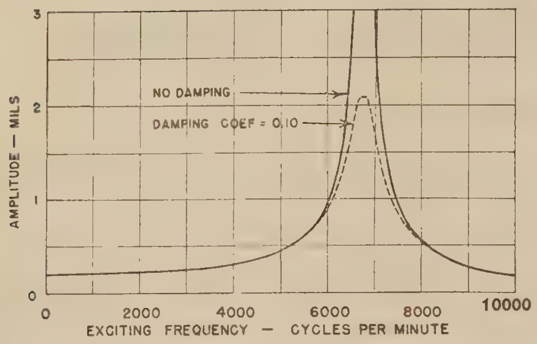

Fig. 1 Vibratory Response of a Cantilever Beam

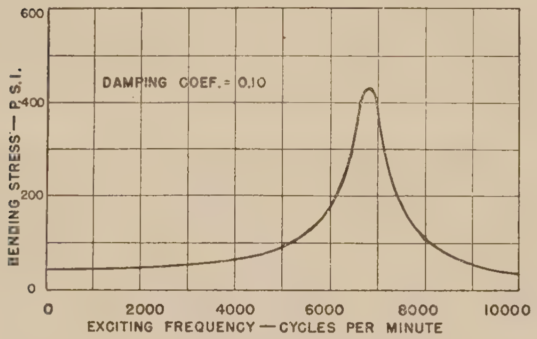

Fig. 2 Vibratory Stress in a Cantilever Beam

critical (at 6800 cycles) is 0.00208 which is 10 times the amplitude at low frequencies.

For each deflection which is shown in Fig. 1, it would be possible to calculate the moment and stress in the material. This has been done in Fig. 2. At low frequencies the stress of 43.2 psi is equal to that produced by the exciting force of 0.6 lb acting statically. At other frequencies, the stress is proportional to deflection, and at resonance it amounts to 432 psi, or 10 times the stress at low frequency. The factor 10 is the magnification factor. It is equal to the reciprocal of the damping coefficient.

This method of applying the magnification factor to the static deflection applies strictly to a concentrated mass on a weightless spring. Its application to deflection and stress of a turbine blade is an approximation which is sufficiently accurate for first-mode vibrations. It is not necessarily suitable for higher modes or for other types of structure.

Those familiar with alternating-current theory will recognize these curves to be the same as those obtained with resonant electric circuits. Magnification factor shown here is the same as the *Q*-factor which applies to series resonance in an electric circuit.

The stress of 432 psi may appear low. It is low because a relatively high damping coefficient was used, in order to obtain a resonance curve which would plot well on a lantern slide. In actual turbine blades, the damping coefficient may be 0.005. This gives a magnification factor of 200 which would make the foregoing stress equal to 8640 psi.

Causes of Damping in a Turbine

The factors which produce damping in turbine blades may be classified as elastic hysteresis, steam damping, and rubbing friction. Elastic hysteresis is internal friction in the blade material as it goes through the stress cycle. It varies widely with composition of the material and with temperature. It is difficult to determine experimentally; several investigators do not agree very well on the values. There is, however, enough information to permit a rough determination of the damping coefficient.

Another cause of damping is the resistance of the steam surrounding the blade. A rational method of determining the magnitude of steam damping would be to treat the velocity of vibratory motion as a change in blade speed, and to calculate the resultant change in tangential steam force. Application of this method shows the resultant damping forces to be rather small (less than hysteresis damping), and they usually are neglected.

The third cause of damping is rubbing friction between surfaces. There is always some minute sliding at the points of contact between the blade and the rotor, and between adjacent blades. The value of this damping is extremely variable, depending upon the design and on the fit which is obtained. Blades which are packed tightly together and are fitted accurately with considerable press fit, will have low frictional damping. Blades which are loose in the groove, or which are poorly fitted may have very high damping. In such cases the frictional damping will be many times that obtained by steam and hysteresis. This can be observed easily by striking the blades of a turbine rotor. Tight blades will ring clearly for a considerable time after striking. If the blades are loose, they have a dead sound because the vibratory energy is damped out almost immediately after striking. A natural reaction to this fact would be the suggestion that blades be installed loose to prevent vibration. This expedient might well be successful but one would hesitate to install loose blades, because of the possibility of wear caused by the movement. Furthermore, a blade which is poorly fitted may sometimes have its natural frequency lowered so that it falls into a resonant condition. It also may fail in the root, while tightly packed blades could not fail this way because they do not bend below the packing piece. Because of the uncertain nature of frictional damping, it is neglected in calculations.

A possible fourth source of damping is impact. It is closely related to frictional damping and may occur to some extent between adjacent faces of blade roots. There are patents on devices such as hollow blades containing loose rods or balls which are intended to cause impact damping if the blade vibrates. It is doubtful that these will ever find extensive application to marine turbines.

It thus appears that elastic hysteresis is the most dependable source of damping. Fig. 3 shows curves of the magnification factors of 13 and 14 per cent chromium stainless steel. These curves, based on data from an article by Andrew Gemant,[3] are expressed as a function of the vibratory stress.

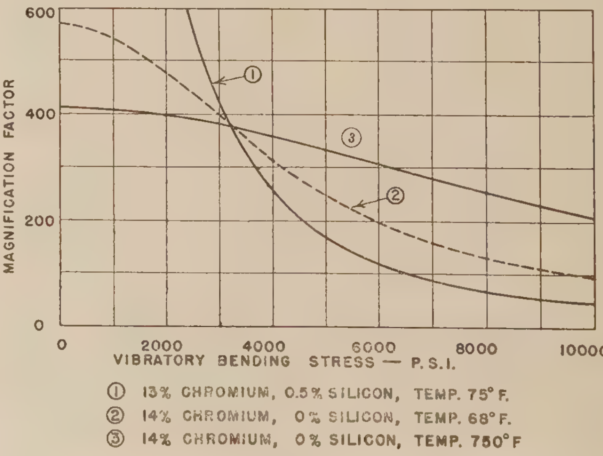

Fig. 3 Magnification Factor for Stainless Steel

---

[3] "Dependence on Stress of Damping Capacity of Alloys," by Andrew Gemant, *Mechanical Engineering*, vol. 67, 1945, p. 33.

Exciting Forces Acting on Turbine Blades

It was mentioned previously that there are always variations present in the tangential steam forces acting on blades. These may be due to many causes. Among them is the variation of pressure around the periphery of the wheel. Pressure variations cause variations in the steam velocity acting on the blade. These variations are difficult to measure experimentally because of the large number of pressure readings which must be obtained. Fig. 4, however, shows an approximate curve of pressure variation based on measurements at five points around the periphery of the last low-pressure stage of a turbine. One curve shows the discharge pressure and the other the inlet pressure for this stage. The last curve shows the variation in the Btu drop in the stage. In this case the maximum variation was about 12 per cent of the average heat drop. This is probably an extreme case since it is the last stage of a heavily loaded turbine.

Similar effects will be found at any point in the turbine where steam is being admitted or extracted. Designers frequently go to considerable pains to distribute steam uniformly in bleeder belts, chests, inlet belts, and in the space between the high-pressure first and second stages. In spite of their best efforts variations still exist.

Lack of uniformity in nozzles or blading also may be a source of uneven steam force. The discontinuity at the horizontal joint in the casing is a further possibility. It is difficult to keep the spacing of the nozzles, which span the joint, the same as that in the remainder of the ring. The conditions at the joint then may result in a different size of nozzle jet and, possibly, a different discharge angle. The blade rotating past these points will experience two impulses at each revolution.

The most severe form of excitation which occurs in turbines is known as impulse excitation. It usually occurs only in the high-pressure first stage and in astern turbines. In these stages steam is admitted to the wheel over a portion of the periphery, usually less than 180 deg. As the blade rotates, it enters the steam arc, receiving a sudden application of the full steam force. When it passes out of the steam arc, the sudden removal of the steam force is equally severe. The force variation is thus equal to 100 per cent.

Fortunately, the blades which receive this punishment are among the shortest and most rugged in the whole turbine. In spite of this, impulse excitation has been a serious problem to shore power plants, and it resulted in a number of failures before the cause was discovered. The shore turbines which suffered these breakdowns were high-pressure topping turbines which used large quantities of high-pressure high-temperature steam (1200 psi, 950 F). Conditions as severe as this have not yet been imposed on marine turbines and therefore failures of first-stage blading have been few. Present trends in marine steam conditions may bring on this trouble, and the designer must be alert to avoid it. A mild form of impulse excitation might be set up by damage which would partially close some of the nozzles in any turbine stage.

Blade vibration also may be excited by external forces. In one case, blade failure in a small geared turbogenerator was attributed to vibration set up by errors in the gear-tooth spacing. It is also possible that errors in the roundness of the journal may cause a motion which could set blading in vibration.

With the exception of impulse excitation, our knowledge of the magnitude of exciting forces is quite limited. We do know, however, that they are present in sufficient magnitude to cause failure of improperly designed blades. The uncertainty concerning the exciting forces and, to a considerable extent, the damping forces has led some of the large turbine manufacturers to adopt an empirical approach to the problem.

Harmonic Analysis of Exciting Forces

Regardless of what may be the pattern of the exciting forces, it will be repeated periodically, usually once for each revolution of the turbine. Any periodically varying set of values, such as the exciting forces acting on a turbine blade, can be broken up into a series of sine and cosine curves. The frequencies of these harmonic components will be integral multiples of the frequency of the original curve.

For example, take the lower curve in Fig. 4, showing the distribution of heat drop around the circumference of the wheel. Assuming that the steam force, acting on a blade, is proportional to the heat drop, a curve of force variation has been plotted in Fig. 5 (solid curve). Each blade will be subjected to this force variation at each revolution.

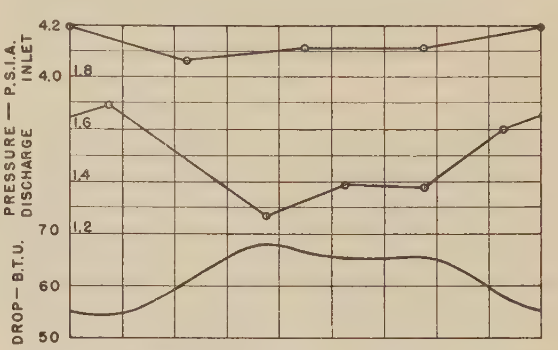

Fig. 4 Pressure and Heat Drop in a Turbine Exhaust Stage

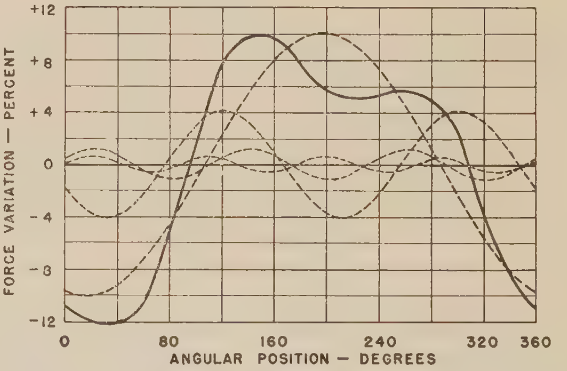

Fig. 5 Harmonic Analysis of Force Variation in a Turbine Exhaust Stage

By applying a Fourier analysis, the first four harmonics have been obtained. These also are shown in Fig. 5 (dotted curves.) Their amplitudes and phase angles are given in Table 1.

TABLE 1 AMPLITUDES AND PHASE ANGLES

Harmonic	Amplitude, per cent	Phase angle, deg
1	10.1	+253
2	4.1	+206
3	1.1	+ 24
4	0.6	+ 3

There was no justification in carrying this analysis beyond the fourth harmonic because there were so few points on the original curves from which the drop was calculated. It should be observed how the harmonics decrease in amplitude as their order increases. This is generally to be expected but it is not always so.

To illustrate the exciting forces generated by impulse excitation, the diagram shown in Fig. 6 has been assumed. Here the nozzle arc is assumed to be 90 deg with instantaneous application and removal of the load taking place at the ends of the arc. The instantaneous application and removal of the load is a rather severe assumption, but it is much less tedious to apply and therefore is more convenient for preliminary design purposes. Analysis of this diagram gives an infinite series of harmonics with every 4th one (4th, 8th, 12th, etc.) equal to zero. The values of the first ten harmonics in per cent of the steam loading *F*, are given in Table 2. Even the 30th harmonic has an amplitude of 2 per cent, which is sufficient to set up a vibration of considerable magnitude. This gives some indication of why impulse excitation can be so destructive. Further troublesome characteristics of impulse excitation will be brought out in the next section.

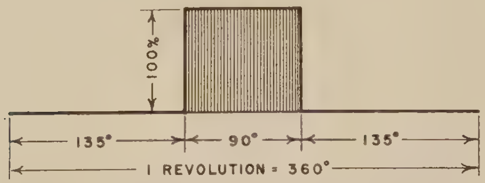

Fig. 6 Steam-Loading Diagram for High-Pressure First-Stage Blading

TABLE 2 VALUES OF FIRST TEN HARMONICS

No. of harmonic	Intensity, per cent
1	45.0
2	31.8
3	15.0
4	0
5	9.0
6	10.6
7	6.4
8	0
9	5.0
10	6.4

Tuning of Turbine Blades

Whenever the frequency of one of the various harmonics of the exciting force coincides with a natural frequency of the blade, resonance will occur. As explained earlier, the vibration amplitude will be equal to the static deflection produced by the component, multiplied by the magnification factor. Assume, for instance, that a blade is subjected to a steady steam force of 6 lb plus a certain harmonic whose magnitude is 5 per cent. The harmonic force will then have an amplitude of 0.3 lb. The static deflection is then considered to be the deflection which would be produced by a force of 0.3 lb uniformly distributed over the blade. If the magnification factor is 200, the deflection at resonance would correspond to that produced by a force of 60 lb. The resultant vibratory stress also would be equal to that produced by a 60-lb load, and would thus be 10 times the stress produced by the total steam load which acts statically on the blade. Such bending stresses when superposed on the already high centrifugal stresses may cause fatigue failure if the turbine runs for long periods at a resonant condition.

As already mentioned, experience with turbines indicates that the lower harmonics usually have the largest amplitudes. There have been many failures which were caused by the 4th or lower harmonics. There also have been some failures at higher-order harmonics. It is therefore necessary to avoid resonance at the 4th and lower harmonics or, when it cannot be avoided, have it occur at a reduced speed where the centrifugal stress acting on the blade will be less than at full power.

A convenient means of visualizing this problem is the Campbell diagram, named for the late Wilfred Campbell of the General Electric Company, who did much of the pioneer work on turbine vibration. The Campbell diagram is shown in Fig. 7. It consists of a series of curves of frequency (usually cycles per minute) plotted versus turbine revolutions per minute. On this diagram each harmonic is represented by a straight line passing through the origin. These lines give the frequencies of the exciting forces corresponding to the various harmonics, at all speeds of the turbine. The second harmonic will have twice the slope of the first, the third harmonic three times, etc. Usually, about eight harmonics are drawn.

After the frequencies of all of the important exciting forces have been plotted on the Campbell diagram, the natural frequencies of the blading are plotted. When the turbine is not rotating, the natural frequency of a blade (or group of blades joined by a shroud band), has a particular value which is called the static frequency. When the turbine is running, the centrifugal force has a stiffening effect on the blade, raising its natural frequency. This is the running frequency. These frequencies also can be plotted on the Campbell diagram. The curves for two stages, A and B, are shown in Fig. 7. The running frequency is fairly close to static frequency up to about half speed of the turbine. Above this speed the frequency increases appreciably. At maximum speed the increase in frequency is usually around 15 per cent for the longest blades.

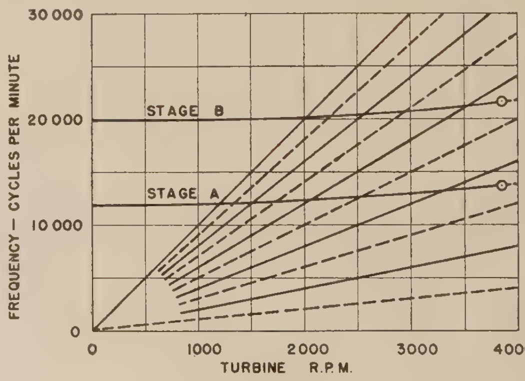

Fig. 7 Campbell Diagram

With the blade frequencies added, the Campbell diagram is complete. Each point at which the blade-frequency curve crosses one of the harmonics, represents a condition of resonance. There are thus numerous resonant conditions for each blade. Most of them are excited by high-order harmonics and are therefore not serious. The lowest order of resonance is the one of which to beware, because it occurs at the highest turbine speed and probably will have the largest exciting force.

Turning now to the curve for blade A, in Fig. 7, it can be seen that at maximum speed, resonance does not occur, and the blade frequency lies halfway between the 3rd and 4th harmonics. If the natural frequency of 13,500 is divided by the turbine rpm of 3850, the result is 3.5. This is usually called 3.5 vibrations per revolution. This value is not a coincidence. As originally laid out, this blade had 4.1 vibrations per revolution, which was very close to a dangerous resonant condition. It was not considered practical to stiffen the blade sufficiently to raise it to 4.5 vibrations per revolution, so, the blade section was reduced in order to lower the frequency to 3.5 vibrations per revolution. This process is called tuning. It is a fairly lengthy design process involving considerable work.

Referring back to the Campbell diagram, it will be seen that at 3300 rpm, stage A is in resonance with the 4th harmonic. At this condition, however, the steam load on the blade is less than at full power (probably down to 70 per cent of the full-power value) and therefore the magnitude of the exciting force is reduced proportionately. In addition to this, the centrifugal stress in the blade is down to 12,200 psi, instead of the 16,600 psi which it had at full power. The total steam load on this blade at full power is 6.5 lb per blade, producing a steam bending stress of 550 psi. At 3300 rpm the bending stress may be assumed to be about 390 psi, (70 per cent of 550). If this steam force contained a 4th harmonic with a magnitude of 5 per cent of the steady steam force, and the vibration magnification factor were 200, the vibratory stress would be 390 × 0.05 × 200 = 3900 psi.

A comparison of the blade stresses at full speed (3850 rpm) and at 3300 rpm, is given in Table 3.

TABLE 3 BLADE STRESSES AT 3850 AND AT 3300 RPM (STAGE A)

(a) Rpm	3300	3850
(b) Centrifugal stress, psi	12200	16600
(c) Static steam stress, psi	390	550
(d) Total steady stress (b + c), psi	12590	17150
(e) Vibratory stress, psi	3900	negligible
(f) Maximum stress (d + e), psi	16490	17150
(g) Minimum stress (d — e), psi	8690	17150

Thus it can be seen that although 4th-order resonance has not been avoided, it has been located at a speed where less severe stresses are encountered. Had 4th-order resonance occurred at full speed, the steady stresses would be 17,150 psi, and the vibratory stresses 5500 psi, leading to a maximum stress of 22,650 psi, and a minimum stress of 11,650 psi.

Stage B has been handled in a similar manner except that it is tuned to have the full-power condition fall between the 5th and 6th harmonics. Unless a blade is very highly stressed, it does not appear necessary to tune for harmonics above the 6th. Assuming the vibratory stress at resonance in stage B to be 10 times the steam bending stress, it will compare with stage A, as in Table 4.

TABLE 4 COMPARISON OF STRESSES IN STAGES A AND B

Stage	Resonant rpm	Harmonic	Centrifugal stress, psi	Steam bending stress, psi	Total steady stress, psi	Vibratory stress, psi
A	3300	4	12200	390	12590	3900
B	3550	6	12500	510	13010	5100

Although the stress in stage B is higher than that in stage A, when calculated by this arbitrary method, it should be remembered that the exciting force of the 6th harmonic will be much less than the 4th, and the factor of 10 is therefore rather severe.

It is in connection with tuning that one of the most objectionable features of impulse excitation becomes apparent. First-stage blades, which are subjected to impulse excitation, have high natural frequencies which ordinarily would put them well out of reach of vibration trouble. Their frequencies may be 25 or more vibrations per revolution. It was, however, mentioned in the preceding section, that even the 30th harmonic of impulse excitation may have an exciting force of 2 per cent. Thus these blades will be subjected to sizable exciting forces. Even assuming that it were possible to tune a blade accurately enough to obtain 24.5 vibrations per revolution, it would be in resonance at 25 vibrations per revolution when the speed dropped 2 per cent. This change is no more than that which would be encountered in going from light draft to load draft, or from clean bottom to foul bottom. It is thus impossible to avoid resonance at, or very close to, maximum speed. Therefore the blades must be designed to withstand such conditions. This can be done by keeping low bending stress and using materials which have good damping properties at the operating temperatures. Thirteen per cent chromium stainless steel has relatively good damping properties.

In the process of tuning, there are several ways of changing the frequency, and usually two or more of them are used together. In discussing the methods it would be well to consider the equation for the frequency of a cantilever beam of constant section, which shows the effect of several of the factors which determine blade frequency. This equation is

$$F_s = 660\sqrt{\frac{EI}{Wl^4}} = \sqrt{\frac{EI}{\rho A l^4}}$$

where

F_s = static frequency, cycles per min (cpm)
E = modulus of elasticity, psi
I = moment of inertia of cross section, in.^{4}
l = length of beam (length of blade), in.
ρ = density of material, lb per cu in.
A = area of cross section, sq in.
W = weight per in. of beam = ρA, lb per in.

In this equation, E and ρ may be considered fixed, since the material is usually settled in advance. That leaves the possibility of altering A, I, and l. Increasing the value of I, will increase the frequency. If a small increase is desired, it can be accomplished by thickening the blade slightly. If a large increase is needed, the necessary thickening would restrict the steam passage too much. In this case the entire blade section may be increased, maintaining the same geometric proportions. Either process increases the area A simultaneously. Moment of inertia, however, increases as the 4th power of the linear dimensions, while A increases as the 2nd. Thus frequency will increase about in proportion to the increase in lateral dimensions.

Another method of changing frequency is to change l. Since frequency varies as l^2, this method is effective. It is usually an increase in frequency which is desired and, in this case, l would be decreased. This, however, may be a costly process because it will lower the efficiency of the stage. Therefore height decreases are used rather sparingly.

The third method of altering frequency is to taper the blade, or alter the taper on one which already has it. Tapering a blade not only increases the blade frequency, but it is most effective in reducing centrifugal stress. If the stage A in Fig. 7 were made with constant cross section (using the base section), its static frequency would be about 13 per cent lower, and the centrifugal stress 70 per cent higher. Tapered blades are also "twisted" frequently. This is done to suit the angle of the incoming steam.

Shroud bands and lacing wires affect the frequency. Shroud bands do not necessarily raise the frequency. They do stiffen the blades, but the added mass sometimes counteracts the added stiffness. In some cases, however, shroud-band alterations can be used as an aid in tuning. Lacing wires increase the frequency, particularly when there are two rows of them. Altering their size will alter the frequency.

Application of any of these methods of tuning usually is limited by the action of some other factor such as loss of thermodynamic efficiency, increase in stress, or difficulty of manufacture. It is for this reason that several methods may be applied simultaneously to obtain the desired result.

The subject of tuning cannot be dismissed without some mention of the calculating methods which must be applied with every change. Only the briefest discussion of them can be given in this paper because a detailed treatment would result in the writing of a textbook.

The calculation of a tapered twisted blade is a tedious process. It is necessary first to calculate maximum and minimum moments of inertia and weight per inch of blade at several sections (usually at least three sections are taken and a curve is drawn through the three points thus obtained). For the actual frequency calculation, the Rayleigh method is frequently used. In this method, the potential and kinetic energy must be calculated for a given assumed deflection curve. Ordinarily, the static-deflection curve, obtained by loading the blade with its own weight, is taken as the assumed curve. In this case, the calculation is represented by the equation

$$F_s = 188 \sqrt{\frac{\int wydl}{\int wy^2dl}}$$

where

w = weight per unit length of blade
y = ordinate of deflection curve
dl = differential length

If the assumed curve is reasonably close to the shape of the actual vibration curve, a good approximation is obtained. In using the static-deflection curve, the error seldom exceeds 2 per cent. If greater accuracy is required, it is necessary to make a second approximation, based upon the first calculation.

Twisted blades present a problem because the axes of the cross sections do not lie in one plane. This requires using two reference planes at right angles and working with co-ordinates. An expedient which has been used to avoid this, is to work two approximate calculations. In the first, the minimum moments of inertia for all sections are rotated into a single plane and the frequency calculated. This gives a frequency which is too low. The other calculation uses the moment of inertia, of each section, about an axis parallel to the minimum axis of the base section. This gives a frequency which is too high. By interpolating between these two frequencies and using factors obtained from tests, it is possible to obtain frequencies which are close enough for preliminary design work.

Final blade-frequency calculations involve the effect of the shroud band or lacing wires. In this case the structure is indeterminate and requires the application of strain-energy methods.

Finally, it is necessary to calculate the effect of centrifugal force. For blades of constant cross section, Campbell used the formula

$$F_r = \sqrt{F_s^2 + BN^2}$$

$$B = 1.56 \times \frac{R}{l} + 1.17$$

where

F_s = static frequency
F_r = running frequency
l = blade length
R = radius to base of blade
N = rpm of turbine

This formula may also be used for preliminary calculations on tapered blades. For final calculations, it is necessary to calculate the radial shortening caused by the lateral bending of the blade, and then calculate the potential energy which is stored up by producing this radial shortening against the action of centrifugal forces. The effect of centrifugal force on the vibration of a turbine blade is analogous in some ways, to the effect of gravity on the frequency of a pendulum.

BLADE TESTING

Consideration of the Campbell diagram shows that an error of a few per cent in the calculation of blade frequency could lead to disaster. Therefore it is natural that testing should be an important phase of blade design. In this way the various factors affecting frequency can be determined, and empirical design coefficients chosen. For this purpose a vibrator can be used to determine the natural frequencies of blading. The vibrator, illustrated in Fig. 8, was built from a loud-speaker. The cone was sawed off and a small threaded nut cemented to the moving element. One end of a small aluminum rod ($^3/_{32}$ in. diam) is screwed into this nut, and the other end is attached to the blade by means of a spring clip. The permanent-magnet field of the speaker has been replaced by an electromagnet of considerably greater field strength. By supplying an alternating current to the coil of the speaker, a corresponding alternating force of about 0.5 lb peak value can be obtained. A Hewlett-Packard 200-B, 1-watt oscillator is used for this purpose, and it supplies sufficient power to vibrate most turbine blades. The oscillator frequency is varied until resonance occurs, and the frequency can be read on the oscillator dial. By using a micrometer drive for the dial and calibrating with a cathode-ray oscillograph, very high precision can be obtained when needed.

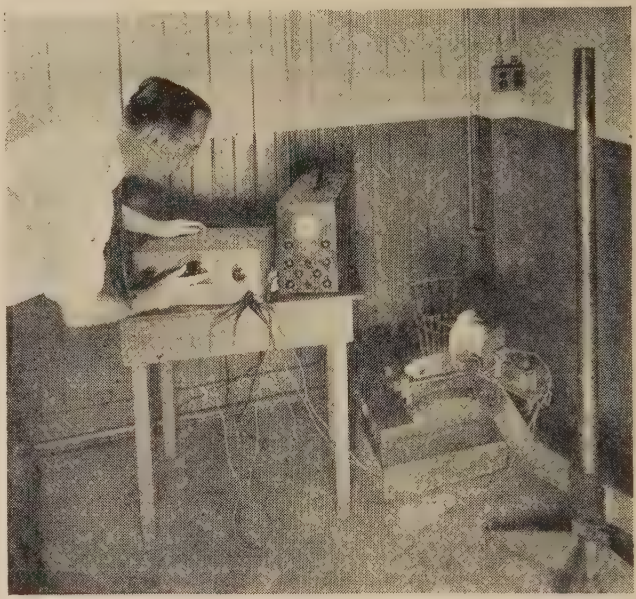

FIG. 8 VIBRATOR FOR DETERMINING NATURAL FREQUENCIES OF TURBINE BLADES

Single blades to be tested are clamped to a heavy metal slab, usually using filler blocks which cover the root and packing piece. When testing an entire group of blades, complete with shroud band, the blades are mounted in a grooved block which simulates a section of the turbine rotor. Such a group can be seen in Fig. 8.

Another type of testing which is necessary in blade designing is the combined tensile and fatigue test. In this test a tensile load is applied to the blade to simulate centrifugal force. At the same time, vibratory stresses are simulated by the application of a lateral alternating force. A machine for making such tests is shown in Fig. 9. A beam, weight-loaded at the end, applies the tensile load (up to 21,000 lb). A connecting rod, attached to an adjustable eccentric, applies a bending deflection to the blade. The eccentric is driven by a motor with a speed range of 1000 to 2200 rpm. The bending stress in the blade is checked by means of bonded resistance-wire (SR-4) strain gages. This machine is used to determine the fatigue strength of blading, and also for comparative tests of modifications to blade roots. It was used in

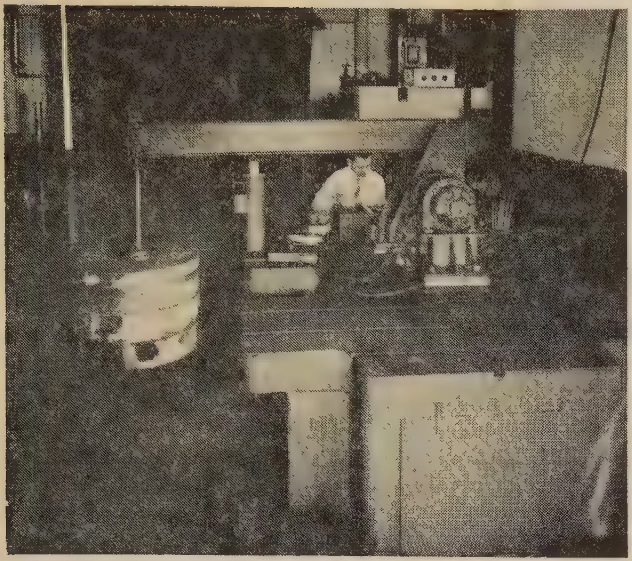

FIG. 9 MACHINE FOR MAKING COMBINED TENSILE AND FATIGUE TESTS

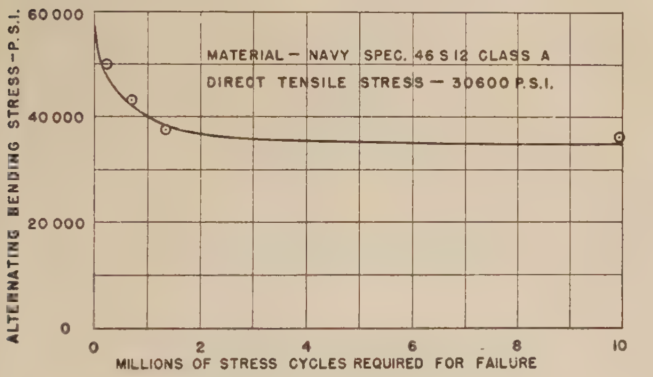

FIG. 10 FATIGUE TEST OF 2-IN. TURBINE BLADE

arriving at the size of fillet to be used in the roots of the stages, A and B, which were shown in Fig. 7.

In making combined tensile and fatigue tests, a certain tensile load is applied, and then a series of tests are run at different bending stresses. Each test is continued until the specimen either breaks or withstands 10,000,000 stress cycles. A curve of bending stress versus number of cycles is then plotted. Such a curve is shown in Fig. 10. It will be noticed that the curve falls rapidly at first and then levels off. At 10,000,000 cycles the curve is practically flat. With ferrous materials, it is assumed that a specimen which withstands 10,000,000 stress cycles will last indefinitely. In this paper the ordinate of the curve at 10,000,000 cycles will be called the endurance limit. This term must be used with caution because endurance limit is usually used to indicate the fatigue strength of the material subjected to alternating stress only. In this case there is a combination of steady stress and alternating stress. A separate endurance limit can be obtained for each value of steady stress.

The several values of endurance limit may be plotted on a curve such as that shown in Fig. 11. Here, endurance limit is plotted as the ordinate and steady stress as the abscissa. In the plot shown in Fig. 11 there are only two points. The tests were all run with 30,600 psi steady stress, which gave one of the points. The other point is the steady stress corresponding to zero alternating stress. This is simply the tensile strength of the material. These have been joined by a straight line. Published literature on the subject indicates that this is a reasonable assumption to use when intermediate points are lacking. The resulting curve shows the strength of a particular blade for any combination of steady and vibratory stress. However, the curve should be representative of other blades of similar design.

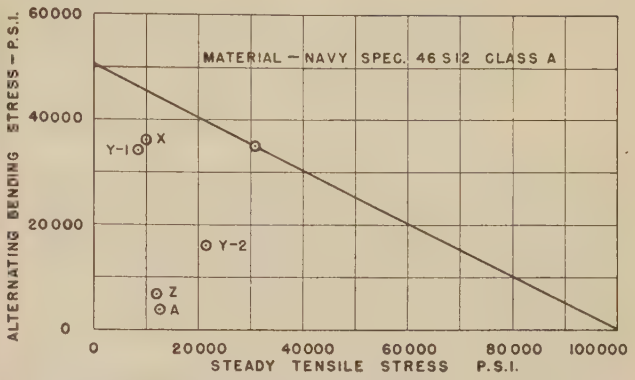

FIG. 11 FATIGUE-STRENGTH DIAGRAM FOR 2-IN. TURBINE BLADE

FACTOR OF SAFETY

In most stress problems it is desirable to calculate a factor of safety. In turbine-blade vibration there is much that is not known and that is why designers prefer statistical methods aided by comparative stress and vibration calculations. The magnitudes of both exciting and damping forces are in considerable doubt. One manufacturer multiplies the steady steam bending stress by 10, adds it to the centrifugal stress at full power and considers that the working stress for the blade. This appears to be a reasonably rational approach when it is considered that it is equivalent to a harmonic exciting component of 5 per cent of the steady steam force, and an amplification factor of 180. The 5 per cent factor appears quite conservative in the light of the few measurements of variations in steam force which are available (except in the case of impulse excitation). In fact, it is difficult to see how this figure could be approached in a carefully designed turbine, unless there were some damage to blading or nozzles.

The amplification of 180 also appears reasonable for 13 per cent chromium stainless-iron blading in a low-pressure turbine. The 5 per cent exciting force and amplification of 200 which have been assumed several times in this paper are very nearly identical with it. What this method does appear to need is an additional factor whereby the decreasing intensity of higher harmonics could be considered.

Returning now to Fig. 11, we can plot the stresses for stage A from Table 3 of a previous section. The bending stress required for failure at the given static stress of 12,590 psi, is 44,000 psi, giving a factor of safety of 44,000 ÷ 3900 = 11.3. At first glance this might seem to be an excessively high factor of safety. It is conservative, but turbine blades are subject to corrosion fatigue. Metals subjected to alternating stresses in an atmosphere of steam or water, have much lower endurance limits than in air. Because of this it would be reasonable to divide the foregoing factor of safety by 2, thus obtaining 5.6.

Four failures have been plotted in Fig. 11. The blades involved had the characteristics given in Table 5.

In each case the bending stresses have been multiplied by 10 before plotting in Fig. 11. Blades X and Y-1 both failed after several years of service. Both were in the last row of the high-pressure turbine, where they were subjected to relatively large variations in heat drop around the periphery. Since both had approximately 12 vibrations per revolution, they would not ordi-

TABLE 5 CHARACTERISTICS OF BLADES WHICH FAILED

Manufacturer	Turbine	Cent. stress, psi	Steam bending stress, psi	Total static stress, psi	Vibrations per rev	Failure
X	HP	6410	3610	10020	11.9	Blade
Y (case 1)	HP	5000	3390	8390	12.5	Blade
Y (case 2)	LP	19800	1590	21390	4.0	Shroud
Z	LP	11200	700	11900	4.2	Root

narily be expected to give trouble. The bending stresses were, however, so high that even with the small excitation obtained from the 12th harmonic they succumbed to corrosion fatigue. In considering these stresses, it must be remembered that the factor of 10 is excessive for the high-order vibration. The remedy for such blade trouble is to lower the bending stress by using a heavier blade section.

With blade Y-2, 4th-order resonance was encountered at full power. The blade itself did not fail but the vibration was sufficiently severe to crack the shroud band. Broken shroud bands are liable to jam and tear up the blading. In the case of blade Z, failure was attributed to axial vibration of the wheel. However, exact diagnosis of blade failure is usually difficult, and the proximity to 4th-order resonance appears suspicious.

In connection with design, it should be emphasized that great care must be exercised in proportioning all fillets on turbine blading. A sharp re-entrant corner at the base of the blade, or in the root can be the starting point for a fatigue crack which will cause the failure of an otherwise successful blade.

CONCLUSION

From the foregoing illustrations and discussion, it can be seen that the design of blading to resist vibration is far from an exact science. In spite of this, high efficiencies are being obtained, while blade failures from fatigue have been reduced to a point where they are considerably less than failures from other causes.

Theory of the Mechanical Properties of Hot Plastics

By S. J. LORING,[1] EASTON, CONN.

This paper describes a theory of large strain, rubberlike elasticity combined with stress relaxation, which is the character of the behavior of hot plastics indicated by a series of unpublished high extension rate tests on such materials as polystyrene, polyethylene, acetate, etc., in the molten or "soft" state.

NOMENCLATURE

a_{ij} = natural strain components
A_{ij} = auxiliary strain quantities defined in terms of a_{ij}
C = pressure gradient in channel or tube flow
D = "diffusion coefficient" representing effect of thermal agitation of molecules on their phase-space co-ordinates
f = representative molecular force
$f(x_i)$ = designation for arbitrary function in channel- and tube-flow analysis
f_{11}, f_{22} = functions representing stresses due only to elastic strain in channel and tube flows
F_{22} = function representing stress due only to elastic strain in tube flows
F_1, F_2, F_3 = forces on sides of parallelepiped of material
G = modulus of rigidity entering specific strain-energy functions
h = semiheight of channel or radius of tube
H, H' = auxiliary parameters in analysis of channel and tube flows
i, j, k = "dummy" indexes ranging over values 1, 2, 3
K = constant of proportionality between representative molecular force f and length r
l_{ij} = direction cosines relating directions of x_1, x_2, x_3 and y_1, y_2, y_3 axes
L_1, L_2, L_3 = fixed reference lengths
m_{ij} = direction cosines relating directions of x_1, x_2, x_3 and z_1, z_2, z_3 axes
M_{ij} = auxiliary strain quantities defined in terms of a_{ij} and m_{ij}
n = exponent in specific relaxation and strain-energy functions
N = number of molecules per unit volume
p = hydrostatic tension independent of elastic strain in incompressible materials
p_0 = constant hydrostatic tension in channel or tube-flow analysis
q = volume rate of flow per unit width in channel
Q = volume rate of flow in tube
r = representative length of chain molecule
r_0 = reference value of r
R_1, R_2, R_3 = functions describing relaxation process
s = shearing rate in simple shear
S = dimensionless measure of shearing rate s
t = time
T = "relaxation time" entering specific relaxation functions
v_0 = constant of integration in flow-velocity integrals for channel or tube
v_1, v_2, v_3 = flow-velocity components in x_1, x_2, x_3 directions
v_r = "drift" velocity of phase-space co-ordinates of a molecule due to molecular force
W = work done on unit volume of material by external forces
x_1, x_2, x_3 = fixed direction Cartesian co-ordinates; in dealing with strain a single prime (′) denotes position of point in unstrained condition, and double prime (″) in strained condition
X, X' = auxiliary parameters in analysis of channel or tube flows
x, y, z = Cartesian co-ordinates in phase space
y_1, y_2, y_3 = Cartesian co-ordinates with same origin as x_1, x_2, x_3, but directed along lines in unstrained condition which become principal axes in strained condition. Single and double primes (′), (″) have same significance as for x_1, x_2, x_3
z_1, z_2, z_3 = Cartesian co-ordinates with same origin as x_1, x_2, x_3, but directed along lines of principal strain in strained condition. Single and double primes (′), (″) have same significance as for x_1, x_2, x_3
$\alpha_1, \alpha_2, \alpha_3$ = principal extension-strain ratios—referring to elastic strain in Sections 3, 4, and 5
η = viscosity coefficient for Newtonian liquid
η_c = apparent viscosity for flow in channel
η_s = apparent viscosity for simple shear flow
η_t = apparent viscosity for flow in tube
θ = angle between principal strain axis z_1, and axis x_1 in two-dimensional strain
θ_1 = angle between unrotated principal axis y_1, and axis x_1 in two-dimensional strain
$\lambda_1, \lambda_2, \lambda_3$ = parameters in linear relations between M_{ij} and m_{ij}
μ = assumed constant of proportionality between v_r and molecular force f
ρ = distribution function in phase space
ρ_0 = equilibrium distribution function
$\sigma_1, \sigma_2, \sigma_3$ = principal stresses
σ_{11}, σ_{22} = tension stresses on x_1, x_2 co-ordinate plane
τ = shear stress on x_1, x_2 co-ordinate planes
Φ, Φ' = auxiliary functions for channel flow
ψ = strain-energy function

1 INTRODUCTION

The mechanical stress-flow properties of hot plastics are of considerable practical importance in the study of various plastic-manufacturing processes, such as extruding, molding, injection molding, etc. The results of a series of tension tests on several hot plastic materials, which are reported by the author,[2] indi-

---

[1] Consulting Engineer. Mem. ASME.

Contributed by the Rubber and Plastics Division and presented at the Annual Meeting, New York, N. Y., November 27–December 2, 1949, of THE AMERICAN SOCIETY OF MECHANICAL ENGINEERS.

NOTE: Statements and opinions advanced in papers are to be understood as individual expressions of their authors and not those of the Society. Paper No. 49—A-60.

[2] "Report on Tensile Tests on Hot Plastics at High Extension Rates"; report prepared for Plax Corporation by S. J. Loring, December, 1948.

cate that the flow properties of these materials result from a rubberlike large deflection elasticity combined with a stress relaxation property.

The elastic and relaxation properties combine to produce flow characteristics which are in many ways similar to those of the classical Maxwell liquid. The classical Maxwell liquid theory, however, implies that the elastic strains are of infinitesimal, or at least very small magnitude as is also assumed in the classical theory of elasticity. In contrast, the subject materials exhibit very large elastic strains, with extension ratios of the order of 2 or even 10, and these large elastic strains have profound effects upon the behavior of the materials as compared to the classical Maxwell liquid.

The important novel effects introduced by large elastic strain as opposed to small strain originate from two principal sources. One source of novel effects lies in the geometrical properties of large strain itself, which are considerably more complex than those of small or infinitesimal strain. The other source of new complexities is the fact that both the elastic and relaxation rates are affected by the changes in internal structural arrangement of the materials which must accompany large strain; these rates no longer can be considered linear as in classical theories.

A theory of the mechanical behavior of materials exhibiting large-strain elasticity and stress relaxation is developed in the present paper, in which consideration is given both to the geometrical properties of large strain and to the nonlinearity of elasticity and relaxation which accompany large strain.

The theory is based upon the mathematical treatment of large strain presented in Section 2. This treatment differs from most other treatments of large strain in that it is developed from the specification of the state of strain at the individual points of a body rather than a general specification of the state of distortion of the body as a whole. The strain at the individual points is then related differentially to the distortion of the body as a whole by specifying its time rate of change in terms of flow velocities. This point of view appears simpler than the usual one because the current strain condition can be followed during the course of a deformation without the complexities and ambiguities that arise in relating the positions of points in the body directly to their original or unstrained positions. The viewpoint is, in addition, particularly well adapted to the treatment of the relaxation process in flows, which leads to real ambiguities with the older method.[3]

In Section 3 the mathematical specification of general elastic and relaxation properties is developed from a phenomenological and macroscopic point of view. It is pointed out at the end of that section that numerical implementation of this specification requires data relating to the internal structure of the materials.

A simple molecular representation of internal structure is set up in Section 4, and analyzed by the methods of statistical mechanics to illustrate the structural significance of the phenomenological concepts introduced to describe the macroscopic mechanical behavior. This analysis leads to definite mathematical functions which describe the elasticity and relaxation of the simplified representation, and which may be used as starting points for interpretation of test data on actual materials.

General solutions for the steady-state flows in channels and tubes are developed in Section 5, and their numerical application is illustrated by carrying out numerical computations with strain-energy and relaxation functions which are in accord with the tensile test data of the author.[2] Comparison is made with some test data on flows through channels and tubes, and the agreement with the theory is encouraging.

Regarding extensions in the applications of this theory, it is interesting to note that the principal novel concepts in large elastic strain are very similar to those described by Bailey[4] as orientation in cold plastics. It appears that the understanding of the mechanical properties of hot plastics may be extended and lead to understanding of the more complex properties of cold plastics.

In any event, it is hoped that the theory in its present form will serve as a basis for interpretation of observations on the mechanical behavior of hot plastics, and when fully implemented by such observations, will serve as a basis for rational and quantitative treatment of some of the flow problems involved in the manufacture of plastic articles.

2 Geometry of Large Strains

(*a*) *The Notion of Strain.* Since the properties of large strain differ in a number of ways from those of the small strain of classical theory, some of the commonly accepted attributes of small strain must be discarded in treating large strain. For this reason the developments of this section are introduced by an account of the general notion of strain of unrestricted magnitude. This account is directed to the viewpoint to be adopted in the following treatment of large strain.

A complete and detailed description of circumstances in which the relative positions of the points of a body change requires the notion of strain. Consideration of those circumstances will serve to bring out the basic concepts involved in the notion of strain.

Note first that change in the relative positions of the points of a body implies a comparison of two states of deformation of the body. Therefore two distinct configurations of the points of a body must be involved in the notion of strain; specifically, the comparison of the two configurations is involved.

Changes in relative position of distant points of the body result from vectorial addition of the changes of relative position of a number of closer intermediate points, and they are, therefore, implied by the latter changes. The closer the points of the body that are individually identified the more complete the description of the relative state of distortion in the two configurations.

In the limit, a complete description of a distortion of a body can consist of a catalog of the relative position changes of all its pairs of points which lie an infinitesimal distance apart. Such a catalog may be conceived as being composed of sections each of which is devoted to a particular point and contains the information for all pairs of points separated by an infinitesimal distance and of which the particular point is a member. Multiple listings required for this arrangement of the catalog will, of course, not affect its completeness, which is all that matters for the present purposes.

The information contained in that section of the catalog described in the preceding paragraph which is devoted to a particular point is just the information which is contained in a specification of the state of strain at the point. The mechanics of this specification, and its properties, form the subject matter of the present treatment.

Most classical treatments of strain are restricted to the case of "small" strains, in which case the changes in the distances between pairs of neighboring points are very small compared to these distances themselves. This restriction is inappropriate for the present purposes and is completely abandoned. In the treatment which follows no assumption is made as to the magnitude of the changes which take place in the distances between neighboring points, except that they are continuous from point to point and remain finite.

---

[3] See, for example, footnote,[5] and discussion just prior to that reference.

[4] "Stretch Orientation of Styrene and Its Interesting Results," by James Bailey, *India Rubber World*, vol. 118, May, 1948, pp. 225–231.

(*b*) *Specification of Strain at a Point.* In order to specify the strain at a point in a body, a set of Cartesian co-ordinates x_1, x_2, x_3 is set up with the origin at the point in question. The directions of these axes remain fixed, but the origin stays on the point of the body and moves with it during a deformation.

Let the x_1, x_2, x_3-co-ordinates of any neighboring point be designated by x_1', x_2', x_3' "before the deformation," and let them be designated by x_1'', x_2'', x_3'' "after the deformation." Specification of the strain at the point consists of a general expression for x_1'', x_2'', x_3'' in terms of x_1', x_2', x_3' in which, however, these coordinates are limited to infinitesimal values.

Any relationship between x_1'', x_2'', x_3'' and x_1', x_2', x_3' can be expressed as power series in x_1', x_2', x_3'. The constant term in the series for each of x_1'', x_2'', x_3'' is zero since, by definition, the reference axes move with the reference point in the body, that is, $x_1' = x_2' = x_3' = 0$ always implies that $x_1'' = x_2'' = x_3'' = 0$. Furthermore, since x_1', x_2', x_3' are limited to infinitesimal values, powers above the first may be neglected in the series. Accordingly, the most general expression for strain at a point is

$$\left.\begin{aligned} x_1'' &= a_{11}x_1' + a_{12}x_2' + a_{13}x_3' \\ x_2'' &= a_{21}x_1' + a_{22}x_2' + a_{23}x_3' \\ x_3'' &= a_{31}x_1' + a_{32}x_2' + a_{33}x_3' \end{aligned}\right\} \ldots\ldots\ldots\ldots [1]$$

The strain is specified by the nine quantities $a_{11} \ldots a_{33}$ which will be called the natural strain components. Though they are in a different form, the natural strain components are equivalent to the strain components usually employed in the classical theory of elasticity. However, as remarked before, in this work no assumption is made as to the magnitudes of the strain components except that they remain finite.

In the exposition which follows a number of equations will be encountered which, like Equations [1], have groups of similar terms in which only the indexes change. It will be convenient to shorten the writing out of these equations by use of the standard summation symbol Σ, and the letter indexes i, j, k, which range over the values 1, 2, and 3. The index to which the summation refers will be indicated by placing this index under the summation sign, and the ranges of other indexes will be indicated in parentheses after each expression. Thus Equations [1] can be written

$$x_i'' = \sum_j a_{ij}x_j', \text{ (for } i = 1, 2, 3) \ldots\ldots\ldots\ldots [1a]$$

(*c*) *Resolution of Strain Into Three Principal Strains and a Rotation.* For treatment of the generalized types of elasticity and relaxation to be discussed in the sequel it is convenient to reduce the specification of a strain to a standard and uniquely simple form rather than to use the natural strain components of Equations [1].

It will be shown that any strain specified by Equations [1] is equivalent to, and can be resolved into three simple extensions along three suitably directed mutually perpendicular axes, plus a rigid-body rotation. The three simple extensions of this resolution are called the principal strains. Thus, according to this resolution, there are only three really independent components of strain proper; in addition to these three principal strains, the natural strain components a_{ij} also specify the orientation of the principal axes of strain and a rigid-body rotation. The resolution into principal strains will isolate these three aspects of a general strain given by Equations [1].

To effect this resolution introduce two additional sets of Cartesian co-ordinates with origins also staying on the point of the body which is the origin of the x_1, x_2, x_3 axes. These new coordinates are designated y_1, y_2, y_3 and z_1, z_2, z_3; their axes differ from x_1, x_2, x_3 only in orientation, and expressions relating the co-ordinates themselves to x_1, x_2, x_3 are

$$y_i = \sum_j l_{ij}x_j, \text{ (for } i = 1, 2, 3) \ldots\ldots\ldots\ldots [2]$$

and

$$z_i = \sum_j m_{ij}x_j, \text{ (for } i = 1, 2, 3) \ldots\ldots\ldots\ldots [3]$$

In these relations l_{ij} and m_{ij} (for $i, j = 1, 2, 3$) are, respectively, sets of direction cosines relating two sets of orthogonal axes. They each satisfy the well-known identities for such direction cosines which express the orthogonality of the two sets of axes. These identities are used in subsequent derivations and will be written here for the m_{ij} for reference purposes

$$\sum_j m_{ij}^2 = 1, \text{ (for } i = 1, 2, 3) \ldots\ldots\ldots\ldots [4]$$

$$\sum_j m_{ij}m_{kj} = 0, \text{ (for } i \neq k, \text{ and } i, k = 1, 2, 3) \ldots\ldots [5]$$

It may be noted that Equations [5] comprise only three equations since for these equations i is specified to be not equal to k, and interchange of i and k does not change the terms of the summation. The terms that would result from $i = k$ in Equation [5] are the terms of Equations [4]. From the identities, Equations [4] and [5], the following similar identities can be derived

$$\sum_i m_{ij}^2 = 1, \text{ (for } j = 1, 2, 3) \ldots\ldots\ldots\ldots [4a]$$

$$\sum_i m_{ij}m_{ik} = 0, \text{ (for } j \neq k, \text{ and } j, k = 1, 2, 3) \ldots\ldots [5a]$$

Observations can be made concerning the identities, Equations [4*a*] and [5*a*], which are entirely similar to those already made concerning Equations [4] and [5].

Similar identities hold, of course, for the l_{ij}.

In a fashion similar to that already specified for x_1, x_2, x_3, the single prime (′) is used to designate the y- and z-co-ordinates of points in the body before deformation, and the double prime (″) after deformation.

For each given strain, the orientation of the y- and z-axes, that is, l_{ij} and m_{ij}, are set as follows: The z_1, z_2, z_3 co-ordinate axes are directed along the three principal strain axes in the deformed body. The points of the body in the neighborhood of the reference point which lie on these principal strain axes after deformation will have lain along three mutually perpendicular straight lines before the deformation took place; these lines, however, generally have different directions than the principal strain axes in the deformed state, because of the rigid-body rotation component of the strain. The y_1, y_2, y_3 axes are directed along the three mutually perpendicular lines thus defined. It is seen then that the orientation of the z-axes, i.e., the m_{ij}, locates the principal axes of strain in the deformed body; and also that the difference in orientation between the z-axes and the y-axes, i.e., the m_{ij} and the l_{ij}, determine the rigid-body rotation part of the strain.

Let the three principal extension "strain ratios" be designated by α_1, α_2, and α_3. The strain expressed by Equations [1] is, then, asserted to be equivalent to a strain specified by

$$\left.\begin{aligned} z_1'' &= \alpha_1 y_1' \\ z_2'' &= \alpha_2 y_2' \\ z_3'' &= \alpha_3 y_3' \end{aligned}\right\} \ldots\ldots\ldots\ldots\ldots\ldots [6]$$

or

$$z_i'' = \alpha_i y_i', \text{ (for } i = 1, 2, 3) \ldots\ldots\ldots\ldots [6a]$$

The problem at hand is to show that a strain given by Equations [6] can be made to coincide with any given by Equations [1], by suitable choices of the principal strain ratios α_i and of the direction cosines m_{ij} and l_{ij}; and further to determine the α_i, m_{ij}, and l_{ij} in terms of the natural strain components a_{ij} of Equations [1]. The balance of this subsection is devoted to this problem.

Use the relations of Equations [2] and [3] to express Equations [6] in terms of the x_1, x_2, x_3 co-ordinates; thus

$$\sum_j m_{ij}x_j'' = \alpha_i \sum_j l_{ij}x_j', \text{ (for } i = 1, 2, 3) \ldots\ldots [7]$$

Now, solve these three equations for x_1'', x_2'', x_3'', respectively, by multiplying the respective equations first by m_{i1} and adding, then by m_{i2} and adding, and finally by m_{i3} and adding. This process solves the equations for x_1'', x_2'', x_3'' by virtue of the identities, Equation [4a] and [5a]. The coefficients of the x_j' in the resulting equations solved for the x_i'', by comparison with Equations [1], are seen to be equal to the natural strain components a_{ij}. Thus

$$a_{ij} = \sum_k \alpha_k l_{kj} m_{ki}, \text{ (for } i, j = 1, 2, 3) \ldots\ldots [8]$$

There is a total of nine separate equations in Equations [8], one for each of the nine a_{ij}.

In order to obtain explicit equations for the direction cosines m_{ij}, start by forming the following nine equations from Equations [8], with the help of the identities, Equations [4] and [5]

$$\sum_i a_{ij} m_{ki} = \alpha_k l_{kj}, \text{ (for } k, j = 1, 2, 3) \ldots\ldots [9]$$

In these equations the m_{ij} occur only in the left-hand sides, while the l_{ij} occur only on the right. Now, with the help of the identities of the type of Equations [5] in the direction cosines l_{ij}, the three combinations

$$\alpha_i \alpha_k \sum_j l_{ij} l_{kj} = 0, \text{ (for } i \neq k;\ i, k = 1, 2, 3) \ldots [10]$$

of the right-hand sides of Equations [9] may be formed which are identically zero. There are only three distinct relations, Equations [10] since $i \neq k$, and interchange of i and k does not change the relation. The corresponding left-hand sides of the combinations, Equations [10], of [9], which are equal to zero by Equations [10], comprise three equations in the m_{ij}. These three equations in combination with the identities, Equations [4] and [5], serve to determine the values of all the m_{ij}.

The three equations in the m_{ij} are most conveniently written with the help of the following auxiliary notation: Let

$$A_{ij} = A_{ji} = \sum_k a_{ik} a_{jk}, \text{ (for } i, j = 1, 2, 3) \ldots\ldots [11]$$

and further, let

$$M_{ij} = \sum_k A_{kj} m_{ik}, \text{ (for } i, j = 1, 2, 3) \ldots\ldots [12]$$

Note that, if a_{ij} are considered known, the A_{ij} are known constants, while the M_{ij} are "linear combinations" of the m_{ij} with these constants as coefficients. With this notation, the three equations in the m_{ij} may be written as follows

$$\sum_j m_{ij} M_{kj} = 0, \text{ (for } i \neq k;\ i, k = 1, 2, 3) \ldots\ldots [13]$$

There are only three equations implied by Equations [13] since i is specified to be not equal to k, and the notation of Equations [11] and [12] implies that interchange of i and k does not alter the expanded or intrinsic form of Equations [13].

Comparison of Equations [13] with the identities, Equations [5], shows directly that the m_{ij} and their linear combinations M_{ij} must be connected by the relations

$$M_{ij} = \lambda_i m_{ij}, \text{ (for } i, j = 1, 2, 3) \ldots\ldots [14]$$

where λ_i ($i = 1, 2, 3$) are constants which will be determined.

If the three of Equations [14] with any specific index i are substituted into the three of Equations [12] with the same index i, the following three linear homogeneous equations in m_{i1}, m_{i2}, m_{i3} are obtained

$$\left.\begin{array}{rrrl} (A_{11} - \lambda_i)m_{i1} + & A_{21}m_{i2} + & A_{31}m_{i3} & = 0 \\ A_{12}m_{i1} + & (A_{22} - \lambda_i)m_{i2} + & A_{32}m_{i3} & = 0 \\ A_{13}m_{i1} + & A_{23}m_{i2} + & (A_{33} - \lambda_i)m_{i3} & = 0 \end{array}\right\} . [15]$$

Furthermore, if these equations are to have solutions for the three unknowns m_{i1}, m_{i2}, m_{i3} which are not all zero—which must be the case because of Equations [4]—then the determinant of the coefficients must vanish. Thus

$$\begin{vmatrix} (A_{11} - \lambda_i) & A_{21} & A_{31} \\ A_{12} & (A_{22} - \lambda_i) & A_{32} \\ A_{13} & A_{23} & (A_{33} - \lambda_i) \end{vmatrix} = 0 \ldots\ldots [16]$$

The numerical values of m_{i1}, m_{i2}, m_{i3} can be obtained for any root λ_i satisfying Equations [16] by use of any two of Equations [15] and condition, Equation [4]. The expanded form of Equations [16] is a cubic equation which has three roots λ_1, λ_2, λ_3. These three roots give the values of m_{i1}, m_{i2}, m_{i3} for $i = 1, 2, 3$, respectively. Therefore all the m_{ij} are determined.

The determination of the l_{ij} can be carried out in an entirely similar manner starting with the relations

$$\sum_j a_{ij} l_{kj} = \alpha_k m_{ki}, \text{ (for } i, k = 1, 2, 3) \ldots\ldots [17]$$

In a fashion entirely similar to that for Equations [9], these relations are obtained from Equations [8], with the help of the identities, Equations [4a], [5a]. The determination of the l_{ij} will not be carried out, since the formulas will not be required in the sequel.

Having shown how to determine the numerical values of the direction cosines m_{ij} and l_{ij}, these values may be considered as known. The values of the principal strain ratios α_i can be determined from Equations [9] by forming the three combinations

$$\alpha_i \sum_j l_{ij}^2 = \alpha_i, \text{ (for } k = 1, 2, 3) \ldots\ldots [18]$$

of the right-hand sides. The resulting formulas for α_i are

$$\alpha_i = \sum_{j,k} m_{ij} l_{ik} a_{jk}, \text{ (for } i = 1, 2, 3) \ldots\ldots [19]$$

Here the summation includes a term for each possible combination of j and k for $j, k = 1, 2, 3$. The summation has therefore nine terms, one for each of the a_{jk}.

The resolution of any strain given by Equations [1] into three principal strains in appropriate orthogonal directions and a rigid-body rotation has been effected. The local state of *distortion* of the material of a body near a point is completely specified by the α_i and the m_{ij}. The only role played by the direction cosines l_{ij} in specifying the strain is in defining the rigid-body rotation in conjunction with the m_{ij}. The rigid-body rotation does not contribute to the local distortion of the material at all, and it will be seen that for a number of purposes, the l_{ij} are extraneous, that is, they do not enter a problem at all. In fact, problems of this type would not have unique solutions in terms of the natural strain components a_{ij}, since the latter contain the extraneous rigid-body rotation.

Problems involving relaxation phenomena are often of this type, since the effect of relaxation on the rigid-body rotational component of the strains is in a sense indeterminate, that is, it depends upon the boundary conditions under which a partially relaxed body is allowed to become elastically restored to zero strain. These boundary conditions are unspecified and really extraneous in problems in which the body is never allowed actually to restore itself to zero strain, for example, in a case of steady-state flow.

The general validity of this resolution is therefore of considerable theoretical significance in treating problems of flow in materials exhibiting relaxation properties. This is the main reason for treating the resolution in the completely general manner of the subsection, i.e., in terms of completely general three-dimensional strain. In the present work actual numerical use of the resolution is made in less general special cases.

(*d*) *Rate of Change of Strain Components Due to Flow.* The treatment of problems of flow is facilitated by relating the strains at the points of the body to the distortion of the body as a whole through differential relations for the rate of change of the strain components due to flow velocities. Some of these relations will be derived in their general three-dimensional form both in terms of the natural strain components and in terms of the principal strain components.

The unstrained co-ordinates x_1', x_2', x_3' of a point will not change as a direct result of a flow process;[5] therefore in the present derivations these co-ordinates are considered independent of time. Differentiation of Equations [1] with respect to time gives the relations

$$\frac{\partial x_i''}{\partial t} = \sum_j \frac{da_{ij}}{dt} x_j', \text{ (for } i = 1, 2, 3) \ldots\ldots\ldots [20]$$

The Eulerian velocity components along the x_1, x_2, x_3 co-ordinate directions are denoted by v_1, v_2, v_3. The time rate of change of the displaced co-ordinates x_1'', x_2'', x_3'' of the particles of the body in the neighborhood on the reference point are therefore directly

$$\frac{\partial x_i''}{\partial t} = \sum_j x_j'' \frac{\partial v_i}{\partial x_j}, \text{ (for } i = 1, 2, 3) \ldots\ldots\ldots [21]$$

In these Equations [21] the factors x_j'' in the terms of the right-hand side may be expressed in terms of x_j' by use of the relations, Equations [1]. The resulting right-hand sides of Equations [21] therefore become linear expressions in the x_j' and direct comparison of these cofficients with those in Equations [20] gives the expressions for the rates of change of the natural strain components due to flow. These expressions are

$$\frac{da_{ij}}{dt} = \sum_k a_{kj} \frac{\partial v_i}{\partial x_k}, \text{ (for } i, j = 1, 2, 3) \ldots\ldots\ldots [22]$$

The principal strain ratios are given by Equations [19]. Their time derivatives are, accordingly, given by

$$\frac{d\alpha_i}{dt} = \sum_{j,k} \left(m_{ij} l_{ik} \frac{da_{jk}}{dt} + a_{jk} l_{ik} \frac{dm_{ij}}{dt} \right.$$
$$\left. + a_{jk} m_{ij} \frac{dl_{ik}}{dt} \right), \text{ (for } i = 1, 2, 3) \ldots\ldots\ldots\ldots [23]$$

The second and third terms in the summation of this equation vanish. This can be shown as follows: Sum the third terms with respect to j, and use Equations [9] to eliminate $a_{jk}m_{ij}$; the total contribution of this third term is thus seen to be

$$\sum_k \alpha_i l_{ik} \frac{dl_{ik}}{dt} = \frac{\alpha_i}{2} \frac{d}{dt} (\sum_k l_{ik}^2) = 0$$

Similarly, sum the second terms with respect to k and use Equations [17]; the contribution of this term is

$$\sum_j \alpha_i m_{ij} \frac{dm_{ij}}{dt} = \frac{\alpha_i}{2} \frac{d}{dt} (\sum_j m_{ij}^2) = 0$$

Thus only the first term in the summation on the right side of Equation [23] remains. Substitute Equations [22] into this first term and use Equations [17] to eliminate $a_{jk}l_{ik}$ factors; the resulting form of Equation [23] is

$$\frac{d\alpha_i}{dt} = \alpha_i \sum_{j,k} m_{ij} m_{ik} \frac{\partial v_j}{\partial x_k}, \text{ (for } i = 1, 2, 3) \ldots\ldots [24]$$

It remains to determine the expressions for the rates of change of the direction cosines. These expressions will be derived only for the two-dimensional case in the next section.

(*e*) *Case of Two-Dimensional Flow and Strain.* The definition of two-dimensional strain in the x_1, x_2-plane is that the deflection vector of all particles lies in the x_1, x_2-plane, and all particles with the same x_1, x_2-co-ordinates have the same deflection vector.

Referring to Equations [1], the condition on the natural strain components a_{ij} for two-dimensional strain in the x_1, x_2-plane are

$$a_{13} = a_{31} = a_{23} = a_{32} = 0; \quad a_{33} = 1 \ldots\ldots\ldots\ldots [25]$$

The corresponding two-dimensional flow is

$$\frac{\partial v_1}{\partial x_3} = \frac{\partial v_2}{\partial x_3} = v_3 = 0 \ldots\ldots\ldots\ldots\ldots\ldots [26]$$

The relations for principal strains, principal strain directions, and rates of change of these due to flow are to be derived for this case of two-dimensional strain and flow.

The A_{ij} of Equations [11] for two-dimensional strain are

$$\left.\begin{array}{c} A_{13} = A_{31} = A_{23} = A_{32} = 0; \quad A_{33} = 1 \\ A_{11} = a_{11}^2 + a_{12}^2 \\ A_{22} = a_{21}^2 + a_{22}^2 \\ A_{12} = A_{21} = a_{11}a_{21} + a_{12}a_{22} \end{array}\right\} \ldots\ldots [27]$$

Thus Equations [15] for the direction cosines m_{ij} become

$$\left.\begin{array}{r} (a_{11}^2 + a_{12}^2 - \lambda_i)m_{i1} + (a_{11}a_{21} + a_{12}a_{22})m_{i2} = 0 \\ (a_{11}a_{21} + a_{12}a_{22})m_{i1} + (a_{21}^2 + a_{22}^2 - \lambda_i)m_{i2} = 0 \\ (1 - \lambda_i)m_{i3} = 0 \end{array}\right\} \ldots [28]$$

The determinantal equation for λ_i is

$$(1 - \lambda_i)[\lambda_i^2 - (a_{11}^2 + a_{12}^2 + a_{21}^2 + a_{22}^2)\lambda_i$$
$$+ (a_{11}a_{22} - a_{12}a_{21})^2] = 0 \ldots\ldots\ldots [29]$$

The root $\lambda_3 = 1$ is determined by the first factor in Equation [29]; substitution of this root into the first two of Equations [28] gives, with the help of Equations [4] and [4*a*]

$$m_{13} = m_{31} = m_{23} = m_{32} = 0; \quad m_{33} = 1 \ldots\ldots\ldots [30]$$

With the values of Equations [30], the remaining direction cosines may be expressed as

$$m_{11} = m_{22} = \cos\theta; \quad m_{12} = -m_{21} = \sin\theta \ldots\ldots\ldots [31]$$

where θ is the angle between the z_1 (principal) axis and the x_1-axis. The meaning of Equations [30] is of course that the axes z_1 and z_2 lie in the x_1, x_2-plane. The relative positions of these axes are shown in Fig. 1.

In order to determine the value of the angle θ, first determine the roots of the quadratic factor of Equation [29]. These roots are

---

[5] The unstrained co-ordinates might be considered to change as an "indirect" result of a flow due to a relaxation phenomenon. For the present, however, only the direct results of flow are being considered. It will be seen later that this delicate question is sidestepped by use of the resolution into principal strains. In fact, this is the really fundamental reason for introducing this resolution.

$$\left.\begin{aligned}\lambda_1 &= \frac{1}{2}\Big[(a_{11}^2 + a_{12}^2 + a_{21}^2 + a_{22}^2)\\ &\quad + \sqrt{(a_{11}^2 + a_{12}^2 - a_{21}^2 - a_{22}^2)^2 + 4(a_{11}a_{21} + a_{12}a_{22})^2}\Big]\\ \lambda_2 &= \frac{1}{2}\Big[(a_{11}^2 + a_{12}^2 + a_{21}^2 + a_{22}^2)\\ &\quad - \sqrt{(a_{11}^2 + a_{12}^2 - a_{21}^2 - a_{22}^2)^2 + 4(a_{11}a_{21} + a_{12}a_{22})^2}\Big]\end{aligned}\right\} \quad \ldots [32]$$

Substitution of either of these values with Equations [31] into either of the first two of Equations [28] will determine the angle θ. The result is most easily expressed as

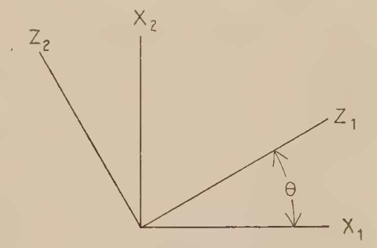

FIG. 1 POSITION OF PRINCIPAL STRAIN AXES z_1, z_2 FOR TWO-DIMENSIONAL STRAIN IN x_1, x_2-PLANE

$$\tan 2\theta = \frac{2(a_{11}a_{21} + a_{12}a_{22})}{a_{11}^2 + a_{12}^2 - a_{21}^2 - a_{22}^2} \quad \ldots\ldots\ldots\ldots [33]$$

An expression for the rate of change of the angle θ is obtained by direct differentiation of Equation [33] with respect to time. This expression is

$$\begin{aligned}2\,(\sec^2 2\theta) \times \frac{d\theta}{dt} &= \frac{2(a_{21} - a_{11} \tan 2\theta)da_{11}/(dt) + 2(a_{22} - a_{12} \tan 2\theta)da_{12}/(dt)}{a_{11}^2 + a_{12}^2 - a_{21}^2 - a_{22}^2}\\ &+ \frac{2(a_{11} + a_{21} \tan 2\theta)da_{21}/(dt) + 2(a_{12} + a_{22} \tan 2\theta)da_{22}/(dt)}{a_{11}^2 + a_{12}^2 - a_{21}^2 - a_{22}^2}\end{aligned} \quad \ldots\ldots\ldots\ldots [34]$$

Expressions [22] for the rate of change of the natural strain components due to flow become, for the two-dimensional case

$$\left.\begin{aligned}\frac{da_{11}}{dt} &= a_{11}\frac{\partial v_1}{\partial x_1} + a_{21}\frac{\partial v_1}{\partial x_2}; & \frac{da_{12}}{dt} &= a_{12}\frac{\partial v_1}{\partial x_1} + a_{22}\frac{\partial v_1}{\partial x_2}\\ \frac{da_{21}}{dt} &= a_{11}\frac{\partial v_2}{\partial x_1} + a_{21}\frac{\partial v_2}{\partial x_2}; & \frac{da_{22}}{dt} &= a_{12}\frac{\partial v_2}{\partial x_1} + a_{22}\frac{\partial v_2}{\partial x_2}\end{aligned}\right\} \quad \ldots [35]$$

Substitution of these relations into Equation [34] gives

$$\left.\begin{aligned}2(\sec^2 2\theta) \times \frac{d\theta}{dt} &= \left[\frac{-2(a_{11}^2 + a_{12}^2)\tan 2\theta}{a_{11}^2 + a_{12}^2 - a_{21}^2 - a_{22}^2} + \tan 2\theta\right]\frac{\partial v_1}{\partial x_1}\\ &+ \left[\frac{2(a_{21}^2 + a_{22}^2)}{a_{11}^2 + a_{12}^2 - a_{21}^2 - a_{22}^2} - \tan^2 2\theta\right]\frac{\partial v_1}{\partial x_2}\\ &+ \left[\frac{2(a_{11}^2 + a_{12}^2)}{a_{11}^2 + a_{12}^2 - a_{21}^2 - a_{22}^2} + \tan^2 2\theta\right]\frac{\partial v_2}{\partial x_1}\\ &+ \left[\frac{2(a_{21}^2 + a_{22}^2)\tan 2\theta}{a_{11}^2 + a_{12}^2 - a_{21}^2 - a_{22}^2} + \tan 2\theta\right]\frac{\partial v_2}{\partial x_2}\end{aligned}\right\} \quad \ldots [36]$$

The set of Equations [8] specialized for the two-dimensional case with the help of Equations [30] and [31] give

$$\left.\begin{aligned}a_{11} &= \alpha_1 l_{11} \cos\theta - \alpha_2 l_{21} \sin\theta\\ a_{12} &= \alpha_1 l_{12} \cos\theta - \alpha_2 l_{22} \sin\theta\\ a_{21} &= \alpha_1 l_{11} \sin\theta + \alpha_2 l_{21} \cos\theta\\ a_{22} &= \alpha_1 l_{12} \sin\theta + \alpha_2 l_{22} \cos\theta\end{aligned}\right\} \quad \ldots\ldots\ldots\ldots [37]$$

Further, reasoning similar to that used to derive Equations [31] shows that l_{11}, l_{12}, l_{21}, and l_{22} in the two-dimensional case may be expressed as

$$l_{11} = l_{22} = \cos\theta_1;\quad l_{12} = -l_{21} = \sin\theta_1 \ldots\ldots\ldots [38]$$

From Equations [37] and [38] the following relations may be obtained which are independent of the angle θ_1 of Equations [38]

$$\left.\begin{aligned}a_{11}^2 + a_{12}^2 &= \alpha_1^2 \cos^2\theta + \alpha_2^2 \sin^2\theta\\ a_{21}^2 + a_{22}^2 &= \alpha_1^2 \sin^2\theta + \alpha_2^2 \cos^2\theta\end{aligned}\right\} \quad \ldots\ldots\ldots\ldots [39]$$

from which, finally

$$\left.\begin{aligned}\frac{2(a_{11}^2 + a_{12}^2)}{a_{11}^2 + a_{12}^2 - a_{21}^2 - a_{22}^2} &= \frac{\alpha_1^2 + \alpha_2^2}{\alpha_1^2 - \alpha_2^2} \times \sec 2\theta + 1\\ \frac{2(a_{21}^2 + a_{22}^2)}{a_{11}^2 + a_{12}^2 - a_{21}^2 - a_{22}^2} &= \frac{\alpha_1^2 + \alpha_2^2}{\alpha_1^2 - \alpha_2^2} \times \sec 2\theta - 1\end{aligned}\right\} \quad \ldots [40]$$

Substitution of the relations, Equations [40], into [36] yields the final expression for the rate of change of the principal strain directions with flow in the two-dimensional case. This final expression is

$$\begin{aligned}2\,\frac{d\theta}{dt} &= \left(\frac{\alpha_1^2 + \alpha_2^2}{\alpha_1^2 - \alpha_2^2} \times \sin 2\theta\right)\left(\frac{\partial v_2}{\partial x_2} - \frac{\partial v_1}{\partial x_1}\right)\\ &+ \left(\frac{\alpha_1^2 + \alpha_2^2}{\alpha_1^2 - \alpha_2^2} \times \cos 2\theta\right)\left(\frac{\partial v_2}{\partial x_1} + \frac{\partial v_1}{\partial x_2}\right) + \left(\frac{\partial v_2}{\partial x_1} - \frac{\partial v_1}{\partial x_2}\right)\end{aligned} \quad \ldots\ldots [41]$$

The important characteristic of this expression is that it involves only the quantities α_1, α_2, θ which describe the "strained" condition at a point; quantities relating back to the unstrained condition, that is, the l_{ij} or angle θ_1 of Equation [38], do not enter the expression at all. Thus the question of whether the unstrained condition at a point of a body is changing due, for example, to a relaxation process, has been sidestepped. Previous reference has been made to this result.[5] In this connection it should also be noted that Equations [24] for the rate of change of the principal strain ratios is also independent of the quantities l_{ij}.

(*f*) *Case of Steady-State Simple Shear Flow.* A particularly simple and important case of two-dimensional strain and flow is the case of a steady-state simple shear flow. Steady flows of materials through tubes and channels are often of this character. The relations of the preceding subsection can be further specialized for this case.

The flow considered is a flow in the x_1-direction for which

$$\frac{\partial v_1}{\partial x_2} = s = \text{const};\quad v_2 = v_3 = \frac{\partial v_1}{\partial x_1} = 0 \ldots\ldots\ldots [42]$$

A flow of this character results in two-dimensional strain in the x_1, x_2-plane, for which $\alpha_3 = 1$. With Equations [31] and [42] the relations, Equations [24] for rate of change of the principal strain ratios become

$$\left.\begin{aligned}\frac{d\alpha_1}{dt} &= \alpha_1 s \sin\theta\cos\theta &&= \frac{1}{2}\alpha_1 s \sin 2\theta\\ \frac{d\alpha_2}{dt} &= -\alpha_1 s \sin\theta\cos\theta &&= -\frac{1}{2}\alpha_2 s \sin 2\theta\\ \frac{d\alpha_3}{dt} &= 0\end{aligned}\right\} \quad \ldots\ldots [43]$$

For the rate of change of the principal strain directions, Equation [41] gives

$$\frac{d\theta}{dt} = \frac{s}{2}\left(\frac{\alpha_1^2 + \alpha_2^2}{\alpha_1^2 - \alpha_2^2}\cos 2\theta - 1\right) \qquad [44]$$

3 Phenomenological Description of Large-Strain Elasticity With Stress Relaxation

(*a*) *Axiomatic Basis of Description.* The phenomenological description of the stress-strain properties of materials, exhibiting large-strain elasticity with stress relaxation, is developed from the following axiomatic statements:

1 The state of stress is dependent solely upon the state of "elastic" strain.

2 The time rate of change of elastic strain is equal to the time rate of "geometric" strain plus a spontaneous time rate of change which depends only upon the current elastic strain, and corresponds to the relaxation process.

The second statement defines the new concept of elastic strain which the first requires. This axiomatic foundation can be restated at greater length, and in a manner which emphasizes the meanings of the terms elastic and geometric strain.

Geometric strain has been treated in Section 2; it specifies the relative movements of the individual particles of a material. The time rates of change of the principal (geometric) strain ratios due to flow of a material are given by Equations [24], and of the principal (geometric) strain directions, for the two-dimensional case, by Equation [41]. Elastic strain is specified in the same terms as geometric strain, but differs in that its time rate of change is equal to the rate of change of geometric strain plus an additional term which describes a spontaneous relaxation of elastic strain. Because of this additional relaxation term, elastic strain does not specify relative movements of the individual particles of a material, though it is related to the history of these movements in a definite way. It is asserted axiomatically that the state of stress in the material is a function only of the elastic strain thus defined, and that the relaxation rate of elastic strain depends only upon the elastic strain itself.

The distinction between geometric strain and elastic strain may be illustrated further by stating how each might, in theory at least, be observed. The state of geometric strain would be observed by marking a number of particles of the material and noting how their relative positions change. The state of elastic strain might be observed by cutting a small cubical element out of a material under flow or stress, and, removing it from its environment, allowing it immediately to assume its natural zero-stress shape. The geometric strain which would have to be imposed to bring the element back to its cubical shape and size when cut would be the elastic strain in the material under the flow or stress condition, or would be closely related to it.[6]

The materials treated will further be assumed to be incompressible, and to have a property of isotropy generalized for the case of large elastic strain. This generalized property of isotropy is defined as follows:

1 When a material is in an elastically unstrained state, its mechanical behavior is identical in all directions in the material.

2 When a material is in an elastically strained state, its mechanical behavior in any direction depends only upon the relation of this direction to the principal strain directions, and upon the principal elastic strains themselves.

It may be noted that the difference between this generalized isotropy and the classical isotropy is that isotropic behavior is not postulated for the superposition of one elastic strain upon another. The analytical difference between large and small strains is of this character; superposition of large strains does not follow a simple addition law, while superposition of small strains does.

A numerical determination of the stress corresponding to any specified deformation process in a material requires mathematical expressions for the spontaneous time rate of change of elastic strain due to the relaxation process, and a mathematical relation between the state of elastic strain and the state of stress. The formulation of these mathematical expressions is the principal aim of the theory.

(*b*) *Elastic Strain and Relaxation Relations.* In accordance with the method of specification of large strain developed in Section 2, the state of elastic strain may be specified by the three principal strain ratios α_1, α_2, α_3, and the principal strain direction cosines m_{ij}, or, in the two-dimensional case, the angle θ. Henceforth this notation will be used without alteration to specify elastic strain. Special mention will be made if geometric strain is referred to, and it is different from elastic strain.

The time rate of change of the principal elastic-strain ratios is given by

$$\frac{d\alpha_1}{dt} = \left(\frac{d\alpha_1}{dt}\right)_{\text{geom}} + \left(\frac{d\alpha_1}{dt}\right)_{\text{relax}} \qquad [45]$$

with two similar equations for α_2 and α_3. The terms $(d\alpha_i/dt)_{\text{geom}}$ are the rates of change of the elastic strain corresponding to change of geometric strain; in a flow these terms are given by Equation [24], in which α_i on the right side is the elastic-strain ratio. The terms $(d\alpha_i/dt)_{\text{relax}}$ describe the relaxation property of the material, and, as properties of the material, these terms must be characteristic functions of the elastic-strain state only. As a result of the assumed property of isotropy these terms must be functions only of the principal strain ratios α_1, α_2, α_3, and are designated by R_1, R_2, R_3; thus

$$\left.\begin{aligned} \left(\frac{d\alpha_1}{dt}\right)_{\text{relax}} &= R_1(\alpha_1, \alpha_2, \alpha_3) \\ \left(\frac{d\alpha_2}{dt}\right)_{\text{relax}} &= R_2(\alpha_1, \alpha_2, \alpha_3) \\ \left(\frac{d\alpha_3}{dt}\right)_{\text{relax}} &= R_3(\alpha_1, \alpha_2, \alpha_3) \end{aligned}\right\} \qquad [46]$$

A further consequence of the property of isotropy is that R_1, R_2, R_3 must be obtainable from each other by interchanging the variables α_1, α_2, α_3; thus there is actually only a single relaxation function to be determined.

It is also a consequence of the property of isotropy that the directions of principal elastic strain are not changed by relaxation. Equation [41] is therefore valid for the change of elastic-strain direction in two dimensions provided that α_1 and α_2 on the right-hand side are elastic strains.

A set of geometric-strain ratios which correspond to zero volume change in a material must satisfy the relation

$$\alpha_1 \times \alpha_2 \times \alpha_3 = 1 \qquad [47]$$

The rates of change of geometric strain for incompressible materials must therefore satisfy the relation obtained by setting the time derivative of the left side of Equation [47] to zero

$$\frac{1}{\alpha_1}\left(\frac{d\alpha_1}{dt}\right)_{\text{geom}} + \frac{1}{\alpha_2}\left(\frac{d\alpha_2}{dt}\right)_{\text{geom}} + \frac{1}{\alpha_3}\left(\frac{d\alpha_3}{dt}\right)_{\text{geom}} = 0 \qquad [48]$$

However, there appears to be no fundamental reason that the rates of change of elastic strain, $R_i = (d\alpha_i/dt)_{\text{relax}}$, must also satisfy Relation [48]. If they do not for a particular material, then, even though the material be incompressible, the Relation [47] need not hold for the elastic strain. This is actually the case for the simple molecular representation analyzed in Section 4, and is the reason for the reservation referred to previously.[6]

---

[6] This reservation is made for a reason which will be referred to in the sequel.

(*c*) *Stresses and Strain-Energy Function.* For rapidly applied geometric strain it is evident from Equation [45] that, since the terms $(d\alpha_i/dt)_{\text{relax}} = R_i$ are functions of α_1, α_2, α_3, the relative effect of relaxation upon the elastic strain becomes small, and the resulting elastic strain is nearly equal to the applied geometric strain. In the limit of very rapidly applied geometric strain the elastic and geometric strains become identical. This fact has important theoretical consequences.

Together with the axiomatic assumption that the stress depends only upon elastic strain the possibility of coincidence of elastic and geometric strain establishes the existence of a strain-energy function ψ. This function is equal to the recoverable strain energy per unit volume stored up as a result of the action of the elastic stresses. As a result of the assumed property of isotropy, ψ depends only upon the principal elastic-strain ratios in such a way that its values are unaltered by any interchange of α_1, α_2, α_3.

A further result of the possibility of coincidence of elastic and geometric strain is that the principle of virtual work can be used to obtain expressions for the stresses in terms of elastic strain from the strain-energy function. In such application of the principle of virtual work, elastic-strain increments are treated as geometric-strain increments.

It may be recalled that any stress condition at a point is equivalent to three principal tension (or compression) stresses, to be denoted by σ_1, σ_2, σ_3, acting across planes normal to the three principal stress directions. It is a consequence of the property of isotropy that the principal elastic-strain directions and the principal stress directions coincide. The zero stress condition $\sigma_1 = \sigma_2 = \sigma_3 = 0$ will be associated with the elastically unstrained condition $\alpha_1 = \alpha_2 = \alpha_3 = 1$.

The relation between stresses and strains can be derived from the strain-energy function by considering the virtual work done on an elemental volume of material during a small virtual deformation specified by elastic strain changes $\delta\alpha_1$, $\delta\alpha_2$, $\delta\alpha_3$. As remarked before, elastic-strain changes can be identified with geometric-strain changes for the purpose of applying the principle of virtual work.

Consider an element of material in the shape of a rectangular parallelepiped with sides normal to the principal strain directions. The lengths of the sides of the parallelepiped must remain proportional to the elastic-strain ratios in any virtual deformation, and can therefore be represented by $\alpha_1 L_1$, $\alpha_2 L_2$, $\alpha_3 L_3$, where L_1, L_2, L_3 are constant lengths.

On the assumption of isotropy, as defined previously, the stress condition is one with principal stresses σ_1, σ_2, σ_3 acting on the faces of the parallelepiped, which have been placed normal to the principal strain directions. The force on each face of the parallelepiped, therefore, acts normal to the face. The magnitudes of these forces, designated by F_1, F_2, F_3, are equal to the products of the stresses and areas of the respective sides, and are

$$\left.\begin{aligned} F_1 &= \alpha_2\alpha_3 L_2 L_3 \sigma_1 \\ F_2 &= \alpha_1\alpha_3 L_1 L_3 \sigma_2 \\ F_3 &= \alpha_1\alpha_2 L_1 L_2 \sigma_3 \end{aligned}\right\} \qquad [49]$$

The parallelepiped and these forces are indicated in the diagram of Fig. 2. The work per unit volume δW done by the forces F_1, F_2, F_3 during a virtual displacement corresponding to elastic- (and geometric-) strain changes $\delta\alpha_1$, $\delta\alpha_2$, $\delta\alpha_3$ is

$$\delta W = \frac{F_1 L_1 \delta\alpha_1 + F_2 L_2 \delta\alpha_2 + F_3 L_3 \delta\alpha_3}{\alpha_1\alpha_2\alpha_3 L_1 L_2 L_3} = \frac{\sigma_1 \delta\alpha_1}{\alpha_1} + \frac{\sigma_2 \delta\alpha_2}{\alpha_2} + \frac{\sigma_3 \delta\alpha_3}{\alpha_3} \qquad [50]$$

The second form of this expression follows from the first by virtue of Equations [49]. This work is equal to the change $\delta\psi$ in the value of the strain-energy function corresponding to the elastic-strain changes $\delta\alpha_1$, $\delta\alpha_2$, $\delta\alpha_3$. Thus

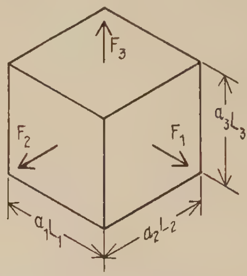

FIG. 2 FORCES ON AN ELEMENT OF VOLUME

$$\delta W = \delta\psi = \frac{\partial\psi}{\partial\alpha_1}\,\delta\alpha_1 + \frac{\partial\psi}{\partial\alpha_2}\,\delta\alpha_2 + \frac{\partial\psi}{\partial\alpha_3}\,\delta\alpha_3 \qquad [51]$$

Both Equations [50] and [51] are valid for any arbitrary values of $\delta\alpha_1$, $\delta\alpha_2$, $\delta\alpha_3$; accordingly, the coefficients of each corresponding differential in the two expressions must be equal. Thus the required stress-strain relations are

$$\left.\begin{aligned} \sigma_1 &= \alpha_1 \frac{\partial\psi}{\partial\alpha_1} \\ \sigma_2 &= \alpha_2 \frac{\sigma\psi}{\partial\alpha_2} \\ \sigma_3 &= \alpha_3 \frac{\sigma\psi}{\sigma\alpha_3} \end{aligned}\right\} \qquad [52]$$

In the case of an incompressible material the virtual displacements must be restricted to those which correspond to no volume change, that is, to those for which

$$\frac{\delta\alpha_1}{\alpha_1} + \frac{\delta\alpha_2}{\alpha_2} + \frac{\delta\alpha_3}{\alpha_3} = 0 \qquad [53]$$

It may be noted that in this case a hydrostatic pressure (tension) component

$$\sigma_1 = \sigma_2 = \sigma_3 = p$$

will not cause any virtual work by Equation [50] and correspondingly, may exist independent of the virtual-work expressions, Equation [53]. For incompressible materials the stress-strain relation which replaces Equations [52] is

$$\left.\begin{aligned} \sigma_1 &= \alpha_1 \frac{\partial\psi}{\partial\alpha_1} + p \\ \sigma_2 &= \alpha_2 \frac{\partial\psi}{\partial\alpha_2} + p \\ \sigma_3 &= \alpha_3 \frac{\partial\psi}{\partial\alpha_3} + p \end{aligned}\right\} \qquad [54]$$

where p is an arbitrary hydrostatic tension which must be determined by external circumstances.

(*d*) *Recapitulation.* A quantitative and mathematical description of the stress-strain behavior of a material exhibiting large-strain elasticity and stress relaxation has been developed from a purely phenomenological viewpoint on the basis of two fundamental and axiomatic assumptions. The materials have further been assumed to be incompressible, and to possess a generalized property of isotropy.

The description is made in terms of a strain-energy function ψ, and relaxation functions R_1, R_2, and R_3; each of these functions is a characteristic function of the principal elastic strains α_1, α_2, α_3. The description is quantitatively complete when the values of these functions are known. It may be remarked that, as a result of the assumed isotropy, when any one of R_1, R_2, or R_3 is given, the others follow by interchange of the arguments α_1, α_2, α_3; thus there are in reality only two independent functions to be determined, ψ and (say) R_1.

If applications are limited to the case of infinitesimal strains, that is, α_1, α_2, α_3, differing only by infinitesimals from unity, then the functions ψ and R might be replaced by the first terms of their Taylor series expansions about the point $\alpha_1 = \alpha_2 = \alpha_3 = 1$. This approximation leads to the classical Maxwell liquid theory.

However, when large deformations occur the behavior becomes more complex, and the abbreviated Taylor expansions are not adequate. It is necessary to use the complete functions or something closely resembling them. The functions ψ and R are properties of a material, and express the characteristics of internal structure which govern stress-strain behavior. They must be derived, therefore, either from a consideration of the internal structure of the materials or from rather extensive empirical observations or both.

4 A MOLECULAR REPRESENTATION OF MATERIALS EXHIBITING LARGE-STRAIN ELASTICITY AND RELAXATION

(*a*) *Purpose of Molecular Representation.* Plausible forms for the strain-energy and relaxation relations are to be obtained from an analysis of the behavior of a mechanical representation of the molecular structure of rubberlike materials. The large deformation elasticity, which is characteristic of rubberlike materials, is attributed to the bulk properties of highly elongated chainlike molecules of which these materials generally consist. The molecular representation proposed here is based upon the general descriptions given by several authors[7] of these molecules.

This molecular representation is introduced primarily to illustrate the structural significance of the phenomenological concepts of elastic strain and relaxation which have been introduced in the preceding section. Detailed characteristics are not expected to be quantitatively realistic, but have been chosen to a large extent to lead to simple and exact mathematical solutions for mechanical behavior. However, the analysis of this model from an internal structural point of view does implement the phenomenological description already given, and the resulting forms for the strain-energy and relaxation functions serve as starting points for the interpretation of empirical observations, and can eventually be refined therefrom.

(*b*) *Description of Molecular Representation.* The molecular structure of the materials is represented by a matrix composed of a great number of structurally identical, highly elongated, chainlike molecules which behave in bulk as though they were embedded in an incompressible liquidlike medium. Each of the molecules assumes a more or less twisted and folded configuration, and is intertwined with numerous neighboring molecules. The whole assembly of molecules is in a state of continuous thermal agitation as a result of which the individual molecules have a certain mobility or freedom of movement. This mobility is, however, also restrained in some degree by the interlaced configuration of the molecules.

Although, for purposes of visualization, the concept of a surrounding liquidlike medium in which the elongated molecules are embedded will be retained, the actual existence of a physical medium is not necessarily implied. The use of the concept may be considered merely as a graphic description of certain bulk properties of the matrix of intertwined molecules. The specific properties attributed to this surrounding "medium" are incompressibility and lack of resistance to change of shape.

It is assumed that at any particular instant the thermal motion of each individual molecule can be considered as a vibration about a defined position of equilibrium. The only effect of the thermal motions upon macroscopic mechanical properties is considered to be their statistical effect upon the mobility of the equilibrium positions of the molecules. All effects of the equilibrium configurations of the molecules are assumed to be represented by the lengths r between the two end points of each one, and by the directions of these lengths. The assumed form of this representation is as follows: The internal force within any molecule as well as its force interaction with its surroundings is equivalent to a simple tension force f tending to draw its end points together. The force f is proportional to the length r, thus

$$f = Kr \qquad [55]$$

where K is a characteristic proportionality constant or stiffness with the dimensions (force)÷(length). The total effect of each molecular configuration upon the potential energy of the material is just the internal molecular potential energy of the force, Equation [55]. Thus the total potential energy of the material arising from molecular configurations is the sum of the contributions dW of each individual molecule

$$dW = \int f x dr = \frac{1}{2} Kr^2 \qquad [56]$$

In any process involving only mechanical deformation the potential energy can be identified with the strain energy. Thus in such processes the sum of the contributions, Equation [56], for all molecules within a small volume of the material divided by the volume gives the value of the strain-energy function ψ for the material within the volume.

When the material is deformed, the equilibrium configurations of the molecules are assumed to change in accordance with the deformation as though their end points floated freely with the corresponding motion of the surrounding liquidlike medium. The molecular configuration may also change spontaneously with time under the sustained action of the forces, Equation [55], and also as a result of the random thermal agitation. The balance of these changes of molecular configuration, which give rise to the bulk properties of the material, are treated by the methods of statistical mechanics.

(*c*) *Statistical Mechanics of Molecular Representation.* The properties and macroscopic state of a material depend only upon certain statistical averages of the parameters which describe the detailed configurations of the individual molecules. In the case of the molecular representation now being considered these statistical averages involve only the magnitudes and directions of the effective molecular lengths, which have been designated by the symbol r.

For purposes of description it is convenient to think of these lengths and directions as being represented by vectors extending out from the origin of co-ordinates in a "phase space." The directions and lengths of the molecules are thus represented by the same vectors in the phase space as they would be represented by in their actual physical positions; in the phase space, however, these vectors all issue out from the origin of co-ordinates. Cartesian co-ordinates in the phase space are designated by x, y, z. The molecular length vectors are, accordingly, represented by the points in the phase space at the outer ends of the vectors, or by the x, y, z-co-ordinates of these points. Thus in phase space

---

[7] See, for example: J. Frenkel, Kinetic Theory of Liquids, Oxford, England, 1946, especially Chapter 8.

$$r^2 = x^2 + y^2 + z^2 \quad [57]$$

A statistical description is required of the configurations of the molecules within an element of volume of the material which is small enough that the macroscopic state, i.e., the stress, strain and temperature, may be considered constant throughout, but which is large enough to contain a very great number of molecules. In the phase space the end points of the vectors representing the individual molecular configurations will form a "cloud," the density of which describes the distribution of configurations over the various possibilities. Quantitative description of this cloud of points in the phase space is afforded by a "distribution function" ρ, which is a function of the phase-space co-ordinates x, y, z, with values such that the fraction of the molecules which have phase-space configuration vectors in the range

$$\left.\begin{array}{l} x_0 < x < x_0 + \Delta x \\ y_0 < y < y_0 + \Delta y \\ z_0 < z < z_0 + \Delta z \end{array}\right\} \quad [58]$$

is given by

$$\rho(x_0, y_0, z_0)\,\Delta x\,\Delta y\,\Delta z \quad [59]$$

The magnitudes of the increments Δx, Δy, Δz in Expressions [58] and [59] are understood to be large enough to include a representative number of vector end points, yet small enough that ρ is sensibly constant over the range of Expression [58]. Because of the immense number of molecules in even a very small macroscopic element of material, this requirement should not cause any theoretical difficulties.

An immediate consequence of the definition of the distribution function ρ is that it must at all times satisfy the relation

$$\int_{-\infty}^{\infty}\int_{-\infty}^{\infty}\int_{-\infty}^{\infty} \rho\, dx\, dy\, dz = 1 \quad [60]$$

It must also be remarked that, since the statistics of the molecular configurations may change with time, ρ must also be considered a function of time t as well as the phase-space co-ordinates x, y, z.

Let N denote the number of molecules per unit volume of the material; this number is a constant for any particular incompressible material. On the basis of the assumptions which have been made the value of the strain-energy function is, from Equations [56] and [57]

$$\psi = \frac{NK}{2}\int_{-\infty}^{\infty}\int_{-\infty}^{\infty}\int_{-\infty}^{\infty} (x^2 + y^2 + z^2)\rho\, dx\, dy\, dz \quad [61]$$

The conditions which govern the variation of the distribution function ρ are now to be set up. Thermal agitation itself causes a random change in the directions and magnitudes of the effective molecular lengths, that is, in their x, y, z-phase space components. The over-all thermal-agitation effect on the distribution function is, therefore, represented by the diffusion equation

$$\left(\frac{\partial\rho}{\partial t}\right)_{\text{thermal agitation}} = D\left(\frac{\partial^2\rho}{\partial x^2} + \frac{\partial^2\rho}{\partial y^2} + \frac{\partial^2\rho}{\partial x^2}\right) \quad [62]$$

in which the constant D is a "diffusion coefficient," and measures the balance between thermal-agitation forces and molecular-restraint forces due to intertwining of the molecules. The physical dimensions of D are (length)^2 ÷ (time). For purposes of this simplified theory D is considered a constant.

The effect of the internal molecular tension force, Equation [55], acting against the restraint of the molecules due to intertwining, may be represented in the phase space by a central attracting force acting upon the cloud of vector points against a viscous resistance to movement. The central force will cause an inward radial drift of the vector end points with a velocity v_r proportional to the force; thus

$$v_r = -\mu f = -\mu K r = -\mu K\sqrt{x^2 + y^2 + z^2} \quad [63]$$

The coefficient μ in this equation has the dimensions (length) ÷ (force × time), and is considered constant. The effect of this drift velocity in the phase space upon the distribution function is as follows

$$\left(\frac{\partial\rho}{\partial t}\right)_{\text{molecular force}} = -\frac{1}{r^2}\frac{\partial}{\partial r}\{\rho r^2 v_r\} = \frac{\mu K}{r^2}\frac{\partial}{\partial r}\{\rho r^3\}$$
$$= \mu K\left(r\frac{\partial\rho}{\partial r} + 3\rho\right) = \mu K\left(x\frac{\partial\rho}{\partial x} + y\frac{\partial\rho}{\partial y} + z\frac{\partial\rho}{\partial z} + 3\rho\right) \quad [64]$$

Combination of Equations [62] and [64] by the principle of direct superposition yields the following differential equation for the distribution function ρ, which holds in the absence of motion due to externally applied deformations

$$\frac{\partial\rho}{\partial t} = D\left(\frac{\partial^2\rho}{\partial x^2} + \frac{\partial^2\rho}{\partial y^2} + \frac{\partial^2\rho}{\partial z^2}\right) + \mu K\left(x\frac{\partial\rho}{\partial y} + y\frac{\partial\rho}{\partial y} + z\frac{\partial\rho}{\partial z} + 3\rho\right) \quad [65]$$

The constants D and μK of this equation are molecular constants in terms of which the bulk properties eventually will be expressed. For the present purposes they may be considered merely as constants of the material which might be evaluated from experimental observation.

The equilibrium distribution function ρ_0, for which $\partial\rho_0/\partial t = 0$, is the solution of the equation formed from Equation [65] by setting the time derivative $\partial\rho/\partial t$ equal to zero. Thus the equation for ρ_0 is

$$D\left(\frac{\partial^2\rho_0}{\partial x^2} + \frac{\partial^2\rho_0}{\partial y^2} + \frac{\partial^2\rho_0}{\partial z^2}\right) + \mu K\left(x\frac{\partial\rho_0}{\partial y} + y\frac{\partial\rho_0}{\partial y} + z\frac{\partial\rho_0}{\partial z} + 3\rho_0\right) = 0 \quad [66]$$

The solution of Equation [66], which also satisfies condition [60], which may be verified by substitution into these relations, is

$$\rho_0 = \frac{e^{-(x^2+y^2+z^2)/r_0^2}}{(r_0\sqrt{\pi})^3} \quad [67]$$

where

$$r_0^2 = \frac{2D}{\mu K} \quad [68]$$

is a fixed reference value of the effective molecular length r.

The distribution function ρ_0 of Equation [67] represents the material in a condition of statistical equilibrium. This function is directionally symmetrical so that the cumulative effect of the molecular forces, Equation [55], must be hydrostatic tension which can be balanced by the action of the surrounding liquid-like medium. Except for an arbitrary hydrostatic pressure p (see Equations [54]), which can have no effect on strain energy because of the assumed incompressibility of the material, the equilibrium distribution function corresponds to the zero stress condition, which is also the condition of no elastic strain

$$\alpha_1 = \alpha_2 = \alpha_3 = 1$$

A structural representation of elastic strain can be described by means of the distribution function ρ. Consider a body having initially the equilibrium distribution function ρ_0 to be deformed rapidly enough that relaxation effects during the deformation may be neglected. Without loss of generality this deformation can be considered to correspond with a strain having principal strain directions along the co-ordinate axes x, y, z of phase space. The strain imposed is arbitrary, except that it must conform to the condition of incompressibility

$$\alpha_1 \times \alpha_2 \times \alpha_3 = 1 \ldots\ldots\ldots\ldots\ldots\ldots [69]$$

During deformation the end points of the molecules are assumed, as stated before, to follow freely the movement of the surrounding medium. Thus a molecule which had an effective length vector specified by the phase-space co-ordinates x_1, y_1, z_1 before the deformation, would have the co-ordinates x_1', y_1', z_1' after the deformation, where

$$\left.\begin{aligned} x_1' &= \alpha_1 x_1 \\ y_1' &= \alpha_2 y_1 \\ z_1' &= \alpha_3 z_1 \end{aligned}\right\} \ldots\ldots\ldots\ldots\ldots\ldots [70]$$

The distribution function immediately after the deformation is obtained by substituting according to Equations [70] the values (x'/α_1), (y'/α_2), (z'/α_3) for x, y, z in Equation [67]. After this substitution is made, interest is restricted to the transformed phase-space co-ordinates x', y', z'; therefore the primes may be dropped from the notation without confusion. The distribution function immediately after the deformation is, accordingly

$$\rho = \frac{1}{\alpha_1\alpha_2\alpha_3 r_0{}^3 \pi^{3/2}} \times e^{-[(x/\alpha_1)^2 + (y/\alpha_2)^2 \div (z/\alpha_3)^2] \div r_0{}^2} \ldots [71]$$

The factor $\alpha_1\alpha_2\alpha_3$ has been inserted into Equation [71] in order to satisfy formally the Condition [60]; this factor is, by Equation [69], equal to unity and so does not change the values of ρ in Equation [71].

(*d*) *Determination of Relaxation and Strain-Energy Functions.* Relaxation effects can now be examined by considering the material to be held by external forces in a deformed state, represented initially by the distribution function, Equation [71], and the principal strain ratios α_1, α_2, α_3. The nonequilibrium Equation [65] for the distribution function is to be applied starting at $t = 0$ with the distribution function, Equation [71]

It may be verified by substitution of Equation [71] into Equation [65] that the solution for ρ under these conditions is a distribution function of the same form as Equation [71], but with α_1, α_2, α_3 functions of time governed by the following differential relations

$$\left.\begin{aligned} \left(\frac{d\alpha_1}{dt}\right)_{\text{relax}} &= R_1 = -\frac{1}{2T}\left(\alpha_1 - \frac{1}{\alpha_1}\right) \\ \left(\frac{d\alpha_2}{dt}\right)_{\text{relax}} &= R_2 = -\frac{1}{2T}\left(\alpha_2 - \frac{1}{\alpha_2}\right) \\ \left(\frac{d\alpha_3}{dt}\right)_{\text{relax}} &= R_3 = -\frac{1}{2T}\left(\alpha_3 - \frac{1}{\alpha_3}\right) \end{aligned}\right\} \ldots\ldots [72]$$

where $T = 1/(2\mu K)$ has the dimension time, and is of the nature of the "relaxation" time of the classical Maxwell liquid.

It can be seen, therefore, that the general solution for the distribution function ρ under any history of external deformation is an expression of the form, Equation [71], where the variables α_1, α_2, α_3 change with applied deformations in the same way that geometric strain does, and in addition have spontaneous time rates of change, or relaxation, given by Equations [72]. The variation of α_1, α_2, α_3 is thus governed by conditions of the type specified by Equations [45].

Substitution of the general distribution function, Equation [71], into Equation [61] gives for the strain-energy function ψ, the expression[8]

$$\psi = \frac{G}{2}\,(\alpha_1{}^2 + \alpha_2{}^2 + \alpha_3{}^2) \ldots\ldots\ldots\ldots [73]$$

where $G = 1/2(NKr_0{}^2)$, and has the dimensions (force) ÷ (length)^2 of a modulus of elasticity; it corresponds to the shear modulus of the classical Maxwell liquid. Thus since the strain-energy function has the arguments α_1, α_2, α_3, and these variables are governed by relations of the form, Equation [45], it is clear that these variables are the structural representations of elastic strain.

5 Application of the Theory to Flows in Channels and Tubes

(*a*) *Remarks on Applications.* Although the general stress-strain behavior of materials exhibiting large strain elasticity with relaxation is specified when the strain-energy and relaxation functions are known, the application of this specification to determine flows of materials under particular conditions is in itself a difficult task. The general problem is one of extreme complexity so that reliance must be placed on special techniques developed for specific problems.

As an illustration of the special techniques which may be employed, solutions are presented here for the important cases of steady-state flows in long uniform channels of infinite width, and in long straight circular tubes. These solutions are based on the observation that in steady-state flows in long tubes or channels, all particles of the material move in straight lines parallel with the tube or channel walls; the flow velocity does not vary in the direction of flow, but varies only in a direction normal to the flow. Consequently, the flow environment of each particle of the material is a steady-state simple shear parallel with the walls. The elastic strain of an element in a steady-state simple shear flow approaches a limiting steady value which is determined by equating to zero the net change of elastic strain, which is the sum of the changes due to change of geometric strain in the flow and that due to the relaxation process. This limiting steady elastic strain will prevail in the flows within long tubes and channels.

Thus, in these cases, the stresses can be determined directly in terms of the shearing rate. The flows themselves can be determined from the shearing-rate distributions which satisfy the stress-equilibrium conditions.

The course of these analyses is first indicated for general strain-energy and relaxation functions, and then illustrated by numerical examples using the following forms for strain-energy function ψ, and relaxation functions R_i

$$\left.\begin{aligned} \psi &= \frac{2G}{n^2}\,(\alpha_1{}^n + \alpha_2{}^n + \alpha_3{}^n) \\ R_i &= -\frac{\alpha_i}{nT}\,(1 - \alpha_i{}^{-n}) \end{aligned}\right\} \ldots\ldots\ldots\ldots [74]$$

where n is a dimensionless constant. These are generalized

---

[8] The indicated integrations of Equation [61] are carried out with the help of the known definite integrals

$$\int_{-\infty}^{\infty} e^{-(x/a)^2}\,dx = a\sqrt{\pi}\,; \quad \int_{-\infty}^{\infty} x^2 e^{-(x/a)^2}\,dx = a^3\sqrt{\pi}/2\,.$$

forms of the functions derived in the previous section which appear to fit data of the author[2] rather well with values of n in the range 1.1 to 1.5. For $n = 2$ these functions coincide with those of Equations [72] and [73]. The constants G and T have the same dimensions of an elastic modulus or stress and time, respectively, as those of Equations [72] and [73], and also have the same significance. For infinitesimal strain the Functions [74] for any value of n describe a classical Maxwell liquid; these functions were set up so that G and T will have their classical significance for each value of n. It may be noted that the behaviors specified by Equations [74] at infinitesimal strains are independent of the value of n.

The forms of Equations [74] were suggested in the course of a rather extensive study of the previous data.[2] Though these forms do fit the data of that reference within the experimental error, the data give relatively little information on the relaxation process because relaxation was a comparatively small factor in determining the stress at the rapid extension rates of those tests. The factor α_i in the relaxation functions R_i of Equations [74], which governs the relaxation rate at large extension ratios, was broadly verified by these tests; however, the tests give virtually no information on the factor $(1 - \alpha_i^{-n})$, which governs the relaxation rates for low stresses.

The strain-energy and relaxation functions, Equations [74], are presented, therefore, not as wholly realistic forms, but as the best information available at present upon which to base numerical examples.

Presentation of the analysis of the data which led to these forms will be postponed until the data from further tests, which will give information on the relaxation at low stresses, are available.

(*b*) *Elastic Strain and Stresses in Steady-State Simple Shear Flow.* Consider a two-dimensional flow referred to plane Cartesian co-ordinates x_1 and x_2, in which the direction of flow at every point is parallel to the x_1-axis, and the velocity of flow is independent of time and of the x_1-co-ordinate. Each particle of the material travels along a straight line parallel to the x_1-axis, and is subject to a continuous simple shear deformation at an unvarying rate specified by $s = (dv_1)/(dx_2)$. The geometrical strain relationships for this case have been analyzed in Section 2 to which reference is made.

Expressions for the rates of change of elastic strain and of the angle of the principal elastic strain directions due only to the geometric flow are given by Equations [43] and [44]. The net changes of these quantities when relaxation effects are included are, following relations, Equations [45] and [46]

$$\left.\begin{aligned}\frac{d\alpha_1}{dt} &= \frac{1}{2}\, s\alpha_1 \sin 2\theta + R_1\\ \frac{d\alpha_2}{dt} &= -\frac{1}{2}\, s\alpha_2 \sin 2\theta + R_2\\ \frac{d\alpha_3}{dt} &= R_3\\ \frac{d\theta}{dt} &= \frac{s}{2}\left[\frac{\alpha_1^2 + \alpha_2^2}{\alpha_1^2 - \alpha_2^2} \times \cos 2\theta - 1\right]\end{aligned}\right\} \quad \ldots\ldots [75]$$

As just described, in the parallel flows being considered, each element of the material is subject to a steady-state shearing rate s. The values of α_1, α_2, α_3, and θ will, therefore, adjust themselves in a period of time to the steady-state condition

$$\frac{d\alpha_1}{dt} = \frac{d\alpha_2}{dt} = \frac{d\alpha_3}{dt} = \frac{d\theta}{dt} = 0 \quad \ldots\ldots\ldots\ldots [76]$$

which, with Equations [75] yield four equations to determine the four quantities which specify the elastic strain as functions of shearing rate s.

The principal stresses σ_1, σ_2, and σ_3 are then given, for the incompressible case, by Equations [54]. The principal stress σ_3 acts in the direction normal to the plane of flow, while σ_1 and σ_2 act at an angle θ to the x_1- and x_2-axes, respectively, or along the z_1- and z_2-axes in Fig. 1. The in-plane direct stresses σ_{11} and σ_{22} acting normal, respectively, to the x_1- and x_2-axes, and the shear stress τ acting on each of these planes are given by

$$\left.\begin{aligned}\sigma_{11} &= \frac{1}{2}(\sigma_1 + \sigma_2) + \frac{1}{2}(\sigma_1 - \sigma_2)\cos 2\theta\\ \sigma_{22} &= \frac{1}{2}(\sigma_1 + \sigma_2) - \frac{1}{2}(\sigma_1 - \sigma_2)\cos 2\theta\\ \tau &= \frac{1}{2}(\sigma_1 - \sigma_2)\sin 2\theta\end{aligned}\right\} \quad \ldots\ldots [77]$$

The positions and directions of these stresses are shown in Fig. 4.

A principal result of this analysis can be represented by an "apparent viscosity for simple shear" η_s, which is defined by

$$\eta_s = \tau/s \quad \ldots\ldots\ldots\ldots\ldots\ldots\ldots\ldots [78]$$

Since the shear stress τ is a function of s, this apparent viscosity is also a function of s. The apparent viscosity thus defined has the same dimensions, (force) × (time) ÷ (length)^2, as the coefficient of viscosity of a Newtonian liquid, and has, for the particular flows being considered, a similar significance.

With the forms of Equations [74] for the relaxation functions, the conditions, Equations [76] for steady-state shear may be written

$$\left.\begin{aligned}\alpha_1 &= \left(1 - \frac{nS}{2}\sin 2\theta\right)^{-1/n}\\ \alpha_2 &= \left(1 + \frac{nS}{2}\sin 2\theta\right)^{-1/n}\\ \alpha_3 &= 1\\ \cos 2\theta &= \frac{\alpha_1^2 - \alpha_2^2}{\alpha_1^2 + \alpha_2^2}\end{aligned}\right\} \quad \ldots\ldots\ldots\ldots [79]$$

into which the dimensionless measure of shearing rate $S = sT$ has been introduced.

The relations, Equations [79], can be solved explicitly for a series of values of the dimensionless shearing rate S by assigning a set of values to the quantity $(nS/2)\sin 2\theta$. Then α_1 and α_2 are determined explicitly for the first two of Equations [79], and θ by the last. The results of computations of this kind, and the subsequent determination of stresses and apparent viscosity are presented in Table 1, for $n = 5/4$ and $3/2$. The apparent viscosities are shown plotted as functions of the dimensionless shearing rate S in Fig. 3.

The case $n = 2$ allows a very simple analytical solution for the stresses. In this case the first two of Equations [79] may be written

$$\alpha_1^2 = \frac{1}{1 - S\sin 2\theta}; \quad \alpha_2^2 = \frac{1}{1 + S\sin 2\theta} \quad \ldots\ldots [80]$$

When these expressions are substituted into the last of Equations [79], the results are

$$\cos 2\theta = S\sin 2\theta; \quad \text{or} \quad \cot 2\theta = S \quad \ldots\ldots\ldots [81]$$

The principal stresses, from Equations [54], are

$$\left.\begin{aligned} \sigma_1 &= G\alpha_1^2 + p = \frac{G}{1 - \cos 2\theta} + p \\ \sigma_2 &= G\alpha_2^2 + p = \frac{G}{1 + \cos 2\theta} + p \\ \sigma_3 &= p \end{aligned}\right\} \quad \ldots\ldots\ldots [82]$$

The in-plane stresses on the co-ordinate planes, from Equations [74] are

$$\sigma_{11} - \sigma_{22} = 2GS^2; \quad \tau = GS \ldots\ldots\ldots\ldots [83]$$

The apparent viscosity defined by Equation [78] is, in this special case, independent of shearing rate, and is equal to GT; this result is in accord with the Maxwell liquid behavior.

(*c*) *Flow in Long Channels of Infinite Width.* In a typical steady-state flow at some distance from the entrance or exit of a long channel with parallel walls and of infinite width, all particles of the flowing material move in parallel straight lines which are also parallel with the walls. The flow is symmetrical with respect to a plane parallel to and lying midway between the channel walls. Since each element of the material is deformed in simple shear, acting parallel with the channel walls and in the direction of flow, the steady-state stress condition is given in terms of shearing rate by the analysis of the preceding subsection. The results of that analysis can be used in conjunction with the stress equilibrium conditions to determine the velocity and stress distributions in such channel flows.

Let Cartesian co-ordinates x_1, x_2, x_3 be set up in a channel with the x_1-axis lying in the mid-plane in the direction of flow, the x_3-axis in the mid-plane at right angles to the flow, and the x_2-axis normal to the channel walls. Let the distance between the channel walls be designated by $2h$. The stresses in the plane of flow on a typical element of the material are those given by Equation [77], and are indicated in Fig. 4 which also shows the co-ordinate system and channel.

The equations of equilibrium for the stresses in the plane of flow indicated in Fig. 4 are

$$\left.\begin{aligned} \frac{\partial \sigma_{11}}{\partial x_1} + \frac{\partial \tau}{\partial x_2} &= 0 \\ \frac{\partial \sigma_{22}}{\partial x_2} + \frac{\partial \tau}{\partial x_1} &= 0 \end{aligned}\right\} \quad \ldots\ldots\ldots\ldots\ldots\ldots [84]$$

According to Equations [54], the principal stresses for an incompressible material may be considered to consist of two parts: the hydrostatic tension p which is independent of the elastic

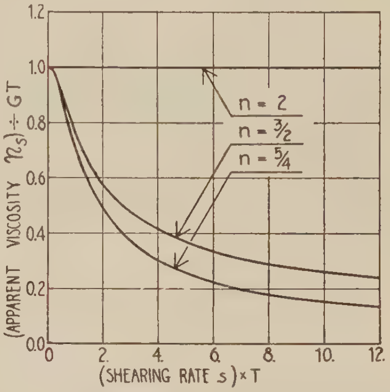

FIG. 3 APPARENT VISCOSITY FOR SIMPLE SHEAR VERSUS SHEARING RATE

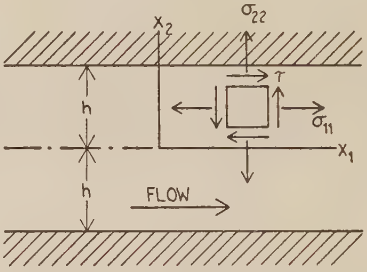

FIG. 4 CO-ORDINATES AND STRESSES ON TYPICAL ELEMENT FOR FLOW IN CHANNEL

TABLE 1 STRESSES AND ELASTIC STRAINS FOR STEADY-STATE SIMPLE SHEAR FLOW FOR THE STRAIN ENERGY AND RELAXATION FUNCTIONS OF EQUATION [74]

$S = sT = T(dv)/(dx)$

S	$\theta°$	α_1	α_2	$\frac{\sigma_{11} - \sigma_{22}}{G}$	$\frac{\tau}{G}$	$\frac{\eta_s}{GT}$
0.0	45.0	1.00	1.00	0.0	0.0	1.000
0.337	35.9	1.20	0.864	0.21	0.317	0.949
0.793	26.9	1.51	0.764	0.90	0.615	0.776
1.613	18.5	2.08	0.687	2.41	0.893	0.553
2.383	14.0	2.62	0.654	3.88	1.032	0.433
2.972	11.9	3.03	0.639	5.02	1.107	0.373
3.822	9.7	3.62	0.625	6.70	1.191	0.312
5.165	7.6	4.56	0.612	9.46	1.291	0.250
7.660	5.4	6.31	0.598	14.89	1.452	0.186
9.413	4.5	7.54	0.593	18.93	1.499	0.159
12.164	3.6	9.48	0.589	25.64	1.598	0.131
17.313	2.5	13.13	0.584	39.03	1.738	0.100
30.982	1.5	22.87	0.579	79.09	2.004	0.065
∞	$45.8 \div S$	$0.718S$	0.574	$1.057 \times S^{5/4}$	$0.845 \times S^{1/4}$	$0.846 \div S^{3/4}$
			$n = 3/2$			
0.0	45.0	1.00	1.00	0.0	0.0	1.000
0.277	37.4	1.16	0.886	0.15	0.268	0.969
0.621	29.6	1.41	0.799	0.65	0.546	0.879
1.166	21.7	1.84	0.732	1.82	0.858	0.735
1.630	17.5	2.23	0.702	3.00	1.048	0.643
1.966	15.3	2.52	0.689	3.94	1.162	0.591
2.431	13.0	2.92	0.676	5.32	1.300	0.535
3.131	10.6	3.54	0.664	7.61	1.478	0.472
4.357	8.0	4.64	0.652	12.14	1.740	0.399
5.177	6.9	5.39	0.647	15.52	1.892	0.366
6.422	5.6	6.53	0.643	21.12	2.101	0.327
8.617	4.3	8.55	0.639	32.29	2.425	0.281
14.012	2.7	13.57	0.634	65.71	3.077	0.220
22.516	1.7	21.55	0.632	132.44	3.889	0.173
∞	$38.2 \div S$	$0.840\ S$	0.631	$1.225 \times S^{3/2}$	$0.817 \times S^{1/2}$	$0.817 \div S^{1/2}$

strain; and the parts $(\alpha_i \partial \psi)/(\partial \alpha_i)$ which depend only upon the elastic strain. It will be convenient to consider the stresses entering Equations [84], which are given in terms of the principal stresses by Equations [77], to be composed of the corresponding two parts; thus

$$\left.\begin{aligned} \sigma_{11} &= (\sigma_{11} - p) + p = f_{11}(x_2) + p \\ \sigma_{22} &= (\sigma_{22} - p) + p = f_{22}(x_2) + p \\ \sigma_3 &= p \\ \tau &= \tau(x_2) \end{aligned}\right\} \dots\dots\dots [85]$$

The stresses $(\sigma_{11} - p)$, $(\sigma_{22} - p)$, and τ depend only upon elastic strain and therefore, in the present flows, must be functions only of the co-ordinate x_2. This dependence is indicated in Equations [85] by introducing the functions f_{11} and f_{22} of x_2 only for $(\sigma_{11} - p)$ and $(\sigma_{22} - p)$, and by writing $\tau = \tau(x_2)$. Since the partial derivatives of f_{11}, f_{22} and τ with respect to x_1 are zero, use of the forms, Equations [85], in the equilibrium relations, Equations [84], reduces the latter to

$$\left.\begin{aligned} \frac{\partial p}{\partial x_1} + \frac{d\tau}{dx_2} &= 0 \\ \frac{\partial p}{\partial x_2} + \frac{df_{22}}{dx_2} &= 0 \end{aligned}\right\} \dots\dots\dots\dots\dots\dots [86]$$

The second of Equations [86] contains only derivatives with respect to x_2, and may be integrated at once to give

$$p = f(x_1) - f_{22}(x_2) \dots\dots\dots\dots\dots\dots [87]$$

where $f(x_1)$ is an as yet undetermined function of x_1 only. Now, since τ and therefore also $(d\tau)/(dx_2)$ are functions of x_2 only, it follows from the first of Equations [86] that $(\partial p)/(\partial x_1)$ must be independent of x_1. It then follows from the form of p in Equation [87] that $(\partial p)/(\partial x_1)$ must be a constant; therefore Equation [87] may be written

$$p = Cx_1 + p_0 - f_{22} \dots\dots\dots\dots\dots\dots [88]$$

where p_0 is a constant of integration. Substitute this result into the first of Equations [86], thus

$$\frac{d\tau}{dx_2} = -C; \quad \text{or} \quad \tau = -Cx_2 \dots\dots\dots\dots [89]$$

Since by symmetry the shear stress on the midplane $x_2 = 0$ must be zero, there is no constant of integration in the expression for τ. Putting these results into the Equations [85], the general solution of the equilibrium equations for flow in a channel is

$$\left.\begin{aligned} \sigma_{11} &= Cx_1 + p_0 + f_{11} - f_{22} \\ \sigma_{22} &= Cx_1 + p_0 \\ \sigma_3 &= Cx_1 + p_0 - f_{22} \\ \tau &= -Cx_2 \end{aligned}\right\} \dots\dots\dots\dots [90]$$

As remarked before, f_{11} and f_{22} depend only upon x_2; thus the constant C is the pressure gradient in the direction of flow.

The analysis of the steady-state shear conditions of the previous subsection has expressed the steady-state shearing rate $s = (dv_1)/(dx_2)$ as a function of the shearing stress τ; therefore, with Equations [90] for the channel flows

$$\frac{dv_1}{dx_1} = s(\tau) = -s(-\tau) = -s(Cx_2) \dots\dots\dots [91]$$

Here $s(\tau) = -s(-\tau)$ follows from the necessary odd character of the shearing rate-shear stress relations. From the values of s the values of elastic strain and the stresses $(\sigma_{11} - p) = f_{11}$ and $(\sigma_{22} - p) = f_{22}$ follow from the steady-state shear analysis.

The velocity distribution over the channel is determined from Equations [91] by the integration

$$v_1 = v_0 + \int_0^{x_2} (dv_1/dx_2)dx_2 = v_0 - \int_0^{x_2} s(Cx_2)dx_2 \dots [92]$$

where the constant of integration v_0 is determined to make $v_1 = 0$ at the channel wall $x_2 = h$. Values of v_1 in the negative range of x_2 follow by symmetry. The volume rate of flow per unit width of the channel, denoted by q, is determined by a second integration

$$q = 2\int_0^h v_1 dx_2 \dots\dots\dots\dots\dots\dots [93]$$

The over-all resistance of a material to flow can be expressed conveniently by analogy to the flow of a Newtonian liquid. For Newtonian liquids the relationship between the volume flow rate q, the pressure gradient C, and the viscosity coefficient η is

$$q = \frac{2h^3C}{3\eta} \dots\dots\dots\dots\dots\dots [94]$$

An "apparent viscosity coefficient for flow in a channel" η_c may be defined in terms of the q given by Equation [93] and h and C by analogy to Equation [94]; thus

$$\eta_c = \frac{2h^3C}{3q} \dots\dots\dots\dots\dots\dots [95]$$

The solution, Equations [90], is perfectly general for all materials of the type considered, and holds in particular for materials of which the behavior is specified by the functions, Equations [74]. For these materials the dimensionless shearing rate $S = sT$ is a function of the dimensionless stress quantity τ/G. It is convenient to write Equations [91] in the following form for these materials

$$\frac{dv_1}{dx_2} = \frac{S(\tau/G)}{T} = -\frac{1}{T} \times S\left(\frac{Cx_2}{G}\right) \dots\dots\dots [96]$$

The integration specified in Equation [92] is written in terms of the dimensionless variables

$$X = \frac{Cx_2}{G};\ H = \frac{Ch}{G} \dots\dots\dots\dots\dots\dots [97]$$

thus

$$v_1 = \frac{G}{CT}\phi(H, X) \dots\dots\dots\dots\dots\dots [98]$$

where

$$\phi(H, X) = \int_0^H SdX - \int_0^X SdX \dots\dots\dots [99]$$

The integral for the volume output rate q may be written

$$q = \frac{2G^2}{C^2T}\Phi = \frac{2h^2}{T} \times \frac{\Phi}{H^2} \dots\dots\dots\dots [100]$$

where

$$\Phi = \int_0^H \phi/(H, X)dX \dots\dots\dots\dots [101]$$

The apparent viscosity coefficient for flow in a channel is, from Equations [95] and [100]

$$\eta_c = GT \times \frac{H^3}{3\Phi} \dots\dots\dots\dots\dots\dots [102]$$

The dimensionless measure of apparent viscosity $\eta_c/(GT)$ is a function of the single variable H, defined by Equations [97].

The dimensionless measure of the volume output rate qT/h^2 is also a function of H by Equation [100]. Therefore, $\eta_c/(GT)$ is a function of qT/h^2, and their relationship characterizes the resistance to flow of these materials.

Numerical computations have been made for the case $n = 5/4$, using the relationship between S and τ/G given in Table 1. The results of these computations are summarized in Table 2, the $\eta_c/(GT)$ versus qT/h^2 plot in Fig. 6, and the velocity-distribution curves in Fig. 5.

Previous data of the author[2] indicate that the constants for polyethylene at 300 F are approximately as follows: $n = 5/4$, $G = 5$ psi, $T = 0.1$ sec, $GT = 0.5$ lb sec/in.^{2} = 34,500 poises. As an example of an application of the numerical computations, the apparent viscosity for flow through a channel of height 0.01 in., and at a volume rate of 0.025 cu. in. per sec per in. width will be found. Thus

$$h = 0.005;\; qT/h^2 = 0.025 \times 0.1/0.000025 = 100$$

$$\eta_c/GT = 0.74(qT/h^2)^{-3/4} = 0.74/31.6 = 0.0234$$

$$\eta_c = 0.0234 \times 34{,}500 = 810 \text{ poises}$$

Values of this general order were found in measurements on the extrusion of polyethylene sheet at the Plax Corporation in June, 1947.

(*d*) *Flow in Long Circular Tubes.* The flow in any radial plane of a circular tube can be referred to x_1, x_2-co-ordinates as in Fig. 4, if x_2 is interpreted as the radial co-ordinate, and h the tube radius. The stress notation of the previous subsection also can be used for the tube flow if σ_{22} is interpreted as radial stress, and σ_3 as circumferential stress. In the case of the circular tube the flow and stresses are symmetrical with respect to the tube axis x_1, and the stress-equilibrium equations are

$$\left.\begin{aligned} \frac{\partial\sigma_{11}}{\partial x_1} + \frac{\partial\tau}{\alpha x_2} + \frac{\tau}{x_2} &= 0 \\ \frac{\partial\sigma_{22}}{\partial x_2} + \frac{\partial\tau}{\partial x_1} + \frac{\sigma_{22} - \sigma_3}{x_2} &= 0 \end{aligned}\right\} \ldots\ldots\ldots\ldots [103]$$

As before, the stresses are represented in the form of Equations [85], and it is again noted that τ, f_{11}, and f_{22}, being functions only of elastic strain, must be dependent only upon the radial co-ordinate x_2. The derivatives of these quantities with respect to x_1 vanish, and the equilibrium Equations [103] may accordingly be written

$$\left.\begin{aligned} \frac{\partial p}{\partial x_1} + \frac{1}{x_2}\frac{d}{dx_2}(x_2\tau) &= 0 \\ \frac{\partial p}{\partial x_2} + \frac{1}{x_2}\frac{d}{dx_2}(x_2 f_{22}) &= 0 \end{aligned}\right\} \ldots\ldots\ldots [104]$$

Integration of the second of these equations with respect to x_2 leads to the following form for p

$$p = f(x_1) - F_{22}(x_2) \ldots\ldots\ldots\ldots\ldots\ldots [105]$$

where $f(x_1)$ is an as yet undetermined function of x_1 only, and F_{22} is given by

$$F_{22} = f_{22} + \int \frac{f_{22}}{x_2}\,dx_2 \ldots\ldots\ldots\ldots [106]$$

and is, accordingly, like f_{22} a function of x_2 only.

It is noted as before that the first equation requires that $(\partial p)/(\partial x_1)$ be independent of x_1, and must, from the form of Equation [105], be a constant C. Thus the general solution of the stress equilibrium equations for the tube can be written

TABLE 2 APPARENT VISCOSITY FOR FLOW IN CHANNELS

H	$\dfrac{qT}{h^2}$	$\dfrac{\eta_c}{(GT)}$
0.0	0.0	1.000
0.25	0.170	0.979
0.5	0.372	0.897
0.75	0.635	0.787
1.0	1.06	0.631
1.25	1.85	0.451
1.5	3.39	0.295
1.75	6.06	0.193
2.0	10.3	0.129
>2	0.65×10^4	$1.03 \div H^3$

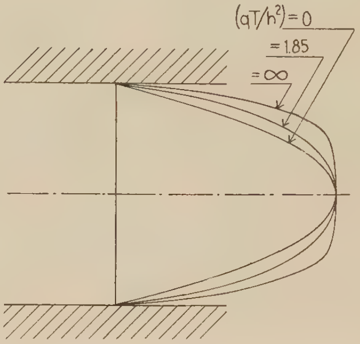

FIG. 5 VELOCITY DISTRIBUTIONS ACROSS CHANNELS

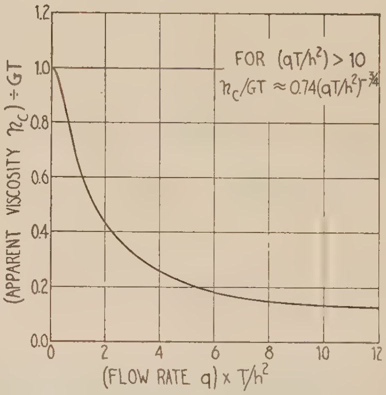

FIG. 6 η_c/GT VERSUS qT/h^2 FOR CHANNELS

$$\left.\begin{aligned} \sigma_{11} &= Cx_1 + p_0 + f_{11} - F_{22} \\ \sigma_{22} &= Cx_1 + p_0 + f_{22} - F_{22} \\ \sigma_3 &= Cx_1 + p_0 - F_{22} \\ \tau &= -Cx_2/2 \end{aligned}\right\} \ldots\ldots\ldots\ldots [107]$$

Again p_0 is a constant of integration, and C represents the pressure gradient in the direction of flow.

The relation for the shearing rate s is

$$\frac{dv_1}{dx_2} = s(\tau) = -s(-\tau) = -s\left(\frac{Cx_2}{2}\right) \ldots\ldots [108]$$

The functions f_{11}, f_{22}, and F_{22} of x_2 in the solution, Equations [107] are determined as before to fit the stress condition, which follows from the elastic strain corresponding to the shearing rate s given by Equation [108]. Equation [92] for the velocity distribution is valid in this case if the argument of s is made $Cx_2/2$. The volume rate of flow through the tube Q is given by

$$Q = 2\pi \int_0^h v_1 x_2\, dx_2 \ldots\ldots\ldots\ldots\ldots [109]$$

It is again convenient to use the analogy to the flow of a Newtonian liquid, this time in a tube, to determine an "apparent viscosity for flow in a tube" η_t as a measure of the over-all resistance to flow of a material. The formula in this case is

$$\eta_t = \frac{\pi h^4 C}{8Q} \qquad [110]$$

For materials governed by the functions, Equations [74], the dimensionless shearing rate $S = sT$ is a function of τ/G; thus in a fashion similar to that used in the channel-flow analysis

$$\frac{dv_1}{dx_2} = \frac{1}{T} S\left(\frac{\tau}{G}\right) = -\frac{1}{T} S\left(\frac{Cx_2}{2G}\right) \qquad [111]$$

This equation differs from Equations [96] only by the factor 2 in the denominator of the argument of S, which comes from Equations [107] or [108]. In this case it is convenient to introduce the variables

$$X' = \frac{Cx_2}{2G}; \quad H' = \frac{Ch}{2G} \qquad [112]$$

The velocity is, accordingly, given by

$$v_1 = \frac{2G}{CT} \phi'(H', X') \qquad [113]$$

where

$$\phi'(H', X') = \int_0^{H'} S dX' - \int_0^{X'} S dX' \qquad [114]$$

The volume output integral Equation [109] gives

$$Q = \frac{16\pi G^3}{C^3 T} \Phi' = \frac{2\pi h^3}{T} \times \frac{\Phi'}{(H')^3} \qquad [115]$$

with

$$\Phi' = \Phi'(H') = \int_0^{H'} \phi'(H', X') X' dX' \qquad [116]$$

The expression for the apparent viscosity η_t is found by substituting the result, Equation [115], into Equation [110], and is

$$\eta_t = GT \times \frac{(H')^4}{8\Phi'} \qquad [117]$$

The dimensionless measure of apparent viscosity $\eta_t/(GT)$ is a function of the parameter H' as is also the dimensionless measure of volume output rate GT/h^3 of Equation [115]; therefore, $\eta_t/(GT)$ is a function of QT/h^3.

Numerical computations have been made for the case $n = 5/4$, and the results are presented in Table 3, and Fig. 7. The velocity distributions are qualitatively similar to those shown in Fig. 5 for the channels.

The viscosity-tube data in Fig. 8 of a report by James Bailey and R. W. Canfield[9] are tabulated in Table 4, where they are also reduced to the form QT/h^3 and $\eta_t/(GT)$ by using values of the constants G and T, which are consistent with the tensile-test data of the author.[2] For values of QT/h^3 above about 0.35, there is good agreement of these measured apparent viscosities with the theoretical values in Fig. 7; the test points of Table 4 have been entered on the plot, Fig. 7. However, at very low rates of flow — QT/h^3 less than 0.3—the measured viscosities are somewhat higher than the theoretical values. This discrepancy may be attributed to the factor $(1 - \alpha_i^{-n})$ of the relaxation functions in Equations [74], which, as remarked before, affect the apparent viscosity at low flow rates. This factor has not been substantiated by the previous tests[2] for the reasons discussed at the beginning of Section 5.

TABLE 3 APPARENT VISCOSITY FOR FLOW IN TUBES

H'	$\frac{QT}{h^3}$	$\frac{\eta_t}{GT}$
0.0	0.0	1.000
0.25	0.201	0.977
0.5	0.443	0.886
0.75	0.767	0.768
1.0	1.31	0.601
1.25	2.35	0.418
1.5	4.44	0.265
1.75	8.05	0.171
2.0	13.8	0.114
>2	$0.88 \times H^4$	$0.90 \div H^3$

TABLE 4 VISCOSITY TUBE DATA OF FIG. 8[a]

Exp no.	h, in.	Q in.^{3}/sec	η_t, poises	$\frac{QT}{h^3}$	$\frac{\eta_t}{GT}$
Temp. = 437 — 440 F; G = 4 psi T = 0.3 sec; GT = 83000 poises					
1	5/8	0.082	350000	0.10	4.21
2	5/8	0.094	345000	0.12	4.15
3	5/8	0.250	258000	0.31	3.11
11	3/8	0.060	82000	0.34	0.99
4	5/8	0.448	86000	0.55	1.04
7	1/4	0.040	70000	0.77	0.84
12	3/8	0.394	29000	2.25	0.35
8	1/4	0.162	35000	3.11	0.42
9	1/4	0.325	20500	6.25	0.25
Temp. = 345 — 350 F; G = 20 psi T = 0.3 sec; GT = 415000 poises					
5	5/8	0.185	500000	0.23	1.20
13	3/8	0.042	655000	0.24	1.58
6	5/8	0.325	315000	0.40	0.76
10	1/4	0.034	325000	0.65	0.77
14	3/8	0.126	235000	0.72	0.57

[a] See footnote 9.

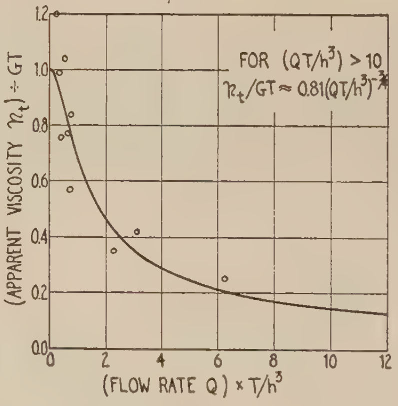

FIG. 7 η_c/GT VERSUS QT/h^3 FOR TUBES

ACKNOWLEDGMENT

The analyses presented in this paper were carried out by the author as a part of the research program of the Plax Corporation of Hartford, Conn., with whose permission they are published. The work was carried out under the general direction of Mr. James Bailey, vice-president and research director of the Plax Corporation, and the author gratefully acknowledges the very valuable guidance of Mr. Bailey in planning and carrying out the work.

Discussion

JAMES BAILEY.[10] On the subject matter of this paper the writer will confine his remarks to reasons why his company felt that a mathematical investigation of the flow of commercially used plastics was necessary.

---

[9] "Report Covering Tests of Viscosity Tubes and Side Entrance Nozzle Made June 19, 20, and 21, 1944;" report prepared for Plax Corporation by James Bailey and R. W. Canfield.

[10] Vice-President and Research Director, Plax Corporation, Hartford, Conn.

Preliminary experiments consisted of measuring the pressure drop through dies, tubes, screen packs, and various commercial apparatus, together with temperature and volume of material per unit of time. These data were analyzed mathematically, using the laws of pure viscous flow, and it was found that the computed viscosity varied over a very wide range.

These experiments were followed by experiments using especially large viscosity tubes having inside bores of $^1/_2$, $^3/_4$, and 1 in., and a length of 14 in. The tubes were equipped with a back-pressure valve at the outlet and four pressure gages arranged along their length. The computed viscosity was found to vary over a range of 17 to 1, when the output varied from a few pounds per hour to 60 lb per hr at the same temperature. Over-all back pressure had no practical effect.

In other experiments, frictional effects, heating effects due to the internal work necessary to maintain the flow, and a relaxation effect at the exit of dies were noted. Tests using a rapid stretching apparatus at controlled temperature showed similar behavior.

All of these effects presented so complicated a picture that it was felt correlation would be possible only by a mathematical procedure.

AUTHOR'S CLOSURE

To supplement Mr. Bailey's remarks on the origin of the studies reported in the paper the writer can add a few remarks on applications and future developments.

In the continuous blowing up of extruded thin-walled polyethylene tubing with internal pressure, a characteristic configuration of tube diameter often occurs wherein the tube diameter first decreases, and finally increases as it is drawn away from the die. This behavior is qualitatively inexplicable in terms of simple viscous flow theory, but is predicted according to the proposed flow theory.

Charts of pressure drop in channels and tubes of various sizes for varying flow rates and temperatures of several materials have been prepared on the basis of the results of section 5 of the paper, and are useful in design of equipment. Studies are also planned on the pressure-development characteristic in the melting section of extruder screws by use of the theory.

Further experimental and theoretical work is expected to improve the quantitative representation of the properties of specific materials, particularly with respect to variations with temperature and flow rate; work with molecular representations appears promising in this respect.

Extrapolation of Static Tests to Predict Operation of Jet Engines in Flight

By C. A. MEYER,[1] SOUTH PHILADELPHIA, PA.

The purpose of this paper is to present a method which enables a prediction of flight performance of a jet engine from data obtainable in the test cell. The range of flight performance obtained by the method is of course limited by the operating range covered in the static tests. The method is also useful in comparing static tests with flight or wind-tunnel data. A curve is also presented which is generally useful in the solution of many flow problems.

NOMENCLATURE

The following nomenclature is used in this paper:

A = exhaust-nozzle area
a = acoustic velocity
c = gas velocity
c_p, c_v = specific heats, and constant pressure and volume
D = diameter
F, F_n = thrust, net thrust
g = acceleration due to gravity
J = mechanical equivalent of heat 778.26 ft-lb/Btu
k = ratio of specific heats (c_p/c_v)
n = rotational speed
p_s, p_t = static and total pressures
p_0 = standard sea-level pressure
R = gas constant
T_s, T_t = static and total absolute temperatures
T_0 = standard sea-level temperature
V = air speed
W_a, W_f = weight rate of air, and fuel flow
δ_{am}, δ_{t2} = relative absolute pressures, P_{am}/P_0, Pt_2/P_0
θ_{am}, δ_{t2} = relative absolute temperatures, T_{am}/T_0, Tt_2/T_0
1, 2 = subscripts referring to stations
am = subscript for ambient

INTRODUCTION

Since the advent of jet propulsion, flight-performance figures of jet engines have been required by airframe builders in order that they could make suitable estimates of performance of proposed airplanes. This need for information was first met by the engine builders by supplying calculated estimates. These calculated estimates of engine performance were obtained by the following:

1 Testing or estimating the performance of the component parts of the engine, such as the compressor, burner, turbine, and exhaust nozzle.

2 Combining by means of calculations the performance of the components to obtain the over-all performance of the jet engine for various flight speeds, altitudes, rotational speeds, and exhaust-nozzle sizes. Later, when jet engines actually were being tested, it became possible to obtain a better estimate of flight performance based on test-cell data rather than by combining the estimated or tested performance of the components.

This paper describes a method of carrying out such an estimate.

The curve, Fig. 1, which in this paper is used to carry out the calculations, will be found to be generally useful in the solution of various flow problems.

JET-MOTOR PERFORMANCE

The static performance of any given jet engine can be represented by the following relations:

$$\text{A function of } \left(\frac{T_{t4}}{\theta_{t2}}\right), \left(\frac{n}{\sqrt{\theta_{t2}}}\right) \text{ and } A = 0 \ldots\ldots\ldots\ldots\ldots [1]$$

$$\text{A function of } \left(\frac{F}{\delta_{t2}}\right), \left(\frac{n}{\sqrt{\theta_{t2}}}\right) \text{ and } A = 0 \ldots\ldots\ldots\ldots\ldots [2]$$

$$\text{A function of } \left(\frac{W_a\sqrt{\theta_{t2}}}{\delta_{t2}}\right), \left(\frac{n}{\sqrt{\theta_{t2}}}\right) \text{ and } A = 0 \ldots\ldots\ldots\ldots [3]$$

$$\text{A function of } \left(\frac{W_f}{\delta_{t2}\sqrt{\theta_{t2}}}\right), \left(\frac{n}{\sqrt{\theta_{t2}}}\right) \text{ and } A = 0 \ldots\ldots\ldots\ldots [4]$$

$$\text{A function of } \left(\frac{P_{t5}}{P_{t2}}\right), \left(\frac{n}{\sqrt{\theta_{t2}}}\right) \text{ and } A = 0 \ldots\ldots\ldots\ldots\ldots [5]$$

The proof of the foregoing relations can be found by means of dimensional analysis of the jet engine.

As an example, the Relation [3] is developed in Appendix 1.

The Relations [1] through [5] give, respectively, the corrected top temperature, the thrust, the air flow, the fuel flow, and the exhaust-nozzle pressure ratio, in terms of the corrected rotational speed, and the exhaust-nozzle area taken as independent variables. It should be noticed that the various quantities given in the Relations [1] through [5] are corrected to the conditions (total pressure and total temperature) at inlet to the compressor. In this way the performance is given independent of the inlet-duct losses. Where the inlet-duct losses are negligible, this is the same as correcting the quantities to the ambient static pressure and temperature, since in this case the total pressure and temperature at the compressor inlet are respectively equal to the ambient static temperature and pressure.

Where it is desired to present the engine performance, including an inlet duct having finite losses, the quantities should be corrected to the ambient conditions.

Another very useful method of presenting jet-engine performance is to consider the engine to be a "hot-gas generator." This method simply presents the performance of the engine exclusive of inlet ducting and exhaust nozzle.

The combination of compressor, burner, and turbine is assumed to generate or supply a quantity of hot gases at a pressure above atmospheric. In the normal jet engine the hot gases are expanded in a nozzle to produce thrust.

---

[1] Thermodynamics Section Engineer, Aviation Gas Turbine Division, Westinghouse Electric Corporation. Jun. ASME.

Contributed by the Oil and Gas Power and Aviation Divisions and presented at the Annual Meeting, New York, N. Y., November 26–29, 1945, of THE AMERICAN SOCIETY OF MECHANICAL ENGINEERS.

NOTE: Statements and opinions advanced in papers are to be understood as individual expressions of their authors and not those of the Society.

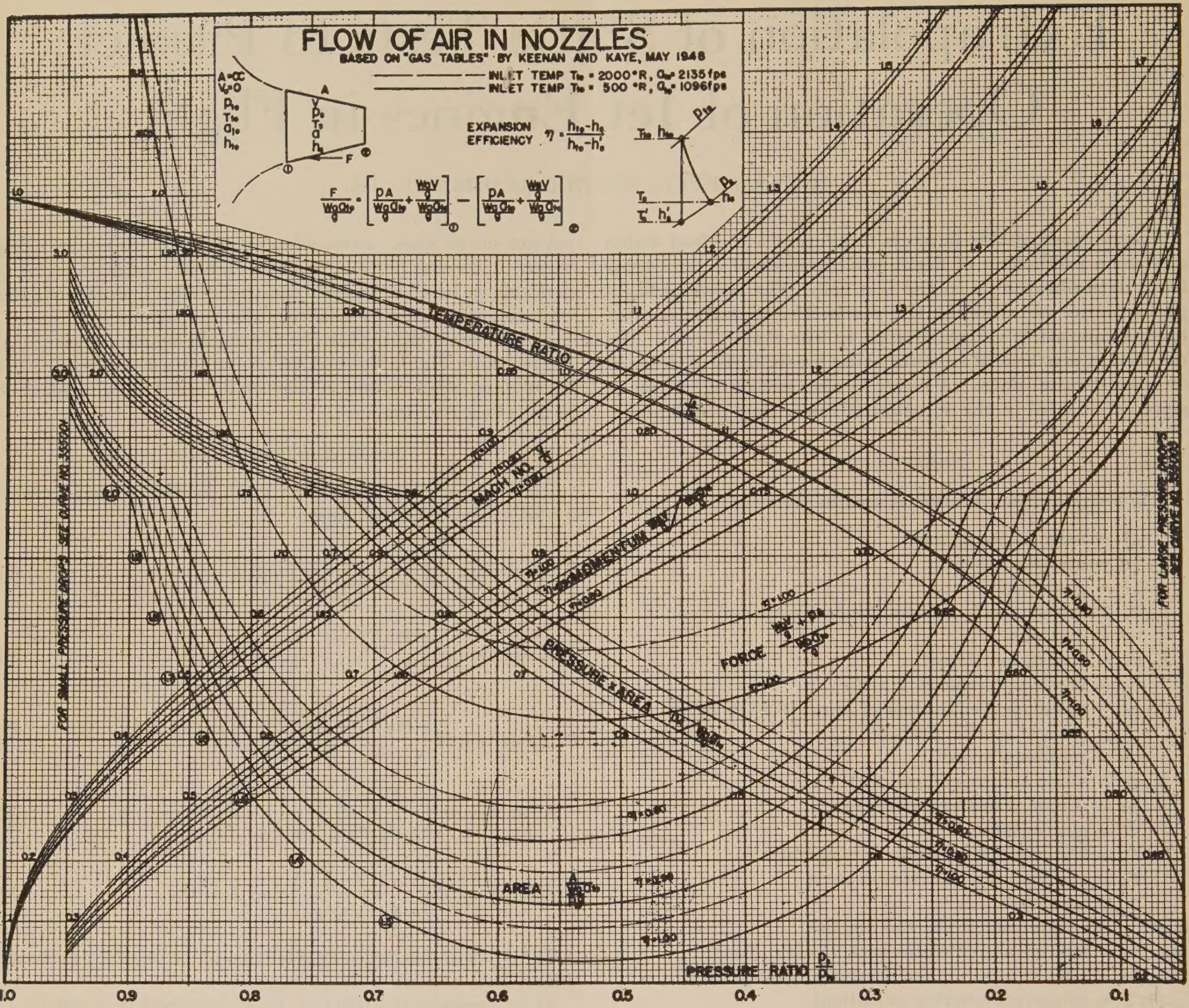

FIG. 1 FLOW OF AIR IN NOZZLES

If we analyze only the combination of compressor, burner, and turbine, we find we can present the performance as follows:

$$\text{A function of}\left(\frac{P_{t5}}{P_{t2}}\right),\left(\frac{T_{t4}}{\theta_{t2}}\right),\left(\frac{n}{\sqrt{\theta_{t2}}}\right)=0\ldots\ldots\ldots\ldots\ldots\ [6]$$

$$\text{A function of}\left(\frac{T_{t5}}{\theta_{t2}}\right),\left(\frac{T_{t4}}{\theta_{t2}}\right),\left(\frac{n}{\sqrt{\theta_{t2}}}\right)=0\ldots\ldots\ldots\ldots\ldots\ [7]$$

$$\text{A function of}\left(\frac{W_a\sqrt{\theta_{t2}}}{\delta_{t2}}\right),\left(\frac{T_{t4}}{\theta_{t2}}\right),\left(\frac{n}{\sqrt{\theta_{t2}}}\right)=0\ldots\ldots\ldots\ldots\ [8]$$

$$\text{A function of}\left(\frac{W_f}{\sqrt{\theta_{t2}}\,\delta_{t2}}\right),\left(\frac{T_{t4}}{\theta_{t2}}\right),\left(\frac{n}{\sqrt{\theta_{t2}}}\right)=0\ldots\ldots\ldots\ldots\ [9]$$

These relations give the generated pressure, the generated gas temperature, the air flow, and the fuel flow in terms of the top temperature and the rotational speed. All values are corrected to the compressor-inlet total pressure and temperature. The Relations [6] through [9] represent the "internal performance" of a jet engine. Once this performance is determined, it can be combined with the characteristics of the inlet ducting and those of the exhaust nozzle to give the over-all performance of the engine.

THE EXTRAPOLATION METHOD

Let us assume we are testing a given jet engine, and during the test we arrange by means of an evacuating device to reduce the back pressure (P_{s7}) below atmosphere, and at the same time we reduce the exhaust-nozzle area so as to maintain the same conditions after the turbine (at point 5). The jet engine would now be operating under conditions which are similar to those in flight, because the total pressure at the compressor inlet will be greater than the static pressure at the outlet of the exhaust nozzle. Furthermore, since the conditions at the exit of the turbine were maintained constant, (p_{t5}/p_{t2}) = const, the internal performance of the jet engine would be unchanged by the reduction of back pressure and nozzle size.

We can now foresee that without performing the foregoing experiment, it is possible to predict a flight operating condition from the static-test data. The flight condition so calculated would correspond to a case with a reduced exhaust-nozzle size.

The method of carrying out such an extrapolation from a static test is summarized in the following:

Let us assume that we have corrected data taken from a single static test and represented by the quantities

$$\left(\frac{F}{\delta_{t2}}\right)_T, \left(\frac{W_a\sqrt{\theta_{t2}}}{\delta_{t2}}\right)_T, \left(\frac{n}{\sqrt{\theta_{t2}}}\right)_T, \left(\frac{T_{t4}}{\theta_{t2}}\right)_T, \left(\frac{W_f}{\delta_{t2}\sqrt{\theta_{t2}}}\right)_T, \left(\frac{P_{t5}}{P_{t2}}\right)_T, A_T$$

The subscript T represents the tested data while E represents extrapolated values.

(*a*) Calculate the corrected jet velocity from the thrust and air flow

$$\left(\frac{C_7}{\sqrt{\theta_{t2}}}\right)_T = g\left(\frac{F}{\delta_{t2}}\right)\Big/\left(\frac{W_a\sqrt{\theta_{t2}}}{\delta_{t2}}\right)$$

(*b*) Assume a reduction in back pressure on the engine. The ratio of original to assumed back pressure becomes the flight (ram) pressure ratio $(P_{t2}/P_{am})_E$ of the extrapolated point so that this pressure ratio can, if desired, be chosen to correspond to a given flight speed.

(*c*) Calculate the isentropic temperature ratio corresponding to the foregoing assumed flight (ram) pressure ratio

$$\left(\frac{P_{t2}}{P_{am}}\right)_E^{\frac{k-1}{k}} = \left(\frac{T_{t2}}{T_{am}}\right)_E = \left(\frac{\theta_{t2}}{\theta_{am}}\right)_E$$

(*d*) To find the required reduction in nozzle area to maintain fixed conditions at point 5, we make use of curve 1, which is explained in Appendix 2. It should be noted that since curve 1 is a general working curve, its nomenclature differs from the remainder of the paper. Enter curve 1 with

$$\frac{P_s}{P_{t0}} = \left(\frac{P_{t2}}{P_{t5}}\right)_T$$

and at an assumed exhaust-nozzle efficiency pick off the dimensionless area

$$\left[\frac{A}{(w_a a_{t0})/(P_{t0}g)}\right]$$

Also pick off the dimensionless velocity

$$\frac{W_aV}{g}\Big/\frac{W_a a_{t0}}{g}$$

(*e*) Enter curve 1 again with

$$\frac{P_s}{P_{t0}} = \left(\frac{P_{t2}}{P_{t5}}\right)_T\Big/\left(\frac{P_{t2}}{P_{am}}\right)_E$$

and again pick off the dimensionless area and velocity at the assumed nozzle efficiency.

(*f*) The ratios of the dimensionless areas and velocities obtained in (*d*) and (*e*) give the required reduction in exhaust-nozzle area and increase in jet velocity. By multiplication, we thus obtain A_E and $(C_7/\sqrt{\theta_{t2}})_E$ which are, respectively, the exhaust-nozzle area, and the corrected jet velocity for the extrapolated point.

(*g*) Calculate the flight speed, corrected to atmospheric conditions, from the flight (ram) pressure ratio assumed under (*b*)

$$\left(\frac{V}{\sqrt{\theta_{am}}}\right)_E = \sqrt{2T_{am}gc_pJ\left[\left(\frac{P_{t2}}{P_{am}}\right)^{\frac{k-1}{k}} - 1\right]}$$

(*h*) Calculate the rotational speed corrected to atmospheric conditions for the extrapolated point using the ram temperature ratio under (*c*)

$$\left(\frac{n}{\sqrt{\theta_{am}}}\right)_E = \left(\frac{n}{\sqrt{\theta_{t2}}}\right)_T\sqrt{\left(\frac{\theta_{t2}}{\theta_{am}}\right)_E}$$

(*i*) Calculate the extrapolated net thrust, corrected to atmospheric conditions from the ram pressure ratio, the air flow, and the jet and flight velocities

$$\left(\frac{F_n}{\delta_{am}}\right)_E = \frac{1}{g}\left(\frac{P_{t2}}{P_{am}}\right)_E\left(\frac{w_a\sqrt{\theta_{t2}}}{\delta_{t2}}\right)_T\left[\left(\frac{C_7}{\sqrt{\theta_{t2}}}\right)_E - \left(\frac{V}{\sqrt{\theta_{am}}}\right)_E\sqrt{\frac{\theta_{am}}{\theta_{t2}}}\right]$$

(*j*) Calculate the corrected air flow

$$\left(\frac{w_a\sqrt{\theta_{am}}}{\delta_{am}}\right)_E = \left(\frac{w_a\sqrt{\theta_{t2}}}{\delta_{t2}}\right)_T\sqrt{\left(\frac{\theta_{am}}{\theta_{t2}}\right)_E}\left(\frac{P_{t2}}{P_{am}}\right)_E$$

(*k*) Calculate the corrected top temperature

$$\left(\frac{T_{t4}}{\theta_{am}}\right)_E = \left(\frac{T_{t4}}{\theta_{t2}}\right)_T\left(\frac{\theta_{t2}}{\theta_{am}}\right)_E$$

Other quantities, such as corrected specific fuel consumption, can be determined easily from the extrapolated quantities found in the foregoing equations.

In summary, the foregoing calculations have given us the net thrust, fuel flow, rotational speed, top temperature, jet velocity, and air flow, corresponding to a given corrected flight speed. All quantities are corrected to the atmospheric conditions before the engine.

DISCUSSION

As a practical application of the method, consider a case in which static tests have been run for various exhaust-nozzle openings. The results of these tests can be extended to flight conditions by extrapolating to smaller exhaust-nozzle areas.

If we are interested in performance data for only one value of exhaust-nozzle area, static tests can be run with various exhaust-nozzle passages which are larger (even diffusing) in size. The results can then be extended to flight conditions by extrapolating to the desired exhaust-nozzle size.

It is also possible to extrapolate in the reverse direction, in order to obtain performance with duct losses. Should it be necessary to extend the range to excessively high duct losses or to represent a case where the boundary layer is removed from the wings and fed into the inlet duct (greatly reducing the effective ram), an actual duct exhibiting such characteristic could be used, or even a simulated inlet duct in the form of a fine-mesh screen could be placed across the inlet.

Fig. 2 shows the flight range covered by the method. This curve assumes that the static tests are run under standard sea-level conditions. As illustrated by this curve, performance can

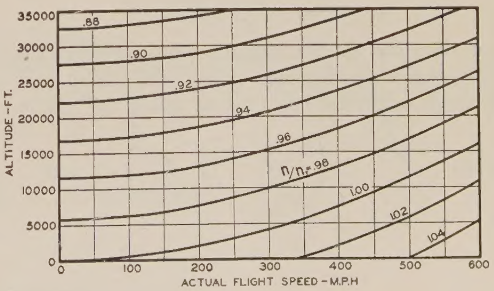

FIG. 2 EXTRAPOLATION RANGE FOR STANDARD SEA-LEVEL TEST CONDITIONS

be obtained only up to 17,000 ft altitude for 600 mph with maximum allowable rotational speed and top temperature. Above this altitude the method will give performance only at reduced rotational speeds and top temperatures.

However, if the static tests are run on a day having a temperature less than the standard sea-level value, the limiting altitude will be increased accordingly. Likewise, it is possible to have the jet engine suck its air through a cooling turbine and in that way reduce the inlet-air temperature considerably below atmospheric. Naturally, this will extend accordingly the range of flight operation obtained; for here we are, in effect, extrapolating from a test condition corresponding to static altitude rather than static sea level.

It should be noted that the following liberties were taken in this extrapolation method:

1 Neglect of Reynolds-number effects.

2 Neglect of the effect caused by change in the properties of the fluid such as specific heat, gas constant, etc.

3 An exhaust-nozzle efficiency was assumed for the added expansion required by the method.

Appendix 1

DEVELOPMENT OF EQUATION [3]

The air mass flow W_a/g through any one of several geometrically similar jet engines depends upon the engine rotational speed n, the size of the engine represented by any convenient reference length D, the adjustable exhaust-nozzle area A, the compressor-inlet total pressure P_{t2}, the compressor-inlet total temperature T_{t2}, and the properties of the working fluid (in this case air) R and c_p.

A function of

$$\left(\frac{W_a}{g}\, nDAP_{t2}T_{t2}Rc_p\right) = 0$$

We have in this analysis neglected to include the fluid viscosity or thermal conductivity. Thus, knowingly, we are neglecting Reynolds-number and Prandtl-number effects on the performance. These effects can be included later when sufficiently accurate test data are available.

By the methods of dimensional analysis, the foregoing relation can be reduced to a new relation between fewer dimensionless variables, for instance, a function of

$$\left(\frac{W_a a_{t2}}{P_{t2}Ag}\right)\left(\frac{nD}{a_{t2}}\right)\frac{A}{D^2}\, k\, \frac{R}{C_p} = 0$$

We have in writing the foregoing relations assumed that the working fluid is a perfect gas with an acoustic velocity

$$a_{t2} = \sqrt{gkRT_{t2}}$$

Rather than use the dimensionless quantities in this relation in plotting engine performance, it has been found more convenient, although somewhat less general, to use the relation

$$\text{A function} \quad \left(\frac{W_a\sqrt{\theta_{t2}}}{\delta_{t2}}\right)\left(\frac{n}{\sqrt{\theta_{t2}}}\right) A = 0 \ldots\ldots\ldots [3]$$

This latter relation is restricted to use for a given-size engine, (D = const), and neglects variations of k and C_p of the working fluid. The inlet temperature and pressure are also given as ratios (θ_{t2} and δ_{t2}) to the standard sea-level total pressure and temperature, respectively.

The quantities appearing in the foregoing relation have dimensions and, therefore, are called "corrected values." They represent the tested values under standard sea-level conditions (for the case without inlet-duct losses), and give more reasonable numerical values for plotting test curves. Others have used, for instance, the quantity $n/\sqrt{T}$ for corrected speed. The numerical values of this quantity for 16,000 rpm and 520 deg R would be 222 rpm/$\sqrt{\text{deg}}$. The inconvenience is apparent.

Relation [3] simply states that the air flow for a given corrected speed and exhaust-nozzle area is proportional to the compressor-inlet total pressure ($\sim \delta_{t2}$) and inversely proportional to the square root of the compressor-inlet total temperature ($\sim \sqrt{\theta_{t2}}$).

The other relations appearing in the paper can easily be developed in a manner similar to the development of Equation [3].

Appendix 2

Fig. 1 is a working curve which is intended for use in the solution of many flow problems.

Often we are given a problem involving a flow through a channel or nozzle in which an area, a total temperature, and a velocity are given at one station, and we are required to find an area, temperature, or velocity at another station.

Fig. 1 has been constructed in such a way that areas, velocities, pressures, Mach numbers, and temperatures along the channel are given as dimensionless quantities in terms of inlet total pressure and temperature or inlet acoustic velocity. All curves are based upon the properties of air as given by Keenan and Kaye and are drawn for 2000 deg R and 500 deg R inlet temperature.

For other inlet temperatures, we interpolate between the curves.

The curve shows the variation of temperature, Mach number, momentum, area, and pressure × area, with the static pressure, all given as dimensionless quantities.

Thus for fixed total conditions, the ratios of the dimensionless velocities at two stations along the nozzle are also the ratio of the velocities. Similarly, the ratios of the dimensionless areas are also the area ratio.

In the problem used in the extrapolation method of this paper we are assuming an extension of the exhaust nozzle with a corresponding reduction in back pressure so as to leave the conditions before the nozzle unaffected. We need only enter the curve with $(P_s/P_{t0}) = (P_{t2}/P_{t5})_T$ and select a dimensionless velocity and area. For, say, a 10 per cent lower back pressure, we need only read the curve again with a value of P_s/P_{t0}, which is 10 per cent lower than the original value. The ratios of dimensionless areas and velocities then give, respectively, the required area reduction, and velocity increase.

The thrust force on the channel is also easily calculated as shown on the curve.